Title
Lamb Wave Propagation in Elastic Plates under various loads

Author
Samajder, Himadri

Publication Date
2015

Peer reviewed|Thesis/dissertation

University of California

Los Angeles

Lamb Wave Propagation in Elastic Plates under various loads

A dissertation submitted in partial satisfaction

of the requirements for the degree

Doctor of Philosophy in Mechanical and Aerospace Engineering

by

Himadri Sekhar Samajder

2015

Abstract of the Dissertation

Lamb Wave Propagation in Elastic Plates under various loads

by

Himadri Sekhar Samajder

Doctor of Philosophy in Mechanical and Aerospace Engineering

University of California, Los Angeles, 2015

Professor Ajit Mal, Co-chair

Professor Robert M'Closkey, Co-chair

Ultrasonic guided waves offer an attractive cost effective tool for inspecting large structures. This is due to the fact that guided waves can propagate a large distance in plate like structural components and are strongly affected by the presence of defects in their propagation path. Propagation characteristics of Lamb waves have been studied extensively over many years, where the waves have been studied at a large distance away from the source, independent of the source influence. The literature on propagation of Lamb waves including the influence of the particular source responsible for the wave motion in the plate is comparatively much more sparse. In this dissertation the propagation of waves in a plate due to different kinds of applied loads is studied. Two dimensional and axisymmetric models are analyzed and the waves are studied both near the source and far away from it. The energy carried by the waves and how they vary depending on the type of applied load are studied. This provides the knowledge base to characterize and ultimately minimize the energy loss in various engineered structures and devices, including in the design of resonators by minimizing the "anchor loss" associated with them.

The dissertation of Himadri Sekhar Samajder is approved.

Ertugrul Taciroglu

William Klug

Christopher Lynch

Robert M'Closkey, Committee Co-chair

Ajit Mal, Committee Co-chair

University of California, Los Angeles

2015

Table of Contents

List of Figures

List of Tables

Acknowledgments

It would not be possible for me to do this work, without the help of many others. First of all, I owe my deepest gratitude to my advisor Prof Ajit Mal. Without his guidance and support every time I needed, and I needed them a lot, I simply would not have made it to this point. I am deeply grateful to my committee members, Prof Klug, Prof M'Closkey, Prof Lynch and Prof Taciroglu for supporting me so much in my research and for being the great teachers from whom I learned my subjects. I am enormously indebted to Prof M'Closkey who supported me financially in a particularly difficult period in my student life and I am thankful to him for letting me work for his exciting project from which I learned new things everyday. I do not have enough words to acknowledge Dr. Amiya Chatterjee's influence on me. His unconditional support and friendship taught me about life and how to carry through difficult days. I will always cherish my friendship I share with my former colleague Dr. Harsh Baid and postdoc Dr. Christoph Schaal. I learned a lot from them and their constant encouragement and companionship made my work enjoyable for me. I will always remember my joyful experience of being the Teaching Assistant of all my beloved students, and quite a few of them, I now have the pleasure to call friends. If they read this, they will know who they are and I must admit that their support, definitely not fully deserved but still the admiration they showed for me and their friendship made me the happiest person. I do not know enough ways to thank my dear friends. They never made me feel, I was away from home. I always received help, even before I asked. I received unconditional support and help from them, even though I fell short reciprocating similarly. They know who they are and I want to say that I will forever be indebted to them. Without my friend Preeti's love and care, I would not be walking today. And what do I say to my niece, sister, mother, father and my family? They know I love them.

Vita

2006	B.Tech. (Mechanical Engineering), WBUT, India.
2008	M.S. (Mechanical Engineering), Texas Tech University, Lubbock, Texas.
2009–2015	Graduate Student Researcher in UCLA Nondestructive Evaluation (NDE) Research Group in Materials Degradation Characterization Laboratory, Los Angeles, California
2009–2015	Teaching Assistant, Mechanical Engineering Department, UCLA. MAE 156A (Advanced Strength of Materials course), MAE 182A (Mathematics of Engineering), MAE 168 (Introduction to Finite Elements), MS online courses (MAE 156A, MAE 168, MAE 256A).
2010	Outstanding Teaching Assistant Award, UCLA MAE Department

Publications

Idesman, A.V., Samajder, H., Aulisa E., Seshaiyer P. Benchmark problems for wave propagation in elastic materials, Computational Mechanics, 2009, 43 (6), 797-814.

Schaal, C., Samajder, H., Baid, H., Mal, A. Rayleigh to Lamb wave conversion at a delamination-like crack. Journal of Sound and Vibration, 2015, 353, 150-163.

Baid, H., Schaal, C., Samajder, H., Mal, A. Dispersion of Lamb waves in a honeycomb composite sandwich panel, Ultrasonics, 2015, 56, 409-416.

Samajder, H., Baid, H., Ricci, F., Mal, A. Lamb waves in a honeycomb composite sandwich plate. In SPIE Smart Structures and Materials+ Nondestructive Evaluation and Health Monitoring (pp. 869505-869505). International Society for Optics and Photonics, 2013, April.

Mal, A., Ricci, F., Samajder, H., Baid, H. NDE of composite structures using ultrasonic guided waves. In SPIE Smart Structures and Materials+ Nondestructive Evaluation and Health Monitoring (pp. 86950E-86950E). International Society for Optics and Photonics, 2013, April.

Schaal, C., Zhang, S., Samajder, H., Mal, A. (2015). Analytical Investigation of the Interaction of Rayleigh and Lamb Waves at a Delamination-like Discontinuity in a Thick Plate. Structural Health Monitoring 2015.

CHAPTER 1

Introduction

Current methods for the detection and characterization of hidden defects in complex structural components are time consuming and costly, often requiring partial disassembly of the structures. Ultrasonic guided waves offer an attractive cost effective tool for inspecting large structures. This is due to the fact that guided waves can propagate a large distance in plate like structural components and are strongly affected by the presence of defects in their propagation path. However, the waves are also affected by other geometrical features (e.g. stringers) in the structure and their application in defects detection and characterization requires a good understanding of the quantitative features of these interactions. While some of these features can be determined through laboratory experiments, numerical simulations can provide the solution for a larger class of problems at a much lower cost.

The need for model-based studies is widely recognized in the NDE and SHM communities and a great deal of work has indeed been carried out dealing with a variety of models. A majority of these studies involve the propagation characteristics of guided waves in plate-like structural components without without externally applied loads and defects. The general features of elastic waves that can be transmitted in isotropic and anisotropic solids have been investigated in great detail [1, 2, 3, 4, 5], motivated by the need to understand the nature of ultrasonic guided waves for applications in both engineering and seismology. In contrast, the literature on the response of anisotropic and multilayered plates to

surface or subsurface sources that are representative of impact or fatigue damage is relatively sparse. The exact solution of three-dimensional problems consisting of multilayered, angle-ply laminates of finite thickness and large lateral dimensions subjected to various types of surface loads, has been given by Mal and Lih [6] and Lih and Mal [7]. Approximate thin-plate theories have also been developed to obtain the analytical solutions for the response of thin isotropic and anisotropic plates to surface loads [8].

The finite element method (FEM) is a versatile tool to analyze this class of problems. In this dissertation a comprehensive approach including experimental and numerical (finite element) methods are used to determine the interaction of ultrasonic guided waves with crack like defects in an aluminum plate and a honeycomb composite sandwich plate. The simpler problem of the aluminum plate is considered for model validation and to understand the basic features of the wave interaction with the defect. The results of the calculations are compared with those obtained in laboratory experiments, showing excellent agreement.

Composite materials are highly susceptible to hidden flaws that may arise from manufacturing flaws and service related defects caused by mechanical or thermal fatigue, foreign object impact and other unexpected events. Hidden defects in composite structures can grow to reach a critical size, become unstable and cause catastrophic failure of the entire structure. An example of such a structural component is a honeycomb composite sandwich panel in which thin composite skins are bonded with adhesives to the two faces of an extremely lightweight and relatively thick metallic honeycomb core. Hidden defects in critical load bearing structural components require reliable and cost effective nondestructive inspection and maintenance strategy for their safe operation. Most of the current inspection techniques, e.g. visual, liquid penetrant, thermal, radiographic or electromagnetic, are time consuming and often require partial disassembly of the structure, resulting in significant expense and loss of service. In addition to acoustic emis-

sion monitoring, active ultrasonic nondestructive evaluation (NDE) is a relatively cost effective technique for defect detection in structural components. The most common ultrasonic method, using a single transducer in the pulse-echo mode, is highly effective in detecting defects that are located directly under the transducer. The method is, however, extremely time-consuming when inspecting large areas, and also insensitive to certain types of defects. Guided waves offer a suitable complementary method for inspecting large plate-like structural components due to the fact that they can travel long distances. In addition, the propagation speed and amplitude of guided waves are strongly influenced by the presence of defects in their propagation path. A careful analysis of waves that are recorded by moveable surface-mounted transducers can lead to significant improvement of the speed and reliability of damage detection and characterization in aircraft and aerospace structures. For successful application of these ultrasonic guided wave techniques to locate and estimate the severity of damages, it is extremely important to understand the propagation characteristics of ultrasonic waves in commonly used composite structural components. The characteristics of the waves are generally quite complex and depend on the laminate layup, direction of wave propagation, frequency, and interface conditions.

In one of his classic papers, Lamb [1] established the existence of guided elastic waves in a plate of finite thickness and infinite lateral dimensions, and determined the theoretical relationship between the phase velocity and frequency of the waves as well as the thickness and elastic properties of the plate. The propagation characteristics of guided waves in more complex media, e.g. isotropic multilayered plates and half spaces, have since been studied by numerous authors [9, 2]. Approximate thin-plate theories, such as the classical plate theory under Kirchoff-Love kinematic assumption, and shear deformation plate theory or Mindlin theory, have been developed to obtain analytical solutions to a variety of problems involving the dynamic response of thin isotropic and anisotropic plates

[10, 11]. Recently, theoretical studies in layered anisotropic media have been carried out, primarily because of the increasing use of composites in aircraft and aerospace structures. Most of these studies involve laminates consisting of a stack of unidirectional fiber-reinforced layers that are modeled as transversely isotropic solids with their symmetry axes on a plane parallel to the surface of the laminate. The velocity of guided waves in such laminates is very sensitive to the thickness, some of the stiffness constants and the condition of the interface between the layers of the laminate. Thus the degradation of these properties can in principle be monitored if the dispersion curves can be determined through nondestructive testing (NDT).

An experimental method based on the so called the Leaky Lamb Wave (LLW) phenomenon has been found to give highly accurate values of the phase velocity of guided waves in laboratory specimens. A nonlinear inversion algorithm has been used to estimate the material properties of the waveguide so that the theoretical dispersion function attains its minimum value in a multidimensional space [12, 13]. Although the method is successful in characterizing relatively small degradation in the material properties of both metallic and composite structural components in laboratory experiments, the requirements of water immersion and of matched pair of equally inclined transducers make the technique impractical for field applications. Other experimental methods to determine the dispersion curves require transducer placement on both faces [14] or on the edges of the plate, or variable angle wedge transducers [15], all of which suffer from various drawbacks for field application. A comprehensive review of recent research on guided waves in composite plates and their use in nondestructive material characterization can be found in Banerjee et al.[16]. Almost all of the wave propagation studies mentioned above involve angle-ply laminates consisting of a stack of unidirectional fiber-reinforced materials with different orientations. In the theoretical models, each ply is assumed to be transversely isotropic with its symmetry axis

on a plane parallel to the surface of the laminate. This homogenized model of the ply has been shown to be adequate when the wavelengths are large compared to the ply thickness. A reasonable homogenized model for the material of the whole woven composite plate is also transversely isotropic but with its symmetry axis normal to the plate surface. This is also true for the honeycomb material where the symmetry axis is parallel to the axis of the cells of the core [17].

In addition to theoretical and experimental studies, the finite element (FE) method is also a versatile tool to analyze this class of problems. For example, a dynamic finite element code has been developed for the calculation of acoustic emission (AE) waveforms in isotropic and anisotropic plates [18, 19]. This code has been for symmetric wave motion and by validated with both experimental measurements and analytical predictions for a variety of source conditions and plate dimensions in isotropic materials. However, although the FE method can handle complex geometries and has the capability to handle reflections from lateral boundaries, it is computationally much more intensive than the analytical methods discussed above, and the the physical properties of the waves are difficult to determine from the numerical solutions. Alternatively, different semi-analytical methods have been developed recently. The waveguide finite element (WFE) method [20] and the spectral finite element (SFE) method [21, 22], are two such modeling techniques. Due to their numerical efciency, these methods have been successfully applied to various kinds of cylindrical structures [23], helical seven-wire cables [24], and even in the presence of parameter uncertainty [25]. However, the WFE method has not been applied to study wave propagation characteristics in complex anisotropic composites and sandwich structures. This research focuses on a woven composite laminate and an aluminum honeycomb sandwich panel with composite face sheets. Due to aforementioned reasons, the theoretical problem for a woven composite plate is a homogeneous plate composed of a transversely isotropic material with symmetry axis normal to its surface. The model of the

honeycomb sandwich panel is a three layered transversely isotropic plate composed of the honeycomb core bonded to the composite skins. Theoretical solutions of the dispersion characteristics for these structures are not available in the literature, and are provided here. In addition to analytical solutions, also efficient numerical solutions are provided using the WFE method. The elastic constants of the two materials (woven composite and aluminum honeycomb) are determined from mixture type theories, and from destructive and ultrasonic nondestructive experiments. Furthermore, an experimental approach that is more amenable to practical implementation in which guided waves are generated and recorded by surface-mounted transducers is proposed and applied within this work. From the experiments, the validity of the assumption of transverse isotropy in the considered frequency range is demonstrated. The experimentally determined dispersion curves are compared with those calculated from theoretical models and from the WFE method. In addition to a woven composite laminate and a honeycomb composite sandwich structure, theory as well as numerical and experimental methods are also applied to an aluminum plate for validation purposes.

NDT and SHM of structures using guided Lamb waves typically compare the characteristics of the Lamb waves generated inside them while they are in service to the characteristics of the Lamb waves generated inside them before they were put into service and hence it could be safely assumed that the structures were free of internal defects. The measurements taken in the damage free structure are called the baseline data and the current measurements are compared against the baseline data to look for signs of internal damages. A more practical approach would be to use updated "baseline" data at a previous time and compare them with current data using a damage index [26]. To eliminate the need of baseline data, Fink [27] proposed the time-reversal process of Lamb waves to be used for SHM. According to the concept of time-reversal process, the source signal, when received at the sensor location is time reversed and emitted back to the source

transducer. In absence of internal defects in the path of propagation, the time-reversed signal when received back at the original source can be reconstructed into the original source signal. But in presence of internal defects, the reconstruction is not possible and the difference in the signals indicate the presence of defects. Time-reversal process of Lamb waves has been used for narrow-band excitation signals are in [28, 29]. Unfortunately, the time-reversal process does not have any advantages over other procedures due to the need to determine the "original source" which is the undamaged structure.

The literature on the interaction of guided waves with cracks and other defects is even sparser. Only a handful of problems of interest for the NDE of real structures have been studied [15, 30]. Often hybrid finite boundary element techniques are employed to characterize guided wave scattering at defects [31, 32]. Shkerdin and Glorieux [33] used an analytical method to study Lamb mode conversion at delaminations in plates, focusing on the dependence of scattering coefficients on size and location of the delamination. More recently, Chakrapani and Dayal [34] studied Rayleigh to Lamb mode conversion in a glass-epoxy laminate numerically and experimentally, and proposed that size and location of the delamination might be identified through a comprehensive analysis of the propagating waves. However, the interaction of waves propagating in thick plate-like structures, such as the aforementioned honeycomb sandwich panels, with delaminations is not well understood, in particular the dependence of scattering coefficients on frequency of the incident wave. In this thesis, a comprehensive approach is used to determine the interaction of ultrasonic guided waves with delamination-like defects in a thick aluminum plate, which is a continuation of the preliminary research work by Mal et al. [30]. The simple problem of the aluminum plate is considered to understand the basic features of the wave interaction with defects, in particular the mode conversion effects at the leading and trailing edges of the defect if the crack is close to the surface. In this case, the small region above the crack acts as a newly formed

waveguide, allowing for the propagation of Lamb waves. While Chakrapani and Dayal [34] did not consider "wave trapping" in the damaged area, in this work, it is shown that, under certain conditions, scattered Lamb waves might be trapped within the delamination zone, since only low transmission of the waves occurs at the trailing edge of the crack.

Support loss, also called anchor loss, has not been thoroughly studied for low-frequency micro-scale resonators. Researchers have used analyzed energy lost in a half-space by various tractions applied on the surface [35, 36, 37]. The substrates to which resonators are attached cannot be considered a half space due to the wavelengths involved when the resonator natural frequencies are below 1 MHz. In this case, the substrate is more accurately modeled as a plate. In this thesis, closed-form expressions for the elastic energy carried away from a source acting on the plate surface are obtained. The source can impart normal forces and moments to the plate surface as an infinite strip (2-D analysis problem) or a circular traction (2-D and 3-D analysis problems). The analysis yields expressions for the far field Lamb wave energy due to the source. In an effort to correlate the Lamb wave energy with the work done by the traction, near-field expressions are also developed in order to derive the driving point impedance at the source. This research attempts to make a connection between the work done by the source over one cycle to the far-field Lamb wave energy. It is shown that these calculations yield the same result. Thus, the far-field analysis represents a simplification for the analytical energy loss computations.

CHAPTER 2

Propagation of Lamb waves in thin plates subjected to surface loads - 2D analysis

In this chapter, the propagation of Lamb waves in an isotropic plate subjected to surface loads is analyzed. It is shown that the wave propagation in the plate can be decomposed into two independent wave motions namely symmetric and antisymmetric about the mid plane of the plate. The dispersion relations and the displacement and stress components for the symmetric and antisymmetric Lamb modes are derived. Then power flow rate through a cross section due to the waves is derived. The rate of power flow into the system by the applied load is calculated and compared with the power carried by the Lamb waves propagating away from the source.

Figure (2.1) shows the plane strain model of the plate that is analyzed. The x axis is positive to the right and the z axis positive upwards.

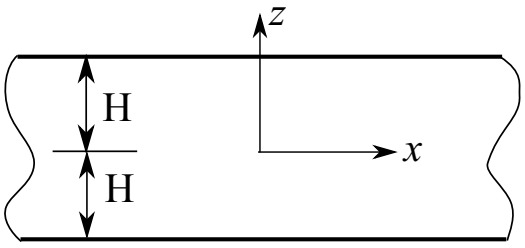

Figure 2.1: Plane strain model of plate

The analysis is done in the frequency-wavenumber domain, by taking double Fourier transforms of the field variables with respect to time (t) and the direction

of propagation of the wave (x). The original field variables $f(x,z,t)$ are transformed into frequency domain to $F(x,z,\omega)$ by taking the Fourier transform with respect to time (t) and then further transformed to $\overline{F}(k,z,\omega)$ according to

$$F(x,z,\omega) = \int_{-\infty}^{\infty} f(x,z,t)\, e^{i\omega t}\, dt \tag{2.1}$$

$$\overline{F}(k,z,\omega) = \int_{-\infty}^{\infty} F(x,z,\omega)\, e^{-ikx}\, dx \tag{2.2}$$

where ω is the circular frequency and k is the wavenumber. The original variables are obtained by taking the inverse Fourier transforms according to

$$f(x,z,t) = \frac{1}{4\pi^2} \int_{-\infty}^{\infty} \int_{-\infty}^{\infty} \overline{F}(k,z,\omega)\, e^{i(kx-\omega t)}\, dk\, d\omega \tag{2.3}$$

The analysis is done in the frequency domain that is on the integrand of Eq.(2.3) for the field variables, shown as follows

$$u(x,z,t) = \overline{U}(k,z,\omega)\, e^{i(kx-\omega t)} \tag{2.4}$$

$$w(x,z,t) = \overline{W}(k,z,\omega)\, e^{i(kx-\omega t)} \tag{2.5}$$

$$\sigma_{xx}(x,z,t) = \overline{S}_{xx}(k,z,\omega)\, e^{i(kx-\omega t)} \tag{2.6}$$

$$\sigma_{zz}(x,z,t) = \overline{S}_{zz}(k,z,\omega)\, e^{i(kx-\omega t)} \tag{2.7}$$

$$\sigma_{xz}(x,z,t) = \overline{S}_{xz}(k,z,\omega)\, e^{i(kx-\omega t)} \tag{2.8}$$

where, $u(x,z,t)$ and $w(x,z,t)$ are the displacements along the x and z directions respectively, and $\sigma_{xx}(x,z,t)$, $\sigma_{zz}(x,z,t)$ are the normal stresses along the x and z directions respectively and $\sigma_{xz}(x,z,t)$ is the shear stress.

Hooke's Law for an isotropic material for 2D plane strain in the xz plane is given

by

$$\sigma_{xx} = \lambda\left(\epsilon_{xx} + \epsilon_{zz}\right) + 2\mu\epsilon_{xx} \tag{2.9}$$

$$\sigma_{zz} = \lambda\left(\epsilon_{xx} + \epsilon_{zz}\right) + 2\mu\epsilon_{zz} \tag{2.10}$$

$$\sigma_{xz} = \mu\gamma_{xz} \tag{2.11}$$

where $\epsilon_{xx}, \epsilon_{zz}$ are the normal strains in the x and the z directions respectively and γ_{xz} is the shear strain. λ and μ are Lamé constants. μ is the shear modulus of the material.

Using the strain displacement kinematic relations

$$\epsilon_{xx} = \frac{\partial u}{\partial x}, \qquad \epsilon_{zz} = \frac{\partial w}{\partial z} \qquad \text{and} \qquad \gamma_{xz} = \frac{\partial u}{\partial z} + \frac{\partial w}{\partial x} \tag{2.12}$$

the stresses can be expressed in terms of displacement components as

$$\begin{aligned}
\sigma_{xx} &= \left(\lambda + 2\mu\right)\frac{\partial u}{\partial x} + \lambda\frac{\partial w}{\partial z} \\
&= \rho c_1^2 \frac{\partial u}{\partial x} + \rho\left(c_1^2 - 2c_2^2\right)\frac{\partial w}{\partial z}
\end{aligned}$$

$$\begin{aligned}
\sigma_{zz} &= \lambda\frac{\partial u}{\partial x} + \left(\lambda + 2\mu\right)\frac{\partial w}{\partial z} \\
&= \rho\left(c_1^2 - 2c_2^2\right)\frac{\partial u}{\partial x} + \rho c_1^2\frac{\partial w}{\partial z}
\end{aligned} \tag{2.13}$$

$$\begin{aligned}
\sigma_{xz} &= \mu\left(\frac{\partial u}{\partial z} + \frac{\partial w}{\partial x}\right) \\
&= \rho c_2^2\left(\frac{\partial u}{\partial z} + \frac{\partial w}{\partial x}\right)
\end{aligned}$$

where ρ is the density of the material and c_1 and c_2 are the longitudinal and shear wave speeds respectively and given by

$$c_1 = \sqrt{\frac{\lambda + 2\mu}{\rho}}, \qquad c_2 = \sqrt{\frac{\mu}{\rho}} \tag{2.14}$$

Using the relations from Equations (2.4,2.5) into Equation (2.13), the stresses are expressed as

$$\sigma_{xx} = \rho \left[c_1^2 ik\overline{U} + \left(c_1^2 - 2c_2^2\right) \frac{\partial \overline{W}}{\partial z} \right] e^{i(kx-\omega t)} \tag{2.15}$$

$$\sigma_{zz} = \rho \left[\left(c_1^2 - 2c_2^2\right) ik\overline{U} + c_1^2 \frac{\partial \overline{W}}{\partial z} \right] e^{i(kx-\omega t)} \tag{2.16}$$

$$\sigma_{xz} = \rho c_2^2 \left[ik\overline{W} + \frac{\partial \overline{U}}{\partial z} \right] e^{i(kx-\omega t)} \tag{2.17}$$

The stress equations of motion in absence of body forces are given by

$$\text{In } x \text{ direction} \qquad \frac{\partial \sigma_{xx}}{\partial x} + \frac{\partial \sigma_{xz}}{\partial z} = \rho \frac{\partial^2 u}{\partial t^2} \tag{2.18}$$

$$\text{In } z \text{ direction} \qquad \frac{\partial \sigma_{xz}}{\partial x} + \frac{\partial \sigma_{zz}}{\partial z} = \rho \frac{\partial^2 w}{\partial t^2} \tag{2.19}$$

Taking the derivatives of the stresses from Equations(2.15-2.17) and substituting them in the equations of motion give

$$\text{In } x \text{ direction} \qquad -c_1^2 k^2 \overline{U} + c_2^2 \frac{\partial^2 \overline{U}}{\partial z^2} + \omega^2 \overline{U} + \left(c_1^2 - c_2^2\right) ik \frac{\partial \overline{W}}{\partial z} = 0 \tag{2.20}$$

$$\text{In } z \text{ direction} \qquad \left(c_1^2 - c_2^2\right) ik \frac{\partial \overline{U}}{\partial z} - c_2^2 k^2 \overline{W} + c_1^2 \frac{\partial^2 \overline{W}}{\partial z^2} + \rho\omega^2 \overline{W} = 0 \tag{2.21}$$

Assuming,

$$\overline{U}\left(k, z, \omega\right) = A\left(k, \omega\right) e^{-\xi z} \tag{2.22}$$

$$\overline{W}\left(k, z, \omega\right) = B\left(k, \omega\right) e^{-\xi z} \tag{2.23}$$

where $A\left(k, \omega\right)$ and $B\left(k, \omega\right)$ are unknown functions and ξ is the unknown parameter describing the z-dependency of $\overline{U}, \overline{W}$.

Substituting Equations (2.22, 2.23) into Equations (2.20, 2.21), the following pair of homogeneous equations are obtained

$$\begin{bmatrix} -c_1^2 k^2 + c_2^2 \xi^2 + \omega^2 & -\left(c_1^2 - c_2^2\right) ik\xi \\ -\left(c_1^2 - c_2^2\right) ik\xi & -c_2^2 k^2 + c_1^2 \xi^2 + \omega^2 \end{bmatrix} \begin{Bmatrix} A\left(k, \omega\right) \\ B\left(k, \omega\right) \end{Bmatrix} = \begin{Bmatrix} 0 \\ 0 \end{Bmatrix} \tag{2.24}$$

For non trivial solution of Equation(2.24), the determinant of the coefficient matrix is set equal to zero, leading to the following fourth order algebraic equation for ξ

$$c_1^2c_2^2\xi^4+\xi^2\left[\omega^2\left(c_1^2+c_2^2\right)-2c_1^2c_2^2k^2\right]+c_1^2c_2^2k^4-\omega^2k^2\left(c_1^2+c_2^2\right)+\omega^4=0 \tag{2.25}$$

which is a quadratic equation in ξ^2. Solving the equation gives the unknown parameter ξ as follows

$$\xi_1=\sqrt{k^2-\frac{\omega^2}{c_1^2}}=\sqrt{k^2-k_1^2}=\eta_1 \tag{2.26}$$

$$\xi_2=-\left(\sqrt{k^2-\frac{\omega^2}{c_1^2}}\right)=-\sqrt{k^2-k_1^2}=-\eta_1 \tag{2.27}$$

$$\xi_3=\sqrt{k^2-\frac{\omega^2}{c_2^2}}=\sqrt{k^2-k_2^2}=\eta_2 \tag{2.28}$$

$$\xi_4=-\left(\sqrt{k^2-\frac{\omega^2}{c_2^2}}\right)=-\sqrt{k^2-k_2^2}=-\eta_2 \tag{2.29}$$

From Equation (2.24), the unknown functions $A\left(k,\omega\right)$ and $B\left(k,\omega\right)$ are related as

$$B\left(k,\omega\right)=\frac{-c_1^2k^2+c_2^2\xi^2+\omega^2}{\left(c_1^2-c_2^2\right)ik\xi}A\left(k,\omega\right)=\alpha A\left(k,\omega\right) \tag{2.30}$$

where the four values of α corresponding to the four values of ξ are given by

$$\alpha_1=\frac{-c_1^2k^2+c_2^2\eta_1^2+\omega^2}{\left(c_1^2-c_2^2\right)ik\eta_1}=\frac{i\eta_1}{k} \tag{2.31}$$

$$\alpha_2=-\frac{i\eta_1}{k}=-\alpha_1 \tag{2.32}$$

$$\alpha_3=\frac{-c_1^2k^2+c_2^2\eta_2^2+\omega^2}{\left(c_1^2-c_2^2\right)ik\eta_2}=\frac{ik}{\eta_2} \tag{2.33}$$

$$\alpha_4=-\frac{ik}{\eta_2}=-\alpha_3 \tag{2.34}$$

Substituting the values of α from Equations (2.31-2.34) into Equation (2.30),

$$B_1(k,\omega) = \alpha_1 A_1(k,\omega) = \frac{i\eta_1}{k} A_1(k,\omega) \tag{2.35}$$

$$B_2(k,\omega) = -\alpha_1 A_2(k,\omega) = -\frac{i\eta_1}{k} A_1(k,\omega) \tag{2.36}$$

$$B_3(k,\omega) = \alpha_3 A_3(k,\omega) = \frac{ik}{\eta_2} A_3(k,\omega) \tag{2.37}$$

$$B_4(k,\omega) = -\alpha_3 A_4(k,\omega) = -\frac{ik}{\eta_2} A_4(k,\omega) \tag{2.38}$$

Substituting Equations (2.26-2.29, 2.35-2.38) in Equations (2.22,2.23) for the displacements

$$\begin{aligned} \overline{U}(k,z,\omega) = {} & A_1(k,\omega)\, e^{-\eta_1 z} + A_2(k,\omega)\, e^{\eta_1 z} \\ & + A_3(k,\omega)\, e^{-\eta_2 z} + A_4(k,\omega)\, e^{\eta_2 z} \end{aligned} \tag{2.39}$$

$$\begin{aligned} \overline{W}(k,z,\omega) = {} & \frac{i\eta_1}{k} A_1(k,\omega)\, e^{-\eta_1 z} - \frac{i\eta_1}{k} A_2(k,\omega)\, e^{\eta_1 z} \\ & + \frac{ik}{\eta_2} A_3(k,\omega)\, e^{-\eta_2 z} - \frac{ik}{\eta_2} A_4(k,\omega)\, e^{\eta_2 z} \end{aligned} \tag{2.40}$$

Using the relations between exponential and hyperbolic sine and cosine,

$$e^{\eta z} = \cosh(\eta z) + \sinh(\eta z) \qquad e^{-\eta z} = \cosh(\eta z) - \sinh(\eta z)$$

the displacements and stresses in the frequency-wavenumber domain can be written as

$$\begin{aligned} \overline{U}(k,z,\omega) = {} & \overline{A}_1 \cosh(\eta_1 z) + \overline{A}_2 \sinh(\eta_1 z) \\ & + \overline{A}_3 \cosh(\eta_2 z) + \overline{A}_4 \sinh(\eta_2 z) \end{aligned} \tag{2.41}$$

$$\begin{aligned} \overline{W}(k,z,\omega) = {} & -\frac{i\eta_1}{k} \overline{A}_1 \sinh(\eta_1 z) - \frac{i\eta_1}{k} \overline{A}_2 \cosh(\eta_1 z) \\ & - \frac{ik}{\eta_2} \overline{A}_3 \sinh(\eta_2 z) - \frac{ik}{\eta_2} \overline{A}_4 \cosh(\eta_2 z) \end{aligned} \tag{2.42}$$

$$\begin{aligned} \overline{S}_{xx}(k,z,\omega) = \frac{i\mu}{k} \Big[& \left(k_2^2 + 2\eta_1^2\right) \left(\overline{A}_1 \cosh(\eta_1 z) + \overline{A}_2 \sinh(\eta_1 z)\right) \\ & + 2k^2 \left(\overline{A}_3 \cosh(\eta_2 z) + \overline{A}_4 \sinh(\eta_2 z)\right) \Big] \end{aligned} \tag{2.43}$$

$$\overline{S}_{zz}(k,z,\omega) = -\frac{i\mu}{k}\Big[\left(2k^2-k_2^2\right)\left(\overline{A}_1\cosh(\eta_1 z)+\overline{A}_2\sinh(\eta_1 z)\right) + 2k^2\left(\overline{A}_3\cosh(\eta_2 z)+\overline{A}_4\sinh(\eta_2 z)\right)\Big] \tag{2.44}$$

$$\overline{S}_{xz}(k,z,\omega) = \frac{\mu}{\eta_2}\Big[2\eta_1\eta_2\left(\overline{A}_1\sinh(\eta_1 z)+\overline{A}_2\cosh(\eta_1 z)\right) + \left(2k^2-k_2^2\right)\left(\overline{A}_3\sinh(\eta_2 z)+\overline{A}_4\cosh(\eta_2 z)\right)\Big] \tag{2.45}$$

where

$$\overline{A}_1 = A_1(k,\omega)+A_2(k,\omega) \qquad \overline{A}_2 = A_2(k,\omega)-A_1(k,\omega) \tag{2.46}$$

$$\overline{A}_3 = A_3(k,\omega)+A_4(k,\omega) \qquad \overline{A}_4 = A_4(k,\omega)-A_3(k,\omega) \tag{2.47}$$

2.1 Lamb wave dispersion relations

Next, the traction free boundary conditions are applied on the top ($z = H$) and bottom ($z = -H$) faces of the plate.

At $z = H$, zero normal stress gives,

$$\begin{aligned}\overline{S}_{zz}(k,H,\omega) &= \left(2k^2-k_2^2\right)\left(\overline{A}_1\cosh(\eta_1 H)+\overline{A}_2\sinh(\eta_1 H)\right)\\ &\quad + 2k^2\left(\overline{A}_3\cosh(\eta_2 H)+\overline{A}_4\sinh(\eta_2 H)\right)\\ &= 0\end{aligned} \tag{2.48}$$

At $z = -H$, zero normal stress gives,

$$\begin{aligned}\overline{S}_{zz}(k,-H,\omega) &= \left(2k^2-k_2^2\right)\left(\overline{A}_1\cosh(\eta_1 H)-\overline{A}_2\sinh(\eta_1 H)\right)\\ &\quad + 2k^2\left(\overline{A}_3\cosh(\eta_2 H)-\overline{A}_4\sinh(\eta_2 H)\right)\\ &= 0\end{aligned} \tag{2.49}$$

From Equations (2.48, 2.49)

$$\begin{aligned}&\left[\left(2k^2-k_2^2\right)\overline{A}_1\cosh(\eta_1 H)+2k^2\overline{A}_3\cosh(\eta_2 H)\right]\pm\\ &\left[\left(2k^2-k_2^2\right)\overline{A}_2\sinh(\eta_1 H)+2k^2\overline{A}_4\sinh(\eta_2 H)\right]=0\end{aligned} \tag{2.50}$$

At $z = H$, zero shear stress gives,

$$\begin{aligned}\overline{S}_{xz}(k, H, \omega) &= 2\eta_1\eta_2\left(\overline{A}_1 \sinh(\eta_1 H) + \overline{A}_2 \cosh(\eta_1 H)\right) \\ &+ \left(2k^2 - k_2^2\right)\left(\overline{A}_3 \sinh(\eta_2 H) + \overline{A}_4 \cosh(\eta_2 H)\right) \\ &= 0\end{aligned} \tag{2.51}$$

At $z = -H$, zero shear stress gives,

$$\begin{aligned}\overline{S}_{xz}(k, -H, \omega) &= 2\eta_1\eta_2\left(-\overline{A}_1 \sinh(\eta_1 H) + \overline{A}_2 \cosh(\eta_1 H)\right) \\ &+ \left(2k^2 - k_2^2\right)\left(-\overline{A}_3 \sinh(\eta_2 H) + \overline{A}_4 \cosh(\eta_2 H)\right) \\ &= 0\end{aligned} \tag{2.52}$$

From Equations (2.51, 2.52),

$$\begin{aligned}&\left[2\eta_1\eta_2\overline{A}_2 \cosh(\eta_1 H) + \left(2k^2 - k_2^2\right)\overline{A}_4 \cosh(\eta_2 H)\right] \pm \\ &\left[2\eta_1\eta_2\overline{A}_1 \sinh(\eta_1 H) + \left(2k^2 - k_2^2\right)\overline{A}_3 \sinh(\eta_2 H)\right] = 0\end{aligned} \tag{2.53}$$

From Equations (2.50,2.53), it is seen that $\overline{A}_1, \overline{A}_3$ are independent of $\overline{A}_2, \overline{A}_4$. Hence two independent motions of the plate can be obtained by setting $\overline{A}_1 = \overline{A}_3 = 0$ and then $\overline{A}_2 = \overline{A}_4 = 0$.

First setting $\overline{A}_2 = \overline{A}_4 = 0$ in Equations (2.50,2.53), the motion governed by $\overline{A}_1, \overline{A}_3$ is derived. $\overline{A}_1, \overline{A}_3$ satisfy

$$\begin{bmatrix} (2k^2 - k_2^2)\cosh(\eta_1 H) & 2k^2 \cosh(\eta_2 H) \\ 2\eta_1\eta_2 \sinh(\eta_1 H) & (2k^2 - k_2^2)\sinh(\eta_2 H) \end{bmatrix} \begin{Bmatrix} \overline{A}_1 \\ \overline{A}_3 \end{Bmatrix} = \begin{Bmatrix} 0 \\ 0 \end{Bmatrix} \tag{2.54}$$

For nontrivial solution of $\overline{A}_1, \overline{A}_3$, the determinant of the coefficient matrix in Equation (2.54) needs to be zero, which gives the dispersion relation for the symmetric Lamb waves in the plate.

$$\left(2k^2 - k_2^2\right)^2 \cosh(\eta_1 H)\sinh(\eta_2 H) - 4k^2\eta_1\eta_2 \sinh(\eta_1 H)\cosh(\eta_2 H) = 0 \tag{2.55}$$

The displacements and stresses in the plate for the symmetric Lamb wave, governed by the coefficients $\overline{A}_1, \overline{A}_3$ are given in the frequency domain by

$$\overline{U}(k,z,\omega) = \overline{A}_1 \cosh(\eta_1 z) + \overline{A}_3 \cosh(\eta_2 z) \tag{2.56}$$

$$\overline{W}(k,z,\omega) = -\frac{i\eta_1}{k}\overline{A}_1 \sinh(\eta_1 z) - \frac{ik}{\eta_2}\overline{A}_3 \sinh(\eta_2 z) \tag{2.57}$$

$$\overline{S}_{xx}(k,z,\omega) = \frac{i\mu}{k}\left[\left(k_2^2 + 2\eta_1^2\right)\overline{A}_1 \cosh(\eta_1 z) + 2k^2\overline{A}_3 \cosh(\eta_2 z)\right] \tag{2.58}$$

$$\overline{S}_{zz}(k,z,\omega) = -\frac{i\mu}{k}\left[\left(2k^2 - k_2^2\right)\overline{A}_1 \cosh(\eta_1 z) + 2k^2\overline{A}_3 \cosh(\eta_2 z)\right] \tag{2.59}$$

$$\overline{S}_{xz}(k,z,\omega) = \frac{\mu}{\eta_2}\left[2\eta_1\eta_2\overline{A}_1 \sinh(\eta_1 z) + \left(2k^2 - k_2^2\right)\overline{A}_3 \sinh(\eta_2 z)\right] \tag{2.60}$$

Similarly, by setting $\overline{A}_1 = \overline{A}_3 = 0$ in Equations (2.50, 2.53), the motion governed by $\overline{A}_2$, $\overline{A}_4$ is derived. $\overline{A}_2$, $\overline{A}_4$ satisfy

$$\begin{bmatrix} (2k^2 - k_2^2)\sinh(\eta_1 H) & 2k^2 \sinh(\eta_2 H) \\ 2\eta_1\eta_2 \cosh(\eta_1 H) & (2k^2 - k_2^2)\cosh(\eta_2 H) \end{bmatrix} \begin{Bmatrix} \overline{A}_2 \\ \overline{A}_4 \end{Bmatrix} = \begin{Bmatrix} 0 \\ 0 \end{Bmatrix} \tag{2.61}$$

For nontrivial solution of $\overline{A}_2, \overline{A}_4$, the determinant of the coefficient matrix in Equation (2.61) needs to be zero, which gives the dispersion relation for the antisymmetric Lamb waves in the plate.

$$\left(2k^2 - k_2^2\right)^2 \sinh(\eta_1 H)\cosh(\eta_2 H) - 4k^2\eta_1\eta_2 \cosh(\eta_1 H)\sinh(\eta_2 H) = 0 \tag{2.62}$$

The displacements and stresses in the plate due the antisymmetric Lamb wave, governed by the coefficients $\overline{A}_2, \overline{A}_4$ are given in the frequency domain by

$$\overline{U}(k,z,\omega) = \overline{A}_2 \sinh(\eta_1 z) + \overline{A}_4 \sinh(\eta_2 z) \tag{2.63}$$

$$\overline{W}\left(k,z,\omega\right)=-\frac{i\eta_1}{k}\overline{A}_2\cosh\left(\eta_1 z\right)-\frac{ik}{\eta_2}\overline{A}_4\cosh\left(\eta_2 z\right) \tag{2.64}$$

$$\overline{S}_{xx}\left(k,z,\omega\right)=\frac{i\mu}{k}\left[\left(k_2^2+2\eta_1^2\right)\overline{A}_2\sinh\left(\eta_1 z\right)+2k^2\overline{A}_4\sinh\left(\eta_2 z\right)\right] \tag{2.65}$$

$$\overline{S}_{zz}\left(k,z,\omega\right)=-\frac{i\mu}{k}\left[\left(2k^2-k_2^2\right)\overline{A}_2\sinh\left(\eta_1 z\right)+2k^2\overline{A}_4\sinh\left(\eta_2 z\right)\right] \tag{2.66}$$

$$\overline{S}_{xz}\left(k,z,\omega\right)=\frac{\mu}{\eta_2}\left[2\eta_1\eta_2\overline{A}_2\cosh\left(\eta_1 z\right)+\left(2k^2-k_2^2\right)\overline{A}_4\cosh\left(\eta_2 z\right)\right] \tag{2.67}$$

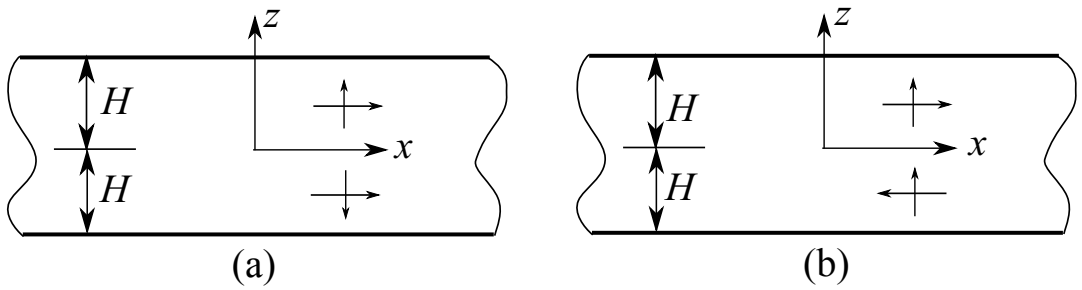

Figure 2.2: (a) Symmetric and (b) Antisymmetric Lamb waves in a plate

Figure (2.2) shows the two independent symmetric and antisymmetric Lamb wave modes propagating in a plate indicating the symmetric and antisymmetric nature of the horizontal and vertical displacements associated with them.

The graphical solutions of Equations (2.55 and 2.62) for the phase velocity c, which is generally a function of frequency, are called the dispersion curves. Figure (2.3) shows the dispersion curves for the symmetric and the antisymmetric modes of Lamb waves propagating in an aluminum plate of thickness 3.175 mm ($\frac{1}{8}''$). The plate has a Young's modulus $E = 69\,\text{MPa}$ and Poisson's ratio $\nu = 0.3269$.

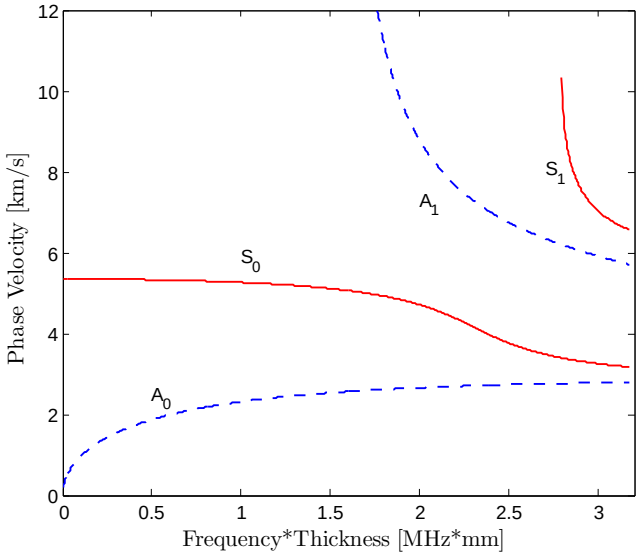

Figure 2.3: Dispersion curves for the phase velocity for an aluminum plate. Symmetric modes are shown as solid lines, antisymmetric as dashed lines

2.2 Cutoff frequencies for higher order symmetric and antisymmetric Lamb wave modes

To determine the cutoff frequencies at which higher order Lamb wave modes start propagating in the plate, the corresponding dispersion equation is solved for the limiting value of the wavenumber k tending to zero, since at the cutoff frequencies the wave speeds of the higher order modes become infinite.

Substituting $k = 0$ in the dispersion relation for symmetric Lamb waves, Equation (2.55) becomes

$$\cosh(\eta_1 H)\sinh(\eta_2 H) = 0 \tag{2.68}$$

For $k = 0$, $\eta_1 H, \eta_2 H, \cosh(\eta_1 H), \sinh(\eta_1 H)$ become

$$\eta_1 H = \sqrt{k^2 - k_1^2} H = i k_1 H \tag{2.69}$$

$$\eta_2 H = \sqrt{k^2 - k_2^2} H = i k_2 H \tag{2.70}$$

$$\cosh(\eta_1 H) = \cosh(i k_1 H) = \cos(k_1 H) \tag{2.71}$$

$$\sinh(\eta_2 H) = \sinh(i k_2 H) = i \sin(k_2 H) \tag{2.72}$$

Substituting Equations (2.69-2.72) in Equation (2.68)

$$\cos(k_1 H) \sin(k_2 H) = 0 \tag{2.73}$$

For, $\cos(k_1 H) = 0$,

$$k_1 H = \left(n - \frac{1}{2}\right)\pi \qquad n = 1, 2, 3, \ldots \tag{2.74}$$

Hence,

$$\frac{2\pi f H}{c_1} = \left(n - \frac{1}{2}\right)\pi \tag{2.75}$$

where, f is the frequency in Hz and c_1 is the longitudinal wave speed. Therefore, the cutoff frequencies for higher order symmetric Lamb wave modes are

$$f = \frac{\left(n - \frac{1}{2}\right)}{2H} c_1 \qquad n = 1, 2, 3, \ldots \tag{2.76}$$

For $\sin(k_2 H) = 0$,

$$k_2 H = n\pi \qquad n = 1, 2, 3, \ldots \tag{2.77}$$

Hence,

$$\frac{2\pi f H}{c_2} = n\pi \tag{2.78}$$

where, f is the frequency in Hz and c_2 is the shear wave speed. Therefore, the cutoff frequencies for higher order symmetric Lamb wave modes are also given by

$$f = \frac{n c_2}{2H} \qquad n = 1, 2, 3, \ldots \tag{2.79}$$

Similarly by substituting $k = 0$ in the dispersion relation for antisymmetric Lamb waves, Equation (2.62) becomes

$$\sinh(\eta_1 H)\cosh(\eta_2 H) = 0 \tag{2.80}$$

For $k = 0$, $\sinh(\eta_1 H), \cosh(\eta_1 H)$ become

$$\sinh(\eta_1 H) = \sinh(ik_1 H) = i\sin(k_1 H) \tag{2.81}$$

$$\cosh(\eta_2 H) = \cosh(ik_2 H) = \cos(k_2 H) \tag{2.82}$$

Substituting Equations (2.69,2.70,2.81,2.82) in Equation (2.80)

$$\sin(k_1 H)\cos(k_2 H) = 0 \tag{2.83}$$

For $\sin(k_1 H) = 0$, the cutoff frequencies for higher order antisymmetric Lamb wave modes are given by

$$f = \frac{nc_1}{2H} \qquad n = 1, 2, 3, \ldots \tag{2.84}$$

For $\cos(k_2 H) = 0$, the cutoff frequencies for higher order antisymmetric Lamb wave modes are are also given by

$$f = \frac{\left(n - \frac{1}{2}\right)}{2H} c_2 \qquad n = 1, 2, 3, \ldots \tag{2.85}$$

2.3 Wave propagation in isotropic plates - Experiments and Results

The general experimental setup for ultrasonic testing is shown in Figure (2.4). Broadband transducers (Digital Wave B225 and B1025) with a fairly flat response in the range of 50 kHz to 600 kHz are placed on the surface of the specimen with the aid of a Plexiglas face sheet, which incorporates an array of holes drilled with an accuracy of 0.1 mm and the diameter of the holes equal to that of the

transducers. The Plexiglas sheet is placed on the surface of the specimen with masking tapes and guarantees identical transducer locations in repeating experiments. Thus only two transducers are needed to obtain data from an array with prescribed positions. The transmission of ultrasound is aided by the application of an ultrasonic gel couplant (Sonotech) between the transducers and the specimen. A 5 cycle sinusoidal tone burst enclosed in a Hann window (also called Hanning window) is generated by an arbitrary waveform generator (NI 5402) and applied to one of the piezoelectric transducers. The sinusoidal tone burst voltage can be expressed as

$$V(t) = \frac{1}{2}\left[1 - \cos\left(\frac{2\pi f t}{n_p}\right)\right]\sin(2\pi f t) \tag{2.86}$$

where f is the central frequency and $n_p = 5$. A four channel signal conditioner (Digital Wave FM-1) is used to boost and filter the received signals in all experiments. The ultrasonic signal is digitized and recorded in a four-channel digital oscilloscope (Agilent 54624A) with up to 200 MHz sampling rate. In order to determine the velocities of the waves, the signals are recorded at various distances x from the source. The test region is thereby located at a sufficient distance away from the edges of the plate structure to avoid superposition with reflected waves from the edges.

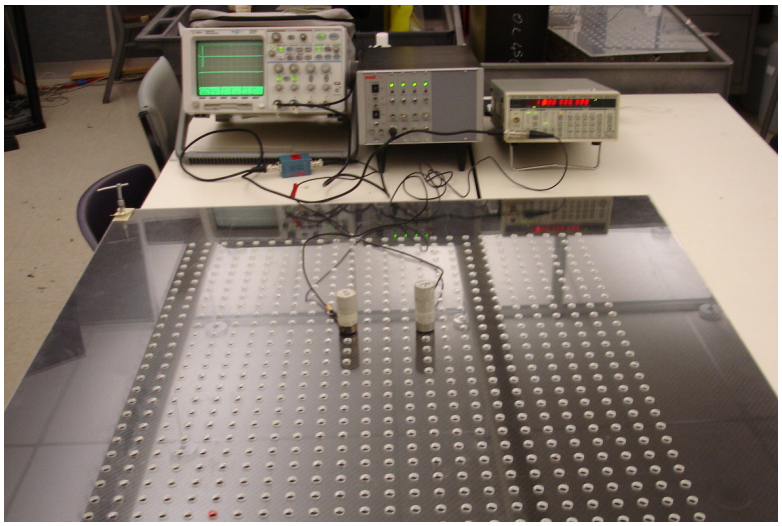

Figure 2.4: The ultrasonic experimental setup including oscilloscope, signal conditioner, signal generator, transducers and Plexiglas face sheet on top of aluminum plate.

Since Lamb waves are dispersive, a direct time-of-flight analysis of the recorded signals to calculate the velocity of the waves would incorporate significant errors. Therefore, the dispersive signals are analyzed using either the short time Fourier transform (STFT) or wavelet transform [38]. In the later case, the digital signals are processed using the AGU-Vallen Wavelet program, allowing a particular frequency component to be tracked in time to obtain its corresponding velocity. The STFT is applied and evaluated in Matlab using the built-in function "spectogram".

In order to verify the velocities of the waves experimentally, measurements are conducted as described above. Specifically, measurements are taken with a distance between actuator and sensor in the range of 7.62 cm to 22.86 cm (3 in. to 9 in.). Due to several limitations in the experimental setup (mostly the transducers), the experimentally analyzed frequency range is 350 kHz to 500 kHz for the S_0 wave and 50 kHz to 250 kHz for the A_0 wave. Figure (2.5) shows typical signals obtained at some of the receiver locations and corresponding STFT plots. It can be seen that in both cases, mostly one type of wave is excited with the laboratory

setup at hand. Nevertheless, the STFT of the signals is only evaluated in the highlighted time intervals to avoid false evaluation of other propagating waves in the signal.

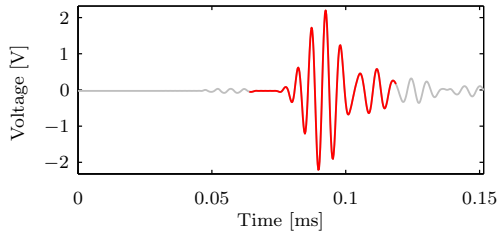

(a) Time signal for $f = 200\,\text{kHz}$ and $\Delta x = 9\,\text{in}$

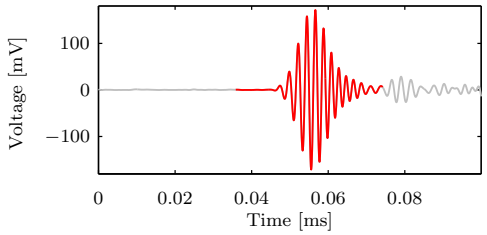

(b) Time signal for $f = 460\,\text{kHz}$ and $\Delta x = 9\,\text{in}$

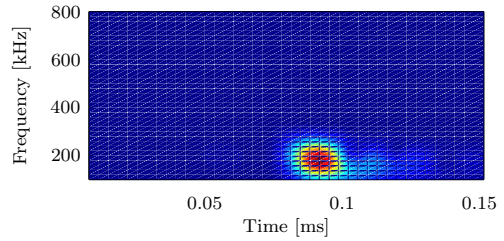

(c) STFT plot for $f = 200\,\text{kHz}$ and $\Delta x = 9\,\text{in}$

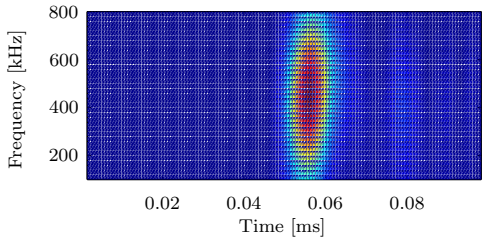

(d) STFT plot for $f = 460\,\text{kHz}$ and $\Delta x = 9\,\text{in}$

Figure 2.5: Time signals and corresponding STFT plots recorded with pitch-catch system at an aluminum plate. STFT is only evaluated in highlighted time interval to avoid false evaluation of other propagating waves in the signal.

The group velocity $c_g = \frac{c}{1-\frac{\omega}{c}\frac{dc}{d\omega}}$ of a wave is the velocity at which energy is transported by the wave and is the velocity obtained in the above experiment. The group velocities are determined by evaluating the center frequency of the excited wave in the STFT datasets. Through a time-of-flight analysis for different distances between actuators and sensors, the velocities are determined from $c_g = \frac{\Delta x}{\Delta t}$ and are represented by the symbol $\times$ in Figure (2.6). It is seen that the experimental results are very close to analytical results. Hence, the pitch-catch system is generally suitable for precise NDE and SHM studies. Experimental investigations of higher order modes are not considered since typically low order modes are used

in NDE systems.

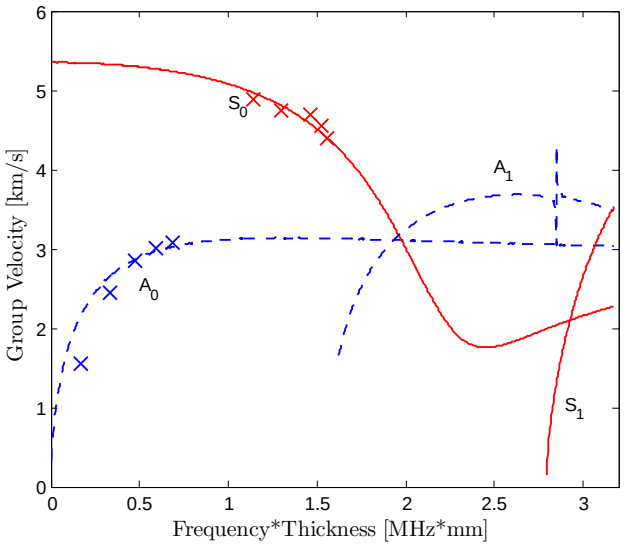

Figure 2.6: Dispersion curves for the group velocity for an aluminum plate. Symmetric modes are shown as solid lines, antisymmetric as dashed lines. Experimental results are marked by $\times$.

2.4 Propagation of Lamb waves in plate for various dynamic surface loads

In this section, the propagation of Lamb waves, under various surface loads are analyzed. The physical problem, with loading applied on the top surface of the plate ($z = H$) is resolved into a corresponding symmetric and an antisymmetric problem, in accordance with the results derived in the last section, (see Figure (2.7)). The applied time-dependent load with intensity p_0 is resolved into the antisymmetric and symmetric loading of intensity $\frac{p_0}{2}$ applied on the top and bottom ($z = -H$) surfaces of the plate. The sum of the values of the different field variables, for the symmetric and the antisymmetric models, give the total field.

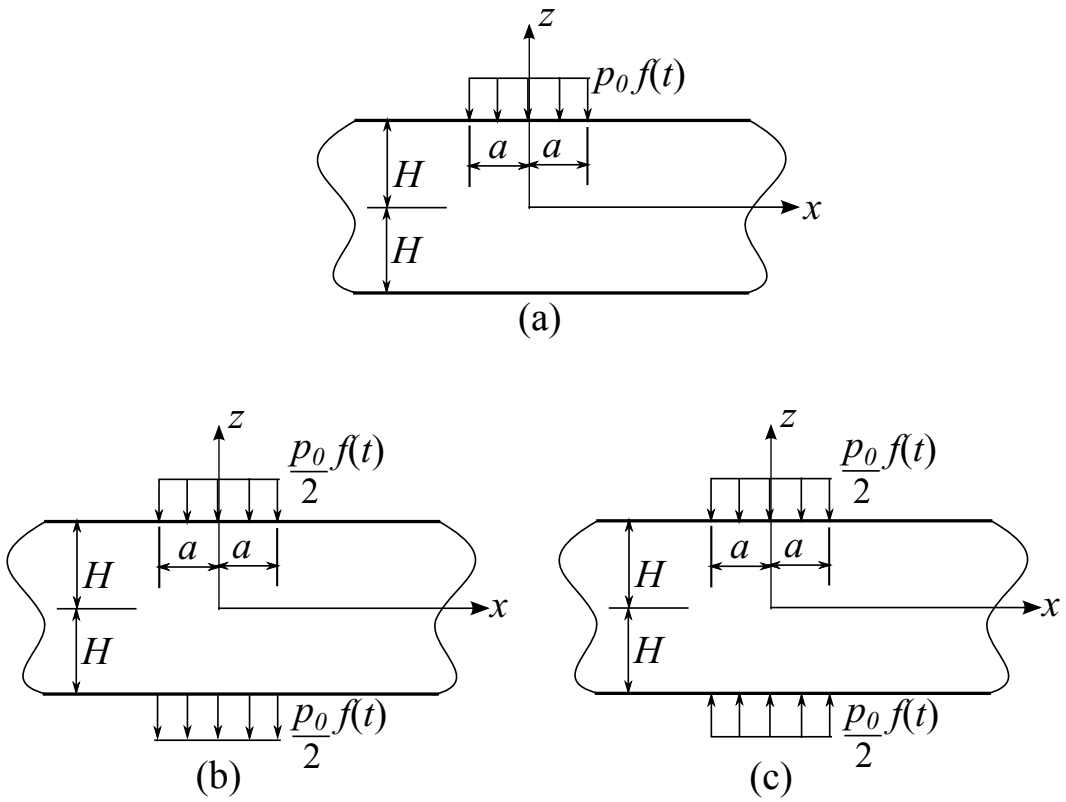

Figure 2.7: (a) Applied loading (b) Antisymmetric loading component and (c) Symmetric loading component in a plate

Like the field variables, the time dependent load $p(x,t)$ is transformed into $P_0(x,\omega)$ in the frequency domain by applying Fourier transform with respect to time. It is then further transformed into $\overline{P}_0(k,\omega)$ by applying the Fourier transform with respect to x-direction. Next, the appropriate boundary conditions are applied.

2.5 Antisymmetric Lamb wave propagation under dynamic vertical load on the top surface of a plate

From Equations (2.66, 2.67), zero shear stress at $z = H$ gives,

$$\overline{S}_{xz}(k,H,\omega) = 2\eta_1\eta_2\overline{A}_2\cosh(\eta_1 H) + \left(2k^2 - k_2^2\right)\overline{A}_4\cosh(\eta_2 z) = 0 \qquad (2.87)$$

which gives,

$$\overline{A}_2 = -\frac{(2k^2 - k_2^2)\cosh(\eta_2 H)}{2\eta_1\eta_2\cosh(\eta_1 H)}\overline{A}_4 \tag{2.88}$$

At $z = H$, the applied normal load gives,

$$\overline{S}_{zz}(k, H, \omega) = -\frac{\overline{P}_0(k, \omega)}{2} \tag{2.89}$$

which gives,

$$\frac{i\mu}{k}\left[\left(2k^2 - k_2^2\right)\overline{A}_2\sinh(\eta_1 H) + 2k^2\overline{A}_4\sinh(\eta_2 H)\right] = \frac{\overline{P}_0}{2} \tag{2.90}$$

Substituting $\overline{A}_2$ from Equation (2.88) into Equation (2.90)

$$\overline{A}_4 = \frac{ik\eta_1\eta_2\cosh(\eta_1 H)}{\mu R_{\mathrm{a}}(k)}\overline{P}_0(k, \omega) \tag{2.91}$$

where, $R_{\mathrm{a}}(k)$ is the antisymmetric Lamb wave denominator and is given by

$$R_{\mathrm{a}}(k) = \left(2k^2 - k_2^2\right)^2\sinh(\eta_1 H)\cosh(\eta_2 H) - 4k^2\eta_1\eta_2\cosh(\eta_1 H)\sinh(\eta_2 H) \tag{2.92}$$

Substituting $\overline{A}_4$ from Equation (2.91) into Equation (2.88)

$$\overline{A}_2 = -\frac{ik(2k^2 - k_2^2)\cosh(\eta_2 H)}{2\mu R_{\mathrm{a}}(k)}\overline{P}_0(k, \omega) \tag{2.93}$$

Using the above values of $\overline{A}_2$ and $\overline{A}_4$, the displacements and the stresses in the plate due to the antisymmetric Lamb wave in the frequency domain are given by

$$\overline{U}(k, z, \omega) = -\frac{ik\overline{P}_0(k, \omega)}{2\mu R_{\mathrm{a}}(k)}\Big[\left(2k^2 - k_2^2\right)\sinh(\eta_1 z)\cosh(\eta_2 H) - 2\eta_1\eta_2\cosh(\eta_1 H)\sinh(\eta_2 z)\Big] \tag{2.94}$$

$$\overline{W}(k, z, \omega) = -\frac{\eta_1\overline{P}_0(k, \omega)}{2\mu R_{\mathrm{a}}(k)}\Big[\left(2k^2 - k_2^2\right)\cosh(\eta_1 z)\cosh(\eta_2 H) - 2k^2\cosh(\eta_1 H)\cosh(\eta_2 z)\Big] \tag{2.95}$$

$$\overline{S}_{xx}(k,z,\omega) = \frac{\overline{P}_0(k,\omega)}{2R_{\mathrm{a}}(k)}\Big[\left(k_2^2+2\eta_1^2\right)\left(2k^2-k_2^2\right)\sinh(\eta_1 z)\cosh(\eta_2 H) \\ -4k^2\eta_1\eta_2\cosh(\eta_1 H)\sinh(\eta_2 z)\Big] \tag{2.96}$$

$$\overline{S}_{zz}(k,z,\omega) = -\frac{\overline{P}_0(k,\omega)}{2R_{\mathrm{a}}(k)}\Big[\left(2k^2-k_2^2\right)^2\sinh(\eta_1 z)\cosh(\eta_2 H) \\ -4k^2\eta_1\eta_2\cosh(\eta_1 H)\sinh(\eta_2 z)\Big] \tag{2.97}$$

$$\overline{S}_{xz}(k,z,\omega) = -\frac{\left(2k^2-k_2^2\right)\eta_1 ik\overline{P}_0(k,\omega)}{R_{\mathrm{a}}(k)}\Big[\cosh(\eta_1 z)\cosh(\eta_2 H) \\ -\cosh(\eta_1 H)\cosh(\eta_2 z)\Big] \tag{2.98}$$

The inverse Fourier transform with respect to the wavenumber k

$$F(x,z,\omega) = \frac{1}{2\pi}\int_{-\infty}^{\infty}\overline{F}(k,z,\omega)\,e^{ikx}\,dk \tag{2.99}$$

gives the field variables in x and the frequency (ω) domain. The integral in Equation (2.99) has simple poles at the roots of the antisymmetric Lamb wave dispersion equation, obtained by equating $R_{\mathrm{a}}(k) = 0$.

Figure (2.8) shows a schematic of the roots in the complex k plane. There are real, imaginary and complex roots. The closed contour in the complex k plane with the anticlockwise direction it is traversed is indicated.

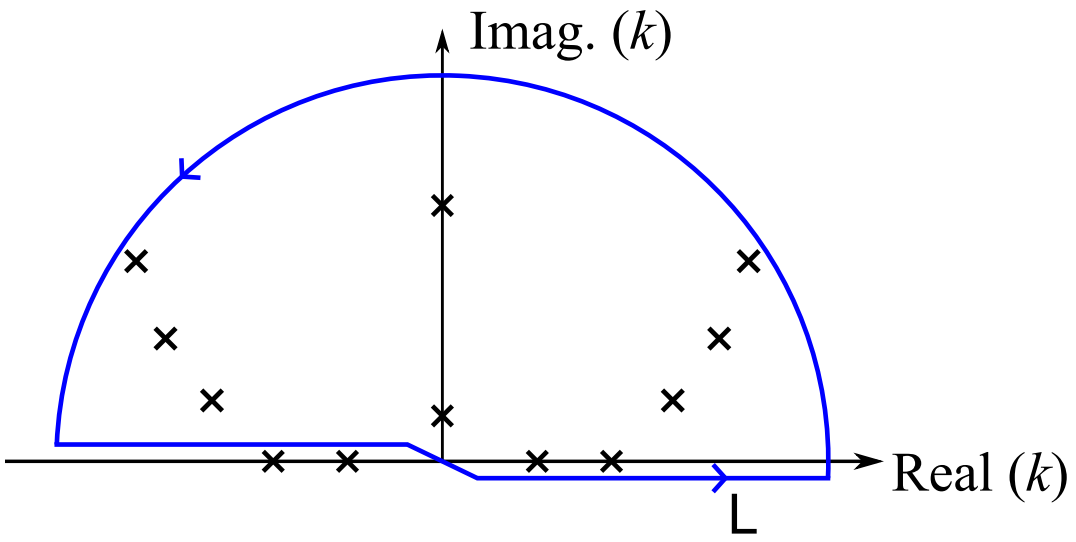

Figure 2.8: Closed contour in the upper half complex k plane enclosing positive real, imaginary and complex poles

To satisfy the radiation boundary condition at $x = \infty$, that is no incoming waves from infinity, the negative real poles are avoided in the contour. All real, imaginary and complex poles in the upper half complex k plane are enclosed in the contour. The field in Equation (2.99) is then given by

$$F(x,z,\omega) = \frac{1}{2\pi} 2\pi i \,(\text{Sum of the residues at the poles } k_{\mathrm{a}} \text{ of } \overline{F}(k,z,\omega)\, e^{ikx}) \tag{2.100}$$

where, $F(x,z,\omega)$ is the field variable due to antisymmetric Lamb waves. k_{a} are the roots of the antisymmetric Lamb wave dispersion equation. The displacements and the stresses can be written as

$$U(x,z,\omega) = \sum_{k_{\mathrm{a}}} \frac{k_{\mathrm{a}} \overline{P}_0(k_{\mathrm{a}},\omega)}{2\mu R'_{\mathrm{a}}(k_{\mathrm{a}})} \Big[\left(2k_{\mathrm{a}}^2 - k_2^2\right) \sinh(\eta_{1\mathrm{a}} z) \cosh(\eta_{2\mathrm{a}} H) - 2\eta_{1\mathrm{a}}\eta_{2\mathrm{a}} \cosh(\eta_{1\mathrm{a}} H) \sinh(\eta_{2\mathrm{a}} z) \Big] e^{ik_{\mathrm{a}} x} \tag{2.101}$$

$$W(x,z,\omega)=\sum_{k_{\mathrm{a}}}-i\frac{\eta_{1\mathrm{a}}\overline{P}_0(k_{\mathrm{a}},\omega)}{2\mu R'_{\mathrm{a}}(k_{\mathrm{a}})}\Big[\left(2k_{\mathrm{a}}^2-k_2^2\right)\cosh(\eta_{1\mathrm{a}}z)\cosh(\eta_{2\mathrm{a}}H) - 2k_{\mathrm{a}}^2\cosh(\eta_{1\mathrm{a}}H)\cosh(\eta_{2\mathrm{a}}z)\Big]e^{ik_{\mathrm{a}}x} \tag{2.102}$$

$$S_{xx}(x,z,\omega)=\sum_{k_{\mathrm{a}}}i\frac{\overline{P}_0(k_{\mathrm{a}},\omega)}{2R'_{\mathrm{a}}(k_{\mathrm{a}})}\Big[\left(k_2^2+2\eta_{1\mathrm{a}}^2\right)\left(2k_{\mathrm{a}}^2-k_2^2\right)\sinh(\eta_{1\mathrm{a}}z)\cosh(\eta_{2\mathrm{a}}H) - 4k_{\mathrm{a}}^2\eta_{1\mathrm{a}}\eta_{2\mathrm{a}}\cosh(\eta_{1\mathrm{a}}H)\sinh(\eta_{2\mathrm{a}}z)\Big]e^{ik_{\mathrm{a}}x} \tag{2.103}$$

$$S_{zz}(x,z,\omega)=\sum_{k_{\mathrm{a}}}-i\frac{\overline{P}_0(k_{\mathrm{a}},\omega)}{2R'_{\mathrm{a}}(k_{\mathrm{a}})}\Big[\left(2k_{\mathrm{a}}^2-k_2^2\right)^2\sinh(\eta_{1\mathrm{a}}z)\cosh(\eta_{2\mathrm{a}}H) - 4k_{\mathrm{a}}^2\eta_{1\mathrm{a}}\eta_{2\mathrm{a}}\cosh(\eta_{1\mathrm{a}}H)\sinh(\eta_{2\mathrm{a}}z)\Big]e^{ik_{\mathrm{a}}x} \tag{2.104}$$

$$S_{xz}(x,z,\omega)=\sum_{k_{\mathrm{a}}}-\frac{\left(2k_{\mathrm{a}}^2-k_2^2\right)\eta_{1\mathrm{a}}k_{\mathrm{a}}\overline{P}_0(k_{\mathrm{a}},\omega)}{R'_{\mathrm{a}}(k_{\mathrm{a}})}\Big[\cosh(\eta_{1\mathrm{a}}z)\cosh(\eta_{2\mathrm{a}}H) - \cosh(\eta_{1\mathrm{a}}H)\cosh(\eta_{2\mathrm{a}}z)\Big]e^{ik_{\mathrm{a}}x} \tag{2.105}$$

where it is understood that the right hand sides of Equations (2.101-2.105) are summed over for all positive real, imaginary and complex values of k_{a}. $R'_{\mathrm{a}}(k_{\mathrm{a}})$ is the derivative of $R_{\mathrm{a}}(k)$, the antisymmetric Lamb wave denominator with respect to k, evaluated at the roots of the antisymmetric Lamb wave dispersion equation

k_{a} and is given by

$$\begin{aligned}
R'_{\mathrm{a}}\left(k_{\mathrm{a}}\right) = & \, 8\left(2k_{\mathrm{a}}^2 - k_2^2\right) k_{\mathrm{a}} \sinh\left(\eta_{1\mathrm{a}} H\right) \cosh\left(\eta_{2\mathrm{a}} H\right) \\
& + \left(2k_{\mathrm{a}}^2 - k_2^2\right)^2 \frac{k_{\mathrm{a}} H}{\eta_{1\mathrm{a}}} \cosh\left(\eta_{1\mathrm{a}} H\right) \cosh\left(\eta_{2\mathrm{a}} H\right) \\
& + \left(2k_{\mathrm{a}}^2 - k_2^2\right)^2 \frac{k_{\mathrm{a}} H}{\eta_{2\mathrm{a}}} \sinh\left(\eta_{1\mathrm{a}} H\right) \sinh\left(\eta_{2\mathrm{a}} H\right) \\
& - 8k_{\mathrm{a}} \eta_{1\mathrm{a}} \eta_{2\mathrm{a}} \cosh\left(\eta_{1\mathrm{a}} H\right) \sinh\left(\eta_{2\mathrm{a}} H\right) \\
& - 4k_{\mathrm{a}}^3 \frac{\eta_{2\mathrm{a}}}{\eta_{1\mathrm{a}}} \cosh\left(\eta_{1\mathrm{a}} H\right) \sinh\left(\eta_{2\mathrm{a}} H\right) \\
& - 4k_{\mathrm{a}}^3 \frac{\eta_{1\mathrm{a}}}{\eta_{2\mathrm{a}}} \cosh\left(\eta_{1\mathrm{a}} H\right) \sinh\left(\eta_{2\mathrm{a}} H\right) \\
& - 4k_{\mathrm{a}}^3 \eta_{2\mathrm{a}} H \sinh\left(\eta_{1\mathrm{a}} H\right) \sinh\left(\eta_{2\mathrm{a}} H\right) \\
& - 4k_{\mathrm{a}}^3 \eta_{1\mathrm{a}} H \cosh\left(\eta_{1\mathrm{a}} H\right) \cosh\left(\eta_{2\mathrm{a}} H\right)
\end{aligned} \tag{2.106}$$

In Equations (2.101-2.106), $\eta_{1\mathrm{a}}$ and $\eta_{2\mathrm{a}}$ are the values of η_1 and η_2 evaluated at k_{a}.

It is noted that at the top and the bottom surface of the plate ($z = \pm H$), the normal stress $S_{zz}\left(x, z, \omega\right)$ from Equation (2.104) becomes zero according to the antisymmetric Lamb wave dispersion equation (Equation (2.62)), seemingly not satisfying the boundary condition in Equation (2.89). But actually, at the top and bottom surfaces of the plate, the integral in Equation (2.99) applied to the normal stress $\overline{S}_{zz}\left(k, z, \omega\right)$ in Equation (2.97) do not have any singularities at the roots of the antisymmetric Lamb wave dispersion equation (Equation (2.62)) and satisfies the applied boundary condition in Equation (2.89).

From Equations (2.101-2.105), it is seen that for the imaginary roots ik_{a} of the dispersion equations, the various field variables have the form

$$F\left(x, z, \omega\right) = \frac{G(k_{\mathrm{a}}, z, \omega)}{R'_{\mathrm{a}}\left(k_{\mathrm{a}}\right)} e^{-k_{\mathrm{a}} x} \tag{2.107}$$

which exponentially decreases for increasing values of x. The complex roots in the upper half complex k plane come in pairs of the the form $k_{\mathrm{a}} = a + ib, -a + ib$.

For the complex roots, the various field variables have the form

$$F(x,z,\omega) = \frac{G(k_{\mathrm{a}},z,\omega)}{R'_{\mathrm{a}}(k_{\mathrm{a}})} e^{\pm iax} e^{-bx} \tag{2.108}$$

which too exponentially decrease for increasing value of x. The antisymmetric Lamb waves propagating to large distances in the plate are the propagating waves given by the residues of the real positive roots.

2.6 Symmetric Lamb wave propagation under dynamic vertical load on the top surface of a plate

From Equations (2.59, 2.60), zero shear stress at $z = H$ gives,

$$\overline{S}_{xz}(k,H,\omega) = 2\eta_1\eta_2\overline{A}_1 \sinh(\eta_1 H) + \left(2k^2 - k_2^2\right)\overline{A}_3 \sinh(\eta_2 z) = 0 \tag{2.109}$$

which gives,

$$\overline{A}_1 = -\frac{(2k^2 - k_2^2)\sinh(\eta_2 H)}{2\eta_1\eta_2 \sinh(\eta_1 H)}\overline{A}_3 \tag{2.110}$$

At $z = H$, the applied normal load gives,

$$\overline{S}_{zz}(k,H,\omega) = -\frac{\overline{P}_0(k,\omega)}{2} \tag{2.111}$$

which gives,

$$\frac{i\mu}{k}\left[\left(2k^2 - k_2^2\right)\overline{A}_1 \cosh(\eta_1 H) + 2k^2\overline{A}_3 \cosh(\eta_2 H)\right] = \frac{\overline{P}_0}{2} \tag{2.112}$$

Substituting $\overline{A}_1$ from Equation (2.110) into Equation (2.112)

$$\overline{A}_3 = \frac{ik\eta_1\eta_2 \sinh(\eta_1 H)}{\mu R_{\mathrm{s}}(k)}\overline{P}_0(k,\omega) \tag{2.113}$$

where, $R_{\mathrm{s}}(k)$ is the symmetric Lamb wave denominator and is given by

$$R_{\mathrm{s}}(k) = \left(2k^2 - k_2^2\right)^2 \cosh(\eta_1 H)\sinh(\eta_2 H) - 4k^2\eta_1\eta_2 \sinh(\eta_1 H)\cosh(\eta_2 H) \tag{2.114}$$

Substituting $\overline{A}_3$ from Equation (2.113) into Equation (2.110)

$$\overline{A}_1 = -\frac{ik\left(2k^2 - k_2^2\right)\sinh\left(\eta_2 H\right)}{2\mu R_{\mathrm{s}}\left(k\right)}\overline{P}_0\left(k,\omega\right) \tag{2.115}$$

Using the above values of $\overline{A}_1$ and $\overline{A}_3$, the displacements and the stresses in the plate due to the symmetric Lamb wave in the frequency domain are given by

$$\overline{U}\left(k,z,\omega\right) = -\frac{ik\overline{P}_0\left(k,\omega\right)}{2\mu R_{\mathrm{s}}\left(k\right)}\Big[\left(2k^2 - k_2^2\right)\cosh\left(\eta_1 z\right)\sinh\left(\eta_2 H\right) - 2\eta_1\eta_2\sinh\left(\eta_1 H\right)\cosh\left(\eta_2 z\right)\Big] \tag{2.116}$$

$$\overline{W}\left(k,z,\omega\right) = -\frac{\eta_1\overline{P}_0\left(k,\omega\right)}{2\mu R_{\mathrm{s}}\left(k\right)}\Big[\left(2k^2 - k_2^2\right)\sinh\left(\eta_1 z\right)\sinh\left(\eta_2 H\right) - 2k^2\sinh\left(\eta_1 H\right)\sinh\left(\eta_2 z\right)\Big] \tag{2.117}$$

$$\overline{S}_{xx}\left(k,z,\omega\right) = \frac{\overline{P}_0\left(k,\omega\right)}{2R_{\mathrm{s}}\left(k\right)}\Big[\left(k_2^2 + 2\eta_1^2\right)\left(2k^2 - k_2^2\right)\cosh\left(\eta_1 z\right)\sinh\left(\eta_2 H\right) - 4k^2\eta_1\eta_2\sinh\left(\eta_1 H\right)\cosh\left(\eta_2 z\right)\Big] \tag{2.118}$$

$$\overline{S}_{zz}\left(k,z,\omega\right) = -\frac{\overline{P}_0\left(k,\omega\right)}{2R_{\mathrm{s}}\left(k\right)}\Big[\left(2k^2 - k_2^2\right)^2\cosh\left(\eta_1 z\right)\sinh\left(\eta_2 H\right) - 4k^2\eta_1\eta_2\sinh\left(\eta_1 H\right)\cosh\left(\eta_2 z\right)\Big] \tag{2.119}$$

$$\overline{S}_{xz}\left(k,z,\omega\right) = -\frac{\left(2k^2 - k_2^2\right)\eta_1 ik\overline{P}_0\left(k,\omega\right)}{R_{\mathrm{s}}\left(k\right)}\Big[\sinh\left(\eta_1 z\right)\sinh\left(\eta_2 H\right) - \sinh\left(\eta_1 H\right)\sinh\left(\eta_2 z\right)\Big] \tag{2.120}$$

The inverse Fourier transform with respect to the wavenumber k

$$F\left(x,z,\omega\right) = \frac{1}{2\pi}\int_{-\infty}^{\infty}\overline{F}\left(k,z,\omega\right)e^{ikx}\,dk \tag{2.121}$$

gives the field variables in x and the frequency (ω) domain. The integral in Equation (2.121) has simple poles at the roots of the symmetric Lamb wave dispersion equation obtained by equating $R_{\mathrm{s}}(k) = 0$.

Figure (2.8) shows a schematic of the roots in the complex k plane. There are real, imaginary and complex roots. The closed contour in the complex k plane with the anticlockwise direction it is traversed is indicated. To satisfy the radiation boundary condition at $x = \infty$, that is no incoming waves from infinity, the negative real poles are avoided in the contour. All real, imaginary and complex poles in the upper half complex k plane are enclosed in the contour. The field in Equation (2.121) is then given by

$$F(x,z,\omega) = \frac{1}{2\pi} 2\pi i \,(\text{Sum of the residues at the poles } k_{\mathrm{s}} \text{ of } \overline{F}(k,z,\omega)\, e^{ikx}) \tag{2.122}$$

where, $F(x,z,\omega)$ is the field variable due to symmetric Lamb waves. k_{s} is the root of the symmetric Lamb wave dispersion equation. The displacements and the stresses can be written as

$$U(x,z,\omega) = \sum_{k_{\mathrm{s}}} \frac{k_{\mathrm{s}} \overline{P}_0(k_{\mathrm{s}},\omega)}{2\mu R_{\mathrm{s}}'(k_{\mathrm{s}})} \Big[\left(2k_{\mathrm{s}}^2 - k_2^2\right) \cosh(\eta_{1\mathrm{s}} z) \sinh(\eta_{2\mathrm{s}} H) - 2\eta_{1\mathrm{s}}\eta_{2\mathrm{s}} \sinh(\eta_{1\mathrm{s}} H) \cosh(\eta_{2\mathrm{s}} z) \Big] e^{ik_{\mathrm{s}}x} \tag{2.123}$$

$$W(x,z,\omega) = \sum_{k_{\mathrm{s}}} -i \frac{\eta_{1\mathrm{s}} \overline{P}_0(k_{\mathrm{s}},\omega)}{2\mu R_{\mathrm{s}}'(k_{\mathrm{s}})} \Big[\left(2k_{\mathrm{s}}^2 - k_2^2\right) \sinh(\eta_{1\mathrm{s}} z) \sinh(\eta_{2\mathrm{s}} H) - 2k_{\mathrm{s}}^2 \sinh(\eta_{1\mathrm{s}} H) \sinh(\eta_{2\mathrm{s}} z) \Big] e^{ik_{\mathrm{s}}x} \tag{2.124}$$

$$S_{xx}(x,z,\omega) = \sum_{k_s} i\frac{\overline{P}_0(k_s,\omega)}{2R_s'(k_s)}\Big[\left(k_2^2+2\eta_{1s}^2\right)\left(2k_s^2-k_2^2\right)\cosh(\eta_{1s}z)\sinh(\eta_{2s}H) - 4k_s^2\eta_{1s}\eta_{2s}\sinh(\eta_{1s}H)\cosh(\eta_{2s}z)\Big]e^{ik_sx} \tag{2.125}$$

$$S_{zz}(x,z,\omega) = \sum_{k_s} -i\frac{\overline{P}_0(k_s,\omega)}{2R_s'(k_s)}\Big[\left(2k_s^2-k_2^2\right)^2\cosh(\eta_{1s}z)\sinh(\eta_{2s}H) - 4k_s^2\eta_{1s}\eta_{2s}\sinh(\eta_{1s}H)\cosh(\eta_{2s}z)\Big]e^{ik_sx} \tag{2.126}$$

$$S_{xz}(x,z,\omega) = \sum_{k_s} -\frac{\left(2k_s^2-k_2^2\right)\eta_{1s}k_s\overline{P}_0(k_s,\omega)}{R_s'(k_s)}\Big[\sinh(\eta_{1s}z)\sinh(\eta_{2s}H) - \sinh(\eta_{1s}H)\sinh(\eta_{2s}z)\Big]e^{ik_sx} \tag{2.127}$$

where it is understood that the right hand side of Equations (2.123-2.127) are summed over for all positive real, imaginary and complex values of k_s. $R_s'(k_s)$ is the derivative of $R_s(k)$, the symmetric Lamb wave denominator with respect to k, evaluated at the roots of the symmetric Lamb wave dispersion equation k_s and is given by

$$\begin{aligned} R_s'(k_s) = {} & 8\left(2k_s^2-k_2^2\right)k_s\cosh(\eta_{1s}H)\sinh(\eta_{2s}H) \\ & + \left(2k_s^2-k_2^2\right)^2\frac{k_sH}{\eta_{1s}}\sinh(\eta_{1s}H)\sinh(\eta_{2s}H) \\ & + \left(2k_s^2-k_2^2\right)^2\frac{k_sH}{\eta_{2s}}\cosh(\eta_{1s}H)\cosh(\eta_{2s}H) \\ & - 8k_s\eta_{1s}\eta_{2s}\sinh(\eta_{1s}H)\cosh(\eta_{2s}H) \\ & - 4k_s^3\frac{\eta_{2s}}{\eta_{1s}}\sinh(\eta_{1s}H)\cosh(\eta_{2s}H) \\ & - 4k_s^3\frac{\eta_{1s}}{\eta_{2s}}\sinh(\eta_{1s}H)\cosh(\eta_{2s}H) \\ & - 4k_s^3\eta_{2s}H\cosh(\eta_{1s}H)\cosh(\eta_{2s}H) \\ & - 4k_s^3\eta_{1s}H\sinh(\eta_{1s}H)\sinh(\eta_{2s}H) \end{aligned} \tag{2.128}$$

In Equations (2.123-2.128), η_{1s} and η_{2s} are the values of η_1 and η_2 evaluated at k_s.

As described for the antisymmetric Lamb waves, at the top and bottom surfaces of the plate, the integral in Equation (2.121) applied to the normal stress $\overline{S}_{zz}(k, z, \omega)$ in Equation (2.119) do not have any singularities at the roots of the symmetric Lamb wave dispersion equation (Equation (2.55)). Hence the normal stress at the top surface of the plate satisfies the boundary condition in Equation (2.111).

From Equations (2.123-2.127), it is seen that for the imaginary roots ik_s of the dispersion equations, the various field variables have the form

$$F(x, z, \omega) = \frac{G(k_s, z, \omega)}{R_s'(k_s)} e^{-k_s x} \tag{2.129}$$

which exponentially decreases for increasing values of x. The complex roots in the upper half complex k plane come in pairs of the the form $k_s = a + ib, -a + ib$. For the complex roots, the various field variables have the form

$$F(x, z, \omega) = \frac{G(k_s, z, \omega)}{R_s'(k_s)} e^{\pm iax} e^{-bx} \tag{2.130}$$

which too exponentially decrease for increasing value of x. The symmetric Lamb waves traveling large distances in the plate are the propagating waves given by the residues of the real positive roots.

2.7 Displacement fields in the plate under applied transient load

The total horizontal and vertical displacements in the plate are given by the corresponding sum of the symmetric and antisymmetric displacements. The displacements are calculated by taking the inverse Fourier transform with respect to frequency (ω) of the sum of Equation (2.101) and Equation (2.123) for the horizontal displacement $u(x, z, t)$ and the sum of Equation (2.102) and Equation (2.124) for the vertical displacement $w(x, z, t)$.

Comparisons of the horizontal displacement $u(x, z, t)$ from the above equations,in an aluminum plate of thickness 1.78 mm, with that calculated by finite element analysis using the commercial software package Abaqus are given below. The loading applied on the top surface of the aluminum plate is a 5 cycle sine load with a frequency of 200 kHz, with amplitude 1 million N/m enclosed in a Hann window given by the form

$$V(t) = \frac{1}{2}\left[1 - \cos\left(\frac{2\pi f t}{n_{\mathrm{p}}}\right)\right]\sin(2\pi f t)$$

The load is uniformly distributed over a length of 1 mm centered at the z axis. Figure (2.9) shows the applied load.

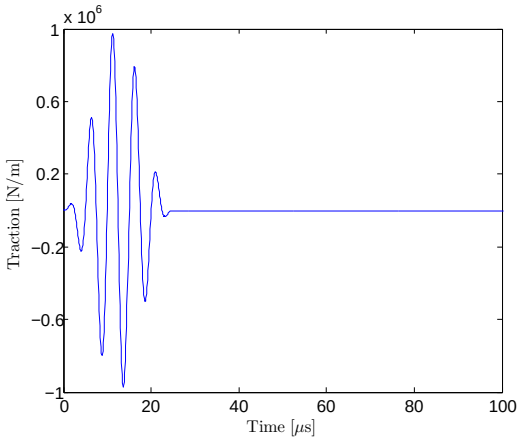

Figure 2.9: Applied tone burst load with center frequency $f = 200$ kHz

Figure (2.10) shows the excellent match between the horizontal displacement at 50 mm distance to the right of the z axis calculated from the above equations to the results from finite element analysis. The results are shown at various depths along the thickness of the plate. The red curves are the results from the finite element analysis using the commercial software package Abaqus. The blue curves are the horizontal displacements computed using 29 modes including the positive real, imaginary and the complex modes. The green curves are the horizontal displacements computed using only the real positive or the right propagating modes. The analytical results using positive real, complex and imaginary modes

are nearly identical to those computed using only the real positive modes as the complex and imaginary modes decay exponentially with distance as discussed earlier. The finite element solutions include reflections from the edge of the plate, which are absent in the analytical solutions for a plate of infinite length. Figure (2.11) shows similar comparisons for the vertical displacements in the plate.

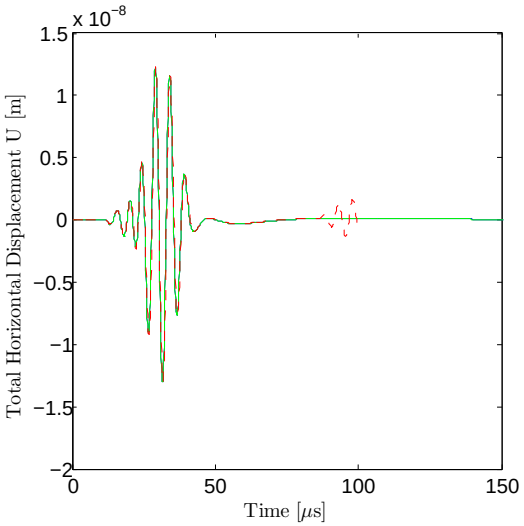

(a) $x = 50\,\text{mm}$, $z = H$, $f = 200\,\text{kHz}$

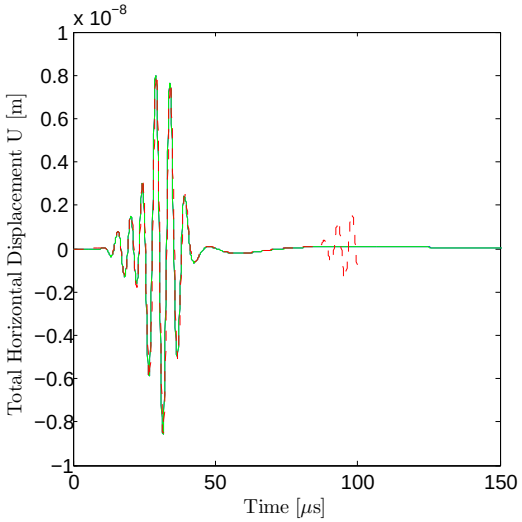

(b) $x = 50\,\text{mm}$, $z = \frac{5H}{7}$, $f = 200\,\text{kHz}$

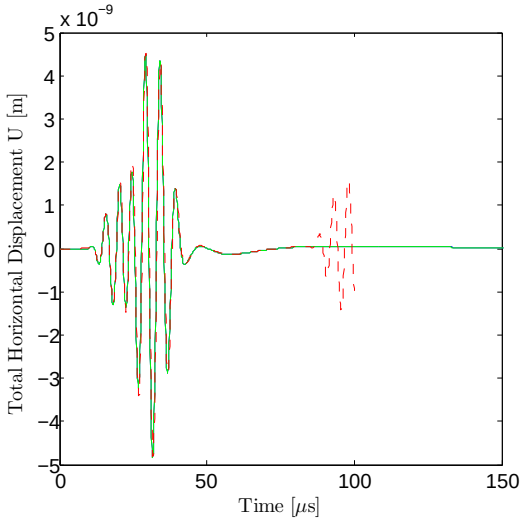

(c) $x = 50\,\text{mm}$, $z = \frac{3H}{7}$, $f = 200\,\text{kHz}$

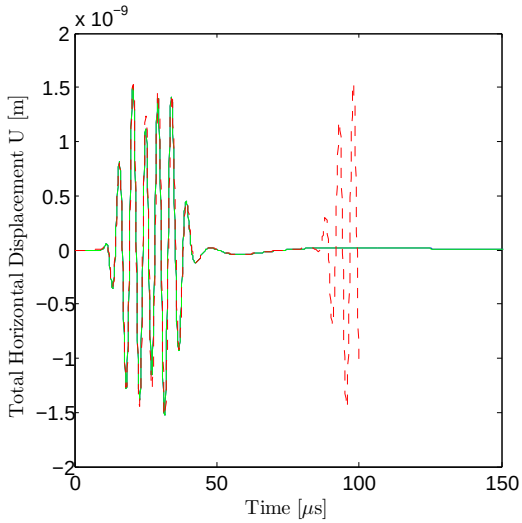

(d) $x = 50\,\text{mm}$, $z = \frac{H}{7}$, $f = 200\,\text{kHz}$

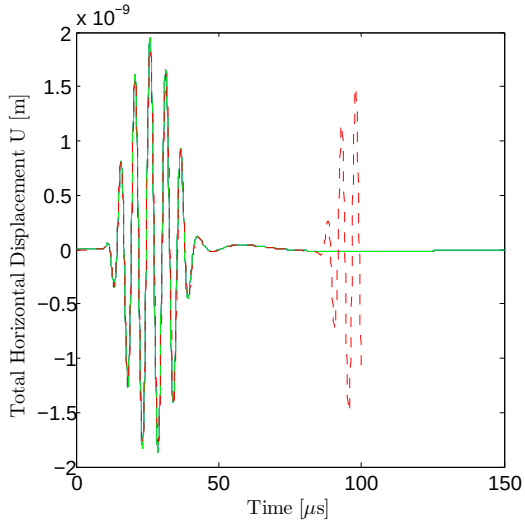

(e) $x = 50\,\text{mm}$, $z = -\frac{H}{7}$, $f = 200\,\text{kHz}$

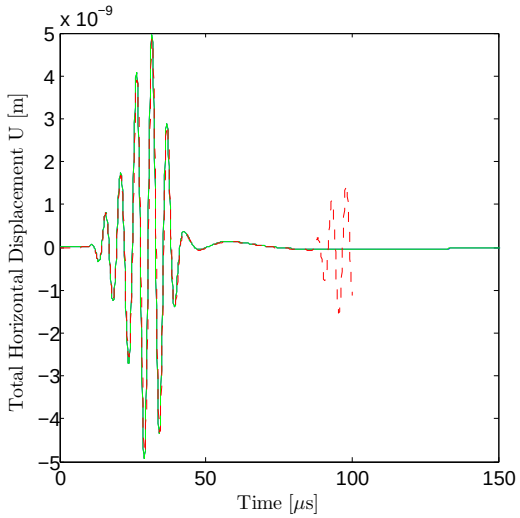

(f) $x = 50\,\text{mm}$, $z = -\frac{3H}{7}$, $f = 200\,\text{kHz}$

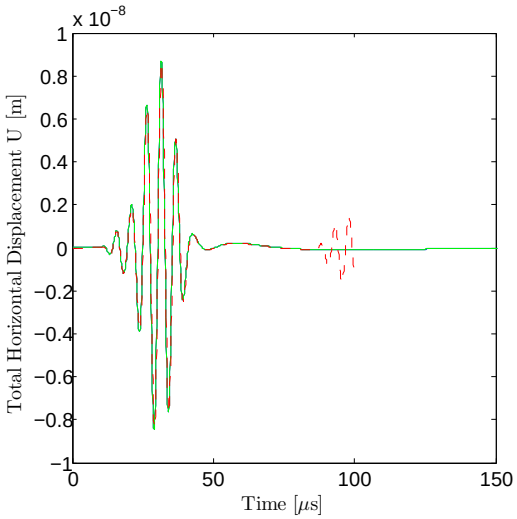

(g) $x = 50\,\text{mm}$, $z = -\frac{5H}{7}$, $f = 200\,\text{kHz}$

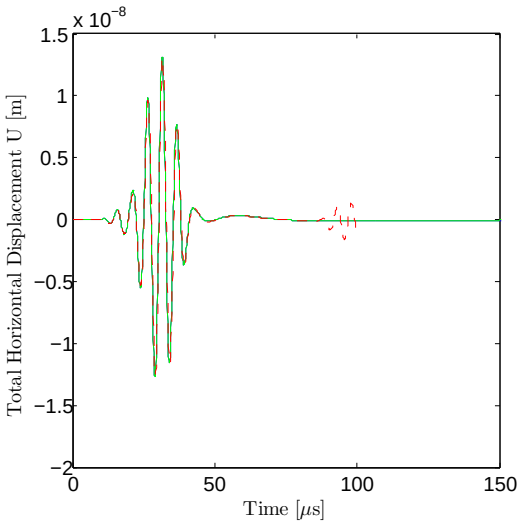

(h) $x = 50\,\text{mm}$, $z = -H$, $f = 200\,\text{kHz}$

Figure 2.10: Horizonal displacements in the aluminum plate. The red curves are the results from finite element analysis using the commercial software package Abaqus. The blue curves are the horizontal displacements computed using 29 modes including the positive real, imaginary and the complex modes. The green curves are the horizontal displacements computed using only the positive real or the right propagating modes.

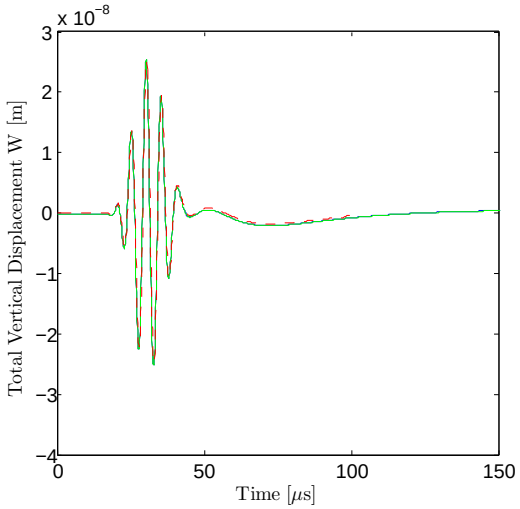

(a) $x = 50\,\text{mm}$, $z = H$, $f = 200\,\text{kHz}$

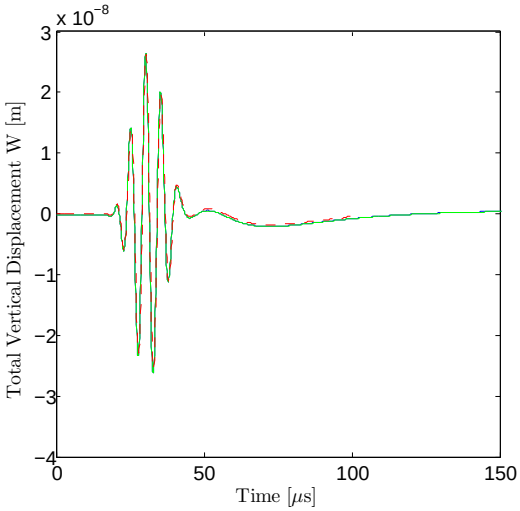

(b) $x = 50\,\text{mm}$, $z = \frac{5H}{7}$, $f = 200\,\text{kHz}$

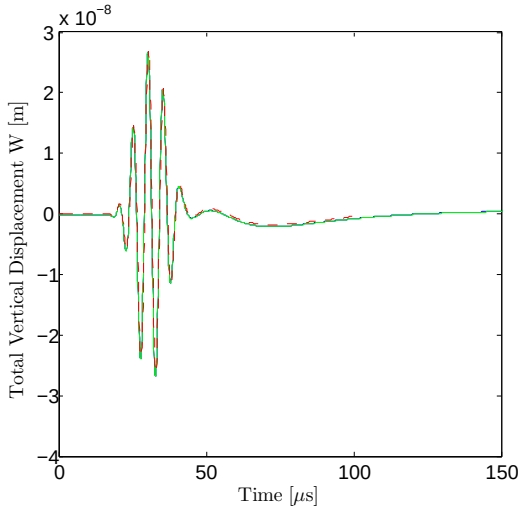

(c) $x = 50\,\text{mm}$, $z = \frac{3H}{7}$, $f = 200\,\text{kHz}$

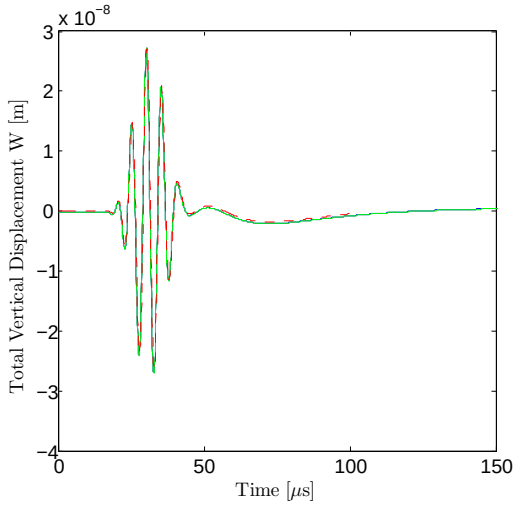

(d) $x = 50\,\text{mm}$, $z = \frac{H}{7}$, $f = 200\,\text{kHz}$

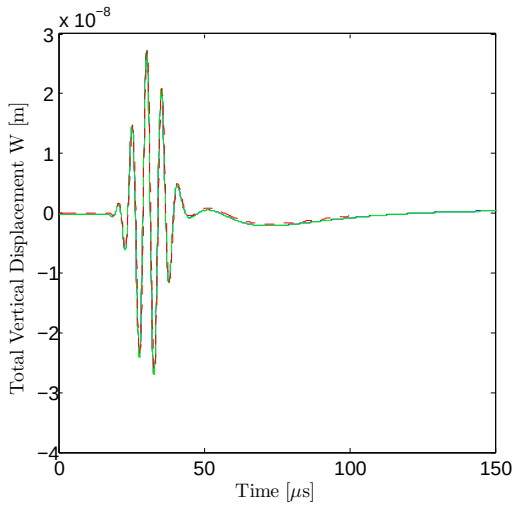

(e) $x = 50\,\text{mm},\ z = -\frac{H}{7},\ f = 200\,\text{kHz}$

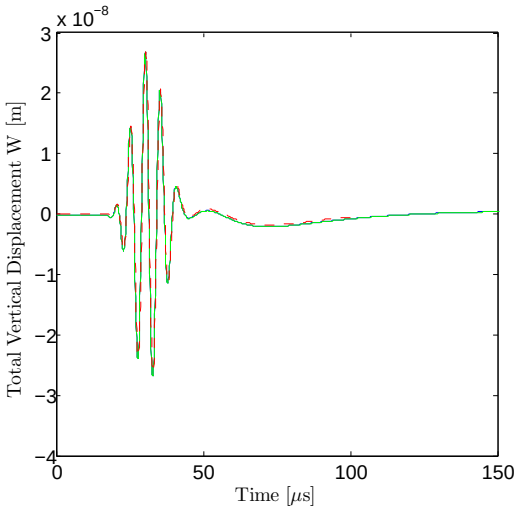

(f) $x = 50\,\text{mm},\ z = -\frac{3H}{7},\ f = 200\,\text{kHz}$

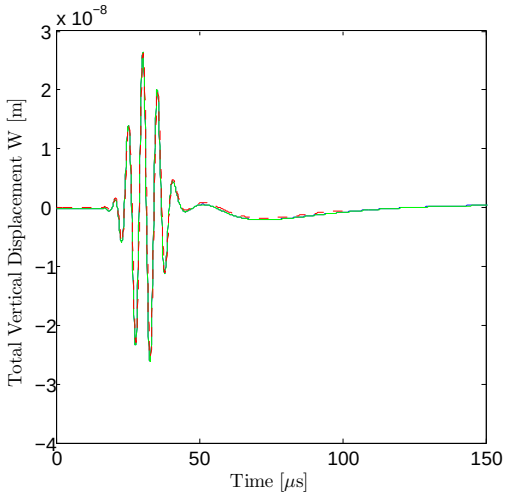

(g) $x = 50\,\text{mm},\ z = -\frac{5H}{7},\ f = 200\,\text{kHz}$

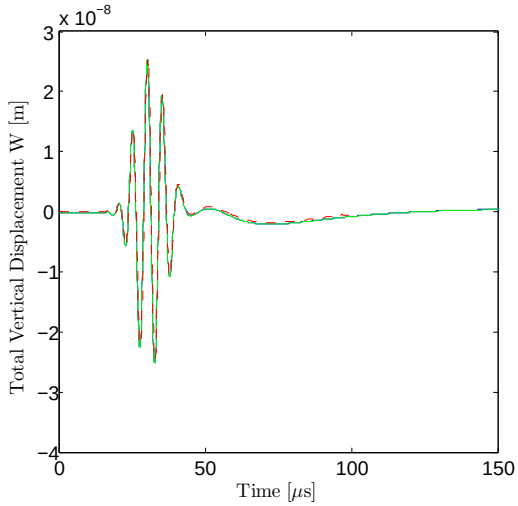

(h) $x = 50\,\text{mm},\ z = -H,\ f = 200\,\text{kHz}$

Figure 2.11: Vertical displacements in the aluminum plate. The red curves are the results from the finite element analysis using the commercial package Abaqus. The blue curves are the vertical displacements computed using 29 modes including the positive real, imaginary and the complex modes. The green curves are the vertical displacements computed using only the positive real or the right propagating modes.

Figure (2.12)shows the horizontal displacement in the same 1.78 mm thick aluminum plate with the same applied load as above at a distance of 1 mm to the

right of the z axis. The red curves are the results from the finite element analysis using the commercial software package Abaqus. The blue curves are the vertical displacements computed using 29 modes including the positive real, imaginary and the complex modes. The green curves are the vertical displacements computed using only the real positive or the right propagating modes. It can be clearly seen that very near the source, the complex and imaginary modes contribute significantly to the displacements. There is excellent match between the results from finite element analysis and those computed analytically using positive real, imaginary and complex modes. Whereas, the green curves computed analytically using only the real positive or the right propagating modes differ significantly from the finite element results. The finite element solutions include reflections from the edge of the plate, which are absent in the analytical solutions for a plate of infinite length. Figure (2.13) shows similar comparisons for the vertical displacements in the plate.

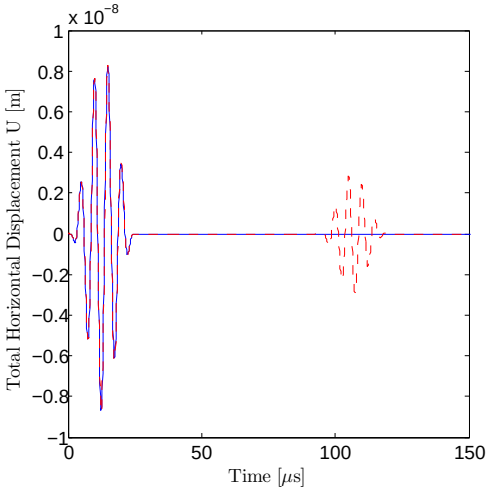

(a) $x = 1\,\text{mm}$, $z = H$, $f = 200\,\text{kHz}$

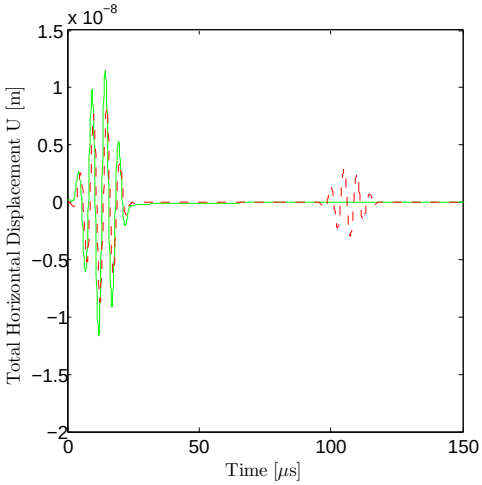

(b) $x = 1\,\text{mm}$, $z = H$, $f = 200\,\text{kHz}$

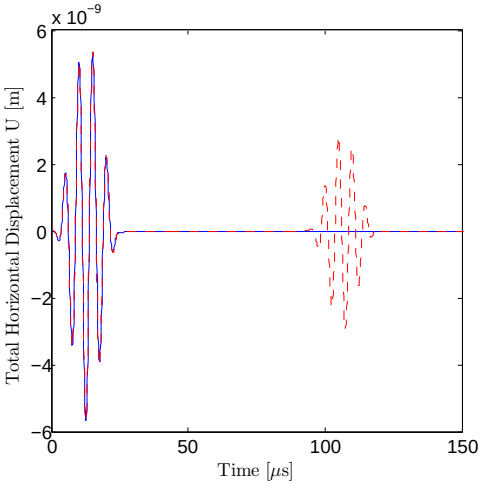

(c) $x = 1\,\text{mm}$, $z = \frac{5H}{7}$, $f = 200\,\text{kHz}$

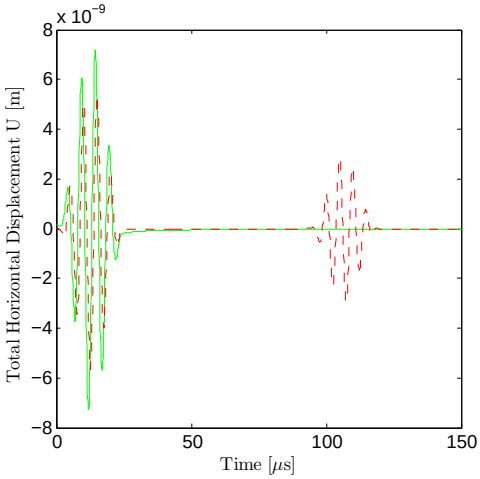

(d) $x = 1\,\text{mm}$, $z = \frac{5H}{7}$, $f = 200\,\text{kHz}$

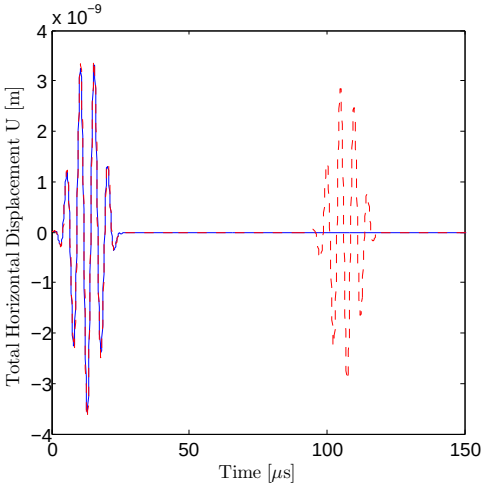

(e) $x = 1\,\text{mm}$, $z = \frac{3H}{7}$, $f = 200\,\text{kHz}$

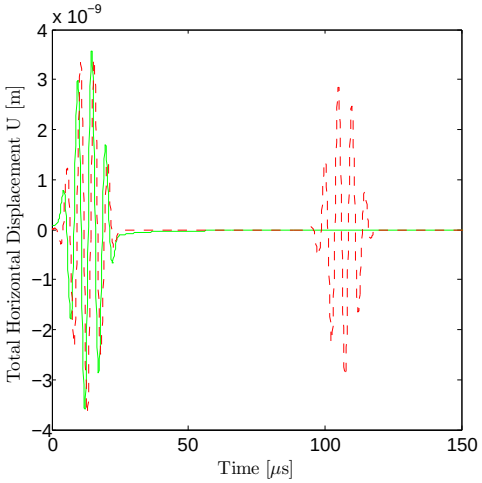

(f) $x = 1\,\text{mm}$, $z = \frac{3H}{7}$, $f = 200\,\text{kHz}$

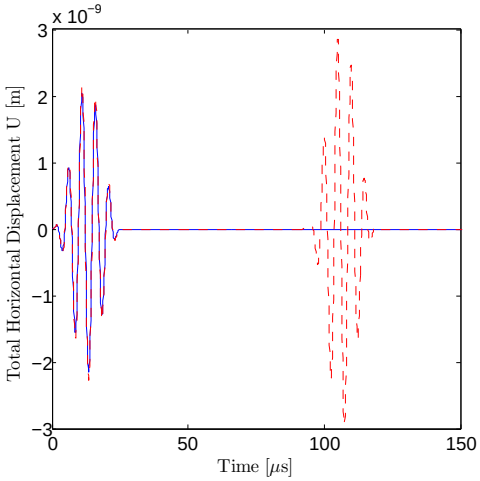

(g) $x = 1\,\text{mm},\ z = \frac{H}{7},\ f = 200\,\text{kHz}$

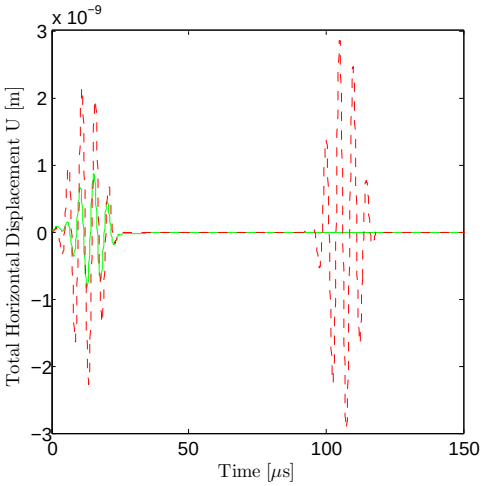

(h) $x = 1\,\text{mm},\ z = \frac{H}{7},\ f = 200\,\text{kHz}$

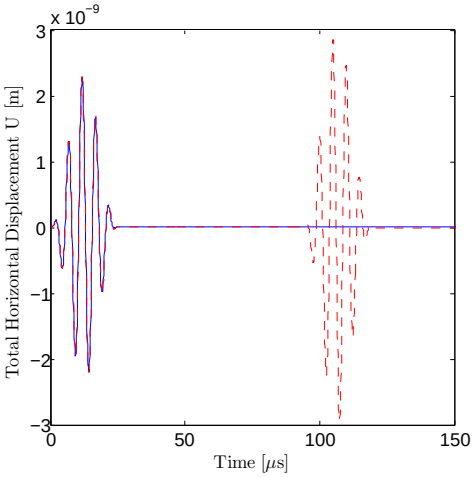

(i) $x = 1\,\text{mm},\ z = -\frac{H}{7},\ f = 200\,\text{kHz}$

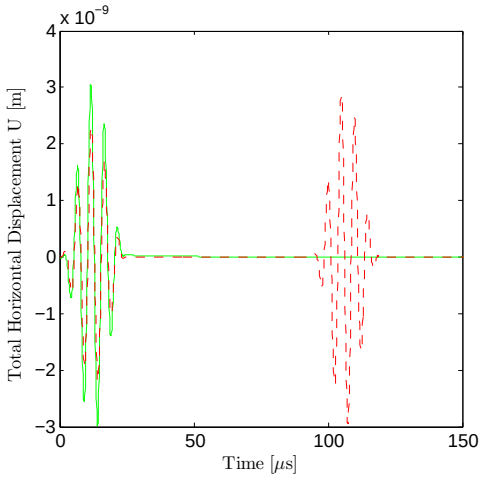

(j) $x = 1\,\text{mm},\ z = -\frac{H}{7},\ f = 200\,\text{kHz}$

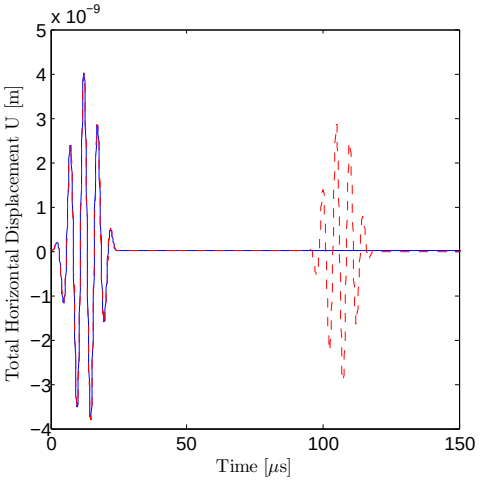

(k) $x = 1\,\text{mm},\ z = -\frac{3H}{7},\ f = 200\,\text{kHz}$

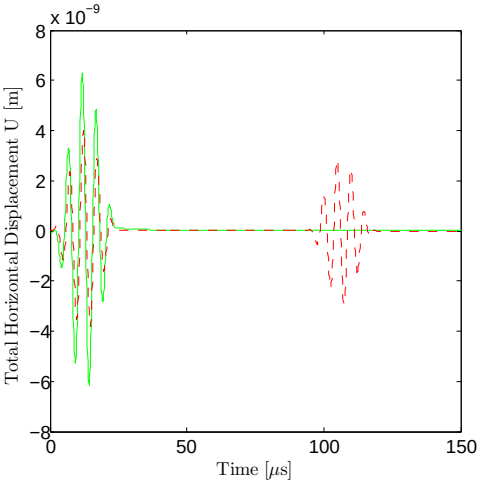

(l) $x = 1\,\text{mm},\ z = -\frac{3H}{7},\ f = 200\,\text{kHz}$

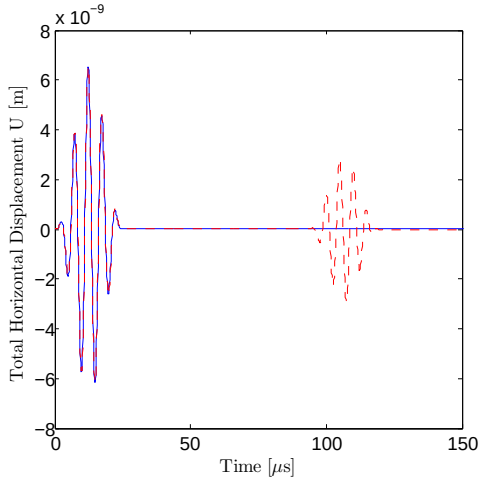

(m) $x = 1\,\text{mm}$, $z = -\frac{5H}{7}$, $f = 200\,\text{kHz}$

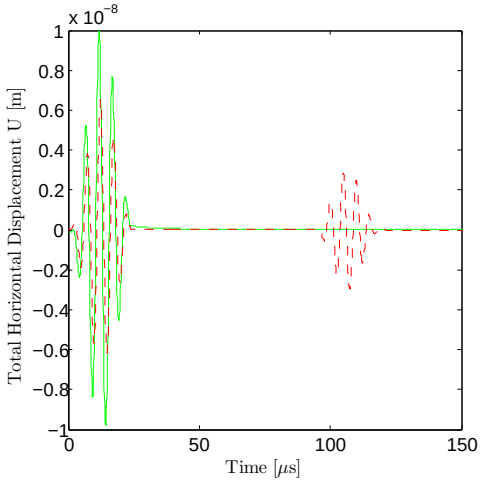

(n) $x = 1\,\text{mm}$, $z = -\frac{5H}{7}$, $f = 200\,\text{kHz}$

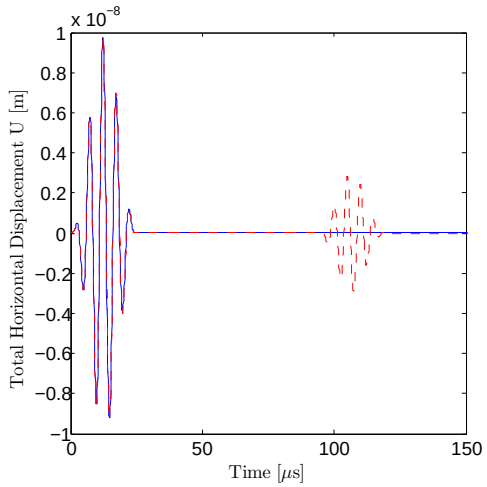

(o) $x = 1\,\text{mm}$, $z = -H$, $f = 200\,\text{kHz}$

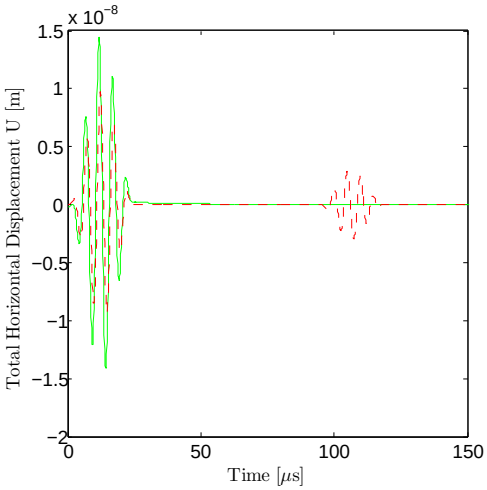

(p) $x = 1\,\text{mm}$, $z = -H$, $f = 200\,\text{kHz}$

Figure 2.12: Horizonal displacements in the aluminum plate. The red curves are the results from the finite element analysis using the commercial software package Abaqus. The blue curves are the horizontal displacements computed using 29 modes including the positive real, imaginary and the complex modes. The green curves are the horizontal displacements computed using only the positive real or the right propagating modes.

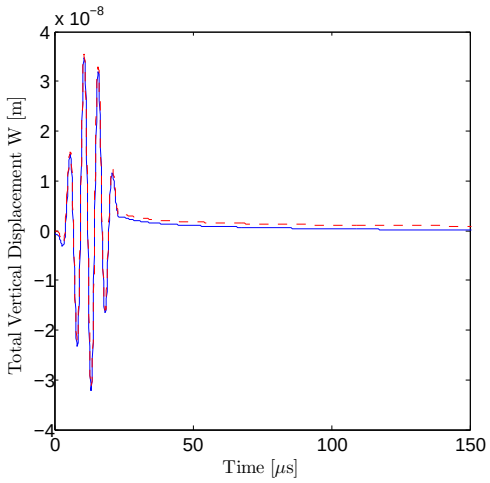

(a) $x = 1\,\text{mm},\ z = H,\ f = 200\,\text{kHz}$

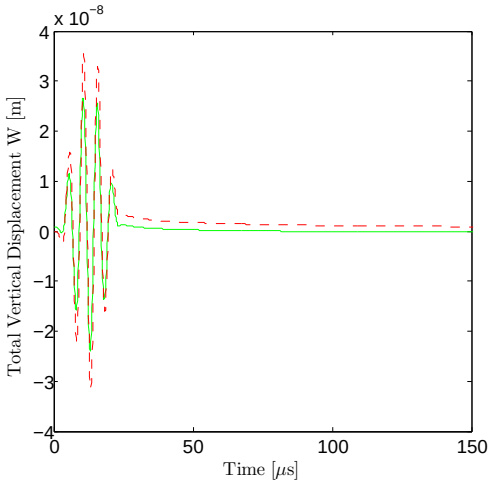

(b) $x = 1\,\text{mm},\ z = H,\ f = 200\,\text{kHz}$

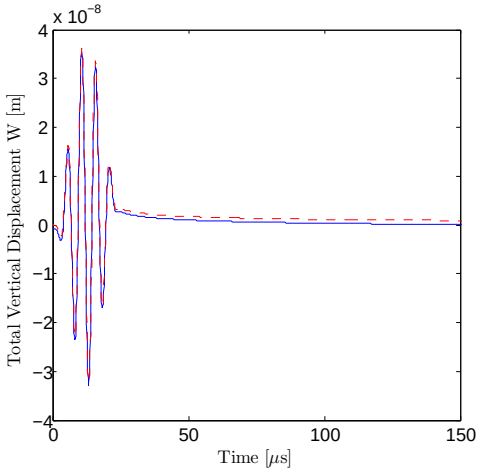

(c) $x = 1\,\text{mm},\ z = \frac{5H}{7},\ f = 200\,\text{kHz}$

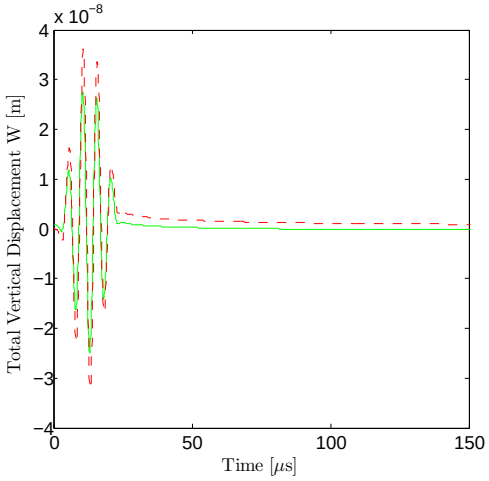

(d) $x = 1\,\text{mm},\ z = \frac{5H}{7},\ f = 200\,\text{kHz}$

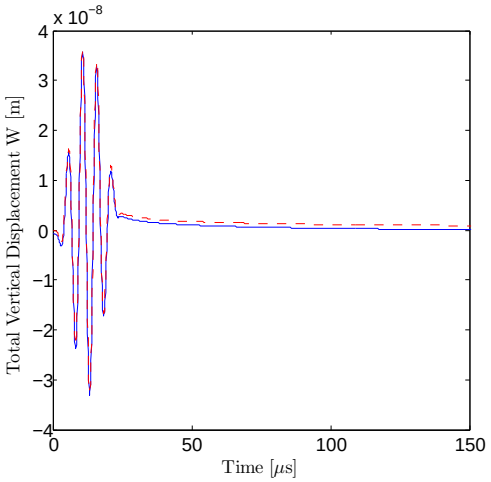

(e) $x = 1\,\text{mm},\ z = \frac{3H}{7},\ f = 200\,\text{kHz}$

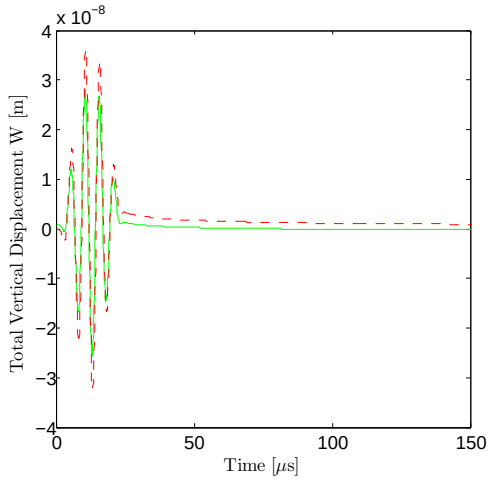

(f) $x = 1\,\text{mm},\ z = \frac{3H}{7},\ f = 200\,\text{kHz}$

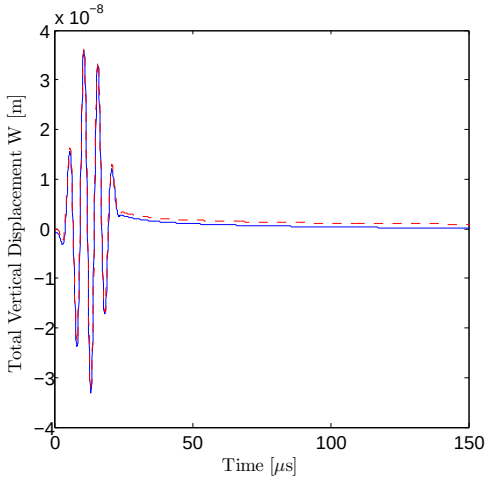

(g) $x = 1\,\text{mm}$, $z = \frac{H}{7}$, $f = 200\,\text{kHz}$

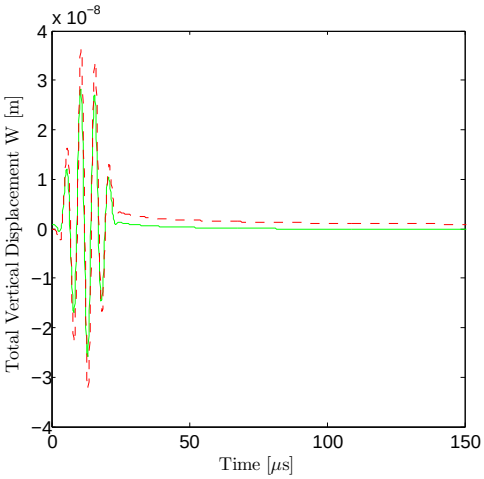

(h) $x = 1\,\text{mm}$, $z = \frac{H}{7}$, $f = 200\,\text{kHz}$

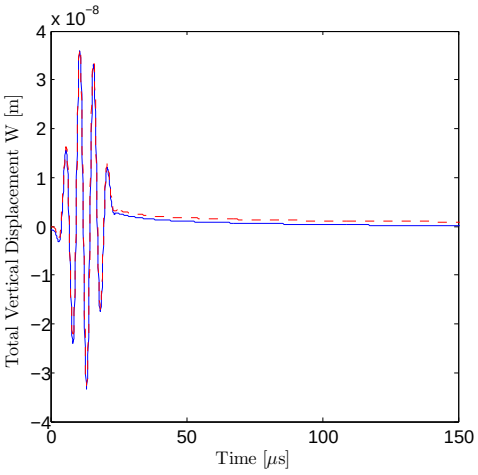

(i) $x = 1\,\text{mm}$, $z = -\frac{H}{7}$, $f = 200\,\text{kHz}$

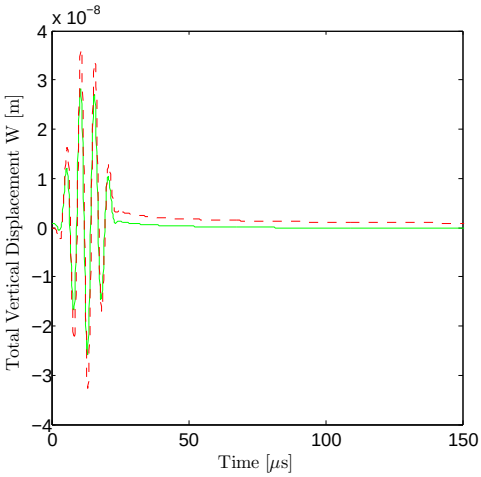

(j) $x = 1\,\text{mm}$, $z = -\frac{H}{7}$, $f = 200\,\text{kHz}$

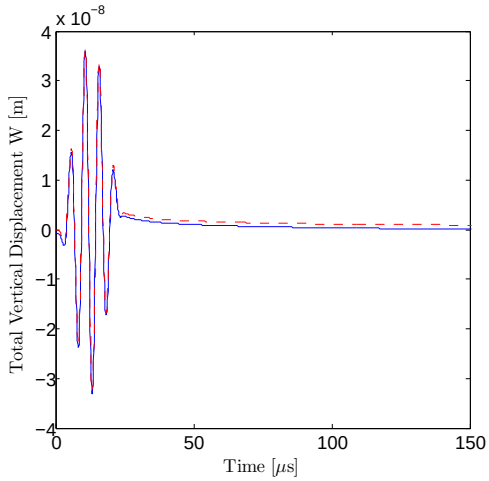

(k) $x = 1\,\text{mm}$, $z = -\frac{3H}{7}$, $f = 200\,\text{kHz}$

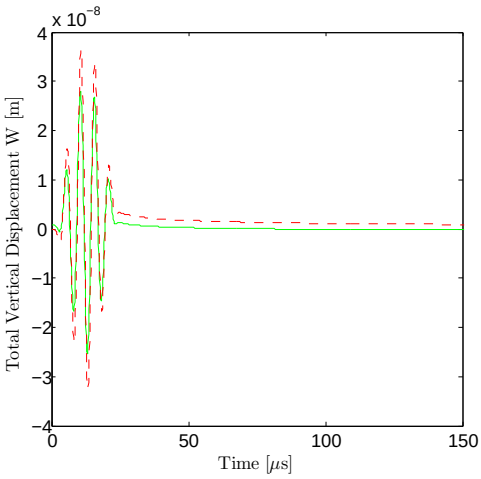

(l) $x = 1\,\text{mm}$, $z = -\frac{3H}{7}$, $f = 200\,\text{kHz}$

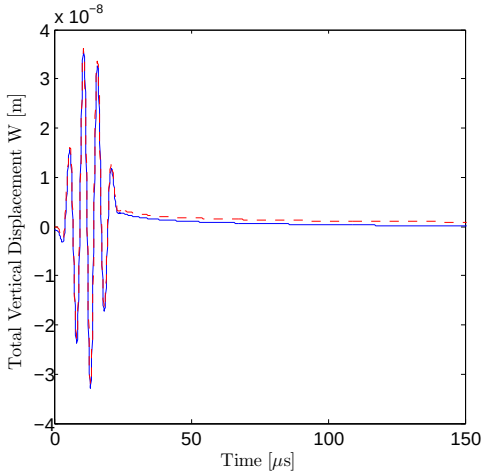

(m) $x = 1\,\text{mm}$, $z = -\frac{5H}{7}$, $f = 200\,\text{kHz}$

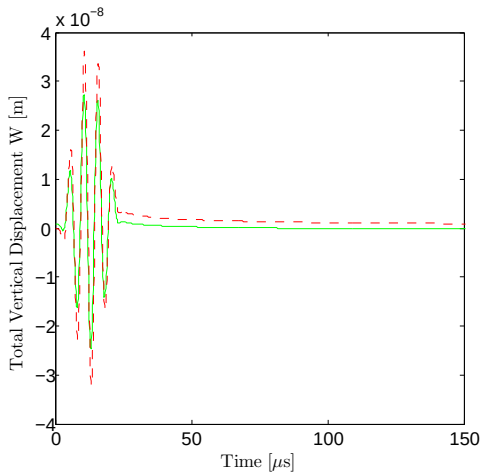

(n) $x = 1\,\text{mm}$, $z = -\frac{5H}{7}$, $f = 200\,\text{kHz}$

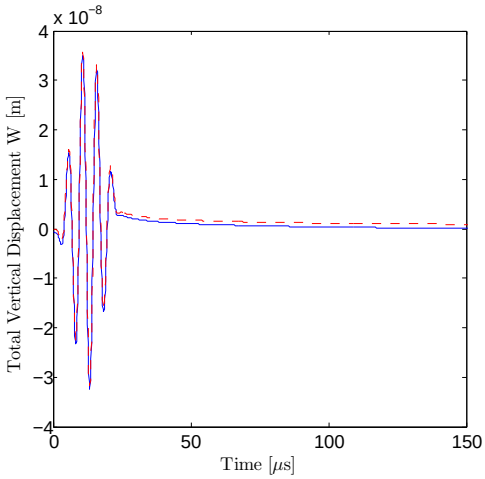

(o) $x = 1\,\text{mm}$, $z = -H$, $f = 200\,\text{kHz}$

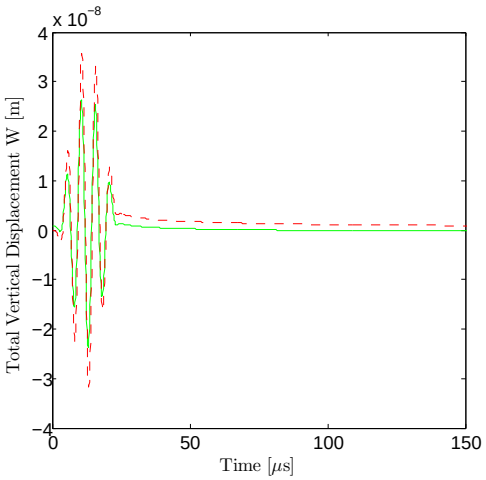

(p) $x = 1\,\text{mm}$, $z = -H$, $f = 200\,\text{kHz}$

Figure 2.13: Vertical displacements in the aluminum plate. The red curves are the results from the finite element analysis using the commercial software package Abaqus. The blue curves are the vertical displacements computed using 29 modes including the positive real, imaginary and the complex modes. The green curves are the vertical displacements computed using only the positive real or the right propagating modes.

The distance in terms of plate thicknesses away from the origin, when the solution due to real, imaginary and complex modes is almost equivalent to the solution due to the positive real (propagating) modes is determined. Figure (2.15) shows the

vertical displacement (W) at the top surface of the same 1.78 mm thick aluminum plate with the same applied loading as stated above. The blue curves are the vertical displacements computed using 29 modes including the positive real, imaginary and the complex modes. The red curves are the vertical displacements computed using only the positive real or the right propagating modes. The displacements are plotted at a distance when the two vertical displacements differ by less than 1% in their maximum amplitude. It is seen that as the frequency increases, the two solutions converge at lesser distances away from the origin. Figure (2.14) plots the percentage error in the maximum amplitude of the vertical displacement at the top surface for various frequencies against the distance away from the origin in terms of plate thickness. Table (2.1) lists the distance away from the origin in terms of plate thicknesses when the two solutions converge for different frequencies. It also lists the percentage difference in the maximum amplitude of the vertical displacement in the two solutions at that distance.

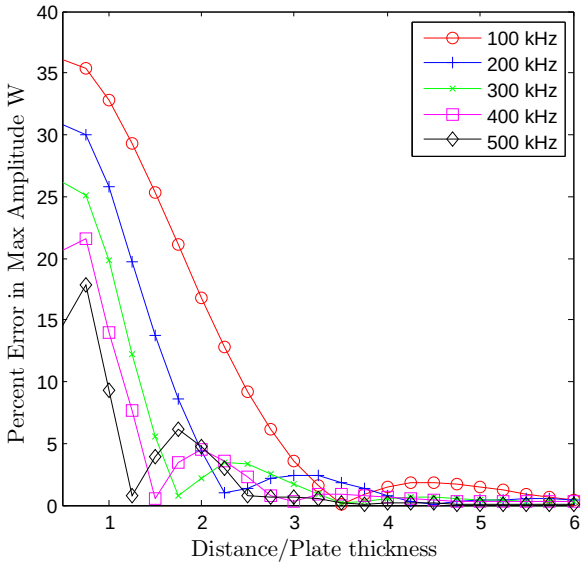

Figure 2.14: Percentage error in maximum amplitude of vertical displacement on the top surface of plate for various frequencies when only the positive real (propagating) modes are considered instead of 29 complex modes.

Table 2.1: Distance away from origin in terms of plate thicknesses when the vertical displacement due to complex, positive real and imaginary modes converge to that due to real positive (propagating) modes

Frequency [kHz]	Distance from origin/plate thickness	Difference in max amplitude (%)
100	5.5	0.91
200	4	0.82
300	3.5	0.14
400	3	0.3
500	2.5	0.72

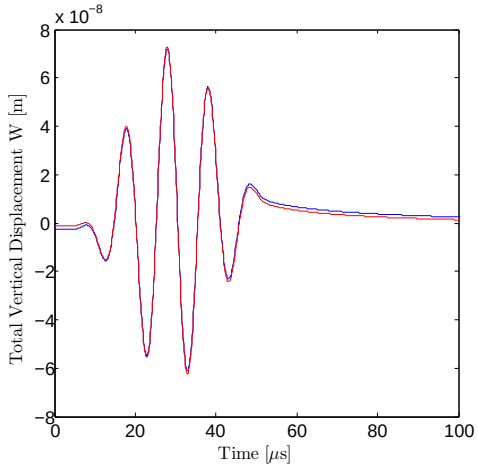

(a) $x = 11H$, $z = H$, $f = 100\,\text{kHz}$

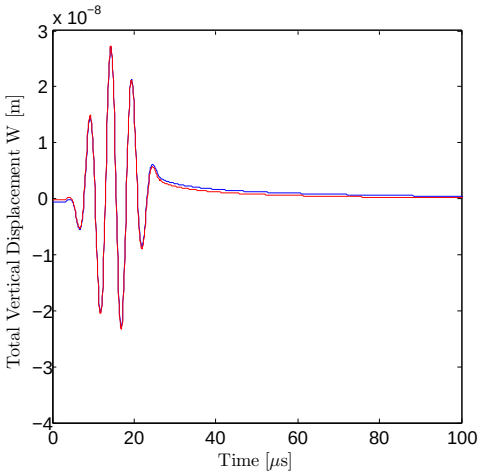

(b) $x = 8H$, $z = H$, $f = 200\,\text{kHz}$

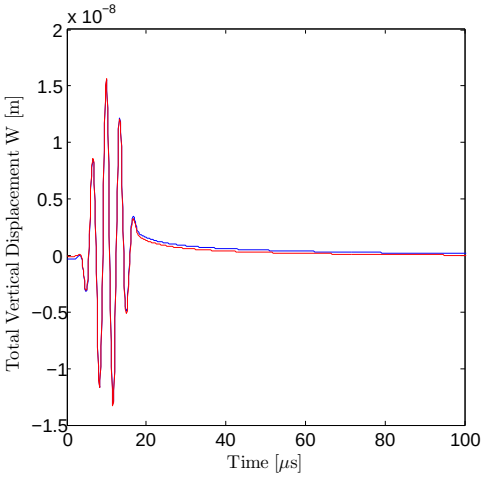

(c) $x = 7H$, $z = H$, $f = 300\,\text{kHz}$

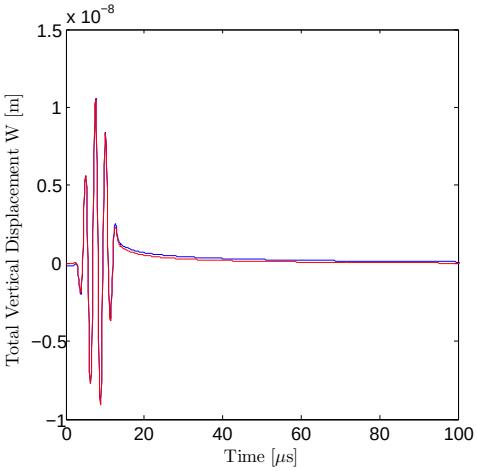

(d) $x = 6H$, $z = H$, $f = 400\,\text{kHz}$

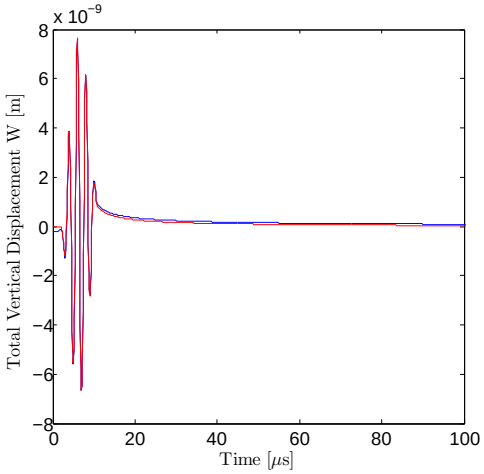

(e) $x = 5H$, $z = H$, $f = 500\,\text{kHz}$

Figure 2.15: Vertical displacements on the top surface of the aluminum plate. The blue curves are the vertical displacements computed using 29 modes including the positive real, imaginary and the complex modes. The red curves are the vertical displacements computed using only the positive real or the right propagating modes.

2.8 Power flow through a plate under applied vertical load

The power that is the rate of energy flow carried by the propagating Lamb waves through a cross section whose unit outward normal is along the positive x axis is calculated. The energy flow per time period ($T = \frac{2\pi}{\omega}$) of a wave in x direction is given by

$$\begin{aligned}\langle P\rangle = -\frac{1}{T}\int_0^T \Bigg(&\text{Real}\left(\sigma_{xx}\left(x,z,t\right)\right)\text{Real}\frac{\partial u\left(x,z,t\right)}{\partial t}\\ &+\text{Real}\left(\sigma_{xz}\left(x,z,t\right)\right)\text{Real}\frac{\partial w\left(x,z,t\right)}{\partial t}\Bigg)\,dt\end{aligned} \tag{2.131}$$

The displacements and the stresses are of the form

$$\begin{aligned}u\left(x,z,t\right) &= U\left(x,z,\omega\right)e^{i(kx-\omega t)}\\ &= \left(U_R + iU_I\right)e^{-i\omega t}\end{aligned} \tag{2.132}$$

$$\begin{aligned}\sigma(x,z,t) &= S(x,z,\omega)\, e^{i(kx-\omega t)} \\ &= (S_R + iS_I)\, e^{-i\omega t}\end{aligned} \tag{2.133}$$

In Equations (2.132,2.133) u, σ represent generic displacement and stress in the time (t) domain, while U_R, U_I, S_R, S_I represent the real and imaginary parts respectively of generic displacement and stress in the frequency (ω) domain. Using Euler's relation $e^{\pm i\omega t} = \cos(\omega t) \pm i \sin(\omega t)$

$$\begin{aligned}\text{Real}(\sigma)\,\text{Real}\left(\frac{\partial u}{\partial t}\right) =& \left(S_R\cos(\omega t) + S_I \sin(\omega t)\right)\left(-\omega U_R \sin(\omega t) + \omega U_I \cos(\omega t)\right) \\ =& \frac{\omega}{2}\left(S_I U_I - S_R U_R\right)\sin(2\omega t) \\ &+ \omega\left(S_R U_I \cos^2(\omega t) - S_I U_R \sin^2(\omega t)\right)\end{aligned} \tag{2.134}$$

Then,

$$\begin{aligned}-\frac{1}{T}\int_0^T \left(\text{Real}(\sigma)\,\text{Real}\left(\frac{\partial u}{\partial t}\right)\right) dt =& -\frac{\omega}{2\pi}\int_0^{\frac{2\pi}{\omega}} \frac{\omega}{2}\left(S_I U_I - S_R U_R\right)\sin(2\omega t)\, dt \\ &-\frac{\omega}{2\pi}\int_0^{\frac{2\pi}{\omega}} \omega\left(S_R U_I \cos^2(\omega t) - S_I U_R \sin^2(\omega t)\right) dt\end{aligned} \tag{2.135}$$

$$-\frac{1}{T}\int_0^T \left(\text{Real}(\sigma)\,\text{Real}\left(\frac{\partial u}{\partial t}\right)\right) dt = -\frac{\omega}{2}\left(S_R U_I - S_I U_R\right) \tag{2.136}$$

$$= -\frac{\omega}{2}\text{Imaginary}\left(US^*\right) \tag{2.137}$$

In the above equation, S^* denotes the complex conjugate of S.

Using the result from Equation (2.137) in Equation (2.131), the power flow in the x direction in the frequency domain is given by

$$\langle P(\omega)\rangle = -\frac{\omega}{2}\text{Imaginary}\left(US^*_{xx} + WS^*_{xz}\right) \tag{2.138}$$

The power flow through a cross section in the plate, whose normal is along the x axis is then obtained by integrating Equation (2.138) along the thickness of the

plate. For a plate with thickness $2H$ along the z axis, the power flow through a section is given by

$$\langle \overline{P}\,(\omega)\rangle = -\frac{\omega}{2}\int_{-H}^{H} \text{Imaginary}\left(US_{xx}^{*} + WS_{xz}^{*}\right)\,dz \tag{2.139}$$

For antisymmetric Lamb wave motion in a plate subjected to a vertical dynamic load on the top surface, the power flow through a cross section is given by

$$\langle \overline{P_{\mathrm{a}}}\,(\omega)\rangle = \langle \overline{P_{\mathrm{a1}}}\,(\omega)\rangle + \langle \overline{P_{\mathrm{a2}}}\,(\omega)\rangle \tag{2.140}$$

where,

$$\begin{aligned}
\langle \overline{P_{\mathrm{a1}}}\,(\omega)\rangle &= -\frac{\omega}{2}\int_{-H}^{H} \text{Imaginary}\left(US_{xx}^{*}\right)\,dz \\
&= \frac{\omega k_{\mathrm{a}}}{8\mu}\frac{|\overline{P}_0\,(k_{\mathrm{a}},\omega)|^2}{\left[R_{\mathrm{a}}'\,(k_{\mathrm{a}})\right]^2} \\
&\Bigg[\left(2k_{\mathrm{a}}^2 - k_2^2\right)^2\left(k_2^2 + 2\eta_{1\mathrm{a}}^2\right)\cosh^2\left(\eta_{2\mathrm{a}}H\right)\left(\frac{\sinh\left(2\eta_{1\mathrm{a}}H\right)}{2\eta_{1\mathrm{a}}} - H\right) - \\
&2\eta_{1\mathrm{a}}\eta_{2\mathrm{a}}\left(2k_{\mathrm{a}}^2 - k_2^2\right)\left(2k_{\mathrm{a}}^2 + k_2^2 + 2\eta_{1\mathrm{a}}^2\right)\cosh\left(\eta_{1\mathrm{a}}H\right)\cosh\left(\eta_{2\mathrm{a}}H\right) \\
&\left(\frac{\sinh\left(\left(\eta_{1\mathrm{a}} + \eta_{2\mathrm{a}}\right)H\right)}{\eta_{1\mathrm{a}} + \eta_{2\mathrm{a}}} - \frac{\sinh\left(\left(\eta_{1\mathrm{a}} - \eta_{2\mathrm{a}}\right)H\right)}{\eta_{1\mathrm{a}} - \eta_{2\mathrm{a}}}\right) + \\
&8\eta_{1\mathrm{a}}^2\eta_{2\mathrm{a}}^2 k_{\mathrm{a}}^2\cosh^2\left(\eta_{1\mathrm{a}}H\right)\left(\frac{\sinh\left(2\eta_{2\mathrm{a}}H\right)}{2\eta_{2\mathrm{a}}} - H\right)\Bigg]
\end{aligned} \tag{2.141}$$

and

$$\begin{aligned}
\langle \overline{P_{\mathrm{a2}}}\,(\omega)\rangle &= -\frac{\omega}{2}\int_{-H}^{H} \text{Imaginary}\left(WS_{xz}^{*}\right)\,dz \\
&= \frac{\omega k_{\mathrm{a}}\eta_{1\mathrm{a}}^2\left(2k_{\mathrm{a}}^2 - k_2^2\right)}{4\mu}\frac{|\overline{P}_0\,(k_{\mathrm{a}},\omega)|^2}{\left[R_{\mathrm{a}}'\,(k_{\mathrm{a}})\right]^2} \\
&\Bigg[\left(2k_{\mathrm{a}}^2 - k_2^2\right)\cosh^2\left(\eta_{2\mathrm{a}}H\right)\left(\frac{\sinh\left(2\eta_{1\mathrm{a}}H\right)}{2\eta_{1\mathrm{a}}} + H\right) - \\
&\left(4k_{\mathrm{a}}^2 - k_2^2\right)\cosh\left(\eta_{1\mathrm{a}}H\right)\cosh\left(\eta_{2\mathrm{a}}H\right) \\
&\left(\frac{\sinh\left(\left(\eta_{1\mathrm{a}} + \eta_{2\mathrm{a}}\right)H\right)}{\eta_{1\mathrm{a}} + \eta_{2\mathrm{a}}} + \frac{\sinh\left(\left(\eta_{1\mathrm{a}} - \eta_{2\mathrm{a}}\right)H\right)}{\eta_{1\mathrm{a}} - \eta_{2\mathrm{a}}}\right) + \\
&2k_{\mathrm{a}}^2\cosh^2\left(\eta_{1\mathrm{a}}H\right)\left(\frac{\sinh\left(2\eta_{2\mathrm{a}}H\right)}{2\eta_{2\mathrm{a}}} + H\right)\Bigg]
\end{aligned} \tag{2.142}$$

In Equations (2.141,2.142), U, W, S_{xx} and S_{xz} are the displacements and stresses for antisymmetric Lamb wave, given by Equations (2.101-2.105).

For symmetric Lamb wave motion in a plate subjected to a vertical dynamic load on the top surface, the power flow through a cross section is given by

$$\langle \overline{P_{\mathrm{s}}}\,(\omega)\rangle = \langle \overline{P_{\mathrm{s1}}}\,(\omega)\rangle + \langle \overline{P_{\mathrm{s2}}}\,(\omega)\rangle \tag{2.143}$$

where,

$$\begin{aligned}
\langle \overline{P_{\mathrm{s1}}}\,(\omega)\rangle &= -\frac{\omega}{2}\int_{-H}^{H} \text{Imaginary}\left(U S_{xx}^{*}\right)\, dz \\
&= \frac{\omega k_{\mathrm{s}}}{8\mu}\frac{\left|\overline{P}_0\left(k_{\mathrm{a}},\omega\right)\right|^2}{\left[R_{\mathrm{s}}'\left(k_{\mathrm{s}}\right)\right]^2} \\
&\Bigg[\left(2k_{\mathrm{s}}^2-k_2^2\right)^2\left(k_2^2+2\eta_{1\mathrm{s}}^2\right)\sinh^2\left(\eta_{2\mathrm{s}}H\right)\left(\frac{\sinh\left(2\eta_{1\mathrm{s}}H\right)}{2\eta_{1\mathrm{s}}}+H\right)- \\
&2\eta_{1\mathrm{s}}\eta_{2\mathrm{s}}\left(2k_{\mathrm{s}}^2-k_2^2\right)\left(2k_{\mathrm{s}}^2+k_2^2+2\eta_{1\mathrm{s}}^2\right)\sinh\left(\eta_{1\mathrm{s}}H\right)\sinh\left(\eta_{2\mathrm{s}}H\right) \\
&\left(\frac{\sinh\left(\left(\eta_{1\mathrm{s}}+\eta_{2\mathrm{s}}\right)H\right)}{\eta_{1\mathrm{as}}+\eta_{2\mathrm{s}}}+\frac{\sinh\left(\left(\eta_{1\mathrm{s}}-\eta_{2\mathrm{s}}\right)H\right)}{\eta_{1\mathrm{s}}-\eta_{2\mathrm{s}}}\right)+ \\
&8\eta_{1\mathrm{s}}^2\eta_{2\mathrm{s}}^2k_{\mathrm{s}}^2\sinh^2\left(\eta_{1\mathrm{s}}H\right)\left(\frac{\sinh\left(2\eta_{2\mathrm{s}}H\right)}{2\eta_{2\mathrm{s}}}+H\right)\Bigg]
\end{aligned} \tag{2.144}$$

and

$$\begin{aligned}
\langle \overline{P_{\mathrm{s2}}}\,(\omega)\rangle &= -\frac{\omega}{2}\int_{-H}^{H} \text{Imaginary}\left(W S_{xz}^{*}\right)\, dz \\
&= \frac{\omega k_{\mathrm{s}}\eta_{1\mathrm{s}}^2\left(2k_{\mathrm{s}}^2-k_2^2\right)}{4\mu}\frac{\left|\overline{P}_0\left(k_{\mathrm{s}},\omega\right)\right|^2}{\left[R_{\mathrm{s}}'\left(k_{\mathrm{s}}\right)\right]^2} \\
&\Bigg[\left(2k_{\mathrm{s}}^2-k_2\right)\sinh^2\left(\eta_{2\mathrm{s}}H\right)\left(\frac{\sinh\left(2\eta_{1\mathrm{s}}H\right)}{2\eta_{1\mathrm{s}}}-H\right)- \\
&\left(4k_{\mathrm{a}}^2-k_2^2\right)\sinh\left(\eta_{1\mathrm{s}}H\right)\sinh\left(\eta_{2\mathrm{s}}H\right) \\
&\left(\frac{\sinh\left(\left(\eta_{1\mathrm{s}}+\eta_{2\mathrm{s}}\right)H\right)}{\eta_{1\mathrm{s}}+\eta_{2\mathrm{s}}}-\frac{\sinh\left(\left(\eta_{1\mathrm{s}}-\eta_{2\mathrm{s}}\right)H\right)}{\eta_{1\mathrm{s}}-\eta_{2\mathrm{s}}}\right)+ \\
&2k_{\mathrm{s}}^2\sinh^2\left(\eta_{1\mathrm{s}}H\right)\left(\frac{\sinh\left(2\eta_{2\mathrm{s}}H\right)}{2\eta_{2\mathrm{s}}}-H\right)\Bigg]
\end{aligned} \tag{2.145}$$

In Equations (2.144,2.145), U, W, S_{xx} and S_{xz} are the displacements and stresses for symmetric Lamb wave, given by Equations (2.123-2.127).

2.9 Work done per cycle by the applied dynamic vertical load

The work done per cycle by the load applied on the top surface of the plate is calculated. The energy flowing across the region on the top surface in the vertical z direction in one cycle is calculated. It is averaged over the time period to given the power. The power flow is integrated over the width $(2a)$ of the region across which the vertical loading is applied, and is compared with the power flow across a vertical section derived already. Similar to before, the power flow in the frequency (ω) domain, in the z direction is now is given by

$$\langle P(\omega)\rangle = -\frac{\omega}{2}\text{Imaginary}\left(W(x,H,\omega)\,S_{zz}(x,H,\omega)\right) \tag{2.146}$$

where, $S_{zz}(x,H,\omega) = -P_0(\omega)$ the applied stress in frequency domain. Since, it is just real, there is no need of the complex conjugate.

Near the source, the contribution of the pure imaginary and the complex roots of the the dispersion equation needs to be added together with the contribution of the real positive roots. The vertical displacement $W(x,z,\omega)$ has the form (see Equations (2.102,2.124))

$$W(x,z,\omega) = i\frac{G(k,z,\omega)}{R'(k)}e^{ikx} \tag{2.147}$$

where $G(k,z,\omega)$ is an even function of k, while $R'(k)$ is an odd function of k.

For pure imaginary roots of the dispersion equations, of the form $k = ik$, the vertical displacement becomes

$$W(x,z,\omega) = i\frac{G(ik,z,\omega)}{R'(ik)}e^{-kx} \tag{2.148}$$

And since, $\frac{G(ik,z,\omega)}{R'(ik)}$ is an odd function of ik, it has the form

$$\frac{G(ik,z,\omega)}{R'(ik)} = iM(k,z,\omega) \tag{2.149}$$

where, $M(k,z,\omega)$ is a real function. Substituting Equation (2.149) in Equation (2.148)

$$W(x,z,\omega) = -M(k,z,\omega)\, e^{-kx} \tag{2.150}$$

which is real together with the applied stress on the top surface. Therefore from Equation (2.146), there is no contribution in the power flow through the top surface from the imaginary roots.

As stated before, the complex roots of the dispersion equations come in pairs of the form $k = a + ib, -a + ib$ in the upper half of the complex k plane. For the complex root $k = a + ib$, the vertical displacement becomes

$$\begin{aligned} W(x,z,\omega) &= i\frac{G(a+ib,z,\omega)}{R'(a+ib)} e^{iax} e^{-bx} \\ &= i\left(r(a,b) + is(a,b)\right) e^{iax} e^{-bx} \qquad (2.151) \\ &= -\left(s(a,b)\cos(ax) + r(a,b)\sin(ax)\right) e^{-bx} \\ &\quad + i\left(r(a,b)\cos(ax) - s(a,b)\sin(ax)\right) e^{-bx} \qquad (2.152) \end{aligned}$$

where $r(a,b)$ and $s(a,b)$ are real functions. And since, $\frac{G(a+ib,z,\omega)}{R'(a+ib)}$ is a real and odd function of $k = a+ib$, the vertical displacement from the complex root $k = -a+ib$ becomes

$$\begin{aligned} W(x,z,\omega) &= i\frac{G(-a+ib,z,\omega)}{R'(-a+ib)} e^{-iax} e^{-bx} \\ &= i\left(-r(a,b) + is(a,b)\right) e^{-iax} e^{-bx} \qquad (2.153) \\ &= -\left(s(a,b)\cos(ax) + r(a,b)\sin(ax)\right) e^{-bx} \\ &\quad - i\left(r(a,b)\cos(ax) - s(a,b)\sin(ax)\right) e^{-bx} \qquad (2.154) \end{aligned}$$

The contribution to power flow through the top surface due to the root $k = a+ib$, then becomes, from Equation (2.146,2.152)

$$\langle P_1(\omega)\rangle = \frac{\omega}{2}\left(r(a,b)\cos(ax) - s(a,b)\sin(ax)\right) e^{-bx} P_0(\omega) \tag{2.155}$$

And the contribution to power flow through the top surface due to the root $k = -a + ib$, then becomes, from Equation (2.146,2.154)

$$\langle P_2(\omega)\rangle = -\frac{\omega}{2}\left(r(a,b)\cos(ax) - s(a,b)\sin(ax)\right)e^{-bx}P_0(\omega) \tag{2.156}$$

From Equations, (2.155) and (2.156), $\langle P_1(\omega)\rangle$ is negative of $\langle P_2(\omega)\rangle$ and their sum is zero. Therefore, the complex roots of the dispersion equation do not have any net contribution to the power flow through the top surface of the plate.

Therefore, only the real roots of the dispersion equations contribute to the energy flow per time period, in the vertical direction through the top surface. The power flowing vertically through the region on which the loading is applied, is obtained by integrating Equation (2.146) along the length of the region from $x = -a$ to $x = a$. It consists of antisymmetric and symmetric components from the real positive roots of the antisymmetric and symmetric dispersion equations.

The power flow through the top surface due to the right propagating antisymmetric Lamb wave motion in a plate subjected to uniform vertical load is given by

$$\langle \overline{P}_{aH}(\omega)\rangle = \frac{\omega k_2^2 \eta_{1a}}{4\mu}\frac{\overline{P}_0(k_a,\omega)}{R'_a(k_a)}P_0(\omega)\frac{\sin(k_a a)}{k_a}\cosh(\eta_{1a}H)\cosh(\eta_{2a}H) \tag{2.157}$$

The power flow through the top surface due to the right propagating symmetric Lamb wave motion in a plate subjected to uniform vertical load is given by

$$\langle \overline{P}_{sH}(\omega)\rangle = \frac{\omega k_2^2 \eta_{1s}}{4\mu}\frac{\overline{P}_0(k_s,\omega)}{R'_s(k_s)}P_0(\omega)\frac{\sin(k_s a)}{k_s}\sinh(\eta_{1s}H)\sinh(\eta_{2s}H) \tag{2.158}$$

The power flow through the top surface due to the right propagating antisymmetric Lamb wave motion in a plate subjected to a linearly varying load is given by

$$\langle \overline{P}_{aH}(\omega)\rangle = -i\frac{\omega k_2^2 \eta_{1a}}{4\mu}\frac{\overline{P}_0(k_a,\omega)}{R'_a(k_a)}P_0(\omega)\left(\frac{\cos(k_a a)}{k_a} - \frac{\sin(k_a a)}{k_a^2 a}\right)\cosh(\eta_{1a}H)\cosh(\eta_{2a}H) \tag{2.159}$$

The power flow through the top surface due to the right propagating symmetric Lamb wave motion in a plate subjected to a linearly varying load is given by

$$\langle \overline{P}_{sH}(\omega) \rangle = -i\frac{\omega k_2^2 \eta_{1s}}{4\mu} \frac{\overline{P}_0(k_s, \omega)}{R_s'(k_s)} P_0(\omega) \left(\frac{\cos(k_s a)}{k_s} - \frac{\sin(k_s a)}{k_s^2 a} \right) \frac{}{\sinh(\eta_{1s} H) \sinh(\eta_{2s} H)} \tag{2.160}$$

The power flow through the top surface due to the left and the right propagating Lamb waves is twice the value given by Equations (2.157,2.158) for uniform vertical load and by Equations (2.159,2.160) for a linearly varying rocking load . And this power flow through the top surface induced by the applied load equals the power flow through two vertical sections left and right of the origin, which again is twice that given by Equations (2.141-2.146). Figure (2.16) compares the above two power flow spectrum in a 1.78 mm thick aluminum plate subjected to a uniform vertical load of intensity 1 N/m over a 1 mm wide region on its top surface. The Young's modulus of the aluminum plate is 69 GPa and its Poisson's ratio is 0.3269. Figure (2.17) compares the above two power flow spectrum in a 1.78 mm thick aluminum plate subjected to a linearly varying load with intensity varying from $-\sqrt{3}$ N/m to $\sqrt{3}$ N/m over a 1 mm wide region on its top surface. The Young's modulus of the aluminum plate is 69 GPa and its Poisson's ratio is 0.3269.

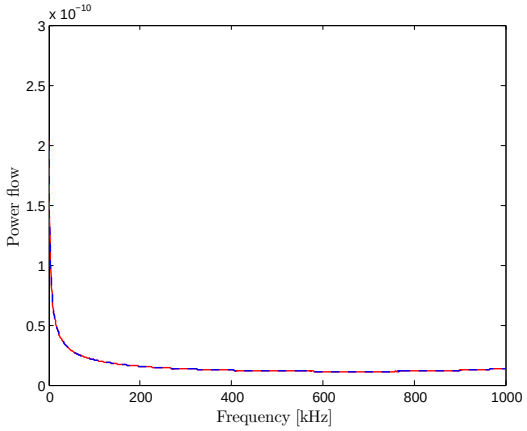

(a) Power flow spectrum

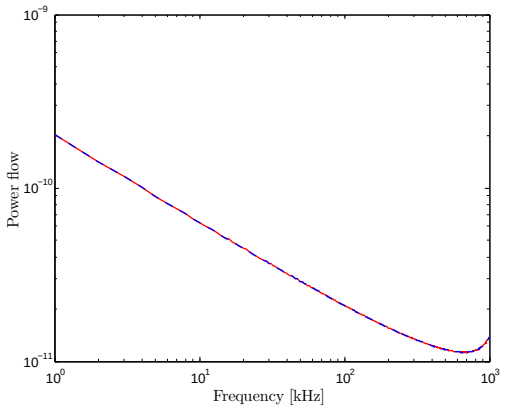

(b) Power flow specttrum in log scale

Figure 2.16: Power flow spectrum due to Lamb waves in a plate subjected to uniform vertical load on its top surface. The red solid curve denotes power flow through vertical cross sections left and right of the origin. The dashed blue curve denotes the power flow through the region on the top surface on which the external load is applied.

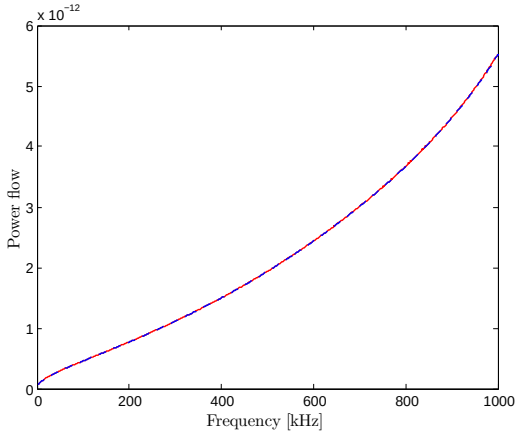

(a) Power flow spectrum

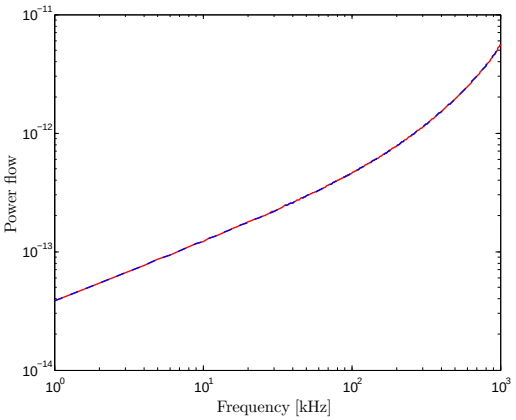

(b) Power flow spectrum in log scale

Figure 2.17: Power flow spectrum due to Lamb waves in a plate subjected to a linearly varying load on its top surface. The red solid curve denotes power flow through vertical cross sections left and right of the origin. The dashed blue curve denotes the power flow through the region on the top surface on which the external load is applied.

2.10 Various vertical loadings applied on the top surface of a plate

The $\overline{P}_0(k,\omega)$ in the above analysis, denotes the the double Fourier transform of the time dependent applied load $p_0(x,t)$. Next, the different $\overline{P}_0(k,\omega)$ that appear for different vertical surface loads and should be used in the formulas for the displacement and stress fields due to the symmetric and antisymmetric Lamb waves are given.

2.10.1 Uniform vertical load

For a vertical loading $p(x,t)$ with intensity $\hat{p}(x)$ over a length $2a$ on the top surface of the plate, centered at the vertical z-axis,

$$p(x,t) = \hat{p}(x) f(t) \tag{2.161}$$

where $f(t)$ is the time-dependence of the load. For an uniform intensity p_0 over a length $2a$ on the top surface of the plate, centered at the vertical z-axis,

$$\hat{p}(x) = p_0 \qquad |x| \leq a \tag{2.162}$$

$$= 0 \qquad |x| > a \tag{2.163}$$

$$\begin{aligned} P_0(x,\omega) &= \int_0^\infty p(x,t)\, e^{i\omega t}\, dt \qquad |x| \leq a, t > 0 \\ &= p_0 \int_0^\infty f(t)\, e^{i\omega t}\, dt \end{aligned} \tag{2.164}$$

$$\overline{P}_0(k,\omega) = \int_{-\infty}^{\infty} P_0(x,\omega)\, e^{-ikx}\, dx \tag{2.165}$$

$$= \int_0^{\infty} \left[\int_{-a}^{a} p_0 e^{-ikx}\, dx \right] f(t)\, e^{i\omega t}\, dt$$

$$= \int_0^{\infty} \left[-\frac{ip_0}{k} \left(e^{ika} - e^{-ika} \right) \right] f(t)\, e^{i\omega t}\, dt$$

$$= \int_0^{\infty} \frac{2p_0 \sin(ka)}{k} f(t)\, e^{i\omega t}\, dt \tag{2.166}$$

2.10.2 Rocking load

For a continuous linearly varying load (see Figure (2.18)) with intensity $-p_0$ at $x = -a$ to intensity p_0 at $x = a$ on the top surface of the plate, centered at the vertical z-axis

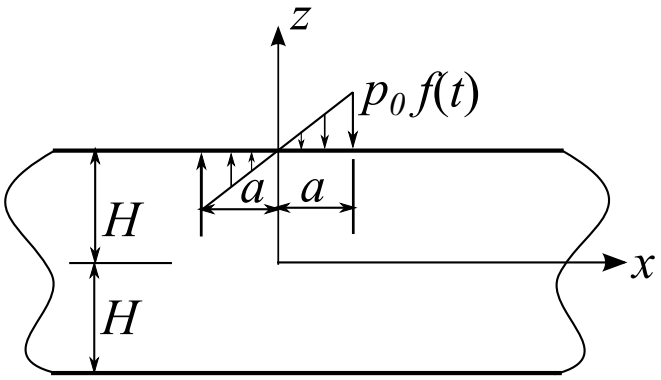

Figure 2.18: Linearly varying (rocking) load

$$\hat{p}(x) = \frac{p_0 x}{a} \qquad |x| \le a \tag{2.167}$$

$$= 0 \qquad |x| > a \tag{2.168}$$

$$P_0(x,\omega) = \int_{-\infty}^{\infty} \frac{p_0 x}{a} f(t)\, e^{i\omega t}\, dt \qquad |x| \le a \tag{2.169}$$

$$\overline{P}_0(k,\omega) = \int_{-\infty}^{\infty} P_0(x,\omega)\, e^{-ikx}\, dx \qquad |x| \le a \tag{2.170}$$

$$= \int_0^{\infty} \left[\int_{-a}^{a} \frac{p_0 x}{a} e^{-ikx}\, dx \right] f(t)\, e^{i\omega t}\, dt$$

$$= \int_0^{\infty} \frac{p_0}{a} \left[x \frac{e^{-ikx}}{-ik} \bigg|_{-a}^{a} - \int_a^a \frac{e^{-ikx}}{-ik} dx \right] f(t)\, e^{i\omega t}\, dt$$

$$= \int_0^{\infty} \left[-\frac{p_0}{ik} \left(e^{ika} + e^{-ika} \right) + \frac{p_0}{k^2 a} \left(e^{-ika} - e^{ika} \right) \right] f(t)\, e^{i\omega t}\, dt$$

$$= \int_0^{\infty} \frac{2ip_0}{k} \left[\cos(ka) - \frac{\sin(ka)}{ka} \right] f(t)\, e^{i\omega t}\, dt \tag{2.171}$$

2.11 Antisymmetric Lamb wave propagation under dynamic shear load on the top surface of a plate

A described in Section (2.4), Figure (2.19) shows the the physical problem with the applied shear load of intensity p_0 on the top surface of the plate, resolved into the antisymmetric and symmetric loading of intensity $\frac{p_0}{2}$ applied on the top and bottom surfaces of the plate

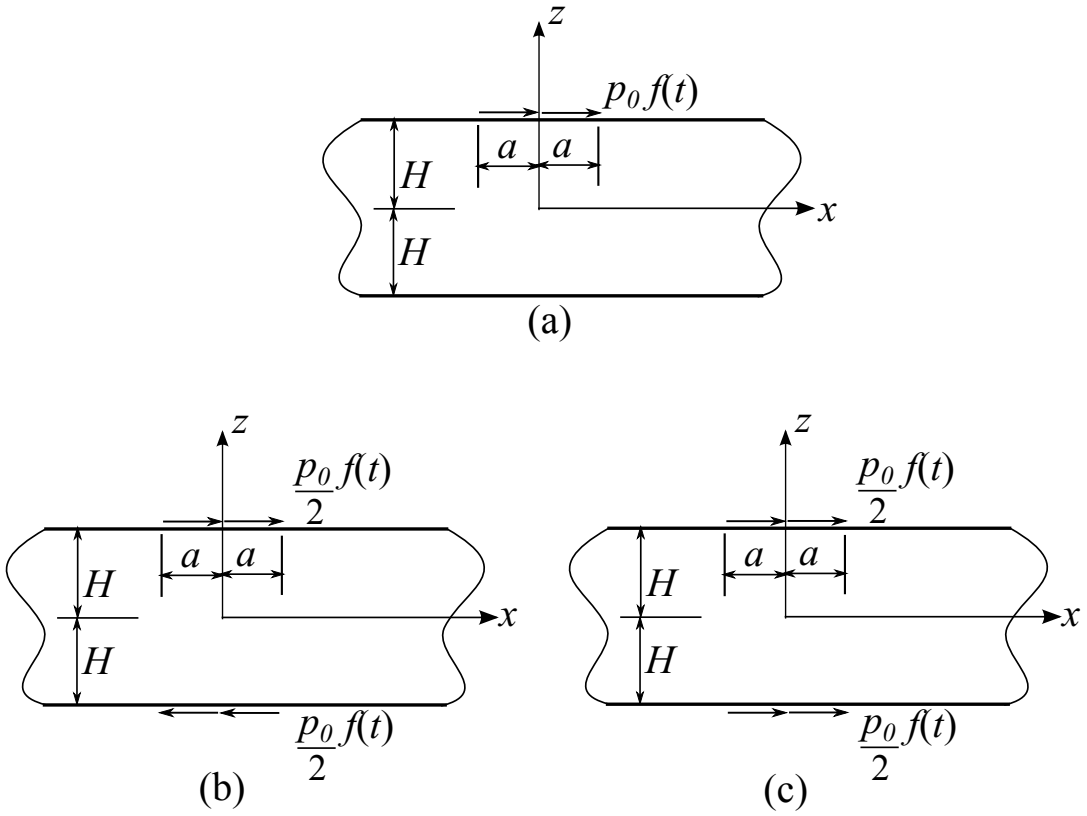

Figure 2.19: (a) Applied loading (b) Antisymmetric loading component and (c) Symmetric loading component in a plate

From Equations (2.66, 2.67), zero normal stress at $z = H$ gives,

$$\overline{S}_{zz}(k, H, \omega) = \left(2k^2 - k_2^2\right)\overline{A}_2 \sinh(\eta_1 H) + 2k^2 \overline{A}_4 \sinh(\eta_2 H) = 0 \tag{2.172}$$

which gives,

$$\overline{A}_4 = -\frac{(2k^2 - k_2^2)\sinh(\eta_1 H)}{2k^2 \sinh(\eta_2 H)}\overline{A}_2 \tag{2.173}$$

At $z = H$, the applied shear load gives,

$$\overline{S}_{xz}(k, H, \omega) = -\frac{\overline{P}_0(k, \omega)}{2} \tag{2.174}$$

which gives,

$$\frac{\mu}{\eta_2}\left[2\eta_1\eta_2\overline{A}_2 \cosh(\eta_1 H) + \left(2k^2 - k_2^2\right)\overline{A}_4 \cosh(\eta_2 H)\right] = \frac{\overline{P}_0}{2} \tag{2.175}$$

Substituting $\overline{A}_4$ from Equation (2.173) into Equation (2.175)

$$\overline{A}_2 = -\frac{k^2 \eta_2 \sinh(\eta_2 H)}{\mu R_{\mathrm{a}}(k)} \overline{P}_0(k,\omega) \tag{2.176}$$

where, $R_{\mathrm{a}}(k)$ is the antisymmetric Lamb wave denominator and is given by

$$R_{\mathrm{a}}(k) = \left(2k^2 - k_2^2\right)^2 \sinh(\eta_1 H)\cosh(\eta_2 H) - 4k^2 \eta_1 \eta_2 \cosh(\eta_1 H)\sinh(\eta_2 H) \tag{2.177}$$

Substituting $\overline{A}_2$ from Equation (2.176) into Equation (2.173)

$$\overline{A}_4 = \frac{\left(2k^2 - k_2^2\right)\eta_2 \sinh(\eta_1 H)}{2\mu R_{\mathrm{a}}(k)} \overline{P}_0(k,\omega) \tag{2.178}$$

Using the above values of $\overline{A}_2$ and $\overline{A}_4$, the displacements and the stresses in the plate due to the antisymmetric Lamb wave in the frequency domain are given by

$$\overline{U}(k,z,\omega) = \frac{\eta_2 \overline{P}_0(k,\omega)}{2\mu R_{\mathrm{a}}(k)} \Big[\left(2k^2 - k_2^2\right)\sinh(\eta_1 H)\sinh(\eta_2 z) - 2k^2 \sinh(\eta_1 z)\sinh(\eta_2 H) \Big] \tag{2.179}$$

$$\overline{W}(k,z,\omega) = \frac{ik\overline{P}_0(k,\omega)}{2\mu R_{\mathrm{a}}(k)} \Big[2\eta_1\eta_2 \cosh(\eta_1 z)\sinh(\eta_2 H) - \left(2k^2 - k_2^2\right)\sinh(\eta_1 H)\cosh(\eta_2 z) \Big] \tag{2.180}$$

$$\overline{S}_{xx}(k,z,\omega) = \frac{ik\eta_2 \overline{P}_0(k,\omega)}{R_{\mathrm{a}}(k)} \Big[\left(2k^2 - k_2^2\right)\sinh(\eta_1 H)\sinh(\eta_2 z) - \left(k_2^2 + 2\eta_1^2\right)\sinh(\eta_1 z)\sinh(\eta_2 H) \Big] \tag{2.181}$$

$$\overline{S}_{zz}(k,z,\omega) = \frac{ik\eta_2 \left(2k^2 - k_2^2\right)\overline{P}_0(k,\omega)}{R_{\mathrm{a}}(k)} \Big[\sinh(\eta_1 z)\sinh(\eta_2 H) - \sinh(\eta_1 H)\sinh(\eta_2 z) \Big] \tag{2.182}$$

$$\overline{S}_{xz}(k,z,\omega) = \frac{\overline{P}_0(k,\omega)}{2R_{\mathrm{a}}(k)}\Big[\left(2k^2-k_2^2\right)^2\sinh(\eta_1 H)\cosh(\eta_2 z) - 4\eta_1\eta_2 k^2\cosh(\eta_1 z)\sinh(\eta_2 H)\Big] \tag{2.183}$$

The inverse Fourier transform with respect to the wavenumber k

$$F(x,z,\omega) = \frac{1}{2\pi}\int_{-\infty}^{\infty}\overline{F}(k,z,\omega)\,e^{ikx}dk \tag{2.184}$$

gives the field variables in x and the frequency (ω) domain. The integral in Equation (2.182) has simple poles at the roots of the antisymmetric Lamb wave dispersion equation obtained by setting $R_{\mathrm{a}}(k) = 0$.

Figure (2.8) shows a schematic of the roots in the complex k plane. There are real, imaginary and complex roots. The closed contour in the complex k plane with the anticlockwise direction it is traversed is indicated. To satisfy the radiation boundary condition at $x = \infty$, that is no incoming waves from infinity, the negative real poles are avoided in the contour. All real, imaginary and complex poles in the upper half complex k plane are enclosed in the contour. The field in Equation (2.184) is then given by

$$F(x,z,\omega) = \frac{1}{2\pi}2\pi i\,(\text{Sum of the residues at the poles } k_{\mathrm{a}} \text{ of } \overline{F}(k,z,\omega)\,e^{ikx}) \tag{2.185}$$

where, $F(x,z,\omega)$ is the field variable due to antisymmetric Lamb waves. k_{a} are the roots of the antisymmetric Lamb wave dispersion equation. The displacements and the stresses can be written as

$$U(x,z,\omega) = \sum_{k_{\mathrm{a}}}\frac{i\eta_{2\mathrm{a}}\overline{P}_0(k_{\mathrm{a}},\omega)}{2\mu R'_{\mathrm{a}}(k_{\mathrm{a}})}\Big[\left(2k_{\mathrm{a}}^2-k_2^2\right)\sinh(\eta_{1\mathrm{a}}H)\sinh(\eta_{2\mathrm{a}}z) - 2k_{\mathrm{a}}^2\sinh(\eta_{1\mathrm{a}}z)\sinh(\eta_{2\mathrm{a}}H)\Big]e^{ik_{\mathrm{a}}x} \tag{2.186}$$

$$W(x,z,\omega) = \sum_{k_a} -\frac{k_a \overline{P}_0(k_a,\omega)}{2\mu R'_a(k_a)} \Big[2\eta_{1a}\eta_{2a}\cosh(\eta_{1a}z)\sinh(\eta_{2a}H) - \left(2k_a^2 - k_2^2\right)\sinh(\eta_{1a}H)\cosh(\eta_{2a}z) \Big] e^{ik_a x} \tag{2.187}$$

$$S_{xx}(x,z,\omega) = \sum_{k_a} -\frac{k_a \eta_{2a} \overline{P}_0(k_a,\omega)}{R'_a(k_a)} \Big[\left(2k_a^2 - k_2^2\right)\sinh(\eta_{1a}H)\sinh(\eta_{2a}z) - \left(k_2^2 + 2\eta_{1a}^2\right)\sinh(\eta_{1a}z)\sinh(\eta_{2a}H) \Big] e^{ik_a x} \tag{2.188}$$

$$S_{zz}(x,z,\omega) = \sum_{k_a} -\frac{k_a \eta_{2a}\left(2k_a^2 - k_2^2\right)\overline{P}_0(k_a,\omega)}{R'_a(k_a)} \Big[\sinh(\eta_{1a}z)\sinh(\eta_{2a}H) - \sinh(\eta_{1a}H)\sinh(\eta_{2a}z) \Big] e^{ik_a x} \tag{2.189}$$

$$S_{xz}(x,z,\omega) = \sum_{k_a} \frac{i\overline{P}_0(k_a,\omega)}{2R'_a(k_a)} \Big[\left(2k_a^2 - k_2^2\right)^2 \sinh(\eta_{1a}H)\cosh(\eta_{2a}z) - 4\eta_{1a}\eta_{2a}k_a^2\cosh(\eta_{1a}z)\sinh(\eta_{2a}H) \Big] e^{ik_a x} \tag{2.190}$$

where it is understood that the right hand side of Equations (2.186-2.190) are summed over for all positive real, imaginary and complex values of k_a. $R'_a(k_a)$ is the derivative of $R_a(k)$, the antisymmetric Lamb wave denominator with respect to k, evaluated at the roots of the antisymmetric Lamb wave dispersion equation k_a and is given by Equation(2.106). Like before, the antisymmetric Lamb waves are the propagating waves given by residues at the real positive roots.

2.12 Symmetric Lamb wave propagation under dynamic shear load on the top surface of a plate

From Equations (2.59, 2.60), zero normal stress at $z = H$ gives,

$$\overline{S}_{zz}(k,H,\omega) = \left(2k^2 - k_2^2\right)\overline{A}_1\cosh(\eta_1 H) + 2k^2\overline{A}_3\cosh(\eta_2 H) = 0 \tag{2.191}$$

which gives,

$$\overline{A}_3 = -\frac{\left(2k^2 - k_2^2\right)\cosh\left(\eta_1 H\right)}{2k^2\cosh\left(\eta_2 H\right)}\overline{A}_1 \tag{2.192}$$

At $z = H$, the applied shear load gives,

$$\overline{S}_{xz}\left(k, H, \omega\right) = \frac{\overline{P}_0\left(k, \omega\right)}{2} \tag{2.193}$$

which gives,

$$\frac{\mu}{\eta_2}\left[2\eta_1\eta_2\overline{A}_1\sinh\left(\eta_1 H\right) + \left(2k^2 - k_2^2\right)\overline{A}_3\sinh\left(\eta_2 H\right)\right] = \frac{\overline{P}_0}{2} \tag{2.194}$$

Substituting $\overline{A}_3$ from Equation (2.192) into Equation (2.194)

$$\overline{A}_1 = -\frac{k^2\eta_2\cosh\left(\eta_2 H\right)}{\mu R_{\mathrm{s}}\left(k\right)}\overline{P}_0\left(k, \omega\right) \tag{2.195}$$

where, $R_{\mathrm{s}}\left(k\right)$ is the symmetric Lamb wave denominator and is given by

$$R_{\mathrm{s}}\left(k\right) = \left(2k^2 - k_2^2\right)^2\cosh\left(\eta_1 H\right)\sinh\left(\eta_2 H\right) - 4k^2\eta_1\eta_2\sinh\left(\eta_1 H\right)\cosh\left(\eta_2 H\right) \tag{2.196}$$

Substituting $\overline{A}_1$ from Equation (2.195) into Equation (2.192)

$$\overline{A}_3 = \frac{\left(2k^2 - k_2^2\right)\eta_2\cosh\left(\eta_1 H\right)}{2\mu R_{\mathrm{s}}\left(k\right)}\overline{P}_0\left(k, \omega\right) \tag{2.197}$$

Using the above values of $\overline{A}_1$ and $\overline{A}_3$, the displacements and the stresses in the plate due to the symmetric Lamb wave in the frequency domain are given by

$$\overline{U}\left(k, z, \omega\right) = \frac{\eta_2\overline{P}_0\left(k, \omega\right)}{2\mu R_{\mathrm{s}}\left(k\right)}\Bigg[\left(2k^2 - k_2^2\right)\cosh\left(\eta_1 H\right)\cosh\left(\eta_2 z\right) - 2k^2\cosh\left(\eta_1 z\right)\cosh\left(\eta_2 H\right)\Bigg] \tag{2.198}$$

$$\overline{W}\left(k, z, \omega\right) = \frac{ik\overline{P}_0\left(k, \omega\right)}{2\mu R_{\mathrm{s}}\left(k\right)}\Bigg[2\eta_1\eta_2\sinh\left(\eta_1 z\right)\cosh\left(\eta_2 H\right) - \left(2k^2 - k_2^2\right)\cosh\left(\eta_1 H\right)\sinh\left(\eta_2 z\right)\Bigg] \tag{2.199}$$

$$\overline{S}_{xx}(k,z,\omega) = \frac{ik\eta_2\overline{P}_0(k,\omega)}{R_s(k)}\Big[\left(2k^2-k_2^2\right)\cosh(\eta_1 H)\cosh(\eta_2 z) - \left(k_2^2+2\eta_1^2\right)\cosh(\eta_1 z)\cosh(\eta_2 H)\Big] \tag{2.200}$$

$$\overline{S}_{zz}(k,z,\omega) = \frac{ik\eta_2\left(2k^2-k_2^2\right)\overline{P}_0(k,\omega)}{R_s(k)}\Big[\cosh(\eta_1 z)\cosh(\eta_2 H) - \cosh(\eta_1 H)\cosh(\eta_2 z)\Big] \tag{2.201}$$

$$\overline{S}_{xz}(k,z,\omega) = \frac{\overline{P}_0(k,\omega)}{2R_s(k)}\Big[\left(2k^2-k_2^2\right)^2\cosh(\eta_1 H)\sinh(\eta_2 z) - 4\eta_1\eta_2 k^2\sinh(\eta_1 z)\cosh(\eta_2 H)\Big] \tag{2.202}$$

The inverse Fourier transform with respect to the wavenumber k

$$F(x,z,\omega) = \frac{1}{2\pi}\int_{-\infty}^{\infty}\overline{F}(k,z,\omega)\,e^{ikx}\,dk \tag{2.203}$$

gives the field variables in x and the frequency (ω) domain. The integral in Equation (2.203) has simple poles at the roots of the symmetric Lamb wave dispersion equation obtained by equating $R_s(k) = 0$.

Figure (2.8) shows a schematic of the roots in the complex k plane. There are real, imaginary and complex roots. The closed contour in the complex k plane with the anticlockwise direction it is traversed is indicated. To satisfy the radiation boundary condition at $x = \infty$, that is no incoming waves from infinity, the negative real poles are avoided in the contour. All real, imaginary and complex poles in the upper half complex k plane are enclosed in the contour. The field in Equation (2.203) is then given by

$$F(x,z,\omega) = \frac{1}{2\pi}2\pi i\,(\text{Sum of the residues at the poles } k_s \text{ of } \overline{F}(k,z,\omega)\,e^{ikx}) \tag{2.204}$$

where, $F(x,z,\omega)$ is the field variable due to symmetric Lamb waves. k_{s} is the root of the symmetric Lamb wave dispersion equation. The displacements and the stresses can be written as

$$U(x,z,\omega) = \sum_{k_{\mathrm{s}}} \frac{i\eta_{2\mathrm{s}}\overline{P}_0(k_{\mathrm{s}},\omega)}{2\mu R_{\mathrm{s}}'(k_{\mathrm{s}})} \Big[\left(2k_{\mathrm{s}}^2 - k_2^2\right)\cosh(\eta_{1\mathrm{s}}H)\cosh(\eta_{2\mathrm{s}}z) - 2k_{\mathrm{s}}^2\cosh(\eta_{1\mathrm{s}}z)\cosh(\eta_{2\mathrm{s}}H)\Big] e^{ik_{\mathrm{s}}x} \tag{2.205}$$

$$W(x,z,\omega) = \sum_{k_{\mathrm{s}}} -\frac{k_{\mathrm{s}}\overline{P}_0(k_{\mathrm{s}},\omega)}{2\mu R_{\mathrm{s}}'(k_{\mathrm{s}})} \Big[2\eta_{1\mathrm{s}}\eta_{2\mathrm{s}}\sinh(\eta_{1\mathrm{s}}z)\cosh(\eta_{2\mathrm{s}}H) - \left(2k_{\mathrm{s}}^2 - k_2^2\right)\cosh(\eta_{1\mathrm{s}}H)\cosh(\eta_{2\mathrm{s}}z)\Big] e^{ik_{\mathrm{s}}x} \tag{2.206}$$

$$S_{xx}(x,z,\omega) = \sum_{k_{\mathrm{s}}} -\frac{k_{\mathrm{s}}\eta_{2\mathrm{s}}\overline{P}_0(k_{\mathrm{s}},\omega)}{R_{\mathrm{s}}'(k_{\mathrm{s}})} \Big[\left(2k_{\mathrm{s}}^2 - k_2^2\right)\cosh(\eta_{1\mathrm{s}}H)\cosh(\eta_{2\mathrm{s}}z) - \left(k_2^2 + 2\eta_{1\mathrm{s}}^2\right)\cosh(\eta_{1\mathrm{s}}z)\cosh(\eta_{2\mathrm{s}}H)\Big] e^{ik_{\mathrm{s}}x} \tag{2.207}$$

$$S_{zz}(x,z,\omega) = \sum_{k_{\mathrm{s}}} -\frac{k_{\mathrm{s}}\eta_{2\mathrm{s}}\left(2k_{\mathrm{s}}^2 - k_2^2\right)\overline{P}_0(k_{\mathrm{s}},\omega)}{R_{\mathrm{s}}'(k_{\mathrm{s}})} \Big[\cosh(\eta_{1\mathrm{s}}z)\cosh(\eta_{2\mathrm{s}}H) - \cosh(\eta_{1\mathrm{s}}H)\cosh(\eta_{2\mathrm{s}}z)\Big] e^{ik_{\mathrm{s}}x} \tag{2.208}$$

$$S_{xz}(x,z,\omega) = \sum_{k_{\mathrm{s}}} \frac{i\overline{P}_0(k_{\mathrm{s}},\omega)}{2R_{\mathrm{s}}'(k_{\mathrm{s}})} \Big[\left(2k_{\mathrm{s}}^2 - k_2^2\right)^2\cosh(\eta_{1\mathrm{s}}H)\sinh(\eta_{2\mathrm{s}}z) - 4\eta_{1\mathrm{s}}\eta_{2\mathrm{s}}k_{\mathrm{s}}^2\sinh(\eta_{1\mathrm{a}}z)\cosh(\eta_{2\mathrm{s}}H)\Big] e^{ik_{\mathrm{s}}x} \tag{2.209}$$

where it is understood that the right hand side of Equations (2.205-2.209) are summed over for all positive real, imaginary and complex values of k_{s}. $R_{\mathrm{s}}'(k_{\mathrm{s}})$ is the derivative of $R_{\mathrm{s}}(k)$, the symmetric Lamb wave denominator with respect to k, evaluated at the roots of the symmetric Lamb wave dispersion equation k_{s} and is given by Equation (2.128). Like before, the symmetric Lamb waves are the propagating waves given by residues at the real positive roots.

2.13 Power flow through a plate under applied shear load

The power flow through a cross section in the plate, whose normal is along the x axis is then obtained by integrating Equation (2.138) along the thickness of the plate. For a plate with thickness $2H$ along the z axis, the power flow though a section is given by

$$\langle \overline{P}\,(\omega)\rangle = -\frac{\omega}{2}\int_{-H}^{H} \text{Imaginary}\left(US_{xx}^{*} + WS_{xz}^{*}\right)\,dz \tag{2.210}$$

For antisymmetric Lamb wave motion in a plate subjected to a dynamic shear load on the top surface, the power flow through a cross section is given by

$$\langle \overline{P_{\text{a}}}\,(\omega)\rangle = \langle \overline{P_{\text{a1}}}\,(\omega)\rangle + \langle \overline{P_{\text{a2}}}\,(\omega)\rangle \tag{2.211}$$

where,

$$\begin{aligned}
\langle \overline{P_{\text{a1}}}\rangle = \frac{\omega\eta_{2\text{a}}^{2}k_{\text{a}}}{4\mu}\frac{|\overline{P}_{0}\,(k_{\text{a}},\omega)|^{2}}{\left[R_{\text{a}}'\,(k_{\text{a}})\right]^{2}} \\
\Bigg[\left(2k_{\text{a}}^{2}-k_{2}^{2}\right)^{2}\sinh^{2}\left(\eta_{1\text{a}}H\right)\left(\frac{\sinh\left(2\eta_{2\text{a}}H\right)}{2\eta_{2\text{a}}}-H\right)- \\
\left(2k_{\text{a}}^{2}-k_{2}^{2}\right)\left(2k_{\text{a}}^{2}+k_{2}^{2}+2\eta_{1\text{a}}^{2}\right)\sinh\left(\eta_{1\text{a}}H\right)\sinh\left(\eta_{2\text{a}}H\right) \\
\left(\frac{\sinh\left(\left(\eta_{1\text{a}}+\eta_{2\text{a}}\right)H\right)}{\eta_{1\text{a}}+\eta_{2\text{a}}}-\frac{\sinh\left(\left(\eta_{1\text{a}}-\eta_{2\text{a}}\right)H\right)}{\eta_{1\text{a}}-\eta_{2\text{a}}}\right)+ \\
2k_{\text{a}}^{2}\left(k_{2}^{2}+2\eta_{1\text{a}}^{2}\right)\sinh^{2}\left(\eta_{2\text{a}}H\right)\left(\frac{\sinh\left(2\eta_{1\text{a}}H\right)}{2\eta_{1\text{a}}}-H\right)\Bigg]
\end{aligned} \tag{2.212}$$

$$\begin{aligned}
\langle \overline{P_{\text{a2}}}\rangle = -\frac{\omega k_{\text{a}}}{8\mu}\frac{|\overline{P}_{0}\,(k_{\text{a}},\omega)|^{2}}{\left[R_{\text{a}}'\,(k_{\text{a}})\right]^{2}} \\
\Bigg[2\eta_{1\text{a}}\eta_{2\text{a}}\left(2k_{\text{a}}^{2}-k_{2}^{2}\right)\left(4k_{\text{a}}^{2}-k_{2}^{2}\right)\sinh\left(\eta_{1\text{a}}H\right)\sinh\left(\eta_{2\text{a}}H\right) \\
\left(\frac{\sinh\left(\left(\eta_{1\text{a}}+\eta_{2\text{a}}\right)H\right)}{\eta_{1\text{a}}+\eta_{2\text{a}}}+\frac{\sinh\left(\left(\eta_{1\text{a}}-\eta_{2\text{a}}\right)H\right)}{\eta_{1\text{a}}-\eta_{2\text{a}}}\right)- \\
8\eta_{1\text{a}}^{2}\eta_{2\text{a}}^{2}k_{\text{a}}^{2}\sinh^{2}\left(\eta_{2\text{a}}H\right)\left(\frac{\sinh\left(2\eta_{1\text{a}}H\right)}{2\eta_{1\text{a}}}+H\right)- \\
\left(2k_{\text{a}}^{2}-k_{2}^{2}\right)^{3}\sinh^{2}\left(\eta_{1\text{a}}H\right)\left(\frac{\sinh\left(2\eta_{2\text{a}}H\right)}{2\eta_{2\text{a}}}+H\right)\Bigg]
\end{aligned} \tag{2.213}$$

For symmetric Lamb wave motion in a plate subjected to a dynamic shear load on the top surface, the power flow through a cross section is given by

$$\langle \overline{P_{\mathrm{s}}}\left(\omega\right)\rangle = \langle \overline{P_{\mathrm{s1}}}\left(\omega\right)\rangle + \langle \overline{P_{\mathrm{s2}}}\left(\omega\right)\rangle \tag{2.214}$$

where,

$$\begin{aligned}
\langle \overline{P_{\mathrm{s1}}}\rangle = \frac{\omega\eta_{2\mathrm{s}}^2 k_{\mathrm{s}}}{4\mu}\frac{\left|\overline{P}_0\left(k_{\mathrm{s}},\omega\right)\right|^2}{\left[R_{\mathrm{s}}'\left(k_{\mathrm{s}}\right)\right]^2} \\
\Bigg[\left(2k_{\mathrm{s}}^2-k_2^2\right)^2\cosh^2\left(\eta_{1\mathrm{s}}H\right)\left(\frac{\sinh\left(2\eta_{2\mathrm{s}}H\right)}{2\eta_{2\mathrm{s}}}+H\right)- \\
\left(2k_{\mathrm{s}}^2-k_2^2\right)\left(2k_{\mathrm{s}}^2+k_2^2+2\eta_{1\mathrm{s}}^2\right)\cosh\left(\eta_{1\mathrm{s}}H\right)\cosh\left(\eta_{2\mathrm{s}}H\right) \\
\left(\frac{\sinh\left(\left(\eta_{1\mathrm{s}}+\eta_{2\mathrm{s}}\right)H\right)}{\eta_{1\mathrm{s}}+\eta_{2\mathrm{s}}}+\frac{\sinh\left(\left(\eta_{1\mathrm{s}}-\eta_{2\mathrm{s}}\right)H\right)}{\eta_{1\mathrm{s}}-\eta_{2\mathrm{s}}}\right)+ \\
2k_{\mathrm{s}}^2\left(k_2^2+2\eta_{1\mathrm{s}}^2\right)\cosh^2\left(\eta_{2\mathrm{s}}H\right)\left(\frac{\sinh\left(2\eta_{1\mathrm{s}}H\right)}{2\eta_{1\mathrm{s}}}+H\right)\Bigg]
\end{aligned} \tag{2.215}$$

$$\begin{aligned}
\langle \overline{P_{\mathrm{s2}}}\rangle = -\frac{\omega k_{\mathrm{s}}}{8\mu}\frac{\left|\overline{P}_0\left(k_{\mathrm{s}},\omega\right)\right|^2}{\left[R_{\mathrm{s}}'\left(k_{\mathrm{s}}\right)\right]^2} \\
\Bigg[2\eta_{1\mathrm{s}}\eta_{2\mathrm{s}}\left(2k_{\mathrm{s}}^2-k_2^2\right)\left(4k_{\mathrm{s}}^2-k_2^2\right)\cosh\left(\eta_{1\mathrm{s}}H\right)\cosh\left(\eta_{2\mathrm{s}}H\right) \\
\left(\frac{\sinh\left(\left(\eta_{1\mathrm{s}}+\eta_{2\mathrm{s}}\right)H\right)}{\eta_{1\mathrm{s}}+\eta_{2\mathrm{s}}}-\frac{\sinh\left(\left(\eta_{1\mathrm{s}}-\eta_{2\mathrm{s}}\right)H\right)}{\eta_{1\mathrm{s}}-\eta_{2\mathrm{s}}}\right)- \\
8\eta_{1\mathrm{s}}^2\eta_{2\mathrm{s}}^2k_{\mathrm{s}}^2\cosh^2\left(\eta_{2\mathrm{s}}H\right)\left(\frac{\sinh\left(2\eta_{1\mathrm{s}}H\right)}{2\eta_{1\mathrm{s}}}-H\right)- \\
\left(2k_{\mathrm{s}}^2-k_2^2\right)^3\cosh^2\left(\eta_{1\mathrm{s}}H\right)\left(\frac{\sinh\left(2\eta_{2\mathrm{s}}H\right)}{2\eta_{2\mathrm{s}}}-H\right)\Bigg]
\end{aligned} \tag{2.216}$$

2.14 Work done per cycle by the applied dynamic shear load

As discussed previously, the power flow through the region on the top surface of the plate, where the shear load is applied, is due to the contribution of the real roots of the dispersion equation that is due to the propagating Lamb waves through the plate.

The power flow through the top surface due to the right propagating antisymmetric Lamb wave motion is given by

$$\langle \overline{P}_{aH}(\omega) \rangle = \frac{\omega k_2^2 \eta_{2a}}{4\mu} \frac{\overline{P}_0(k_a, \omega)}{R'_a(k_a)} P_0(\omega) \frac{\sin(k_a a)}{k_a} \sinh(\eta_{1a} H) \sinh(\eta_{2a} H) \quad (2.217)$$

The power flow through the top surface due to the right propagating symmetric Lamb wave motion is given by

$$\langle \overline{P}_{sH}(\omega) \rangle = \frac{\omega k_2^2 \eta_{2s}}{4\mu} \frac{\overline{P}_0(k_s, \omega)}{R'_s(k_s)} P_0(\omega) \frac{\sin(k_s a)}{k_s} \cosh(\eta_{1s} H) \cosh(\eta_{2s} H) \quad (2.218)$$

The power flow through the top surface due to the left and the right propagating Lamb waves is twice the value given by Equations (2.217,2.218). And this power flow through the top surface induced by the applied load equals the power flow through two vertical sections left and right of the origin, which again is twice that given by Equations (2.212-2.216). Figure (2.20) compares the above two power flow spectrum in a 1.78 mm thick aluminum plate subjected to a uniform shear load of intensity $1 \frac{\mathrm{N}}{m}$ over a 1 mm wide region on its top surface. The Young's modulus of the aluminum plate is 69 GPa and its Poisson's ratio is 0.3269.

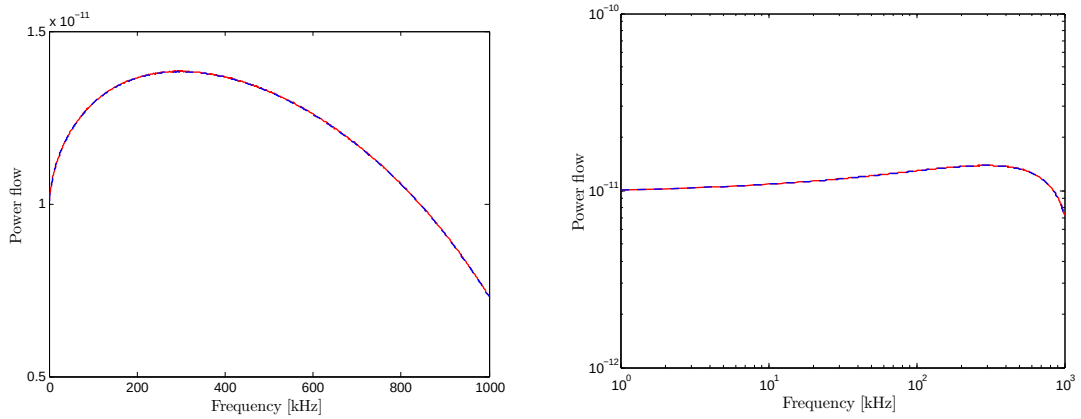

(a) Power flow spectrum

(b) Power flow specttrum in log scale

Figure 2.20: Power flow spectrum due to Lamb waves in a plate subjected to uniform shear load on its top surface. The red solid curve denotes power flow through vertical cross sections left and right of the origin. The dashed blue curve denotes the power flow through the region on the top surface on which the external load is applied.

2.14.1 Uniform shear load

For a shear loading $p(x,t)$ with intensity $\hat{p}(x)$ over a length $2a$ on the top surface of the plate, centered at the vertical z-axis,

$$p(x,t) = \hat{p}(x) f(t) \tag{2.219}$$

where $f(t)$ is the time-dependence of the load. For an uniform intensity p_0 over a length $2a$ on the top surface of the plate, centered at the vertical z-axis,

$$\hat{p}(x) = p_0 \qquad |x| \leq a \tag{2.220}$$

$$= 0 \qquad |x| > a \tag{2.221}$$

$$\begin{aligned} P_0(x,\omega) &= \int_0^\infty p(x,t)\, e^{i\omega t}\, dt \qquad |x| \leq a, t > 0 \\ &= p_0 \int_0^\infty f(t)\, e^{i\omega t}\, dt \end{aligned} \tag{2.222}$$

$$\overline{P}_0(k,\omega) = \int_{-\infty}^\infty P_0(x,\omega)\, e^{-ikx}\, dx \tag{2.223}$$

$$= \int_0^\infty \left[\int_{-a}^a p_0 e^{-ikx}\, dx \right] f(t)\, e^{i\omega t}\, dt$$

$$= \int_0^\infty \left[-\frac{ip_0}{k} \left(e^{ika} - e^{-ika} \right) \right] f(t)\, e^{i\omega t}\, dt$$

$$= \int_0^\infty \frac{2p_0 \sin(ka)}{k} f(t)\, e^{i\omega t}\, dt \tag{2.224}$$

2.15 Energy content in Lamb waves generated under different loading conditions

The power flow through a vertical cross section of a plate on the right of the origin by the Lamb waves are compared. The aluminum plate is 1.78 mm thick with

Young's modulus 69 GPa and Poisson's ratio 0.3269. Both the uniform vertical load and the uniform shear load have an intensity of 1 $\frac{\text{N}}{\text{m}}$ applied over a region of width 1 mm on the top surface of the plate, centered about the origin. To compare the power flow with the rocking load, an equivalent mean square area under the load curve is considered. The rocking load hence has intensity linearly varying from $-\sqrt{3}, \frac{\text{N}}{\text{m}}$ to $\sqrt{3}, \frac{\text{N}}{\text{m}}$ over the 1 mm width on which it is applied. Figure (2.21) shows the comparison between the power flow spectrum of the three different cases. It is seen that the rocking load induces Lamb waves with the least energy within the frequency range considered. For low frequencies, Lamb waves generated due to the uniform vertical load, carries the most amount of energy. For some mid frequencies, in the range considered, the Lamb waves generated due to the uniform shear load carries a little more energy than those generated by the uniform vertical load, but again decreases for higher frequencies.

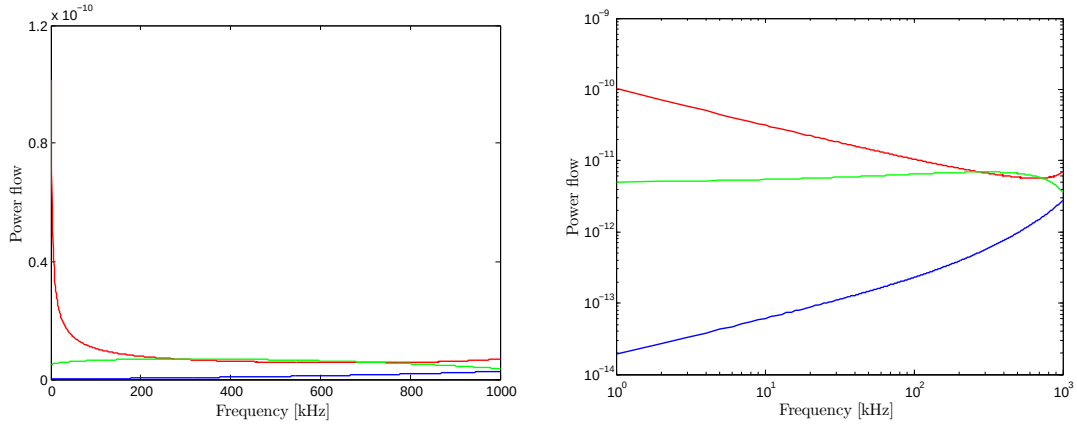

(a) Power flow spectrum

(b) Power flow spectrum in log scale

Figure 2.21: Power flow spectrum through a right vertical cross section due to Lamb waves in a plate subjected to uniform vertical, shear load and rocking load with equal mean square area under the load curve on its top surface. The red curve denotes power flow due to uniform vertical load. The green curve denotes the power flow due to uniform shear load. The blue curve denotes the power flow due to an equivalent rocking load.

CHAPTER 3

Propagation of Lamb waves in thin plates subjected to surface loads - Axisymmetric analysis

In this chapter, the propagation of Lamb waves through an isotropic thin plate subjected to surface loads is analyzed. The dispersion relations and the displacement and stress components for the symmetric and antisymmetric Lamb modes are derived.

Figure 3.1 shows the axisymmetric model of the plate that is analyzed. The radial direction is given by r which as always is positive away from the centre and the z axis positive upwards.

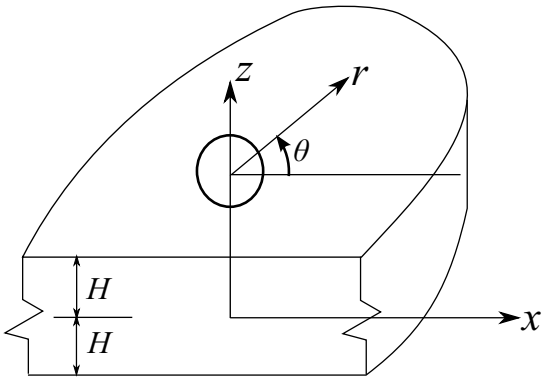

Figure 3.1: Axisymmetric geometry of plate

The analysis is done in the frequency domain, by taking Fourier transform of the field variables with respect to time (t) and Hankel transform in the direction of

propagation of the wave (r). The original field variables $f(r,z,t)$ are transformed into frequency domain to $F(r,z,\omega)$ by taking the Fourier transform with respect to time (t) and then further transformed to $\overline{F}_m(k,z,\omega)$ according to

$$F(r,z,\omega) = \int_{-\infty}^{\infty} f(x,z,t)\, e^{i\omega t}\, dt \tag{3.1}$$

$$\overline{F}_m(k,z,\omega) = \frac{1}{2}\int_{-\infty}^{\infty} F(r,z,\omega)\, r H_m^{(1)}(kr)\; dr \tag{3.2}$$

where ω is the circular frequency and k is the wavenumber and $H_m^{(1)}(kr)$ is the Hankel function of first kind of order m. The original variables are obtained by taking the inverse Fourier and Hankel transforms according to

$$f(r,z,t) = \frac{1}{4\pi}\int_{-\infty}^{\infty}\int_{-\infty}^{\infty} \overline{F}_m(k,z,\omega)\, k H_m^{(1)} e^{-i\omega t}\, dk\, d\omega \tag{3.3}$$

The analysis is done in the frequency domain that is on the integrand of Equation(3.3) for the field variables, shown as follows

$$u(r,z,t) = \overline{U}_1(k,z,\omega)\, k H_1^{(1)}(kr)\, e^{-i\omega t} \tag{3.4}$$

$$w(r,z,t) = \overline{W}_0(k,z,\omega)\, k H_0^{(1)}(kr)\, e^{-i\omega t} \tag{3.5}$$

$$\sigma_{rr}(r,z,t) = \left[\overline{S}_{rr0}(k,z,\omega)\, k H_0^{(1)}(kr) + \overline{S}_{rr1}(k,z,\omega)\, k H_1^{(1)}(kr)\right] e^{-i\omega t} \tag{3.6}$$

$$\sigma_{\theta\theta}(r,z,t) = \left[\overline{S}_{\theta\theta0}(k,z,\omega)\, k H_0^{(1)}(kr) + \overline{S}_{\theta\theta1}(k,z,\omega)\, k H_1^{(1)}(kr)\right] e^{-i\omega t} \tag{3.7}$$

$$\sigma_{zz}(r,z,t) = \overline{S}_{zz0}(k,z,\omega)\, k H_0^{(1)}(kr)\, e^{-i\omega t} \tag{3.8}$$

$$\sigma_{rz}(r,z,t) = \overline{S}_{rz0}(k,z,\omega)\, k H_1^{(1)}(kr)\, e^{-i\omega t} \tag{3.9}$$

where, $u(r,z,t)$ and $w(r,z,t)$ are the displacements along the r and z directions respectively. $H_m^{(1)}$ is the Hankel function of first kind of order m and the subscripts in $\overline{U}, \overline{W}, \overline{S}_{rr}, \overline{S}_{\theta\theta}, \overline{S}_{zz}, \overline{S}_{rz}$ denote the order of the Hankel function of the first kind it is associated with.

Hooke's Law for an isotropic material for axisymmetric analysis is given by

$$\sigma_{rr} = \lambda\left(\epsilon_{rr} + \epsilon_{zz}\right) + 2\mu\epsilon_{rr} \tag{3.10}$$

$$\sigma_{\theta\theta} = \lambda\left(\epsilon_{rr} + \epsilon_{zz} + \epsilon_{\theta\theta}\right) + 2\mu\epsilon_{\theta\theta} \tag{3.11}$$

$$\sigma_{zz} = \lambda\left(\epsilon_{rr} + \epsilon_{zz}\right) + 2\mu\epsilon_{zz} \tag{3.12}$$

$$\sigma_{rz} = \mu\gamma_{rz} \tag{3.13}$$

where $\epsilon_{rr}, \epsilon_{zz}, \epsilon_{\theta\theta}$ are the normal strains in the r and the z and the θ directions respectively and γ_{rz} is the hear strain. λ and μ are Lamé constants. μ is the shear modulus of the material.

Using the strain displacement kinematic relations

$$\epsilon_{rr} = \frac{\partial u}{\partial r}, \qquad \epsilon_{\theta\theta} = \frac{u}{r}, \qquad \epsilon_{zz} = \frac{\partial w}{\partial z} \qquad \text{and} \qquad \gamma_{rz} = \frac{\partial u}{\partial z} + \frac{\partial w}{\partial r} \tag{3.14}$$

the stresses can be expressed in terms of displacement components as

$$\begin{aligned}
\sigma_{rr} &= \left(\lambda + 2\mu\right)\frac{\partial u}{\partial r} + \lambda\left(\frac{u}{r} + \frac{\partial w}{\partial z}\right) \\
&= \rho c_1^2 \frac{\partial u}{\partial r} + \rho\left(c_1^2 - 2c_2^2\right)\left(\frac{u}{r} + \frac{\partial w}{\partial z}\right)
\end{aligned}$$

$$\begin{aligned}
\sigma_{\theta\theta} &= \left(\lambda + 2\mu\right)\frac{u}{r} + \lambda\left(\frac{\partial u}{\partial r} + \frac{\partial w}{\partial z}\right) \\
&= \rho c_1^2 \frac{u}{r} + \rho\left(c_1^2 - 2c_2^2\right)\left(\frac{\partial u}{\partial r} + \frac{\partial w}{\partial z}\right)
\end{aligned} \tag{3.15}$$

$$\begin{aligned}
\sigma_{zz} &= \lambda\left(\frac{\partial u}{\partial r} + \frac{u}{r}\right) + \left(\lambda + 2\mu\right)\frac{\partial w}{\partial z} \\
&= \rho\left(c_1^2 - 2c_2^2\right)\left(\frac{\partial u}{\partial r} + \frac{u}{r}\right) + \rho c_1^2 \frac{\partial w}{\partial z}
\end{aligned}$$

$$\begin{aligned}
\sigma_{rz} &= \mu\left(\frac{\partial u}{\partial z} + \frac{\partial w}{\partial r}\right) \\
&= \rho c_2^2 \left(\frac{\partial u}{\partial z} + \frac{\partial w}{\partial r}\right)
\end{aligned}$$

where ρ is the density of the material and c_1 and c_2 are the longitudinal and shear wave speeds respectively and given by

$$c_1 = \sqrt{\frac{\lambda + 2\mu}{\rho}}, \qquad c_2 = \sqrt{\frac{\mu}{\rho}} \tag{3.16}$$

The derivatives of Hankel functions of the first kind of orders 0 and 1 are given by [39]

$$\frac{d}{dr}H_0^{(1)}(kr) = -kH_1^{(1)}(kr) \tag{3.17}$$

$$\frac{d}{dr}H_1^{(1)}(kr) = kH_0^{(1)}(kr) - \frac{1}{r}H_1^{(1)}(kr) \tag{3.18}$$

$$\frac{d^2}{dr^2}H_0^{(1)}(kr) = -k^2H_0^{(1)}(kr) + \frac{k}{r}H_1^{(1)}(kr) \tag{3.19}$$

$$\frac{d^2}{dr^2}H_1^{(1)}(kr) = -\left(k^2 + \frac{2}{r^2}\right)H_1^{(1)}(kr) - \frac{k}{r}H_0^{(1)}(kr) \tag{3.20}$$

Using the relations from Equations (3.4-3.14) into Equation (3.15), and using the above formulas for the derivatives of the Hankel functions, the stresses are expressed as

$$\sigma_{rr} = \rho\left[c_1^2\overline{U}_1k^2H_0^{(1)}(kr) - 2c_2^2\overline{U}_1\frac{k}{r}H_1^{(1)}(kr) + \left(c_1^2 - 2c_2^2\right)\frac{\partial\overline{W}_0}{\partial z}kH_0^{(1)}(kr)\right]e^{-i\omega t} \tag{3.21}$$

$$\sigma_{\theta\theta} = \rho\left[\left(c_1^2 - 2c_2^2\right)\left(\overline{U}_1k + \frac{\partial\overline{W}_0}{\partial z}\right)kH_0^{(1)}(kr) + 2c_2^2\overline{U}_1\frac{k}{r}H_1^{(1)}(kr)\right]e^{-i\omega t} \tag{3.22}$$

$$\sigma_{zz} = \rho\left[c_1^2\frac{\partial\overline{W}_0}{\partial z} + \left(c_1^2 - 2c_2^2\right)\overline{U}_1k\right]kH_0^{(1)}(kr)\,e^{-i\omega t} \tag{3.23}$$

$$\sigma_{rz} = \rho c_2^2\left[\frac{\partial\overline{U}_1}{\partial z} - \overline{W}_0k\right]kH_1^{(1)}(kr)\,e^{-i\omega t} \tag{3.24}$$

The stress equations of motion in absence of body forces are given by

$$\text{In r direction} \qquad \frac{1}{r}\frac{\partial(r\sigma_{rr})}{\partial r} + \frac{\partial\sigma_{rz}}{\partial z} - \frac{\sigma_{\theta\theta}}{r} = \rho\frac{\partial^2u}{\partial t^2} \tag{3.25}$$

$$\text{In z direction} \qquad \frac{1}{r}\frac{\partial(r\sigma_{rz})}{\partial r} + \frac{\partial\sigma_{zz}}{\partial z} = \rho\frac{\partial^2w}{\partial t^2} \tag{3.26}$$

Taking the derivatives of the stresses from Equations(3.21-3.24) and substituting them in the equations of motion give

$$\text{In r direction} \qquad -c_1^2 k^2 \overline{U}_1 + c_2^2 \frac{\partial^2 \overline{U}_1}{\partial z^2} + \omega^2 \overline{U}_1 - \left(c_1^2 - c_2^2\right) k \frac{\partial \overline{W}_0}{\partial z} = 0 \quad (3.27)$$

$$\text{In z direction} \qquad \left(c_1^2 - c_2^2\right) k \frac{\partial \overline{U}_1}{\partial z} - c_2^2 k^2 \overline{W}_0 + c_1^2 \frac{\partial^2 \overline{W}_0}{\partial z^2} + \omega^2 \overline{W}_0 = 0 \quad (3.28)$$

Assuming,

$$\overline{U}_1 (k, z, \omega) = A (k, \omega) e^{-\xi z} \quad (3.29)$$

$$\overline{W}_0 (k, z, \omega) = B (k, \omega) e^{-\xi z} \quad (3.30)$$

where $A(k, \omega)$ and $B(k, \omega)$ are unknown functions and ξ is the unknown parameter describing the z-dependency of $\overline{U}, \overline{W}$.

Substituting Equations (3.29, 3.30) into Equations (3.27, 3.28), the following pair of homogeneous equations are obtained

$$\begin{bmatrix} -c_1^2 k^2 + c_2^2 \xi^2 + \omega^2 & \left(c_1^2 - c_2^2\right) k\xi \\ -\left(c_1^2 - c_2^2\right) k\xi & -c_2^2 k^2 + c_1^2 \xi^2 + \omega^2 \end{bmatrix} \begin{Bmatrix} A (k, \omega) \\ B (k, \omega) \end{Bmatrix} = \begin{Bmatrix} 0 \\ 0 \end{Bmatrix} \quad (3.31)$$

For non trivial solution of Equation(3.31), the determinant of the coefficient matrix is equal to zero, leading to the following fourth order algebraic equation for ξ

$$c_1^2 c_2^2 \xi^4 + \xi^2 \left[\omega^2 \left(c_1^2 + c_2^2\right) - 2 c_1^2 c_2^2 k^2\right] + c_1^2 c_2^2 k^4 - \omega^2 k^2 \left(c_1^2 + c_2^2\right) + \omega^4 = 0 \quad (3.32)$$

which is a quadratic equation in ξ^2. Solving the equation gives the unknown

parameter ξ as follows

$$\xi_1 = \sqrt{k^2 - \frac{\omega^2}{c_1^2}} = \sqrt{k^2 - k_1^2} = \eta_1 \tag{3.33}$$

$$\xi_2 = -\left(\sqrt{k^2 - \frac{\omega^2}{c_1^2}}\right) = \sqrt{k^2 - k_1^2} = -\eta_1 \tag{3.34}$$

$$\xi_3 = \sqrt{k^2 - \frac{\omega^2}{c_2^2}} = \sqrt{k^2 - k_2^2} = \eta_2 \tag{3.35}$$

$$\xi_4 = -\left(\sqrt{k^2 - \frac{\omega^2}{c_2^2}}\right) = \sqrt{k^2 - k_2^2} = -\eta_2 \tag{3.36}$$

From Equation (3.31), the unknown functions $A(k,\omega)$ and $B(k,\omega)$ are related as

$$B(k,\omega) = \frac{c_1^2 k^2 - c_2^2 \xi^2 - \omega^2}{(c_1^2 - c_2^2)\, k\xi} A(k,\omega) = \alpha A(k,\omega) \tag{3.37}$$

where the four values of α corresponding to the four values of ξ are given by

$$\alpha_1 = \frac{c_1^2 k^2 - c_2^2 \eta_1^2 - \omega^2}{(c_1^2 - c_2^2)\, k\eta_1} = \frac{\eta_1}{k} \tag{3.38}$$

$$\alpha_2 = -\frac{\eta_1}{k} = -\alpha_1 \tag{3.39}$$

$$\alpha_3 = \frac{c_1^2 k^2 - c_2^2 \eta_2^2 - \omega^2}{(c_1^2 - c_2^2)\, k\eta_2} = \frac{k}{\eta_2} \tag{3.40}$$

$$\alpha_4 = -\frac{k}{\eta_2} = -\alpha_3 \tag{3.41}$$

Substituting the values of α from Equations (3.38-3.41) into Equation (3.37),

$$B_1(k,\omega) = \alpha_1 A_1(k,\omega) = \frac{\eta_1}{k} A_1(k,\omega) \tag{3.42}$$

$$B_2(k,\omega) = -\alpha_1 A_2(k,\omega) = -\frac{\eta_1}{k} A_1(k,\omega) \tag{3.43}$$

$$B_3(k,\omega) = \alpha_3 A_3(k,\omega) = \frac{k}{\eta_2} A_3(k,\omega) \tag{3.44}$$

$$B_4(k,\omega) = -\alpha_3 A_4(k,\omega) = -\frac{k}{\eta_2} A_4(k,\omega) \tag{3.45}$$

Substituting Equations (3.42-3.45) in Equations (3.29,3.30) for the displacements

$$\begin{aligned} \overline{U}_1(k,z,\omega) = {} & A_1(k,\omega)\, e^{-\eta_1 z} + A_2(k,\omega)\, e^{\eta_1 z} \\ & + A_3(k,\omega)\, e^{-\eta_2 z} + A_4(k,\omega)\, e^{\eta_2 z} \end{aligned} \tag{3.46}$$

$$\begin{aligned}\overline{W}_0(k,z,\omega) = &\frac{\eta_1}{k}A_1(k,\omega)\,e^{-\eta_1 z} - \frac{\eta_1}{k}A_2(k,\omega)\,e^{\eta_1 z} \\ &+ \frac{k}{\eta_2}A_3(k,\omega)\,e^{-\eta_2 z} - \frac{k}{\eta_2}A_4(k,\omega)\,e^{\eta_2 z}\end{aligned} \tag{3.47}$$

Using the relations between exponential and hyperbolic sine and cosine,

$$e^{\eta z} = \cosh(\eta z) + \sinh(\eta z) \qquad e^{-\eta z} = \cosh(\eta z) - \sinh(\eta z)$$

the displacements and stresses in the frequency domain can be written as

$$\begin{aligned}\overline{U}_1(k,z,\omega) = &\overline{A}_1\cosh(\eta_1 z) + \overline{A}_2\sinh(\eta_1 z) \\ &+ \overline{A}_3\cosh(\eta_2 z) + \overline{A}_4\sinh(\eta_2 z)\end{aligned} \tag{3.48}$$

$$\begin{aligned}\overline{W}_0(k,z,\omega) = &-\frac{\eta_1}{k}\overline{A}_1\sinh(\eta_1 z) - \frac{\eta_1}{k}\overline{A}_2\cosh(\eta_1 z) \\ &- \frac{k}{\eta_2}\overline{A}_3\sinh(\eta_2 z) - \frac{k}{\eta_2}\overline{A}_4\cosh(\eta_2 z)\end{aligned} \tag{3.49}$$

$$\begin{aligned}\overline{S}_{rr0}(k,z,\omega) = \frac{\mu}{k}\Big[&\left(k_2^2 + 2\eta_1^2\right)\left(\overline{A}_1\cosh(\eta_1 z) + \overline{A}_2\sinh(\eta_1 z)\right) \\ &+ 2k^2\left(\overline{A}_3\cosh(\eta_2 z) + \overline{A}_4\sinh(\eta_2 z)\right)\Big]\end{aligned} \tag{3.50}$$

$$\begin{aligned}\overline{S}_{rr1}(k,z,\omega) = -\frac{2\mu}{r}\Big[&\overline{A}_1\cosh(\eta_1 z) + \overline{A}_2\sinh(\eta_1 z) \\ &+ \overline{A}_3\cosh(\eta_2 z) + \overline{A}_4\sinh(\eta_2 z)\Big]\end{aligned} \tag{3.51}$$

$$\overline{S}_{\theta\theta 0}(k,z,\omega) = \frac{\mu}{k}\left(k_2^2 - 2k_1^2\right)\left(\overline{A}_1\cosh(\eta_1 z) + \overline{A}_2\sinh(\eta_1 z)\right) \tag{3.52}$$

$$\begin{aligned}\overline{S}_{\theta\theta 1}(k,z,\omega) = \frac{2\mu}{r}\Big[&\overline{A}_1\cosh(\eta_1 z) + \overline{A}_2\sinh(\eta_1 z) \\ &+ \overline{A}_3\cosh(\eta_2 z) + \overline{A}_4\sinh(\eta_2 z)\Big]\end{aligned} \tag{3.53}$$

$$\overline{S}_{zz0}(k,z,\omega) = -\frac{\mu}{k}\Big[\left(2k^2-k_2^2\right)\left(\overline{A}_1\cosh(\eta_1 z)+\overline{A}_2\sinh(\eta_1 z)\right) + 2k^2\left(\overline{A}_3\cosh(\eta_2 z)+\overline{A}_4\sinh(\eta_2 z)\right)\Big] \tag{3.54}$$

$$\overline{S}_{rz1}(k,z,\omega) = \frac{\mu}{\eta_2}\Big[2\eta_1\eta_2\left(\overline{A}_1\sinh(\eta_1 z)+\overline{A}_2\cosh(\eta_1 z)\right) + \left(2k^2-k_2^2\right)\left(\overline{A}_3\sinh(\eta_2 z)+\overline{A}_4\cosh(\eta_2 z)\right)\Big] \tag{3.55}$$

where

$$\overline{A}_1 = A_1(k,\omega)+A_2(k,\omega) \qquad \overline{A}_2 = A_2(k,\omega)-A_1(k,\omega) \tag{3.56}$$

$$\overline{A}_3 = A_3(k,\omega)+A_4(k,\omega) \qquad \overline{A}_4 = A_4(k,\omega)-A_3(k,\omega) \tag{3.57}$$

3.1 Lamb wave dispersion

Next, the stress free boundary conditions are applied on the top ($z = H$) and bottom ($z = -H$) faces of the plate.

At $z = H$, zero normal stress gives,

$$\begin{aligned}\overline{S}_{zz0}(k,H,\omega) &= \left(2k^2-k_2^2\right)\left(\overline{A}_1\cosh(\eta_1 H)+\overline{A}_2\sinh(\eta_1 H)\right)\\ &\quad+\left(2k^2\right)\left(\overline{A}_3\cosh(\eta_2 H)+\overline{A}_4\sinh(\eta_2 H)\right)\\ &= 0\end{aligned} \tag{3.58}$$

At $z = -H$, zero normal stress gives,

$$\begin{aligned}\overline{S}_{zz0}(k,-H,\omega) &= -\left(2k^2-k_2^2\right)\left(\overline{A}_1\cosh(\eta_1 H)-\overline{A}_2\sinh(\eta_1 H)\right)\\ &\quad-2k^2\left(\overline{A}_3\cosh(\eta_2 H)-\overline{A}_4\sinh(\eta_2 H)\right)\\ &= 0\end{aligned} \tag{3.59}$$

From Equations (3.58, 3.59)

$$\begin{aligned}\left[\left(2k^2-k_2^2\right)\overline{A}_2\sinh(\eta_1 H)+2k^2\overline{A}_4\sinh(\eta_2 H)\right]\pm\\ \left[\left(2k^2-k_2^2\right)\overline{A}_1\cosh(\eta_1 H)+2k^2\overline{A}_3\cosh(\eta_2 H)\right]=0\end{aligned} \tag{3.60}$$

At $z = H$, zero shear stress gives,

$$\begin{aligned}\overline{S}_{rz1}(k, H, \omega) &= 2\eta_1\eta_2\left(\overline{A}_1 \sinh(\eta_1 H) + \overline{A}_2 \cosh(\eta_1 H)\right) \\ &+ \left(2k^2 - k_2^2\right)\left(\overline{A}_3 \sinh(\eta_2 H) + \overline{A}_4 \cosh(\eta_2 H)\right) \\ &= 0\end{aligned} \tag{3.61}$$

At $z = -H$, zero shear stress gives,

$$\begin{aligned}\overline{S}_{rz1}(k, -H, \omega) &= 2\eta_1\eta_2\left(-\overline{A}_1 \sinh(\eta_1 H) + \overline{A}_2 \cosh(\eta_1 H)\right) \\ &+ \left(2k^2 - k_2^2\right)\left(-\overline{A}_3 \sinh(\eta_2 H) + \overline{A}_4 \cosh(\eta_2 H)\right) \\ &= 0\end{aligned} \tag{3.62}$$

From Equations (3.61, 3.62),

$$\begin{aligned}&\left[2\eta_1\eta_2\overline{A}_2 \cosh(\eta_1 H) + \left(2k^2 - k_2^2\right)\overline{A}_4 \cosh(\eta_2 H)\right] \pm \\ &\left[2\eta_1\eta_2\overline{A}_1 \sinh(\eta_1 H) + \left(2k^2 - k_2^2\right)\overline{A}_3 \sinh(\eta_2 H)\right] = 0\end{aligned} \tag{3.63}$$

From Equations (3.60,3.63), it is seen that $\overline{A}_1, \overline{A}_3$ are independent of $\overline{A}_2, \overline{A}_4$. Hence two independent motions of the plate can be obtained by setting $\overline{A}_1 = \overline{A}_3 = 0$ and then $\overline{A}_2 = \overline{A}_4 = 0$ First setting $\overline{A}_2 = \overline{A}_4 = 0$, the motion governed by $\overline{A}_1, \overline{A}_3$ is derived. $\overline{A}_1, \overline{A}_3$ satisfy

$$\begin{bmatrix} (2k^2 - k_2^2)\cosh(\eta_1 H) & 2k^2 \cosh(\eta_2 H) \\ 2\eta_1\eta_2 \sinh(\eta_1 H) & (2k^2 - k_2^2)\sinh(\eta_2 H) \end{bmatrix} \begin{Bmatrix} \overline{A}_1 \\ \overline{A}_3 \end{Bmatrix} = \begin{Bmatrix} 0 \\ 0 \end{Bmatrix} \tag{3.64}$$

For nontrivial solution of $\overline{A}_1, \overline{A}_3$, the determinant of the coefficient matrix in Equation (3.64) needs to be zero, which gives the dispersion relation for the symmetric Lamb waves in the plate.

$$\left(2k^2 - k_2^2\right)^2 \cosh(\eta_1 H)\sinh(\eta_2 H) - 4k^2\eta_1\eta_2 \sinh(\eta_1 H)\cosh(\eta_2 H) = 0 \tag{3.65}$$

The displacements and stresses in the plate for the symmetric Lamb wave, governed by the coefficients $\overline{A}_1, \overline{A}_3$ are given in the frequency domain by

$$\overline{U}_1(k, z, \omega) = \overline{A}_1 \cosh(\eta_1 z) + \overline{A}_3 \cosh(\eta_2 z) \tag{3.66}$$

$$\overline{W}_0(k,z,\omega) = -\frac{\eta_1}{k}\overline{A}_1 \sinh(\eta_1 z) - \frac{k}{\eta_2}\overline{A}_3 \sinh(\eta_2 z) \tag{3.67}$$

$$\overline{S}_{rr0}(k,z,\omega) = \frac{\mu}{k}\left[\left(k_2^2 + 2\eta_1^2\right)\overline{A}_1 \cosh(\eta_1 z) + 2k^2\overline{A}_3 \cosh(\eta_2 z)\right] \tag{3.68}$$

$$\overline{S}_{rr1}(k,z,\omega) = -\frac{2\mu}{r}\left[\overline{A}_1 \cosh(\eta_1 z) + \overline{A}_3 \cosh(\eta_2 z)\right] \tag{3.69}$$

$$\overline{S}_{\theta\theta 0}(k,z,\omega) = \frac{\mu}{k}\left(k_2^2 - 2k_1^2\right)\overline{A}_1 \cosh(\eta_1 z) \tag{3.70}$$

$$\overline{S}_{\theta\theta 1}(k,z,\omega) = \frac{2\mu}{r}\left[\overline{A}_1 \cosh(\eta_1 z) + \overline{A}_3 \cosh(\eta_2 z)\right] \tag{3.71}$$

$$\overline{S}_{zz0}(k,z,\omega) = -\frac{\mu}{k}\left[\left(2k^2 - k_2^2\right)\overline{A}_1 \cosh(\eta_1 z) + 2k^2\overline{A}_3 \cosh(\eta_2 z)\right] \tag{3.72}$$

$$\overline{S}_{rz1}(k,z,\omega) = \frac{\mu}{\eta_2}\left[2\eta_1\eta_2\overline{A}_1 \sinh(\eta_1 z) + \left(2k^2 - k_2^2\right)\overline{A}_3 \sinh(\eta_2 z)\right] \tag{3.73}$$

Similarly, by setting $\overline{A}_1 = \overline{A}_3 = 0$ in Equations (3.60, 3.63), the motion governed by $\overline{A}_2$, $\overline{A}_4$ is derived. $\overline{A}_2$, $\overline{A}_4$ satisfy

$$\begin{bmatrix} (2k^2 - k_2^2)\sinh(\eta_1 H) & 2k^2 \sinh(\eta_2 H) \\ 2\eta_1\eta_2 \cosh(\eta_1 H) & (2k^2 - k_2^2)\cosh(\eta_2 H) \end{bmatrix} \begin{Bmatrix} \overline{A}_2 \\ \overline{A}_4 \end{Bmatrix} = \begin{Bmatrix} 0 \\ 0 \end{Bmatrix} \tag{3.74}$$

For nontrivial solution of $\overline{A}_2, \overline{A}_4$, the determinant of the coefficient matrix in Equation (3.74) needs to be zero, which gives the dispersion relation for the anti-symmetric Lamb waves in the plate.

$$\left(2k^2 - k_2^2\right)^2 \sinh(\eta_1 H)\cosh(\eta_2 H) - 4k^2\eta_1\eta_2 \cosh(\eta_1 H)\sinh(\eta_2 H) = 0 \tag{3.75}$$

The displacements and stresses in the plate due the antisymmetric Lamb wave, governed by the coefficients $\overline{A}_2, \overline{A}_4$ are given in the frequency domain by

$$\overline{U}_1(k,z,\omega) = \overline{A}_2 \sinh(\eta_1 z) + \overline{A}_4 \sinh(\eta_2 z) \tag{3.76}$$

$$\overline{W}_0(k,z,\omega) = -\frac{\eta_1}{k}\overline{A}_2 \cosh(\eta_1 z) - \frac{k}{\eta_2}\overline{A}_4 \cosh(\eta_2 z) \tag{3.77}$$

$$\overline{S}_{rr0}(k,z,\omega) = \frac{\mu}{k}\left[\left(k_2^2 + 2\eta_1^2\right)\overline{A}_2 \sinh(\eta_1 z) + 2k^2\overline{A}_4 \sinh(\eta_2 z)\right] \tag{3.78}$$

$$\overline{S}_{rr1}(k,z,\omega) = -\frac{2\mu}{r}\left[\overline{A}_2 \sinh(\eta_1 z) + \overline{A}_4 \sinh(\eta_2 z)\right] \tag{3.79}$$

$$\overline{S}_{\theta\theta 0}(k,z,\omega) = \frac{\mu}{k}\left(k_2^2 - 2k_1^2\right)\overline{A}_2 \sinh(\eta_1 z) \tag{3.80}$$

$$\overline{S}_{\theta\theta 1}(k,z,\omega) = \frac{2\mu}{r}\left[\overline{A}_2 \sinh(\eta_1 z) + \overline{A}_4 \sinh(\eta_2 z)\right] \tag{3.81}$$

$$\overline{S}_{zz0}(k,z,\omega) = -\frac{\mu}{k}\left[\left(2k^2 - k_2^2\right)\overline{A}_2 \sinh(\eta_1 z) + 2k^2\overline{A}_4 \sinh(\eta_2 z)\right] \tag{3.82}$$

$$\overline{S}_{rz1}(k,z,\omega) = \frac{\mu}{\eta_2}\left[2\eta_1\eta_2\overline{A}_2 \cosh(\eta_1 z) + \left(2k^2 - k_2^2\right)\overline{A}_4 \cosh(\eta_2 z)\right] \tag{3.83}$$

3.2 Propagation of Lamb waves through plate under axisymmetric dynamic surface loads

In this section, the propagation of Lamb waves, under axisymmetric surface load is analyzed. The physical problem, with loading applied on the top surface of the plate ($z = H$) is resolved into a corresponding symmetric and an antisymmetric problem, see Figure (3.2). The applied time-dependent load with intensity p_0 is

resolved into the antisymmetric and symmetric loading of intensity $\frac{p_0}{2}$ applied on the top and bottom ($z = -H$) surfaces of the plate. The sum of the values of the different field variables, for the symmetric and the antisymmetric models, give the total field.

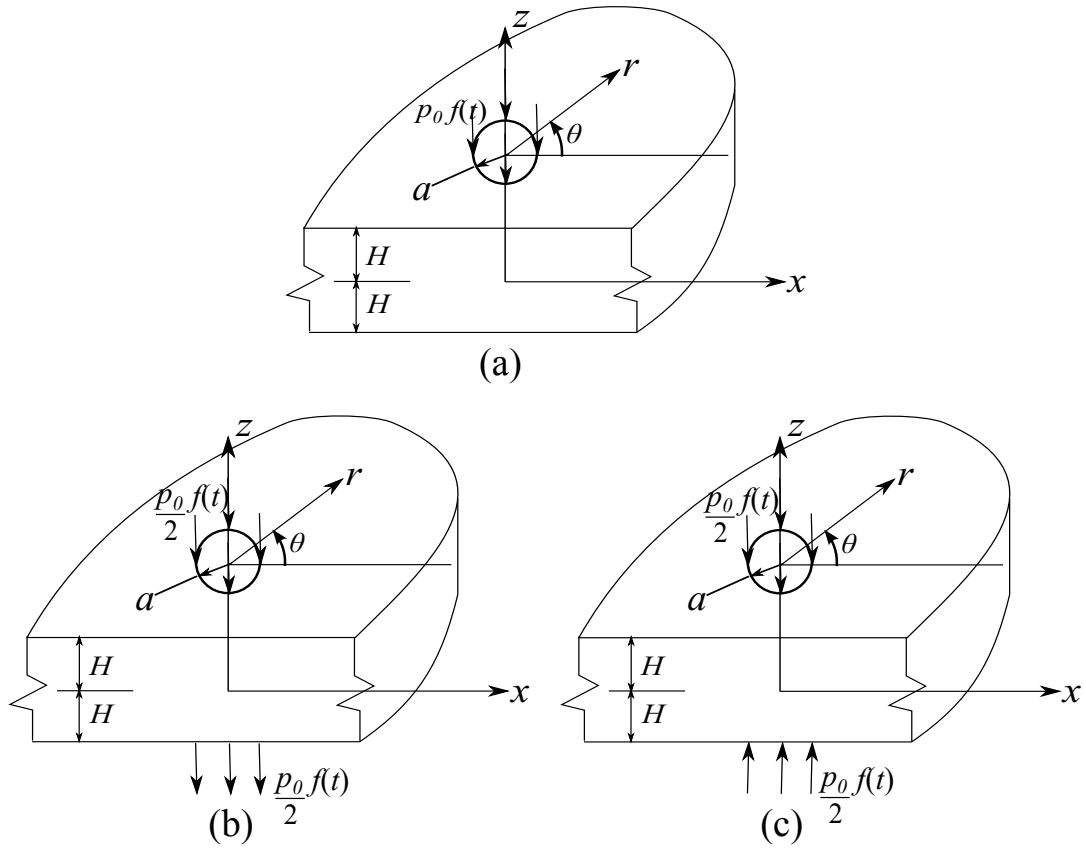

Figure 3.2: (a) Applied loading (b) Antisymmetric loading component and (c) Symmetric loading component in a plate

Like the field variables, the time dependent load $p\,(r,t)$ is transformed into $P_0\,(r,\omega)$ in the frequency domain by applying Fourier transform with respect to time. It is then further transformed into $\overline{P}_0\,(k,\omega)$ by applying the Hankel transform with respect to r-direction. Next, the appropriate boundary conditions are applied.

3.3 Antisymmetric Lamb wave propagation under axisymmetric dynamic surface load

From Equations (3.82, 3.83), zero shear stress at $z = H$ gives,

$$\overline{S}_{rz1}(k, H, \omega) = 2\eta_1\eta_2\overline{A}_2 \cosh(\eta_1 H) + \left(2k^2 - k_2^2\right)\overline{A}_4 \cosh(\eta_2 z) = 0 \tag{3.84}$$

which gives,

$$\overline{A}_2 = -\frac{(2k^2 - k_2^2)\cosh(\eta_2 H)}{2\eta_1\eta_2 \cosh(\eta_1 H)}\overline{A}_4 \tag{3.85}$$

At $z = H$, the applied normal load gives,

$$\overline{S}_{zz0}(k, H, \omega) = -\frac{\overline{P}_0(k, \omega)}{2} \tag{3.86}$$

which gives,

$$\frac{\mu}{k}\left[\left(2k^2 - k_2^2\right)\overline{A}_2 \sinh(\eta_1 H) + 2k^2\overline{A}_4 \sinh(\eta_2 H)\right] = \frac{\overline{P}_0}{2} \tag{3.87}$$

Substituting $\overline{A}_2$ from Equation (3.85) into Equation (3.87)

$$\overline{A}_4 = -\frac{k\eta_1\eta_2 \cosh(\eta_1 H)}{\mu R_{\mathrm{a}}(k)}\overline{P}_0(k, \omega) \tag{3.88}$$

where, $R_{\mathrm{a}}(k)$ is the antisymmetric Lamb wave denominator and is given by

$$R_{\mathrm{a}}(k) = \left(2k^2 - k_2^2\right)^2 \sinh(\eta_1 H)\cosh(\eta_2 H) - 4k^2\eta_1\eta_2 \cosh(\eta_1 H)\sinh(\eta_2 H) \tag{3.89}$$

Substituting $\overline{A}_4$ from Equation (3.88) into Equation (3.85)

$$\overline{A}_2 = \frac{k(2k^2 - k_2^2)\cosh(\eta_2 H)}{2\mu R_{\mathrm{a}}(k)}\overline{P}_0(k, \omega) \tag{3.90}$$

Using the above values of $\overline{A}_2$ and $\overline{A}_4$, the displacements and the stresses in the plate due to the antisymmetric Lamb wave in the frequency domain are given by

$$\overline{U}_1(k, z, \omega) = \frac{k\overline{P}_0(k, \omega)}{2\mu R_{\mathrm{a}}(k)}\Big[\left(2k^2 - k_2^2\right)\sinh(\eta_1 z)\cosh(\eta_2 H) - 2\eta_1\eta_2 \cosh(\eta_1 H)\sinh(\eta_2 z)\Big] \tag{3.91}$$

$$\overline{W}_0(k,z,\omega) = -\frac{\eta_1 \overline{P}_0(k,\omega)}{2\mu R_{\mathrm{a}}(k)} \Big[\left(2k^2 - k_2^2\right) \cosh(\eta_1 z) \cosh(\eta_2 H) - 2k^2 \cosh(\eta_1 H) \cosh(\eta_2 z) \Big] \tag{3.92}$$

$$\overline{S}_{rr0}(k,z,\omega) = \frac{\overline{P}_0(k,\omega)}{2R_{\mathrm{a}}(k)} \Big[\left(k_2^2 + 2\eta_1^2\right) \left(2k^2 - k_2^2\right) \sinh(\eta_1 z) \cosh(\eta_2 H) - 4k^2 \eta_1 \eta_2 \cosh(\eta_1 H) \sinh(\eta_2 z) \Big] \tag{3.93}$$

$$\overline{S}_{rr1}(k,z,\omega) = -\frac{\overline{P}_0(k,\omega)}{rR_{\mathrm{a}}(k)} \Big[\left(2k^2 - k_2^2\right) k \sinh(\eta_1 z) \cosh(\eta_2 H) - 2k\eta_1 \eta_2 \cosh(\eta_1 H) \sinh(\eta_2 z) \Big] \tag{3.94}$$

$$\overline{S}_{\theta\theta 0}(k,z,\omega) = \frac{\overline{P}_0(k,\omega)}{2R_{\mathrm{a}}(k)} \Big[\left(k_2^2 - 2k_1^2\right) \left(2k^2 - k_2^2\right) \sinh(\eta_1 z) \cosh(\eta_2 H) \Big] \tag{3.95}$$

$$\overline{S}_{\theta\theta 1}(k,z,\omega) = \frac{\overline{P}_0(k,\omega)}{rR_{\mathrm{a}}(k)} \Big[\left(2k^2 - k_2^2\right) k \sinh(\eta_1 z) \cosh(\eta_2 H) - 2k\eta_1 \eta_2 \cosh(\eta_1 H) \sinh(\eta_2 z) \Big] \tag{3.96}$$

$$\overline{S}_{zz0}(k,z,\omega) = -\frac{\overline{P}_0(k,\omega)}{2R_{\mathrm{a}}(k)} \Big[\left(2k^2 - k_2^2\right)^2 \sinh(\eta_1 z) \cosh(\eta_2 H) - 4k^2 \eta_1 \eta_2 \cosh(\eta_1 H) \sinh(\eta_2 z) \Big] \tag{3.97}$$

$$S_{rz1}(k,z,\omega) = \frac{\left(2k^2 - k_2^2\right) \eta_1 k \overline{P}_0(k,\omega)}{R_{\mathrm{a}}(k)} \Big[\cosh(\eta_1 z) \cosh(\eta_2 H) - \cosh(\eta_1 H) \cosh(\eta_2 z) \Big] \tag{3.98}$$

The inverse Hankel transform with respect to the wavenumber k

$$F(r,z,\omega) = \frac{1}{2} \int_{-\infty}^{\infty} \overline{F}_m(k,z,\omega)\, k H_m^{(1)}(kr)\, dk \tag{3.99}$$

gives the field variables in the radial (r) and the frequency (ω) domain. The integral in Equation (3.99) has simple poles at the roots of the antisymmetric Lamb wave dispersion equation, obtained by equating $R_{\mathrm{a}}(k) = 0$.

Figure (2.8) shows a schematic of the roots in the complex k plane. There are real, imaginary and complex roots. The closed contour in the complex k plane with the anticlockwise direction it is traversed is indicated. To satisfy the radiation boundary condition at $r = \infty$, that is no incoming waves from infinity, the negative real poles are avoided in the contour. All real, imaginary and complex poles in the upper half complex k plane are enclosed in the contour. The field in Equation (3.99) is then given by

$$\begin{aligned} F(r,z,\omega) = \frac{1}{2} 2\pi i \,(\text{Sum of the residues at the poles} \\ k_{\mathrm{a}} \text{ of } \overline{F}_m(k,z,\omega)\, k H_m^{(1)}(kr)\big) \end{aligned} \tag{3.100}$$

where, $F(r,z,\omega)$ is the field variable due to antisymmetric Lamb waves. k_{a} are the roots of the antisymmetric Lamb wave dispersion equation. The displacements and the stresses can be written as

$$\begin{aligned} U_1(r,z,\omega) = \sum_{k_{\mathrm{a}}} i \frac{\pi k_{\mathrm{a}}^2 \overline{P}_0(k_{\mathrm{a}},\omega)}{2\mu R_{\mathrm{a}}'(k_{\mathrm{a}})} \Big[\left(2k_{\mathrm{a}}^2 - k_2^2\right) \sinh(\eta_{1\mathrm{a}} z) \cosh(\eta_{2\mathrm{a}} H) \\ - 2\eta_{1\mathrm{a}}\eta_{2\mathrm{a}} \cosh(\eta_{1\mathrm{a}} H) \sinh(\eta_{2\mathrm{a}} z) \Big] H_1^{(1)}(k_{\mathrm{a}} r) \end{aligned} \tag{3.101}$$

$$\begin{aligned} W_0(r,z,\omega) = \sum_{k_{\mathrm{a}}} -i \frac{\pi \eta_{1\mathrm{a}} k_{\mathrm{a}} \overline{P}_0(k_{\mathrm{a}},\omega)}{2\mu R_{\mathrm{a}}'(k_{\mathrm{a}})} \Big[\left(2k_{\mathrm{a}}^2 - k_2^2\right) \cosh(\eta_{1\mathrm{a}} z) \cosh(\eta_{2\mathrm{a}} H) \\ - 2k_{\mathrm{a}}^2 \cosh(\eta_{1\mathrm{a}} H) \cosh(\eta_{2\mathrm{a}} z) \Big] H_0^{(1)}(k_{\mathrm{a}} r) \end{aligned} \tag{3.102}$$

$$S_{rr0}\left(r,z,\omega\right)=\sum_{k_{\mathrm{a}}}i\frac{\pi k_{\mathrm{a}}\overline{P}_{0}\left(k_{\mathrm{a}},\omega\right)}{2R_{\mathrm{a}}^{\prime}\left(k_{\mathrm{a}}\right)}\Bigg[\left(k_{2}^{2}+2\eta_{1\mathrm{a}}^{2}\right)\left(2k_{\mathrm{a}}^{2}-k_{2}^{2}\right)\sinh\left(\eta_{1\mathrm{a}}z\right)\cosh\left(\eta_{2\mathrm{a}}H\right)$$
$$-4k_{\mathrm{a}}^{2}\eta_{1\mathrm{a}}\eta_{2\mathrm{a}}\cosh\left(\eta_{1\mathrm{a}}H\right)\sinh\left(\eta_{2\mathrm{a}}z\right)\Bigg]H_{0}^{(1)}\left(k_{\mathrm{a}}r\right) \tag{3.103}$$

$$S_{rr1}\left(r,z,\omega\right)=\sum_{k_{\mathrm{a}}}-i\frac{\pi k_{\mathrm{a}}^{2}\overline{P}_{0}\left(k_{\mathrm{a}},\omega\right)}{rR_{\mathrm{a}}^{\prime}\left(k_{\mathrm{a}}\right)}\Bigg[\left(2k_{\mathrm{a}}^{2}-k_{2}^{2}\right)\sinh\left(\eta_{1\mathrm{a}}z\right)\cosh\left(\eta_{2\mathrm{a}}H\right)$$
$$-2\eta_{1\mathrm{a}}\eta_{2\mathrm{a}}\cosh\left(\eta_{1\mathrm{a}}H\right)\sinh\left(\eta_{2\mathrm{a}}z\right)\Bigg]H_{1}^{(1)}\left(k_{\mathrm{a}}r\right) \tag{3.104}$$

$$S_{\theta\theta0}\left(r,z,\omega\right)=\sum_{k_{\mathrm{a}}}i\frac{\pi k_{\mathrm{a}}\overline{P}_{0}\left(k,\omega\right)}{2R_{\mathrm{a}}^{\prime}\left(k\right)}\Bigg[\left(k_{2}^{2}-2k_{1}^{2}\right)\left(2k^{2}-k_{2}^{2}\right)$$
$$\sinh\left(\eta_{1}z\right)\cosh\left(\eta_{2}H\right)\Bigg]H_{0}^{(1)}\left(k_{\mathrm{a}}r\right) \tag{3.105}$$

$$S_{\theta\theta1}\left(r,z,\omega\right)=\sum_{k_{\mathrm{a}}}i\frac{\pi k_{\mathrm{a}}^{2}\overline{P}_{0}\left(k,\omega\right)}{rR_{\mathrm{a}}^{\prime}\left(k\right)}\Bigg[\left(2k^{2}-k_{2}^{2}\right)\sinh\left(\eta_{1}z\right)\cosh\left(\eta_{2}H\right)$$
$$-2\eta_{1}\eta_{2}\cosh\left(\eta_{1}H\right)\sinh\left(\eta_{2}z\right)\Bigg]H_{1}^{(1)}\left(k_{\mathrm{a}}r\right) \tag{3.106}$$

$$S_{zz0}\left(r,z,\omega\right)=\sum_{k_{\mathrm{a}}}-i\frac{\pi k_{\mathrm{a}}\overline{P}_{0}\left(k_{\mathrm{a}},\omega\right)}{2R_{\mathrm{a}}^{\prime}\left(k_{\mathrm{a}}\right)}\Bigg[\left(2k_{\mathrm{a}}^{2}-k_{2}^{2}\right)^{2}\sinh\left(\eta_{1\mathrm{a}}z\right)\cosh\left(\eta_{2\mathrm{a}}H\right)$$
$$-4k_{\mathrm{a}}^{2}\eta_{1\mathrm{a}}\eta_{2\mathrm{a}}\cosh\left(\eta_{1\mathrm{a}}H\right)\sinh\left(\eta_{2\mathrm{a}}z\right)\Bigg]H_{0}^{(1)}\left(k_{\mathrm{a}}r\right) \tag{3.107}$$

$$S_{rz1}\left(r,z,\omega\right)=\sum_{k_{\mathrm{a}}}-i\frac{\pi\left(2k_{\mathrm{a}}^{2}-k_{2}^{2}\right)\eta_{1\mathrm{a}}k_{\mathrm{a}}^{2}\overline{P}_{0}\left(k_{\mathrm{a}},\omega\right)}{R_{\mathrm{a}}^{\prime}\left(k_{\mathrm{a}}\right)}\Bigg[\cosh\left(\eta_{1\mathrm{a}}z\right)\cosh\left(\eta_{2\mathrm{a}}H\right)$$
$$-\cosh\left(\eta_{1\mathrm{a}}H\right)\cosh\left(\eta_{2\mathrm{a}}z\right)\Bigg]H_{1}^{(1)}\left(k_{\mathrm{a}}r\right) \tag{3.108}$$

where $R'_{\mathrm{a}}(k_{\mathrm{a}})$ is the derivative of $R_{\mathrm{a}}(k)$, the antisymmetric Lamb wave denominator with respect to k, evaluated at the roots of the antisymmetric Lamb wave dispersion equation k_{a} and is given by

$$\begin{aligned}
R'_{\mathrm{a}}(k_{\mathrm{a}}) &= 8\left(2k_{\mathrm{a}}^2 - k_2^2\right) k_{\mathrm{a}} \sinh(\eta_{1\mathrm{a}} H)\cosh(\eta_{2\mathrm{a}} H) \\
&+ \left(2k_{\mathrm{a}}^2 - k_2^2\right)^2 \frac{k_{\mathrm{a}} H}{\eta_{1\mathrm{a}}} \cosh(\eta_{1\mathrm{a}} H)\cosh(\eta_{2\mathrm{a}} H) \\
&+ \left(2k_{\mathrm{a}}^2 - k_2^2\right)^2 \frac{k_{\mathrm{a}} H}{\eta_{2\mathrm{a}}} \sinh(\eta_{1\mathrm{a}} H)\sinh(\eta_{2\mathrm{a}} H) \\
&- 8k_{\mathrm{a}}\eta_{1\mathrm{a}}\eta_{2\mathrm{a}} \cosh(\eta_{1\mathrm{a}} H)\sinh(\eta_{2\mathrm{a}} H) \\
&- 4k_{\mathrm{a}}^3 \frac{\eta_{2\mathrm{a}}}{\eta_{1\mathrm{a}}} \cosh(\eta_{1\mathrm{a}} H)\sinh(\eta_{2\mathrm{a}} H) \\
&- 4k_{\mathrm{a}}^3 \frac{\eta_{1\mathrm{a}}}{\eta_{2\mathrm{a}}} \cosh(\eta_{1\mathrm{a}} H)\sinh(\eta_{2\mathrm{a}} H) \\
&- 4k_{\mathrm{a}}^3 \eta_{2\mathrm{a}} H \sinh(\eta_{1\mathrm{a}} H)\sinh(\eta_{2\mathrm{a}} H) \\
&- 4k_{\mathrm{a}}^3 \eta_{1\mathrm{a}} H \cosh(\eta_{1\mathrm{a}} H)\cosh(\eta_{2\mathrm{a}} H)
\end{aligned} \tag{3.109}$$

In Equations (3.101-3.109), $\eta_{1\mathrm{a}}$ and $\eta_{2\mathrm{a}}$ are the values of η_1 and η_2 evaluated at k_{a}.

For a large argument, the Hankel function of the first kind of order m becomes approximately equals to [39]

$$H_m^{(1)}(x) \approx \sqrt{\frac{2}{\pi x}} e^{i\left(x - \frac{\pi}{4} - \frac{m\pi}{2}\right)}$$

which simplifies to

$$H_0^{(1)}(x) \approx \sqrt{\frac{2}{\pi x}} e^{i\left(x - \frac{\pi}{4}\right)} \qquad H_1^{(1)}(x) \approx -i\sqrt{\frac{2}{\pi x}} e^{i\left(x - \frac{\pi}{4}\right)}$$

Hence for a large distance away from the from the origin, the displacements and the stresses in the frequency domain due to the antisymmetric Lamb waves can be written as

$$\begin{aligned}
U_1(r, z, \omega) = \sum_{k_{\mathrm{a}}} \frac{\sqrt{\pi} k_{\mathrm{a}}^{\frac{3}{2}} \overline{P}_0(k_{\mathrm{a}}, \omega)}{\sqrt{2r}\mu R'_{\mathrm{a}}(k_{\mathrm{a}})} \Big[&\left(2k_{\mathrm{a}}^2 - k_2^2\right) \sinh(\eta_{1\mathrm{a}} z)\cosh(\eta_{2\mathrm{a}} H) \\
&- 2\eta_{1\mathrm{a}}\eta_{2\mathrm{a}} \cosh(\eta_{1\mathrm{a}} H)\sinh(\eta_{2\mathrm{a}} z) \Big] e^{i\left(k_{\mathrm{a}} r - \frac{\pi}{4}\right)}
\end{aligned} \tag{3.110}$$

$$W_0(r,z,\omega)=\sum_{k_\mathrm{a}}-i\frac{\sqrt{\pi k_\mathrm{a}}\eta_{1\mathrm{a}}\overline{P}_0(k_\mathrm{a},\omega)}{\sqrt{2r}\mu R'_\mathrm{a}(k_\mathrm{a})}\Big[\left(2k_\mathrm{a}^2-k_2^2\right)\cosh(\eta_{1\mathrm{a}}z)\cosh(\eta_{2\mathrm{a}}H)-2k_\mathrm{a}^2\cosh(\eta_{1\mathrm{a}}H)\cosh(\eta_{2\mathrm{a}}z)\Big]e^{i\left(k_\mathrm{a}r-\frac{\pi}{4}\right)} \tag{3.111}$$

$$S_{rr0}(r,z,\omega)=\sum_{k_\mathrm{a}}i\frac{\sqrt{\pi k_\mathrm{a}}\,\overline{P}_0(k_\mathrm{a},\omega)}{\sqrt{2r}R'_\mathrm{a}(k_\mathrm{a})}\Big[\left(k_2^2+2\eta_{1\mathrm{a}}^2\right)\left(2k_\mathrm{a}^2-k_2^2\right)\sinh(\eta_{1\mathrm{a}}z)\cosh(\eta_{2\mathrm{a}}H)-4k_\mathrm{a}^2\eta_{1\mathrm{a}}\eta_{2\mathrm{a}}\cosh(\eta_{1\mathrm{a}}H)\sinh(\eta_{2\mathrm{a}}z)\Big]e^{i\left(k_\mathrm{a}r-\frac{\pi}{4}\right)} \tag{3.112}$$

$$S_{rr1}(r,z,\omega)=\sum_{k_\mathrm{a}}-\frac{\sqrt{2\pi}k_\mathrm{a}^{\frac{3}{2}}\overline{P}_0(k_\mathrm{a},\omega)}{r^{\frac{3}{2}}R'_\mathrm{a}(k_\mathrm{a})}\Big[\left(2k_\mathrm{a}^2-k_2^2\right)\sinh(\eta_{1\mathrm{a}}z)\cosh(\eta_{2\mathrm{a}}H)-2\eta_{1\mathrm{a}}\eta_{2\mathrm{a}}\cosh(\eta_{1\mathrm{a}}H)\sinh(\eta_{2\mathrm{a}}z)\Big]e^{i\left(k_\mathrm{a}r-\frac{\pi}{4}\right)} \tag{3.113}$$

$$S_{\theta\theta0}(r,z,\omega)=\sum_{k_\mathrm{a}}i\frac{\sqrt{\pi k_\mathrm{a}}\,\overline{P}_0(k,\omega)}{\sqrt{2r}R'_\mathrm{a}(k)}\Big[\left(k_2^2-2k_1^2\right)\left(2k^2-k_2^2\right)\sinh(\eta_1z)\cosh(\eta_2H)\Big]e^{i\left(k_\mathrm{a}r-\frac{\pi}{4}\right)} \tag{3.114}$$

$$S_{\theta\theta1}(r,z,\omega)=\sum_{k_\mathrm{a}}\frac{\sqrt{2\pi}k_\mathrm{a}^{\frac{3}{2}}\overline{P}_0(k,\omega)}{r^{\frac{3}{2}}R'_\mathrm{a}(k)}\Big[\left(2k^2-k_2^2\right)\sinh(\eta_1z)\cosh(\eta_2H)-2\eta_1\eta_2\cosh(\eta_1H)\sinh(\eta_2z)\Big]e^{i\left(k_\mathrm{a}r-\frac{\pi}{4}\right)} \tag{3.115}$$

$$S_{zz0}(r,z,\omega)=\sum_{k_\mathrm{a}}-i\frac{\sqrt{\pi k_\mathrm{a}}\,\overline{P}_0(k_\mathrm{a},\omega)}{\sqrt{2r}R'_\mathrm{a}(k_\mathrm{a})}\Big[\left(2k_\mathrm{a}^2-k_2^2\right)^2\sinh(\eta_{1\mathrm{a}}z)\cosh(\eta_{2\mathrm{a}}H)-4k_\mathrm{a}^2\eta_{1\mathrm{a}}\eta_{2\mathrm{a}}\cosh(\eta_{1\mathrm{a}}H)\sinh(\eta_{2\mathrm{a}}z)\Big]e^{i\left(k_\mathrm{a}r-\frac{\pi}{4}\right)} \tag{3.116}$$

$$S_{rz1}(r,z,\omega)=\sum_{k_a}\frac{\sqrt{2\pi}\left(2k_a^2-k_2^2\right)\eta_{1a}k_a^{\frac{3}{2}}\overline{P}_0(k_a,\omega)}{\sqrt{r}R_a'(k_a)}\Bigg[\cosh(\eta_{1a}z)\cosh(\eta_{2a}H)$$
$$-\cosh(\eta_{1a}H)\cosh(\eta_{2a}z)\Bigg]e^{i\left(k_ar-\frac{\pi}{4}\right)} \tag{3.117}$$

From Equations (3.110-3.117), it is seen that for the imaginary roots ik_a of the dispersion equations, the various field variables have the form

$$F(x,z,\omega)=\frac{G(k_a,z,\omega)}{R_a'(k_a)}e^{-k_ar-i\frac{\pi}{4}} \tag{3.118}$$

which exponentially decreases for increasing values of r. The complex roots in the upper half complex k plane come in pairs of the the form $k_a=a+ib,-a+ib$. For the complex roots, the various field variables have the form

$$F(x,z,\omega)=\frac{G(k_a,z,\omega)}{R_a'(k_a)}e^{\pm iax-i\frac{\pi}{4}}e^{-br} \tag{3.119}$$

which too exponentially decrease for increasing value of r. The antisymmetric Lamb waves traveling large distances in the plate are the propagating waves given by the residues of the real positive roots.

3.4 Symmetric Lamb wave propagation under axisymmetric dynamic surface load

From Equations (3.72, 3.73), zero shear stress at $z=H$ gives,

$$\overline{S}_{rz1}(k,H,\omega)=2\eta_1\eta_2\overline{A}_1\sinh(\eta_1H)+\left(2k^2-k_2^2\right)\overline{A}_3\sinh(\eta_2z)=0 \tag{3.120}$$

which gives,

$$\overline{A}_1=-\frac{(2k^2-k_2^2)\sinh(\eta_2H)}{2\eta_1\eta_2\sinh(\eta_1H)}\overline{A}_3 \tag{3.121}$$

At $z = H$, the applied normal load gives,

$$\overline{S}_{zz0}\left(k, H, \omega\right) = -\frac{\overline{P}_0\left(k, \omega\right)}{2} \tag{3.122}$$

which gives,

$$\frac{\mu}{k}\left[\left(2k^2 - k_2^2\right)\overline{A}_1 \cosh\left(\eta_1 H\right) + 2k^2\overline{A}_3 \cosh\left(\eta_2 H\right)\right] = \frac{\overline{P}_0}{2} \tag{3.123}$$

Substituting $\overline{A}_1$ from Equation (3.121) into Equation (3.123)

$$\overline{A}_3 = -\frac{k\eta_1\eta_2 \sinh\left(\eta_1 H\right)}{\mu R_{\mathrm{s}}\left(k\right)}\overline{P}_0\left(k, \omega\right) \tag{3.124}$$

where, $R_{\mathrm{s}}\left(k\right)$ is the symmetric Lamb wave denominator and is given by

$$R_{\mathrm{s}}\left(k\right) = \left(2k^2 - k_2^2\right)^2 \cosh\left(\eta_1 H\right)\sinh\left(\eta_2 H\right) - 4k^2\eta_1\eta_2 \sinh\left(\eta_1 H\right)\cosh\left(\eta_2 H\right) \tag{3.125}$$

Substituting $\overline{A}_3$ from Equation (3.124) into Equation (3.121)

$$\overline{A}_1 = \frac{k\left(2k^2 - k_2^2\right)\sinh\left(\eta_2 H\right)}{2\mu R_{\mathrm{s}}\left(k\right)}\overline{P}_0\left(k, \omega\right) \tag{3.126}$$

Using the above values of $\overline{A}_1$ and $\overline{A}_3$, the displacements and the stresses in the plate due to the symmetric Lamb wave in the frequency domain are given by

$$\overline{U}_1\left(k, z, \omega\right) = \frac{k\overline{P}_0\left(k, \omega\right)}{2\mu R_{\mathrm{s}}\left(k\right)}\left[\left(2k^2 - k_2^2\right)\cosh\left(\eta_1 z\right)\sinh\left(\eta_2 H\right) - 2\eta_1\eta_2 \sinh\left(\eta_1 H\right)\cosh\left(\eta_2 z\right)\right] \tag{3.127}$$

$$\overline{W}_0\left(k, z, \omega\right) = -\frac{\eta_1\overline{P}_0\left(k, \omega\right)}{2\mu R_{\mathrm{s}}\left(k\right)}\left[\left(2k^2 - k_2^2\right)\sinh\left(\eta_1 z\right)\sinh\left(\eta_2 H\right) - 2k^2 \sinh\left(\eta_1 H\right)\sinh\left(\eta_2 z\right)\right] \tag{3.128}$$

$$\overline{S}_{rr0}\left(k, z, \omega\right) = \frac{\overline{P}_0\left(k, \omega\right)}{2R_{\mathrm{s}}\left(k\right)}\left[\left(k_2^2 + 2\eta_1^2\right)\left(2k^2 - k_2^2\right)\cosh\left(\eta_1 z\right)\sinh\left(\eta_2 H\right) - 4k^2\eta_1\eta_2 \sinh\left(\eta_1 H\right)\cosh\left(\eta_2 z\right)\right] \tag{3.129}$$

$$\overline{S}_{rr1}(k,z,\omega) = -\frac{\overline{P}_0(k,\omega)}{rR_{\mathrm{s}}(k)}\Big[\left(2k^2-k_2^2\right)k\cosh(\eta_1 z)\sinh(\eta_2 H) - 2k\eta_1\eta_2\sinh(\eta_1 H)\cosh(\eta_2 z)\Big] \tag{3.130}$$

$$\overline{S}_{\theta\theta 0}(k,z,\omega) = \frac{\overline{P}_0(k,\omega)}{2R_{\mathrm{s}}(k)}\Big[\left(k_2^2-2k_1^2\right)\left(2k^2-k_2^2\right)\cosh(\eta_1 z)\sinh(\eta_2 H)\Big] \tag{3.131}$$

$$\overline{S}_{\theta\theta 1}(k,z,\omega) = \frac{\overline{P}_0(k,\omega)}{rR_{\mathrm{s}}(k)}\Big[\left(2k^2-k_2^2\right)k\cosh(\eta_1 z)\sinh(\eta_2 H) - 2k\eta_1\eta_2\sinh(\eta_1 H)\cosh(\eta_2 z)\Big] \tag{3.132}$$

$$\overline{S}_{zz0}(k,z,\omega) = -\frac{\overline{P}_0(k,\omega)}{2R_{\mathrm{s}}(k)}\Big[\left(2k^2-k_2^2\right)^2\cosh(\eta_1 z)\sinh(\eta_2 H) - 4k^2\eta_1\eta_2\sinh(\eta_1 H)\cosh(\eta_2 z)\Big] \tag{3.133}$$

$$S_{rz1}(k,z,\omega) = \frac{\left(2k^2-k_2^2\right)\eta_1 k\overline{P}_0(k,\omega)}{R_{\mathrm{s}}(k)}\Big[\sinh(\eta_1 z)\sinh(\eta_2 H) - \sinh(\eta_1 H)\sinh(\eta_2 z)\Big] \tag{3.134}$$

The inverse Hankel transform with respect to the wavenumber k

$$F(r,z,\omega) = \frac{1}{2}\int_{-\infty}^{\infty}\overline{F}_m(k,z,\omega)\,kH_m^{(1)}(kr)\,dk \tag{3.135}$$

gives the field variables in the radial (r) and the frequency (ω) domain. The integral in Equation (3.135) has simple poles at the roots of the symmetric Lamb wave dispersion equation, obtained by equating $R_{\mathrm{s}}(k) = 0$.

Figure (2.8) shows a schematic of the roots in the complex k plane. There are real, imaginary and complex roots. The closed contour in the complex k plane with the anticlockwise direction it is traversed is indicated. To satisfy the radiation boundary condition at $r = \infty$, that is no incoming waves from infinity, the negative

real poles are avoided in the contour. All real, imaginary and complex poles in the upper half complex k plane are enclosed in the contour. The field in Equation (3.135) is then given by

$$F(r,z,\omega) = \frac{1}{2}2\pi i \left(\text{Sum of the residues at the poles } k_\text{s} \text{ of } \overline{F}_m(k,z,\omega)\, kH_m^{(1)}(kr)\right) \tag{3.136}$$

where, $F(r,z,\omega)$ is the field variable due to symmetric Lamb waves. k_s are the roots of the symmetric Lamb wave dispersion equation. The displacements and the stresses can be written as

$$U_1(r,z,\omega) = \sum_{k_\text{s}} i\frac{\pi k_\text{s}^2 \overline{P}_0(k_\text{s},\omega)}{2\mu R_\text{s}'(k_\text{s})}\Big[\left(2k_\text{s}^2 - k_2^2\right)\cosh(\eta_{1\text{s}}z)\sinh(\eta_{2\text{s}}H) - 2\eta_{1\text{s}}\eta_{2\text{s}}\sinh(\eta_{1\text{s}}H)\cosh(\eta_{2\text{s}}z)\Big]H_1^{(1)}(k_\text{s}r) \tag{3.137}$$

$$W_0(r,z,\omega) = \sum_{k_\text{s}} -i\frac{\pi \eta_{1\text{s}} k_\text{s} \overline{P}_0(k_\text{s},\omega)}{2\mu R_\text{s}'(k_\text{s})}\Big[\left(2k_\text{s}^2 - k_2^2\right)\sinh(\eta_{1\text{s}}z)\sinh(\eta_{2\text{s}}H) - 2k_\text{s}^2\sinh(\eta_{1\text{s}}H)\sinh(\eta_{2\text{s}}z)\Big]H_0^{(1)}(k_\text{s}r) \tag{3.138}$$

$$S_{rr0}(r,z,\omega) = \sum_{k_\text{s}} i\frac{\pi k_\text{s} \overline{P}_0(k_\text{s},\omega)}{2R_\text{s}'(k_\text{s})}\Big[\left(k_2^2 + 2\eta_{1\text{s}}^2\right)\left(2k_\text{s}^2 - k_2^2\right)\cosh(\eta_{1\text{s}}z)\sinh(\eta_{2\text{s}}H) - 4k_\text{s}^2\eta_{1\text{s}}\eta_{2\text{s}}\sinh(\eta_{1\text{s}}H)\cosh(\eta_{2\text{s}}z)\Big]H_0^{(1)}(k_\text{s}r) \tag{3.139}$$

$$S_{rr1}(r,z,\omega) = \sum_{k_\text{s}} -i\frac{\pi k_\text{s}^2 \overline{P}_0(k_\text{s},\omega)}{rR_\text{s}'(k_\text{s})}\Big[\left(2k_\text{s}^2 - k_2^2\right)\cosh(\eta_{1\text{s}}z)\sinh(\eta_{2\text{s}}H) - 2\eta_{1\text{s}}\eta_{2\text{s}}\sinh(\eta_{1\text{s}}H)\cosh(\eta_{2\text{s}}z)\Big]H_1^{(1)}(k_\text{s}r) \tag{3.140}$$

$$S_{\theta\theta 0}(r,z,\omega) = \sum_{k_\text{s}} i\frac{\pi k_\text{s} \overline{P}_0(k,\omega)}{2R_\text{s}'(k)}\Big[\left(k_2^2 - 2k_1^2\right)\left(2k^2 - k_2^2\right)\cosh(\eta_1 z)\sinh(\eta_2 H)\Big]H_0^{(1)}(k_\text{s}r) \tag{3.141}$$

$$S_{\theta\theta 1}(r,z,\omega) = \sum_{k_s} i\frac{\pi k_s^2 \overline{P}_0(k,\omega)}{r R_s'(k)} \Big[\left(2k^2 - k_2^2\right)\cosh(\eta_1 z)\sinh(\eta_2 H) - 2\eta_1\eta_2 \sinh(\eta_1 H)\cosh(\eta_2 z) \Big] H_1^{(1)}(k_s r) \tag{3.142}$$

$$S_{zz0}(r,z,\omega) = \sum_{k_s} -i\frac{\pi k_s \overline{P}_0(k_s,\omega)}{2R_s'(k_s)} \Big[\left(2k_s^2 - k_2^2\right)^2 \cosh(\eta_{1s} z)\sinh(\eta_{2s} H) - 4k_s^2\eta_{1s}\eta_{2s} \sinh(\eta_{1s} H)\cosh(\eta_{2s} z) \Big] H_0^{(1)}(k_s r) \tag{3.143}$$

$$S_{rz1}(r,z,\omega) = \sum_{k_s} -i\frac{\pi\left(2k_s^2 - k_2^2\right)\eta_{1s} k_s^2 \overline{P}_0(k_s,\omega)}{R_s'(k_s)} \Big[\sinh(\eta_{1s} z)\sinh(\eta_{2s} H) - \sinh(\eta_{1s} H)\sinh(\eta_{2s} z) \Big] H_1^{(1)}(k_s r) \tag{3.144}$$

where $R_s'(k_s)$ is the derivative of $R_s(k)$, the symmetric Lamb wave denominator with respect to k, evaluated at the roots of the symmetric Lamb wave dispersion equation k_s and is given by

$$\begin{aligned} R_s'(k_s) = {} & 8\left(2k_s^2 - k_2^2\right) k_s \cosh(\eta_{1s} H)\sinh(\eta_{2s} H) \\ & + \left(2k_s^2 - k_2^2\right)^2 \frac{k_s H}{\eta_{1s}} \sinh(\eta_{1s} H)\sinh(\eta_{2s} H) \\ & + \left(2k_s^2 - k_2^2\right)^2 \frac{k_s H}{\eta_{2s}} \cosh(\eta_{1s} H)\cosh(\eta_{2s} H) \\ & - 8k_s\eta_{1s}\eta_{2s} \sinh(\eta_{1s} H)\cosh(\eta_{2s} H) \\ & - 4k_s^3 \frac{\eta_{2s}}{\eta_{1s}} \sinh(\eta_{1s} H)\cosh(\eta_{2s} H) \\ & - 4k_s^3 \frac{\eta_{1s}}{\eta_{2s}} \sinh(\eta_{1s} H)\cosh(\eta_{2s} H) \\ & - 4k_s^3\eta_{2s} H \cosh(\eta_{1s} H)\cosh(\eta_{2s} H) \\ & - 4k_s^3\eta_{1s} H \sinh(\eta_{1s} H)\sinh(\eta_{2s} H) \end{aligned} \tag{3.145}$$

In Equations (3.137-3.145), η_{1s} and η_{2s} are the values of η_1 and η_2 evaluated at k_s.

Using the approximation to Hankel functions for large arguments, for a large distance away from the origin, the displacements and the stresses in the frequency domain due to the symmetric Lamb waves can be written as

$$U_1(r,z,\omega)=\sum_{k_\mathrm{s}}\frac{\sqrt{\pi}k_\mathrm{s}^{\frac{3}{2}}\overline{P}_0(k_\mathrm{s},\omega)}{\sqrt{2r}\mu R_\mathrm{s}'(k_\mathrm{s})}\Big[\left(2k_\mathrm{s}^2-k_2^2\right)\cosh(\eta_{1\mathrm{s}}z)\sinh(\eta_{2\mathrm{s}}H) - 2\eta_{1\mathrm{s}}\eta_{2\mathrm{s}}\sinh(\eta_{1\mathrm{s}}H)\cosh(\eta_{2\mathrm{s}}z)\Big]e^{i\left(k_\mathrm{s}r-\frac{\pi}{4}\right)} \tag{3.146}$$

$$W_0(r,z,\omega)=\sum_{k_\mathrm{s}}-i\frac{\sqrt{\pi k_\mathrm{s}}\eta_{1\mathrm{s}}\overline{P}_0(k_\mathrm{s},\omega)}{\sqrt{2r}\mu R_\mathrm{s}'(k_\mathrm{s})}\Big[\left(2k_\mathrm{s}^2-k_2^2\right)\sinh(\eta_{1\mathrm{s}}z)\sinh(\eta_{2\mathrm{s}}H) - 2k_\mathrm{s}^2\sinh(\eta_{1\mathrm{s}}H)\sinh(\eta_{2\mathrm{s}}z)\Big]e^{i\left(k_\mathrm{s}r-\frac{\pi}{4}\right)} \tag{3.147}$$

$$S_{rr0}(r,z,\omega)=\sum_{k_\mathrm{s}}i\frac{\sqrt{\pi k_\mathrm{s}}\,\overline{P}_0(k_\mathrm{s},\omega)}{\sqrt{2r}R_\mathrm{s}'(k_\mathrm{s})}\Big[\left(k_2^2+2\eta_{1\mathrm{s}}^2\right)\left(2k_\mathrm{s}^2-k_2^2\right)\cosh(\eta_{1\mathrm{s}}z)\sinh(\eta_{2\mathrm{s}}H) - 4k_\mathrm{s}^2\eta_{1\mathrm{s}}\eta_{2\mathrm{s}}\sinh(\eta_{1\mathrm{s}}H)\cosh(\eta_{2\mathrm{s}}z)\Big]e^{i\left(k_\mathrm{s}r-\frac{\pi}{4}\right)} \tag{3.148}$$

$$S_{rr1}(r,z,\omega)=\sum_{k_\mathrm{s}}-\frac{\sqrt{2\pi}k_\mathrm{s}^{\frac{3}{2}}\overline{P}_0(k_\mathrm{s},\omega)}{r^{\frac{3}{2}}R_\mathrm{s}'(k_\mathrm{s})}\Big[\left(2k_\mathrm{s}^2-k_2^2\right)\cosh(\eta_{1\mathrm{s}}z)\sinh(\eta_{2\mathrm{s}}H) - 2\eta_{1\mathrm{s}}\eta_{2\mathrm{s}}\sinh(\eta_{1\mathrm{s}}H)\cosh(\eta_{2\mathrm{s}}z)\Big]e^{i\left(k_\mathrm{s}r-\frac{\pi}{4}\right)} \tag{3.149}$$

$$S_{\theta\theta0}(r,z,\omega)=\sum_{k_\mathrm{s}}i\frac{\sqrt{\pi k_\mathrm{s}}\,\overline{P}_0(k,\omega)}{\sqrt{2r}R_\mathrm{s}'(k)}\Big[\left(k_2^2-2k_1^2\right)\left(2k^2-k_2^2\right)\cosh(\eta_1 z)\sinh(\eta_2 H)\Big]e^{i\left(k_\mathrm{s}r-\frac{\pi}{4}\right)} \tag{3.150}$$

$$S_{\theta\theta 1}(r,z,\omega)=\sum_{k_s}\frac{\sqrt{2\pi}k_s^{\frac{3}{2}}\overline{P}_0(k,\omega)}{r^{\frac{3}{2}}R_s'(k)}\Big[\left(2k^2-k_2^2\right)\cosh(\eta_1 z)\sinh(\eta_2 H) - 2\eta_1\eta_2\sinh(\eta_1 H)\cosh(\eta_2 z)\Big]e^{i\left(k_s r-\frac{\pi}{4}\right)} \tag{3.151}$$

$$S_{zz0}(r,z,\omega)=\sum_{k_s}-i\frac{\sqrt{\pi k_s}\,\overline{P}_0(k_s,\omega)}{\sqrt{2r}R_s'(k_s)}\Big[\left(2k_s^2-k_2^2\right)^2\cosh(\eta_{1s} z)\sinh(\eta_{2s} H) - 4k_s^2\eta_{1s}\eta_{2s}\sinh(\eta_{1s} H)\cosh(\eta_{2s} z)\Big]e^{i\left(k_s r-\frac{\pi}{4}\right)} \tag{3.152}$$

$$S_{rz1}(r,z,\omega)=\sum_{k_s}\frac{\sqrt{2\pi}\left(2k_s^2-k_2^2\right)\eta_{1s}k_s^{\frac{3}{2}}\overline{P}_0(k_s,\omega)}{\sqrt{r}R_s'(k_s)}\Big[\sinh(\eta_{1s} z)\sinh(\eta_{2s} H) - \sinh(\eta_{1s} H)\sinh(\eta_{2s} z)\Big]e^{i\left(k_s r-\frac{\pi}{4}\right)} \tag{3.153}$$

From Equations (3.146-3.153), it is seen that for the imaginary roots ik_s of the dispersion equations, the various field variables have the form

$$F(x,z,\omega)=\frac{G(k_s,z,\omega)}{R_s'(k_s)}e^{-k_s r-i\frac{\pi}{4}} \tag{3.154}$$

which exponentially decreases for increasing values of r. The complex roots in the upper half complex k plane come in pairs of the the form $k_s=a+ib,-a+ib$. For the complex roots, the various field variables have the form

$$F(x,z,\omega)=\frac{G(k_s,z,\omega)}{R_s'(k_s)}e^{\pm iax-i\frac{\pi}{4}}e^{-br} \tag{3.155}$$

which too exponentially decrease for increasing value of r. The symmetric Lamb waves traveling large distances in the plate are the propagating waves given by the residues of the real positive roots.

3.5 Power flow through a plate under applied axisymmetric load

The power that is the rate of energy flow carried by the propagating Lamb waves at a large distance away from the source through a cylindrical surface whose unit outward normal is along the radial direction r is calculated. The energy flow per time period ($T = \frac{2\pi}{\omega}$) of a wave in r direction is given by

$$\begin{aligned}\langle P \rangle = -\frac{1}{T}\int_0^T \Bigg(&\text{Real}\left(\sigma_{rr}\left(r,z,t\right)\right)\text{Real}\frac{\partial u\left(r,z,t\right)}{\partial t} \\ &+\text{Real}\left(\sigma_{rz}\left(r,z,t\right)\right)\text{Real}\frac{\partial w\left(r,z,t\right)}{\partial t}\Bigg)\, dt\end{aligned} \tag{3.156}$$

The displacements and the stresses are of the form

$$\begin{aligned}u\left(r,z,t\right) &= U_m\left(r,z,\omega\right) kH_m^{(1)}\left(kr\right) e^{-i\omega t} \\ &= \left(U_R + iU_I\right) e^{-i\omega t}\end{aligned} \tag{3.157}$$

$$\begin{aligned}\sigma\left(r,z,t\right) &= S_m\left(r,z,\omega\right) kH_m^{(1)}\left(kr\right) e^{-i\omega t} \\ &= \left(S_R + iS_I\right) e^{-i\omega t}\end{aligned} \tag{3.158}$$

In Equations (3.157,3.158) u, σ represent generic displacement and stress in the time (t) domain, while U_R, U_I, S_R, S_I represent the real and imaginary parts respectively of generic displacement and stress in the frequency (ω) domain.

Using the result from Equation (2.137) in Equation (2.131), the power flow in the r direction in the frequency domain is given by

$$\langle P\left(\omega\right)\rangle = -\frac{\omega}{2}\text{Imaginary}\left(U_1\left(S_{rr0}^* + S_{rr1}^*\right) + W_0 S_{rz1}^*\right) \tag{3.159}$$

In the above equation, S^* denotes the complex conjugate of S.

The power flow through a cylindrical surface in the plate, whose normal is along the radial r axis is then obtained by integrating Equation (3.159) along the thickness of the plate. For a plate with thickness $2H$ along the z axis, the power flow

though a section is given by

$$\langle \overline{P}\,(\omega)\rangle = -\frac{\omega}{2}\int_{-H}^{H} \text{Imaginary}\left(U_1\left(S^*_{rr0}+S^*_{rr1}\right)+W_0 S^*_{rz1}\right) 2\pi r\, dz \tag{3.160}$$

For antisymmetric Lamb wave motion in a plate subjected to an axisymmetric dynamic load on the top surface, the power flow through a cylindrical surface at a large distance away from the source is given by

$$\langle \overline{P_{\mathrm{a}}}\,(\omega)\rangle = \langle \overline{P_{\mathrm{a1}}}\,(\omega)\rangle + \langle \overline{P_{\mathrm{a2}}}\,(\omega)\rangle \tag{3.161}$$

where,

$$\begin{aligned}\langle \overline{P_{\mathrm{a1}}}\,(\omega)\rangle &= -\frac{\omega}{2}\int_{-H}^{H} \text{Imaginary}\left(U_1\left(S^*_{rr0}+S^*_{rr1}\right)\right) 2\pi r\, dz \\ &= \frac{\omega\pi^2 k_{\mathrm{a}}^2}{2\mu}\frac{\left|\overline{P}_0\left(k_{\mathrm{a}},\omega\right)\right|^2}{\left[R'_{\mathrm{a}}\left(k_{\mathrm{a}}\right)\right]^2} \\ &\Bigg[\left(2k_{\mathrm{a}}^2-k_2^2\right)^2\left(k_2^2+2\eta_{1\mathrm{a}}^2\right)\cosh^2\left(\eta_{2\mathrm{a}}H\right)\left(\frac{\sinh\left(2\eta_{1\mathrm{a}}H\right)}{2\eta_{1\mathrm{a}}}-H\right)- \\ &\quad 2\eta_{1\mathrm{a}}\eta_{2\mathrm{a}}\left(2k_{\mathrm{a}}^2-k_2^2\right)\left(2k_{\mathrm{a}}^2+k_2^2+2\eta_{1\mathrm{a}}^2\right)\cosh\left(\eta_{1\mathrm{a}}H\right)\cosh\left(\eta_{2\mathrm{a}}H\right) \\ &\quad \left(\frac{\sinh\left(\left(\eta_{1\mathrm{a}}+\eta_{2\mathrm{a}}\right)H\right)}{\eta_{1\mathrm{a}}+\eta_{2\mathrm{a}}}-\frac{\sinh\left(\left(\eta_{1\mathrm{a}}-\eta_{2\mathrm{a}}\right)H\right)}{\eta_{1\mathrm{a}}-\eta_{2\mathrm{a}}}\right)+ \\ &\quad 8\eta_{1\mathrm{a}}^2\eta_{2\mathrm{a}}^2k_{\mathrm{a}}^2\cosh^2\left(\eta_{1\mathrm{a}}H\right)\left(\frac{\sinh\left(2\eta_{2\mathrm{a}}H\right)}{2\eta_{2\mathrm{a}}}-H\right)\Bigg]\end{aligned} \tag{3.162}$$

and

$$\begin{aligned}\langle \overline{P_{\mathrm{a2}}}\,(\omega)\rangle &= -\frac{\omega}{2}\int_{-H}^{H} \text{Imaginary}\left(W_0 S^*_{rz1}\right) 2\pi r\, dz \\ &= \frac{\omega\pi^2 k_{\mathrm{a}}^2\eta_{1\mathrm{a}}^2\left(2k_{\mathrm{a}}^2-k_2^2\right)}{\mu}\frac{\left|\overline{P}_0\left(k_{\mathrm{a}},\omega\right)\right|^2}{\left[R'_{\mathrm{a}}\left(k_{\mathrm{a}}\right)\right]^2} \\ &\Bigg[\left(2k_{\mathrm{a}}^2-k_2^2\right)\cosh^2\left(\eta_{2\mathrm{a}}H\right)\left(\frac{\sinh\left(2\eta_{1\mathrm{a}}H\right)}{2\eta_{1\mathrm{a}}}+H\right)- \\ &\quad \left(4k_{\mathrm{a}}^2-k_2^2\right)\cosh\left(\eta_{1\mathrm{a}}H\right)\cosh\left(\eta_{2\mathrm{a}}H\right) \\ &\quad \left(\frac{\sinh\left(\left(\eta_{1\mathrm{a}}+\eta_{2\mathrm{a}}\right)H\right)}{\eta_{1\mathrm{a}}+\eta_{2\mathrm{a}}}+\frac{\sinh\left(\left(\eta_{1\mathrm{a}}-\eta_{2\mathrm{a}}\right)H\right)}{\eta_{1\mathrm{a}}-\eta_{2\mathrm{a}}}\right)+ \\ &\quad 2k_{\mathrm{a}}^2\cosh^2\left(\eta_{1\mathrm{a}}H\right)\left(\frac{\sinh\left(2\eta_{2\mathrm{a}}H\right)}{2\eta_{2\mathrm{a}}}+H\right)\Bigg]\end{aligned} \tag{3.163}$$

In Equations (3.162,3.163), U_1, W_0, S_{rr0}, S_{rr1} and S_{rz1} are the displacements and stresses for antisymmetric Lamb wave, given by Equations (3.110-3.117).

For symmetric Lamb wave motion in a plate subjected to a vertical dynamic load on the top surface, the power flow through a cylindrical surface at a large distance away from the source is given by

$$\left\langle \overline{P_{\mathrm{s}}}\left(\omega\right)\right\rangle = \left\langle \overline{P_{\mathrm{s1}}}\left(\omega\right)\right\rangle + \left\langle \overline{P_{\mathrm{s2}}}\left(\omega\right)\right\rangle \tag{3.164}$$

where,

$$\begin{aligned}
\left\langle \overline{P_{\mathrm{s1}}}\left(\omega\right)\right\rangle &= -\frac{\omega}{2}\int_{-H}^{H}\mathrm{Imaginary}\left(U_1\left(S_{rr0}^{*}+S_{rr1}^{*}\right)\right)2\pi r\,dz \\
&= \frac{\omega\pi^2 k_{\mathrm{s}}^2}{2\mu}\frac{\left|\overline{P}_0\left(k_{\mathrm{a}},\omega\right)\right|^2}{\left[R_{\mathrm{s}}'\left(k_{\mathrm{s}}\right)\right]^2} \\
&\Bigg[\left(2k_{\mathrm{s}}^2-k_2^2\right)^2\left(k_2^2+2\eta_{1\mathrm{s}}^2\right)\sinh^2\left(\eta_{2\mathrm{s}}H\right)\left(\frac{\sinh\left(2\eta_{1\mathrm{s}}H\right)}{2\eta_{1\mathrm{s}}}+H\right)- \\
&\quad 2\eta_{1\mathrm{s}}\eta_{2\mathrm{s}}\left(2k_{\mathrm{s}}^2-k_2^2\right)\left(2k_{\mathrm{s}}^2+k_2^2+2\eta_{1\mathrm{s}}^2\right)\sinh\left(\eta_{1\mathrm{s}}H\right)\sinh\left(\eta_{2\mathrm{s}}H\right) \\
&\quad \left(\frac{\sinh\left(\left(\eta_{1\mathrm{s}}+\eta_{2\mathrm{s}}\right)H\right)}{\eta_{1\mathrm{as}}+\eta_{2\mathrm{s}}}+\frac{\sinh\left(\left(\eta_{1\mathrm{s}}-\eta_{2\mathrm{s}}\right)H\right)}{\eta_{1\mathrm{s}}-\eta_{2\mathrm{s}}}\right)+ \\
&\quad 8\eta_{1\mathrm{s}}^2\eta_{2\mathrm{s}}^2k_{\mathrm{s}}^2\sinh^2\left(\eta_{1\mathrm{s}}H\right)\left(\frac{\sinh\left(2\eta_{2\mathrm{s}}H\right)}{2\eta_{2\mathrm{s}}}+H\right)\Bigg]
\end{aligned} \tag{3.165}$$

and

$$\begin{aligned}
\left\langle \overline{P_{\mathrm{s2}}}\left(\omega\right)\right\rangle &= -\frac{\omega}{2}\int_{-H}^{H}\mathrm{Imaginary}\left(W_0S_{rz1}^{*}\right)2\pi r\,dz \\
&= \frac{\omega\pi^2 k_{\mathrm{s}}^2\eta_{1\mathrm{s}}^2\left(2k_{\mathrm{s}}^2-k_2^2\right)}{\mu}\frac{\left|\overline{P}_0\left(k_{\mathrm{s}},\omega\right)\right|^2}{\left[R_{\mathrm{s}}'\left(k_{\mathrm{s}}\right)\right]^2} \\
&\Bigg[\left(2k_{\mathrm{s}}^2-k_2\right)\sinh^2\left(\eta_{2\mathrm{s}}H\right)\left(\frac{\sinh\left(2\eta_{1\mathrm{s}}H\right)}{2\eta_{1\mathrm{s}}}-H\right)- \\
&\quad \left(4k_{\mathrm{a}}^2-k_2^2\right)\sinh\left(\eta_{1\mathrm{s}}H\right)\sinh\left(\eta_{2\mathrm{s}}H\right) \\
&\quad \left(\frac{\sinh\left(\left(\eta_{1\mathrm{s}}+\eta_{2\mathrm{s}}\right)H\right)}{\eta_{1\mathrm{s}}+\eta_{2\mathrm{s}}}-\frac{\sinh\left(\left(\eta_{1\mathrm{s}}-\eta_{2\mathrm{s}}\right)H\right)}{\eta_{1\mathrm{s}}-\eta_{2\mathrm{s}}}\right)+ \\
&\quad 2k_{\mathrm{s}}^2\sinh^2\left(\eta_{1\mathrm{s}}H\right)\left(\frac{\sinh\left(2\eta_{2\mathrm{s}}H\right)}{2\eta_{2\mathrm{s}}}-H\right)\Bigg]
\end{aligned} \tag{3.166}$$

In Equations (3.165,3.166), U_1, W_0, S_{rr0}, S_{rr1} and S_{rz1} are the displacements and stresses for symmetric Lamb wave, given by Equations (3.146-3.153).

3.6 Work done per cycle by the applied dynamic axisymmetric load

The work done per cycle by the load applied on the top surface of the plate is calculated. The energy flowing across the region on the top surface in the vertical z direction in one cycle is calculated. It is averaged over the time period to give the power. The power flow is integrated over the area (πa^2) of the region across which the axisymmetric loading is applied, and is compared with the power flow across the cylindrical surface far away from the source derived already. Similar to before, the power flow in the frequency (ω) domain, in the z direction is now is given by

$$\langle P(\omega)\rangle = -\frac{\omega}{2}\text{Imaginary}\left(W_0(r,H,\omega)\,S_{zz0}(r,H,\omega)\right) \tag{3.167}$$

where, $S_{zz0}(r,H,\omega) = -P_0(\omega)$ the applied stress in frequency domain. Since, it is just real, there is no need of the complex conjugate.

As discussed previously, the power flow through the region on the top surface of the plate, where the axisymmetric load is applied, is due to the contribution of the real roots of the dispersion equation that is due to the propagating Lamb waves through the plate. The power flowing vertically through the region on which the loading is applied, is obtained by integrating Equation (3.167) along the circular area with radius a. It consists of antisymmetric and symmetric components from the real positive roots of the antisymmetric and symmetric dispersion equations.

The power flow through the top surface due to the right propagating antisymmetric Lamb wave motion is given by

$$\langle \overline{P}_{aH}(\omega)\rangle = \frac{\omega\pi^2 k_2^2 \eta_{1\mathrm{a}}}{4\mu}\frac{\overline{P}_0(k_\mathrm{a},\omega)}{R'_\mathrm{a}(k_\mathrm{a})}P_0(\omega)\,aJ_1(k_\mathrm{a}a)\cosh(\eta_{1\mathrm{a}}H)\cosh(\eta_{2\mathrm{a}}H) \tag{3.168}$$

The power flow through the top surface due to the right propagating symmetric Lamb wave motion is given by

$$\langle \overline{P}_{sH}(\omega) \rangle = \frac{\omega \pi^2 k_2^2 \eta_{1s}}{4\mu} \frac{\overline{P}_0(k_s, \omega)}{R_s'(k_s)} P_0(\omega)\, a J_1(k_s a) \sinh(\eta_{1s} H) \sinh(\eta_{2s} H) \quad (3.169)$$

where J_1 is the Bessel function of the first kind of order 1.

The power flow through the top surface due to the left and the right propagating Lamb waves is twice the value given by Equations (3.168,3.169). And this power flow through the top surface induced by the applied load equals the power flow through the cylindrical surface far away from the origin given by Equations (3.161-3.166) by the outward propagating Lamb waves. Figure (3.3) compares the above two power flow spectrum in a 1.78 mm thick aluminum plate subjected to an axisymmetric load of intensity 1 $\frac{\mathrm{N}}{m}$ over a circular area of diameter 1 mm on its top surface. The Young's modulus of the aluminum plate is 69 GPa and its Poisson's ratio is 0.3269.

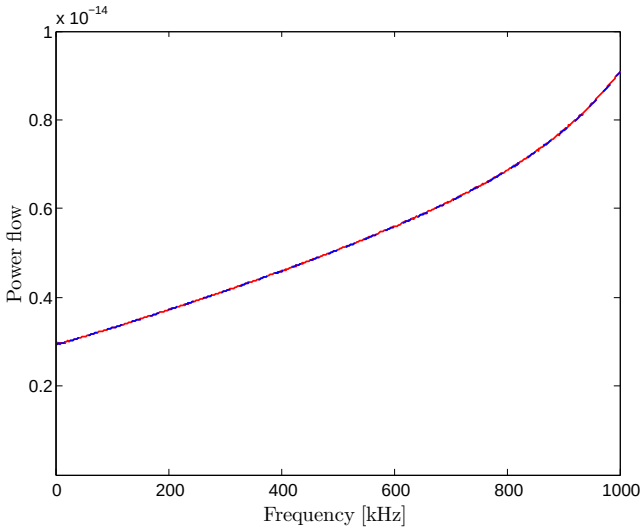

Figure 3.3: Power flow spectrum due to Lamb waves in a plate subjected to axisymmetric load on its top surface. The red solid curve denotes power flow through a cylindrical surface far away from the origin. The dashed blue curve denotes the power flow through the region on the top surface on which the external load is applied.

3.6.1 Axisymmetric load

For an axisymmetric loading $p(r,t)$ with intensity $\hat{p}(r)$ over a circular area of radius a on the top surface of the plate, centered at the vertical z-axis,

$$p(r,t) = \hat{p}(r) f(t) \tag{3.170}$$

where $f(t)$ is the time-dependence of the load. For an uniform intensity p_0 over a circular area of radius a on the top surface of the plate, centered at the vertical z-axis,

$$\hat{p}(r) = p_0 \qquad |r| \leq a \tag{3.171}$$

$$= 0 \qquad |r| > a \tag{3.172}$$

$$\begin{aligned} P_0(r,\omega) &= \int_0^\infty p(r,t)\, e^{i\omega t}\, dt \qquad |r| \leq a, t > 0 \\ &= p_0 \int_0^\infty f(t)\, e^{i\omega t}\, dt \end{aligned} \tag{3.173}$$

$$\overline{P}_0(k,\omega) = \frac{1}{2} \int_{-\infty}^{\infty} P_0(r,\omega)\, r H_0^1(kr)\, dr \qquad r \leq a \tag{3.174}$$

$$= \frac{1}{2} \int_0^\infty \left[\int_0^a p_0 r H_0^1(kr)\, dr \right] f(t)\, e^{i\omega t}\, dt$$

$$= \int_0^\infty \left[p_0 \int_0^a r J_0(kr)\, dr \right] f(t)\, e^{i\omega t}\, dt \tag{3.175}$$

Substituting, $kr = \zeta$,

$$\overline{P}_0(k,\omega) = \int_0^\infty \left[p_0 \int_0^{ak} \frac{\zeta}{k^2} J_0(\zeta)\, d\zeta \right] f(t)\, e^{i\omega t}\, dt$$

$$= \int_0^\infty \left[\frac{p_0}{k^2} \left[\zeta J_1(\zeta) \right]_0^{ak} \right] f(t)\, e^{i\omega t}\, dt \tag{3.176}$$

$$= \int_0^\infty \left[\frac{a p_0}{k} J_1(ak) \right] f(t)\, e^{i\omega t}\, dt$$

CHAPTER 4

Rayleigh and Lamb wave propagation in quasi-isotropic composite media

In this chapter, the dispersion properties of guided waves in a quasi isotropic composite half space and plate is derived analytically. The composite plate is modeled as a transversely isotropic solid with its axis of symmetry as the vertical axis through the plane of the plate. Figure 4.1 shows the plane strain model of the plate that is analyzed. The xy plane is the plane of isotropy and the z axis (shown positive upwards) is the axis of symmetry.

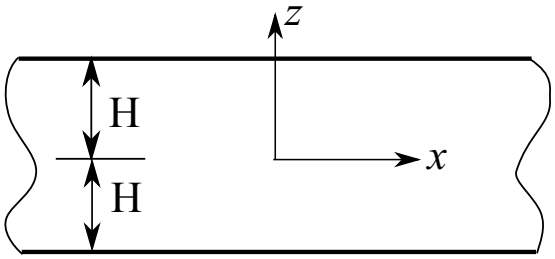

Figure 4.1: Plane strain model of plate

The analysis is done in the frequency domain, by taking double Fourier transforms of the field variables with respect to time (t) and the direction of propagation of the wave (x). The original field variables $f\left(x,z,t\right)$) are transformed into frequency domain to $F\left(x,z,\omega\right)$ by taking the Fourier transform with respect to time (t) and

then further transformed to $\overline{F}(k,z,\omega)$ according to

$$F(x,z,\omega) = \int_{-\infty}^{\infty} f(x,z,t)\, e^{i\omega t} dt \tag{4.1}$$

$$\overline{F}(k,z,\omega) = \int_{-\infty}^{\infty} F(x,z,\omega)\, e^{-ikx} dx \tag{4.2}$$

where ω is the circular frequency and k is the wavenumber. The original variables are obtained by taking the inverse Fourier transforms according to

$$f(x,z,t) = \frac{1}{4\pi^2} \int_{-\infty}^{\infty} \int_{-\infty}^{\infty} \overline{F}(k,z,\omega)\, e^{i(kx-\omega t)} dk d\omega \tag{4.3}$$

The analysis is done in the frequency domain that is on the integrand of Eq.(4.3) for the field variables, shown as follows

$$u(x,z,t) = \overline{U}(k,z,\omega)\, e^{i(kx-\omega t)} \tag{4.4}$$

$$w(x,z,t) = \overline{W}(k,z,\omega)\, e^{i(kx-\omega t)} \tag{4.5}$$

$$\sigma_{xx}(x,z,t) = \overline{S}_{xx}(k,z,\omega)\, e^{i(kx-\omega t)} \tag{4.6}$$

$$\sigma_{zz}(x,z,t) = \overline{S}_{zz}(k,z,\omega)\, e^{i(kx-\omega t)} \tag{4.7}$$

$$\sigma_{xz}(x,z,t) = \overline{S}_{xz}(k,z,\omega)\, e^{i(kx-\omega t)} \tag{4.8}$$

where, $u(x,z,t)$ and $w(x,z,t)$ are the displacements along the x and z directions respectively, and $\sigma_{xx}(x,z,t)$, $\sigma_{zz}(x,z,t)$ are the normal stresses along the x and z directions respectively and $\sigma_{xz}(x,z,t)$ is the shear stress.

The Hooke's Law for a transversely isotropic material with the z axis as the axis of symmetry in 3D is given by

$$\begin{Bmatrix} \sigma_{xx} \\ \sigma_{yy} \\ \sigma_{zz} \\ \sigma_{yz} \\ \sigma_{xz} \\ \sigma_{xy} \end{Bmatrix} = \begin{bmatrix} c_{11} & c_{12} & c_{13} & 0 & 0 & 0 \\ c_{12} & c_{11} & c_{13} & 0 & 0 & 0 \\ c_{13} & c_{13} & c_{33} & 0 & 0 & 0 \\ 0 & 0 & 0 & c_{44} & 0 & 0 \\ 0 & 0 & 0 & 0 & c_{44} & 0 \\ 0 & 0 & 0 & 0 & 0 & \frac{1}{2}(c_{11}-c_{12}) \end{bmatrix} \begin{Bmatrix} \epsilon_{xx} \\ \epsilon_{yy} \\ \epsilon_{zz} \\ \gamma_{yz} \\ \gamma_{xz} \\ \gamma_{xy} \end{Bmatrix} \tag{4.9}$$

which for 2D plane strain in xz plane, reduces to

$$\begin{Bmatrix} \sigma_{xx} \\ \sigma_{zz} \\ \sigma_{xz} \end{Bmatrix} = \begin{bmatrix} c_{11} & c_{13} & 0 \\ c_{13} & c_{33} & 0 \\ 0 & 0 & c_{44} \end{bmatrix} \begin{Bmatrix} \epsilon_{xx} \\ \epsilon_{zz} \\ \gamma_{xz} \end{Bmatrix} \tag{4.10}$$

Using the strain displacement kinematic relations

$$\epsilon_{xx} = \frac{\partial u}{\partial x}, \qquad \epsilon_{zz} = \frac{\partial u}{\partial x} \qquad \text{and} \qquad \gamma_{xz} = \frac{\partial u}{\partial z} + \frac{\partial w}{\partial x} \tag{4.11}$$

the stresses can be expressed in terms of displacement components as

$$\begin{aligned} \sigma_{xx} &= c_{11}\frac{\partial u}{\partial x} + c_{13}\frac{\partial w}{\partial z} \\ \sigma_{zz} &= c_{13}\frac{\partial u}{\partial x} + c_{33}\frac{\partial w}{\partial z} \\ \sigma_{xz} &= c_{44}\left(\frac{\partial w}{\partial x} + \frac{\partial u}{\partial z}\right) \end{aligned} \tag{4.12}$$

Using the relations from Equations (4.4,4.5) into Equation (4.12), the stresses are expressed as

$$\sigma_{xx} = \left[c_{11} ik\overline{U} + c_{13}\frac{\partial \overline{W}}{\partial z}\right] e^{i(kx-\omega t)} \tag{4.13}$$

$$\sigma_{zz} = \left[c_{13} ik\overline{U} + c_{33}\frac{\partial \overline{W}}{\partial z}\right] e^{i(kx-\omega t)} \tag{4.14}$$

$$\sigma_{xz} = c_{44}\left[ik\overline{W} + \frac{\partial \overline{U}}{\partial z}\right] e^{i(kx-\omega t)} \tag{4.15}$$

The stress equations of motion in absence of body forces are given by

$$\text{In x direction} \qquad \frac{\partial \sigma_{xx}}{\partial x} + \frac{\partial \sigma_{xz}}{\partial z} = \rho\frac{\partial^2 u}{\partial t^2} \tag{4.16}$$

$$\text{In z direction} \qquad \frac{\partial \sigma_{xz}}{\partial x} + \frac{\partial \sigma_{zz}}{\partial z} = \rho\frac{\partial^2 w}{\partial t^2} \tag{4.17}$$

where ρ is the density of the material. Taking the derivatives of the stresses from Equations(4.13-4.15) and substituting them in the equations of motion give

$$\text{In x direction} \qquad -c_{11}k^2\overline{U} + c_{44}\frac{\partial^2 \overline{U}}{\partial z^2} + \rho\omega^2\overline{U} + (c_{13}+c_{44})\, ik\frac{\partial \overline{W}}{\partial z} = 0 \tag{4.18}$$

$$\text{In z direction} \qquad (c_{13}+c_{44})\, ik\frac{\partial \overline{U}}{\partial z} - c_{44}k^2\overline{W} + c_{33}\frac{\partial^2 \overline{W}}{\partial z^2} + \rho\omega^2\overline{W} = 0 \tag{4.19}$$

Assuming,

$$\overline{U}\left(k,z,\omega\right)=G\left(k,\omega\right)e^{-\xi z} \tag{4.20}$$

$$\overline{W}\left(k,z,\omega\right)=H\left(k,\omega\right)e^{-\xi z} \tag{4.21}$$

where $G\left(k,\omega\right)$ and $H\left(k,\omega\right)$ are unknown functions and ξ is the unknown parameter describing the z-dependency of $\overline{U},\overline{W}$.

Substituting Equations (4.20, 4.21) into Equations (4.18, 4.19), the following pair of homogeneous equations are obtained

$$\begin{bmatrix} -c_{11}k^2+c_{44}\xi^2+\rho\omega^2 & -\left(c_{13}+c_{44}\right)ik\xi \\ -\left(c_{13}+c_{44}\right)ik\xi & -c_{44}k^2+c_{33}\xi^2+\rho\omega^2 \end{bmatrix}\begin{Bmatrix} G\left(k,\omega\right) \\ H\left(k,\omega\right) \end{Bmatrix}=\begin{Bmatrix} 0 \\ 0 \end{Bmatrix} \tag{4.22}$$

For non trivial solution of Equation(4.22), the determinant of the coefficient matrix is equal to zero, leading to the following fourth order algebraic equation for ξ

$$\begin{aligned} c_{44}c_{33}\xi^4+&\xi^2\left[k^2\left(c_{13}^2+2c_{13}c_{44}-c_{11}c_{33}\right)+\rho\omega^2\left(c_{44}+c_{33}\right)\right] \\ &+c_{11}c_{44}k^2-\rho\omega^2k^2\left(c_{11}+c_{44}\right)+\rho^2\omega^4=0 \end{aligned} \tag{4.23}$$

which is a quadratic equation in ξ^2. Solving the equation gives the unknown parameter ξ as follows

$$\xi^2=\frac{-A\pm\sqrt{A^2-4B}}{2} \tag{4.24}$$

where,

$$A=\frac{\rho\omega^2}{c_{33}}+\frac{\rho\omega^2}{c_{44}}-\frac{k^2c_{11}}{c_{44}}+\frac{k^2c_{13}^2}{c_{44}c_{33}}+\frac{2k^2c_{13}}{c_{33}} \tag{4.25}$$

$$B=\frac{k^4c_{11}}{c_{33}}-\frac{\rho\omega^2k^2c_{11}}{c_{44}c_{33}}-\frac{\rho\omega^2k^2}{c_{33}}+\frac{\rho^2\omega^4}{c_{44}c_{33}} \tag{4.26}$$

Introducing the wave speeds

$$c_{1L}=\sqrt{\frac{c_{11}}{\rho}}\qquad c_{3L}=\sqrt{\frac{c_{33}}{\rho}}\qquad c_{3L}=\sqrt{\frac{c_{44}}{\rho}} \tag{4.27}$$

and using relation between radial frequency (ω), wavenumber (k) and wave speed (c),

$$\omega=kc$$

the coefficients A and B from Equations (4.25, 4.26), can be written as

$$A = \frac{k^2c^2}{c_{3L}^2} + \frac{k^2c^2}{c_{3T}^2} - \frac{k^2\left(c_{11}c_{33} - c_{13}^2 - 2c_{13}c_{44}\right)}{c_{33}c_{44}} \tag{4.28}$$

$$B = \left(\frac{c^2}{c_{3L}^2} - \frac{c_{11}}{c_{33}}\right)\left(\frac{c^2}{c_{3T}^2} - 1\right) \tag{4.29}$$

From Equation (4.24), the four values of ξ are given by

$$\xi_1 = \sqrt{\frac{-A + \sqrt{A^2 - 4B}}{2}} = \eta_1 \tag{4.30}$$

$$\xi_2 = -\sqrt{\frac{-A + \sqrt{A^2 - 4B}}{2}} = -\eta_1 \tag{4.31}$$

$$\xi_3 = \sqrt{\frac{-A - \sqrt{A^2 - 4B}}{2}} = \eta_2 \tag{4.32}$$

$$\xi_4 = -\sqrt{\frac{-A - \sqrt{A^2 - 4B}}{2}} = -\eta_2 \tag{4.33}$$

From Equation (4.22), the unknown functions $G\left(k,\omega\right)$ and $H\left(k,\omega\right)$ are related as

$$H\left(k,\omega\right) = \frac{-c_{11}k^2 + c_{44}\xi^2\rho\omega^2}{\left(c_{13} + c_{44}\right)ik\xi}G\left(k,\omega\right) = \alpha G\left(k,\omega\right) \tag{4.34}$$

where

$$\alpha = \frac{-c_{11}k^2 + c_{44}\xi^2\rho\omega^2}{\left(c_{13} + c_{44}\right)ik\xi} \tag{4.35}$$

Using Equations (4.30-4.33) for ξ,

$$H_1\left(k,\omega\right) = \frac{-c_{11}k^2 + c_{44}\eta_1^2 + \rho\omega^2}{\left(c_{13} + c_{44}\right)ik\eta_1}G_1\left(k,\omega\right) = \alpha_1 G_1\left(k,\omega\right) \tag{4.36}$$

$$H_2\left(k,\omega\right) = \alpha_2 G_2\left(k,\omega\right) = -\alpha_1 G_2\left(k,\omega\right) \tag{4.37}$$

$$H_3\left(k,\omega\right) = \frac{-c_{11}k^2 + c_{44}\eta_2^2 + \rho\omega^2}{\left(c_{13} + c_{44}\right)ik\eta_2}G_3\left(k,\omega\right) = \alpha_3 G_3\left(k,\omega\right) \tag{4.38}$$

$$H_4\left(k,\omega\right) = \alpha_4 G_4\left(k,\omega\right) = -\alpha_3 G_4\left(k,\omega\right) \tag{4.39}$$

Substituting Equations (4.36-4.39) in Equations (4.21.4.22) for the displacements

$$\begin{aligned}\overline{U}\left(k,z,\omega\right) = {} & G_1\left(k,\omega\right)e^{-\eta_1 z} + G_2\left(k,\omega\right)e^{\eta_1 z} \\ & + G_3\left(k,\omega\right)e^{-\eta_2 z} + G_4\left(k,\omega\right)e^{\eta_2 z}\end{aligned} \tag{4.40}$$

$$\begin{aligned}\overline{W}(k,z,\omega) = {} & \alpha_1 G_1(k,\omega)\, e^{-\eta_1 z} - \alpha_1 G_2(k,\omega)\, e^{\eta_1 z} \\ & + \alpha_3 G_3(k,\omega)\, e^{-\eta_2 z} - \alpha_3 G_4(k,\omega)\, e^{\eta_2 z}\end{aligned} \tag{4.41}$$

Using the relations between exponential and hyperbolic sine and cosine,

$$e^{\eta z} = \cosh(\eta z) + \sinh(\eta z) \qquad e^{-\eta z} = \cosh(\eta z) - \sinh(\eta z)$$

the displacements and stresses in the frequency domain can be written as

$$\begin{aligned}\overline{U}(k,z,\omega) = {} & \overline{G}_1 \cosh(\eta_1 z) + \overline{G}_2 \sinh(\eta_1 z) \\ & + \overline{G}_3 \cosh(\eta_2 z) + \overline{G}_4 \sinh(\eta_2 z)\end{aligned} \tag{4.42}$$

$$\begin{aligned}\overline{W}(k,z,\omega) = {} & -\alpha_1 \overline{G}_1 \sinh(\eta_1 z) - \alpha_1 \overline{G}_2 \cosh(\eta_1 z) \\ & - \alpha_3 \overline{G}_3 \sinh(\eta_2 z) - \alpha_3 \overline{G}_4 \cosh(\eta_2 z)\end{aligned} \tag{4.43}$$

$$\begin{aligned}\overline{S}_{xx}(k,z,\omega) = {} & (c_{11} ik - c_{13}\alpha_1\eta_1)\left(\overline{G}_1 \cosh(\eta_1 z) + \overline{G}_2 \sinh(\eta_1 z)\right) \\ & + (c_{11} ik - c_{13}\alpha_3\eta_2)\left(\overline{G}_3 \cosh(\eta_2 z) + \overline{G}_4 \sinh(\eta_2 z)\right)\end{aligned} \tag{4.44}$$

$$\begin{aligned}\overline{S}_{zz}(k,z,\omega) = {} & (c_{13} ik - c_{33}\alpha_1\eta_1)\left(\overline{G}_1 \cosh(\eta_1 z) + \overline{G}_2 \sinh(\eta_1 z)\right) \\ & + (c_{13} ik - c_{33}\alpha_3\eta_2)\left(\overline{G}_3 \cosh(\eta_2 z) + \overline{G}_4 \sinh(\eta_2 z)\right)\end{aligned} \tag{4.45}$$

$$\begin{aligned}\overline{S}_{xz}(k,z,\omega) = c_{44}\Big[& (-ik\alpha_1 + \eta_1)\left(\overline{G}_1 \sinh(\eta_1 z) + \overline{G}_2 \cosh(\eta_1 z)\right) \\ & + (-ik\alpha_3 + \eta_2)\left(\overline{G}_3 \sinh(\eta_2 z) + \overline{G}_4 \cosh(\eta_2 z)\right)\Big]\end{aligned} \tag{4.46}$$

where

$$\overline{G}_1 = G_1(k,\omega) + G_2(k,\omega) \qquad \overline{G}_2 = G_2(k,\omega) - G_1(k,\omega) \tag{4.47}$$

$$\overline{G}_3 = G_3(k,\omega) + G_4(k,\omega) \qquad \overline{G}_4 = G_4(k,\omega) - G_3(k,\omega) \tag{4.48}$$

Next, the stress free boundary conditions are applied on the top ($z = H$) and bottom ($z = -H$) faces of the plate.

At $z = H$, zero normal stress gives,

$$\begin{aligned}\overline{S}_{zz}(k, H, \omega) &= (c_{13}ik - c_{33}\alpha_1\eta_1)\left(\overline{G}_1 \cosh(\eta_1 H) + \overline{G}_2 \sinh(\eta_1 H)\right) \\ &+ (c_{13}ik - c_{33}\alpha_3\eta_2)\left(\overline{G}_3 \cosh(\eta_2 H) + \overline{G}_4 \sinh(\eta_2 H)\right) \\ &= 0\end{aligned} \tag{4.49}$$

At $z = -H$, zero normal stress gives,

$$\begin{aligned}\overline{S}_{zz}(k, -H, \omega) &= (c_{13}ik - c_{33}\alpha_1\eta_1)\left(\overline{G}_1 \cosh(\eta_1 H) - \overline{G}_2 \sinh(\eta_1 H)\right) \\ &+ (c_{13}ik - c_{33}\alpha_3\eta_2)\left(\overline{G}_3 \cosh(\eta_2 H) - \overline{G}_4 \sinh(\eta_2 H)\right) \\ &= 0\end{aligned} \tag{4.50}$$

From Equations (4.49, 4.50)

$$\begin{aligned}&\left[(c_{13}ik - c_{33}\alpha_1\eta_1)\overline{G}_1 \cosh(\eta_1 H) + (c_{13}ik - c_{33}\alpha_3\eta_2)\overline{G}_3 \cosh(\eta_2 H)\right] \pm \\ &\left[(c_{13}ik - c_{33}\alpha_1\eta_1)\overline{G}_2 \sinh(\eta_1 H) + (c_{13}ik - c_{33}\alpha_3\eta_2)\overline{G}_4 \sinh(\eta_2 H)\right] = 0\end{aligned} \tag{4.51}$$

At $z = H$, zero shear stress gives,

$$\begin{aligned}\overline{S}_{xz}(k, H, \omega) &= (-ik\alpha_1 + \eta_1)\left(\overline{G}_1 \sinh(\eta_1 H) + \overline{G}_2 \cosh(\eta_1 H)\right) \\ &+ (-ik\alpha_3 + \eta_2)\left(\overline{G}_3 \sinh(\eta_2 H) + \overline{G}_4 \cosh(\eta_2 H)\right) \\ &= 0\end{aligned} \tag{4.52}$$

At $z = -H$, zero shear stress gives,

$$\begin{aligned}\overline{S}_{xz}(k, -H, \omega) &= (-ik\alpha_1 + \eta_1)\left(-\overline{G}_1 \sinh(\eta_1 H) + \overline{G}_2 \cosh(\eta_1 H)\right) \\ &+ (-ik\alpha_3 + \eta_2)\left(-\overline{G}_3 \sinh(\eta_2 H) + \overline{G}_4 \cosh(\eta_2 H)\right) \\ &= 0\end{aligned} \tag{4.53}$$

From Equations (4.52, 4.53),

$$\begin{aligned}&\left[(-ik\alpha_1 + \eta_1)\overline{G}_2 \cosh(\eta_1 H) + (-ik\alpha_3 + \eta_2)\overline{G}_4 \cosh(\eta_2 H)\right] \pm \\ &\left[(-ik\alpha_1 + \eta_1)\overline{G}_1 \sinh(\eta_1 H) + (-ik\alpha_3 + \eta_2)\overline{G}_3 \sinh(\eta_2 H)\right] = 0\end{aligned} \tag{4.54}$$

From Equations (4.51,4.54), it is seen that $\overline{G}_1, \overline{G}_3$ are independent of $\overline{G}_2, \overline{G}_4$. Hence two independent motions of the plate can be obtained by setting $\overline{G}_1 =$

$\overline{G}_3 = 0$ and then $\overline{G}_2 = \overline{G}_4 = 0$ First setting $\overline{G}_2 = \overline{G}_4 = 0$, the motion governed by $\overline{G}_1, \overline{G}_3$ is derived. $\overline{G}_1, \overline{G}_3$ satisfy

$$\begin{bmatrix} (c_{13}ik - c_{33}\alpha_1\eta_1)\cosh(\eta_1 H) & (c_{13}ik - c_{33}\alpha_3\eta_2)\cosh(\eta_2 H) \\ (-ik\alpha_1 + \eta_1)\sinh(\eta_1 H) & (-ik\alpha_3 + \eta_2)\sinh(\eta_2 H) \end{bmatrix} \begin{Bmatrix} \overline{G}_1 \\ \overline{G}_3 \end{Bmatrix} = \begin{Bmatrix} 0 \\ 0 \end{Bmatrix} \tag{4.55}$$

For nontrivial solution of $\overline{G}_1, \overline{G}_3$, the determinant of the coefficient matrix in Equation (4.55) needs to be zero, which gives the dispersion relation for the symmetric Lamb waves in the plate.

$$\frac{\sinh(\eta_1 H)\cosh(\eta_2 H)}{\cosh(\eta_1 H)\sinh(\eta_2 H)} = \frac{(c_{13}ik - c_{33}\alpha_1\eta_1)(-ik\alpha_3 + \eta_2)}{(c_{13}ik - c_{33}\alpha_3\eta_2)(-ik\alpha_1 + \eta_1)} \tag{4.56}$$

Substituting the expressions for α_1, α_3 from Equations (4.36,4.38), the above dispersion relation for the symmetric Lamb waves can be written as

$$\begin{aligned} \frac{\sinh(\eta_1 H)\cosh(\eta_2 H)}{\cosh(\eta_1 H)\sinh(\eta_2 H)} &= \\ \frac{\eta_1}{\eta_2}\frac{\left[-c_{13}^2k^2 - c_{13}c_{44}k^2 + c_{33}c_{11}k^2 - c_{33}c_{44}\eta_1^2 - c_{33}\rho\omega^2\right]}{\left[-c_{13}^2k^2 - c_{13}c_{44}k^2 + c_{33}c_{11}k^2 - c_{33}c_{44}\eta_2^2 - c_{33}\rho\omega^2\right]}\frac{\left[c_{11}k^2 - \rho\omega^2 + c_{13}\eta_2^2\right]}{\left[c_{11}k^2 - \rho\omega^2 + c_{13}\eta_1^2\right]} &= \\ \frac{\eta_1}{\eta_2}\frac{\left[c_{13}\left\{\eta_2^2 - \frac{c_{11}k^2}{c_{13}}\left(\frac{\rho c^2}{c_{11}} - 1\right)\right\}\right]}{\left[c_{13}\left\{\eta_1^2 - \frac{c_{11}k^2}{c_{13}}\left(\frac{\rho c^2}{c_{11}} - 1\right)\right\}\right]}\frac{\left[-c_{33}c_{44}\left\{\eta_1^2 + \frac{c_{13}}{c_{33}}k^2\left(\frac{c_{13}}{c_{44}} + 1\right) + \frac{c_{11}}{c_{44}}k^2\left(\frac{\rho c^2}{c_{11}} - 1\right)\right\}\right]}{\left[-c_{33}c_{44}\left\{\eta_2^2 + \frac{c_{13}}{c_{33}}k^2\left(\frac{c_{13}}{c_{44}} + 1\right) + \frac{c_{11}}{c_{44}}k^2\left(\frac{\rho c^2}{c_{11}} - 1\right)\right\}\right]} &= \\ \frac{\eta_1}{\eta_2}\frac{\left[\eta_2^2 - \frac{c_{11}k^2}{c_{13}}\left(\frac{\rho c^2}{c_{11}} - 1\right)\right]}{\left[\eta_1^2 - \frac{c_{11}k^2}{c_{13}}\left(\frac{\rho c^2}{c_{11}} - 1\right)\right]}\frac{\left[\eta_1^2 + \frac{c_{13}}{c_{33}}k^2\left(\frac{c_{13}}{c_{44}} + 1\right) + \frac{c_{11}}{c_{44}}k^2\left(\frac{\rho c^2}{c_{11}} - 1\right)\right]}{\left[\eta_2^2 + \frac{c_{13}}{c_{33}}k^2\left(\frac{c_{13}}{c_{44}} + 1\right) + \frac{c_{11}}{c_{44}}k^2\left(\frac{\rho c^2}{c_{11}} - 1\right)\right]} & \end{aligned} \tag{4.57}$$

Defining

$$A_1 = \frac{\eta_1}{k} \qquad A_2 = \frac{\eta_2}{k} \tag{4.58}$$

the above dispersion relation (Equation (4.57)) for the symmetric Lamb waves can be written as

$$\begin{aligned} \frac{\sinh(kA_1 H)\cosh(kA_2 H)}{\cosh(kA_1 H)\sinh(kA_2 H)} &= \frac{\tanh(kA_1 H)}{\tanh(kA_2 H)} = \\ \frac{A_1}{A_2}\frac{\left[A_2^2 - \frac{c_{11}}{c_{13}}\left(\frac{c^2}{c_{1L}^2} - 1\right)\right]}{\left[A_1^2 - \frac{c_{11}}{c_{13}}\left(\frac{c^2}{c_{1L}^2} - 1\right)\right]}\frac{\left[A_1^2 + \frac{c_{13}}{c_{33}}\left(\frac{c_{13}}{c_{44}} + 1\right) + \frac{c_{11}}{c_{44}}\left(\frac{c^2}{c_{1L}^2} - 1\right)\right]}{\left[A_2^2 + \frac{c_{13}}{c_{33}}\left(\frac{c_{13}}{c_{44}} + 1\right) + \frac{c_{11}}{c_{44}}\left(\frac{c^2}{c_{1L}^2} - 1\right)\right]} & \end{aligned} \tag{4.59}$$

Similarly, by setting $\overline{G}_1 = \overline{G}_3 = 0$ in Equations (4.51, 4.54), the motion governed by $\overline{G}_2$, $\overline{G}_4$ is derived. $\overline{G}_2$, $\overline{G}_4$ satisfy

$$\begin{bmatrix} (c_{13}ik - c_{33}\alpha_1\eta_1)\sinh(\eta_1 H) & (c_{13}ik - c_{33}\alpha_3\eta_2)\sinh(\eta_2 H) \\ (-ik\alpha_1 + \eta_1)\cosh(\eta_1 H) & (-ik\alpha_3 + \eta_2)\cosh(\eta_2 H) \end{bmatrix} \begin{Bmatrix} \overline{G}_2 \\ \overline{G}_4 \end{Bmatrix} = \begin{Bmatrix} 0 \\ 0 \end{Bmatrix} \tag{4.60}$$

For nontrivial solution of $\overline{G}_2, \overline{G}_4$, the determinant of the coefficient matrix in Equation (4.60) needs to be zero, which gives the dispersion relation for the symmetric Lamb waves in the plate.

$$\frac{\cosh(\eta_1 H)\sinh(\eta_2 H)}{\sinh(\eta_1 H)\cosh(\eta_2 H)} = \frac{(c_{13}ik - c_{33}\alpha_1\eta_1)(-ik\alpha_3 + \eta_2)}{(c_{13}ik - c_{33}\alpha_3\eta_2)(-ik\alpha_1 + \eta_1)} \tag{4.61}$$

Substituting the expressions for α_1, α_3 from Equations (4.36,4.38), the above dispersion relation for the antisymmetric Lamb waves can be written as

$$\begin{aligned} \frac{\cosh(\eta_1 H)\sinh(\eta_2 H)}{\sinh(\eta_1 H)\cosh(\eta_2 H)} &= \\ \frac{\eta_1}{\eta_2}\frac{\left[-c_{13}^2k^2 - c_{13}c_{44}k^2 + c_{33}c_{11}k^2 - c_{33}c_{44}\eta_1^2 - c_{33}\rho\omega^2\right]}{\left[-c_{13}^2k^2 - c_{13}c_{44}k^2 + c_{33}c_{11}k^2 - c_{33}c_{44}\eta_2^2 - c_{33}\rho\omega^2\right]}\frac{\left[c_{11}k^2 - \rho\omega^2 + c_{13}\eta_2^2\right]}{\left[c_{11}k^2 - \rho\omega^2 + c_{13}\eta_1^2\right]} &= \\ \frac{\eta_1}{\eta_2}\frac{\left[c_{13}\left\{\eta_2^2 - \frac{c_{11}k^2}{c_{13}}\left(\frac{\rho c^2}{c_{11}} - 1\right)\right\}\right]}{\left[c_{13}\left\{\eta_1^2 - \frac{c_{11}k^2}{c_{13}}\left(\frac{\rho c^2}{c_{11}} - 1\right)\right\}\right]}\frac{\left[-c_{33}c_{44}\left\{\eta_1^2 + \frac{c_{13}}{c_{33}}k^2\left(\frac{c_{13}}{c_{44}} + 1\right) + \frac{c_{11}}{c_{44}}k^2\left(\frac{\rho c^2}{c_{11}} - 1\right)\right\}\right]}{\left[-c_{33}c_{44}\left\{\eta_2^2 + \frac{c_{13}}{c_{33}}k^2\left(\frac{c_{13}}{c_{44}} + 1\right) + \frac{c_{11}}{c_{44}}k^2\left(\frac{\rho c^2}{c_{11}} - 1\right)\right\}\right]} &= \\ \frac{\eta_1}{\eta_2}\frac{\left[\eta_2^2 - \frac{c_{11}k^2}{c_{13}}\left(\frac{\rho c^2}{c_{11}} - 1\right)\right]}{\left[\eta_1^2 - \frac{c_{11}k^2}{c_{13}}\left(\frac{\rho c^2}{c_{11}} - 1\right)\right]}\frac{\left[\eta_1^2 + \frac{c_{13}}{c_{33}}k^2\left(\frac{c_{13}}{c_{44}} + 1\right) + \frac{c_{11}}{c_{44}}k^2\left(\frac{\rho c^2}{c_{11}} - 1\right)\right]}{\left[\eta_2^2 + \frac{c_{13}}{c_{33}}k^2\left(\frac{c_{13}}{c_{44}} + 1\right) + \frac{c_{11}}{c_{44}}k^2\left(\frac{\rho c^2}{c_{11}} - 1\right)\right]} & \end{aligned} \tag{4.62}$$

Defining, as before

$$A_1 = \frac{\eta_1}{k} \qquad A_2 = \frac{\eta_2}{k} \tag{4.63}$$

the above dispersion relation (Equation (4.62)) for the antisymmetric Lamb waves can be written as

$$\begin{aligned} \frac{\cosh(kA_1 H)\sinh(kA_2 H)}{\sinh(kA_1 H)\cosh(kA_2 H)} = \frac{\tanh(kA_2 H)}{\tanh(kA_1 H)} &= \\ \frac{A_1}{A_2}\frac{\left[A_2^2 - \frac{c_{11}}{c_{13}}\left(\frac{c^2}{c_{1L}^2} - 1\right)\right]}{\left[A_1^2 - \frac{c_{11}}{c_{13}}\left(\frac{c^2}{c_{1L}^2} - 1\right)\right]}\frac{\left[A_1^2 + \frac{c_{13}}{c_{33}}\left(\frac{c_{13}}{c_{44}} + 1\right) + \frac{c_{11}}{c_{44}}\left(\frac{c^2}{c_{1L}^2} - 1\right)\right]}{\left[A_2^2 + \frac{c_{13}}{c_{33}}\left(\frac{c_{13}}{c_{44}} + 1\right) + \frac{c_{11}}{c_{44}}\left(\frac{c^2}{c_{1L}^2} - 1\right)\right]} & \end{aligned} \tag{4.64}$$

The graphical solutions of Equations (4.59 and 4.64) for the phase velocity c, which is generally a function of frequency, are called the dispersion curves. Figure (4.2) shows the dispersion curves for the symmetric and the antisymmetric modes of Lamb waves propagating in an aluminum plate of thickness 1.78 mm ($\frac{1}{8}''$) with the properties given in Table (4.1).

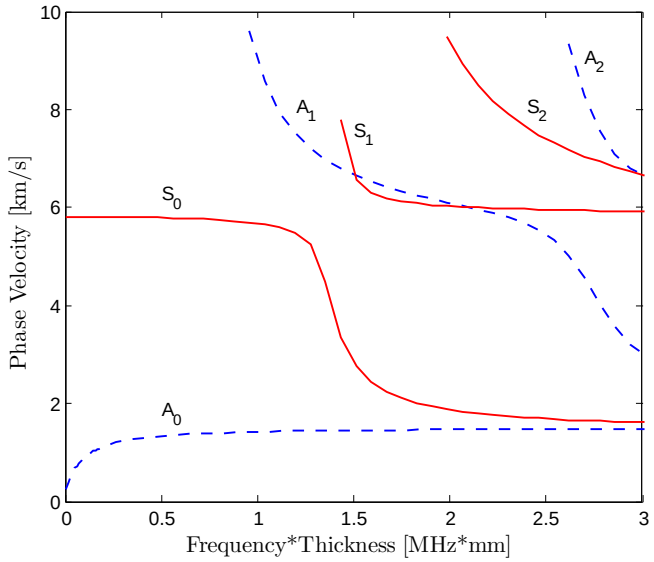

Figure 4.2: Dispersion curves for the phase velocity for a composite plate. Symmetric modes are shown as solid lines, antisymmetric as dashed lines

4.1 Low and high frequency limits of the symmetric and antisymmetric Lamb waves in a transversely isotropic plate

From the dispersion equations for symmetric and antisymmetric Lamb waves in a transversely isotropic plate, the limits of the waves speeds as the frequency tends to zero and to ∞ are evaluated.

As the frequency $\omega \to \infty$, for symmetric Lamb waves from Equation (4.59)

$$\begin{aligned}&\frac{\tanh\left(kA_1H\right)}{\tanh\left(kA_2H\right)} = \\ &\frac{A_1}{A_2}\frac{\left[A_2^2 - \frac{c_{11}}{c_{13}}\left(\frac{c^2}{c_{1L}^2}-1\right)\right]}{\left[A_1^2 - \frac{c_{11}}{c_{13}}\left(\frac{c^2}{c_{1L}^2}-1\right)\right]}\frac{\left[A_1^2 + \frac{c_{13}}{c_{33}}\left(\frac{c_{13}}{c_{44}}+1\right) + \frac{c_{11}}{c_{44}}\left(\frac{c^2}{c_{1L}^2}-1\right)\right]}{\left[A_2^2 + \frac{c_{13}}{c_{33}}\left(\frac{c_{13}}{c_{44}}+1\right) + \frac{c_{11}}{c_{44}}\left(\frac{c^2}{c_{1L}^2}-1\right)\right]} = 1\end{aligned} \tag{4.65}$$

which precisely is the governing equation for Rayleigh waves in a transversely isotropic half-space as derived in Section (4.4).

As the frequency $\omega \to \infty$, for antisymmetric Lamb waves from Equation (4.64)

$$\begin{aligned}&\frac{\tanh\left(kA_2H\right)}{\tanh\left(kA_1H\right)} = \\ &\frac{A_1}{A_2}\frac{\left[A_2^2 - \frac{c_{11}}{c_{13}}\left(\frac{c^2}{c_{1L}^2}-1\right)\right]}{\left[A_1^2 - \frac{c_{11}}{c_{13}}\left(\frac{c^2}{c_{1L}^2}-1\right)\right]}\frac{\left[A_1^2 + \frac{c_{13}}{c_{33}}\left(\frac{c_{13}}{c_{44}}+1\right) + \frac{c_{11}}{c_{44}}\left(\frac{c^2}{c_{1L}^2}-1\right)\right]}{\left[A_2^2 + \frac{c_{13}}{c_{33}}\left(\frac{c_{13}}{c_{44}}+1\right) + \frac{c_{11}}{c_{44}}\left(\frac{c^2}{c_{1L}^2}-1\right)\right]} = 1\end{aligned} \tag{4.66}$$

which precisely is the governing equation for Rayleigh waves in a transversely isotropic half-space as derived in Section (4.4).

As the frequency $\omega \to 0$, for the symmetric Lamb waves from Equation (4.59)

$$\begin{aligned}&\frac{\tanh\left(kA_1H\right)}{\tanh\left(kA_2H\right)} = \frac{kA_1H}{kA_2H} = \\ &\frac{A_1}{A_2}\frac{\left[A_2^2 - \frac{c_{11}}{c_{13}}\left(\frac{c^2}{c_{1L}^2}-1\right)\right]}{\left[A_1^2 - \frac{c_{11}}{c_{13}}\left(\frac{c^2}{c_{1L}^2}-1\right)\right]}\frac{\left[A_1^2 + \frac{c_{13}}{c_{33}}\left(\frac{c_{13}}{c_{44}}+1\right) + \frac{c_{11}}{c_{44}}\left(\frac{c^2}{c_{1L}^2}-1\right)\right]}{\left[A_2^2 + \frac{c_{13}}{c_{33}}\left(\frac{c_{13}}{c_{44}}+1\right) + \frac{c_{11}}{c_{44}}\left(\frac{c^2}{c_{1L}^2}-1\right)\right]}\end{aligned} \tag{4.67}$$

which gives,

$$\begin{aligned}&\left[A_2^2 - \frac{c_{11}}{c_{13}}\left(\frac{c^2}{c_{1L}^2}-1\right)\right]\left[A_1^2 + \frac{c_{13}}{c_{33}}\left(\frac{c_{13}}{c_{44}}+1\right) + \frac{c_{11}}{c_{44}}\left(\frac{c^2}{c_{1L}^2}-1\right)\right] = \\ &\left[A_1^2 - \frac{c_{11}}{c_{13}}\left(\frac{c^2}{c_{1L}^2}-1\right)\right]\left[A_2^2 + \frac{c_{13}}{c_{33}}\left(\frac{c_{13}}{c_{44}}+1\right) + \frac{c_{11}}{c_{44}}\left(\frac{c^2}{c_{1L}^2}-1\right)\right]\end{aligned} \tag{4.68}$$

Simplifying Equation (4.68),

$$(A_1 - A_2)\left[\frac{c_{11}}{c_{13}}\left(\frac{c^2}{c_{1L}^2}-1\right) + \frac{c_{13}}{c_{33}}\left(\frac{c_{13}}{c_{44}}+1\right) + \frac{c_{11}}{c_{44}}\left(\frac{c^2}{c_{1L}^2}-1\right)\right] = 0 \tag{4.69}$$

Since $A_1 = A_2$ gives non physical velocity, from Equation (4.69)

$$\frac{c_{13}}{c_{33}}\left(\frac{c_{13}}{c_{44}}+1\right) + \frac{c_{11}}{c_{44}}\left(\frac{c^2}{c_{1L}^2}-1\right) = \frac{c_{11}}{c_{13}}\left(1 - \frac{c^2}{c_{1L}^2}\right) \tag{4.70}$$

which can be solved for the limiting velocity of the symmetric Lamb wave c, as the frequency $\omega \to 0$ given by

$$\begin{aligned} c &= \sqrt{\frac{\frac{c_{11}}{c_{13}} - \frac{c_{13}}{c_{33}}\left(\frac{c_{13}}{c_{44}} + 1\right) + \frac{c_{11}}{c_{44}}}{\frac{1}{c_{1L}^2}\left(\frac{c_{11}}{c_{44}} + \frac{c_{11}}{c_{13}}\right)}} \\ &= c_{1L}\sqrt{1 - \frac{c_{13}^2}{c_{11}c_{33}}} \end{aligned} \tag{4.71}$$

As the frequency $\omega \to 0$, for the antisymmetric Lamb waves from Equation (4.64)

$$\frac{\tanh(kA_2H)}{\tanh(kA_1H)} = \frac{kA_2H\left(1 - \frac{(kA_2H)^2}{3}\right)}{kA_1H\left(1 - \frac{(kA_1H)^2}{3}\right)} = \frac{A_1}{A_2}\frac{(A_2^2 - D)}{(A_1^2 - D)}\frac{(A_1^2 + E)}{(A_2^2 + E)} \tag{4.72}$$

where,

$$D = \frac{c_{11}}{c_{13}}\left(\frac{c^2}{c_{1L}^2} - 1\right) \tag{4.73}$$

$$E = \frac{c_{13}}{c_{33}}\left(\frac{c_{13}}{c_{44}} + 1\right) + \frac{c_{11}}{c_{44}}\left(\frac{c^2}{c_{1L}^2} - 1\right) \tag{4.74}$$

From Equation (4.72),

$$\frac{A_2}{A_1}\left(1 - \frac{(kA_2H)^2}{3}\right)\left(1 + \frac{(kA_1H)^2}{3}\right) = \frac{A_1}{A_2}\frac{(A_2^2 - D)}{(A_1^2 - D)}\frac{(A_1^2 + E)}{(A_2^2 + E)} \tag{4.75}$$

$$1 + \frac{(kA_1H)^2}{3} - \frac{(kA_2H)^2}{3} - \frac{(A_1A_2)^2(kH)^4}{9} = \frac{A_1^2}{A_2^2}\frac{(A_2^2 - D)}{(A_1^2 - D)}\frac{(A_1^2 + E)}{(A_2^2 + E)} \tag{4.76}$$

Since $\omega \to 0$, neglecting the higher order fourth term in the left hand side of Equation (4.76),

$$1 + \frac{(kH)^2}{3}\left(A_1^2 - A_2^2\right) = \frac{A_1^2}{A_2^2}\frac{(A_2^2 - D)}{(A_1^2 - D)}\frac{(A_1^2 + E)}{(A_2^2 + E)} \tag{4.77}$$

which can be solved for the limiting velocity (c) of the antisymmetric Lamb wave as the frequency tends to zero. Figure (4.3) shows the very close match between the limiting velocity of the antisymmetric Lamb wave in a transversely isotropic

plate by solving Equation (4.77) to the velocity of the antisymmetric Lamb wave at low frequencies obtained by solving the antisymmetric Lamb wave dispersion equation (4.64).

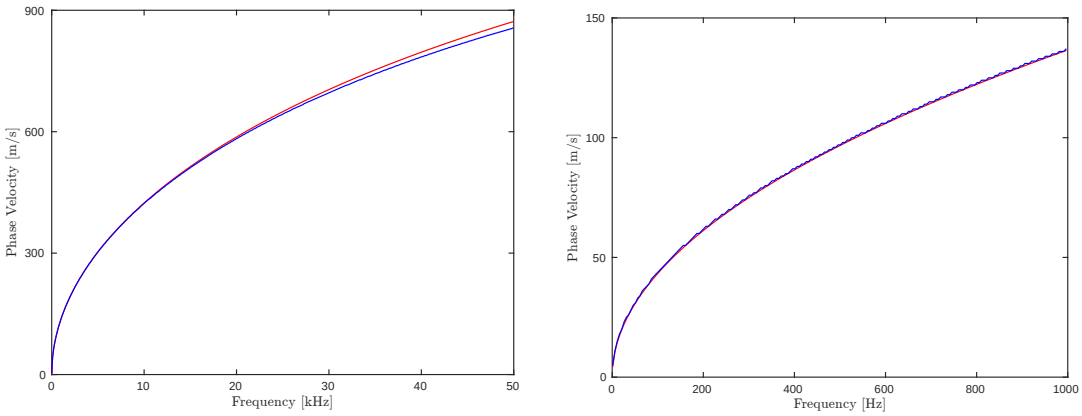

(a) (b)

Figure 4.3: Antisymmetric Lamb wave speeds in a transversely isotropic plate at low frequencies. The blue curve is obtained from solution of the dispersion equation and the red curve is the solution of the low frequency approximation. Figure (b) shows a zoomed version of Figure (a) to show the close match.

4.2 Reduction of results in transversely isotropic plate to isotropic plate

The results obtained above for propagation of Lamb waves in a transversely isotropic plate are validated by reducing them to corresponding results in an isotropic plate.

The material constants and wave speeds in a transversely isotropic material are reduced for an isotropic material into

$$c_{11} = c_{22} = c_{33} = \lambda + 2\mu = \rho c_1^2 = \mu \frac{k_2^2}{k_1^2} \tag{4.78}$$

$$c_{12} = c_{13} = c_{21} = c_{23} = c_{31} = c_{32} = \lambda = \rho\left(c_1^2 - 2c_2^2\right) = \frac{\mu}{k_1^2}\left(k_2^2 - 2k_1^2\right) \tag{4.79}$$

$$c_{44} = c_{55} = c_{66} = \mu = \rho c_2^2 \tag{4.80}$$

$$c_{1L} = c_{3L} = c_1 \tag{4.81}$$

$$c_{3T} = c_2 \tag{4.82}$$

Equations (4.28,4.29) for A, B reduces to

$$\begin{aligned} A &= \frac{k^2c^2}{c_{3L}^2} + \frac{k^2c^2}{c_{3T}^2} - \frac{k^2\left(c_{11}c_{33} - c_{13}^2 - 2c_{13}c_{44}\right)}{c_{33}c_{44}} \\ &= k^2\left[\frac{c^2}{c_1^2} + \frac{c^2}{c_2^2} - 2\right] = -\left(\eta_{1\text{iso}}^2 + \eta_{2\text{iso}}^2\right) \end{aligned} \tag{4.83}$$

where, $\eta_{1\text{iso}}^2 = k^2 - k_1^2$ and $\eta_{2\text{iso}}^2 = k^2 - k_2^2$.

$$\begin{aligned} B &= \left(\frac{c^2}{c_{3L}^2} - \frac{c_{11}}{c_{33}}\right)\left(\frac{c^2}{c_{3T}^2} - 1\right) \\ &= k^4\left(\frac{c^2}{c_1^2} - 1\right)\left(\frac{c^2}{c_2^2} - 1\right) = \eta_{1\text{iso}}^2\eta_{2\text{iso}}^2 \end{aligned} \tag{4.84}$$

Equations (4.30,4.32,4.58,4.73,4.74) become,

$$\eta_1 = \sqrt{\frac{-A + \sqrt{A^2 - 4B}}{2}} = \eta_{1\text{iso}} \tag{4.85}$$

$$\eta_2 = \sqrt{\frac{-A - \sqrt{A^2 - 4B}}{2}} = \eta_{2\text{iso}} \tag{4.86}$$

$$A_1 = \frac{\eta_1}{k} = \frac{\eta_{1\text{iso}}}{k} = \sqrt{1 - \left(\frac{c}{c_1}\right)^2} \tag{4.87}$$

$$A_2 = \frac{\eta_2}{k} = \frac{\eta_{2\text{iso}}}{k} = \sqrt{1 - \left(\frac{c}{c_2}\right)^2} \tag{4.88}$$

$$D = \frac{c_{11}}{c_{13}}\left(\frac{c^2}{c_{1L}^2} - 1\right) = \frac{c_1^2}{c_1^2 - 2c_2^2}\left(\frac{c^2}{c_1^2} - 1\right) \tag{4.89}$$

$$E = \frac{c_{13}}{c_{33}}\left(\frac{c_{13}}{c_{44}} + 1\right) + \frac{c_{11}}{c_{44}}\left(\frac{c^2}{c_{1L}^2} - 1\right) = \frac{2c_2^2}{c_1^2} + \frac{c^2}{c_2^2} - 3 \tag{4.90}$$

The other terms in the dispersion equations (4.59,4.64) also simplify to

$$\frac{(A_2^2 - D)}{(A_1^2 - D)} = \frac{c_1^2\left(2c_2^2 - c^2\right)}{2c_2^2\left(c_1^2 - c^2\right)} \tag{4.91}$$

$$\frac{(A_1^2 + E)}{(A_2^2 + E)} = \frac{2c_2^2 - c^2}{2c_2^2} \tag{4.92}$$

Hence, the symmetric Lamb wave dispersion equation (4.59) becomes for an isotropic plate,

$$\frac{\tanh\left(\eta_{1\text{iso}}H\right)}{\tanh\left(\eta_{2\text{iso}}H\right)} = \frac{c_1\left(2c_2^2 - c^2\right)^2}{4c_2^3\sqrt{c_1^2 - c^2}\sqrt{c_2^2 - c^2}} = \frac{\left(2k^2 - k_2^2\right)^2}{4k^2\eta_{1\text{iso}}\eta_{2\text{iso}}} \tag{4.93}$$

which is exactly the symmetric Lamb wave dispersion equation in an isotropic plate derived in Equation (2.55).

Similarly, the antisymmetric Lamb wave dispersion equation (4.64) becomes for an isotropic plate,

$$\frac{\tanh\left(\eta_{2\text{iso}}H\right)}{\tanh\left(\eta_{1\text{iso}}H\right)} = \frac{c_1\left(2c_2^2 - c^2\right)^2}{4c_2^3\sqrt{c_1^2 - c^2}\sqrt{c_2^2 - c^2}} = \frac{\left(2k^2 - k_2^2\right)^2}{4k^2\eta_{1\text{iso}}\eta_{2\text{iso}}} \tag{4.94}$$

which is exactly the antisymmetric Lamb wave dispersion equation in an isotropic plate derived in Equation (2.62).

Likewise, the low frequency approximation to the symmetric Lamb wave speed in a transversely isotropic plate given by Equation (4.71), reduces for an isotropic plate into

$$c = 2c_2\sqrt{1 - \frac{c_2^2}{c_1^2}} \tag{4.95}$$

known as the plate wave velocity.

4.3 Wave propagation in composite plates - Experiments and Results

The considered laminate consists of 8 layers of 2/2 twill woven carbon fibers with a $[0°/45°/0°/45°]_s$ stacking sequence. The fabric, a balanced weave, has 12 yarns-per-inch in both the warp and fill directions, and each yarn is composed of 3000 strands of T300 carbon fibers. The matrix that binds the material is Unibond 1070 epoxy. The overall thickness of the laminate is 1.78 mm and its density is $1276\,\mathrm{kg/m^3}$.

The effective properties of the laminate are determined through destructive and nondestructive (wave propagation) experiments, and from mixture type theories [18]. The Young's Modulus E_{yy} is determined from a standard uniaxial tension test in the $y-$ direction from which E_{yy} is found to be 38.8 GPa. The Poisson's ratio ν_{xy} in the xy plane is determined from the same test by measuring strains in both the x and y directions using extensometers mounted on the specimen, yielding $\nu_{xy} = 0.31$. The shear modulus G_{yz} and the elastic constant E_{zz} for the composite face sheet are determined from the equations [40]

$$G_{yz} = v_{yz}^2 \rho \tag{4.96}$$

and

$$E_{zz} = \frac{\rho E_{yy}\left(1 - v_{xy}\right) v_{11}^2}{E_{yy}\left(1 - v_{xy}\right) + 2\rho v_{xz}^2 v_{xx}^2} \tag{4.97}$$

where v_{xx} and v_{yz} are the longitudinal and shear wave velocities, respectively, of a wave propagating along the thickness direction of the laminate. The measured velocities from through transmission tests of ultrasonic waves are $v_{xx} = 2880\,\mathrm{m/s}$, $v_{yz} = 1517\,\mathrm{m/s}$. These results are found to be nearly independent of the frequency of the ultrasonic waves. E_{zz} can then be calculated with 2.6 by assuming a value for ν_{xz} (here: estimated from mixture type theories [41]). The estimated effective properties of the composite laminate obtained from the mixture type

theory and destructive and nondestructive experiments are given in Table4.1. It can be seen that there is reasonable agreement between the theoretical and experimental values of the material constants. In the remainder of this thesis, the experimentally determined properties are used.

Table 4.1: Geometry and effective material parameters for a woven composite laminate, when transversely isotropic behavior is assumed

	$2H$ [mm]	E_{11} [GPa]	E_{33} [GPa]	ν_{12}	ν_{13}	G_{13} [GPa]	ρ [kg/m^3]
Experiment	1.78	38.8	9.77	0.3137	0.324	2.937	1276
Theory	1.78	44.795	10.753	0.320	0.324	3.881	1276

The stiffness constants c_{ij} can be calculated from their well known relationships with the material constants E_{ij}, G_{ij} and ν_{ij} by

$$c_{11} = \frac{E_{xx}\left(1-\nu_{zy}\nu_{yz}\right)}{\left(1+\nu_{xy}\right)\left(1-\nu_{xy}-2\nu_{zy}\nu_{yz}\right)} \tag{4.98}$$

$$c_{33} = \frac{E_{zz}\left(1-\nu_{xy}\right)}{\left(1-\nu_{xy}-2\nu_{zy}\nu_{yz}\right)} \tag{4.99}$$

$$c_{12} = \frac{E_{xx}\left(\nu_{xy}+\nu_{zy}\nu_{yz}\right)}{\left(1+\nu_{xy}\right)\left(1-\nu_{xy}-2\nu_{zy}\nu_{yz}\right)} \tag{4.100}$$

$$c_{13} = \frac{E_{zz}\nu_{yz}}{\left(1-\nu_{xy}-2\nu_{zy}\nu_{yz}\right)} \tag{4.101}$$

$$c_{44} = G_{zx} \tag{4.102}$$

For the woven composite laminate, ultrasonic guided Lamb wave experiments are conducted and wave signals are recorded at distances of 50.8 mm to 254 mm (2 in. to 10 in.) from the source transducer, using the setup described in Section (2.3). The group velocities of the S_0 wave in the frequency range of 200 kHz to 500 kHz, and of the A_0 wave in the range of 100 kHz to 220 kHz are determined by evaluating peaks of the center frequency of the excited wave in the STFT data-sets of the recorded time domain signals.

In Figure (4.4) symmetric waves are shown as solid lines, antisymmetric as dashed

lines; experimental results are marked by $\times$. Good agreement with experimental results is achieved for both the S_0 and A_0 modes.

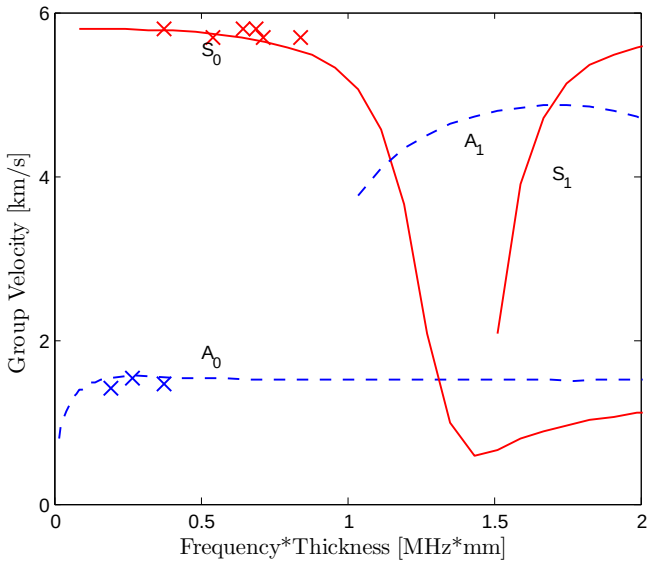

Figure 4.4: Dispersion curves for the group velocity for a composite plate. Symmetric modes are shown as solid lines, antisymmetric as dashed lines. Experimental results are marked by $\times$.

Additional wave propagation tests are carried out to validate the assumption of transverse isotropy by measuring the velocity of Lamb waves for different directions (angles) of propagation. The results for A_0 waves, propagating along three directions ($0°, 45°$ and $90°$), are summarized in Table (4.2), confirming the symmetry of the material on the xy-plane.

Table 4.2: Group velocity of the A_0 wave for different angles of propagation in the xy plane of composite plate.

Frequency [kHz]	c_g for 0° [m/s]	c_g for 45° [m/s]	c_g for 90° [m/s]
100	1529	1539	1551
150	1579	1516	1569
200	1597	1494	1565
250	1545	1563	1551

4.4 Rayleigh wave propagation in a quasi-isotropic half space

In this section a similar procedure is followed to derive the equation governing the propagation of Rayleigh waves in a transversely isotropic half space. Rayleigh waves are surface waves and they exponentially decrease in amplitude along the depth of the medium. They are non dispersive in nature, unlike Lamb waves. At high frequencies, the speeds of both the symmetric and the antisymmetric Lamb wave modes asymptotically tend towards the speed of propagation of the Rayleigh waves.

Figure (4.5) shows the model of the half space. z- direction denotes depth and is positive in the downward direction. x- direction denotes the direction of propagation of the wave. The origin is taken on the free surface.

Using exactly the same derivation as above for Lamb waves, the parameter ξ, describing the z-dependency of $\overline{U}$, $\overline{V}$ are derived (see Equations (4.30-4.33). But the field variables cannot become infinite at $z = \infty$. This physical constraint results in $\xi_2 = \xi_4 = 0$. Therefore, the displacements and stresses in the frequency

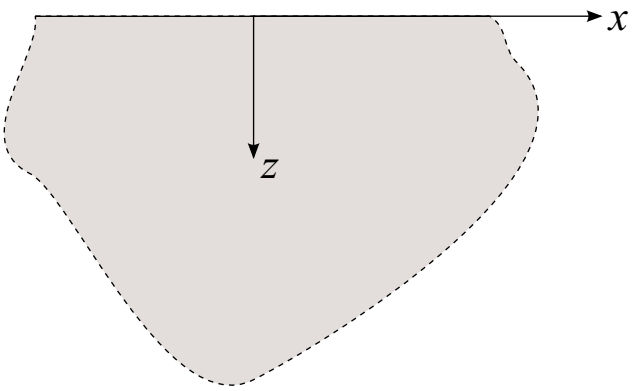

Figure 4.5: Geometry of the half space

domain can be written as

$$\overline{U}\left(k,z,\omega\right)=G_1\left(k,\omega\right)e^{-\eta_1 z}+G_3\left(k,\omega\right)e^{-\eta_2 z} \tag{4.103}$$

$$\overline{W}\left(k,z,\omega\right)=\alpha_1 G_1\left(k,\omega\right)e^{-\eta_1 z}+\alpha_3 G_3\left(k,\omega\right)e^{-\eta_2 z} \tag{4.104}$$

$$\overline{S}_{xx}\left(k,z,\omega\right)=\left(c_{11}ik-c_{13}\alpha_1\eta_1\right)\overline{G}_1 e^{-\eta_1 z}+\left(c_{11}ik-c_{13}\alpha_3\eta_2\right)\overline{G}_3 e^{-\eta_2 z} \tag{4.105}$$

$$\overline{S}_{zz}\left(k,z,\omega\right)=\left(c_{13}ik-c_{33}\alpha_1\eta_1\right)\overline{G}_1 e^{-\eta_1 z}+\left(c_{13}ik-c_{33}\alpha_3\eta_2\right)\overline{G}_3 e^{-\eta_2 z} \tag{4.106}$$

$$\overline{S}_{xz}\left(k,z,\omega\right)=c_{44}\left[\left(ik\alpha_1-\eta_1\right)\overline{G}_1 e^{-\eta_1 z}+\left(ik\alpha_3-\eta_2\right)\overline{G}_3 e^{-\eta_2 z}\right] \tag{4.107}$$

Next, the stress free boundary conditions are applied on the top surface ($z=H$) of the half space.

At $z=0$, zero normal stress gives,

$$\begin{aligned}\overline{S}_{zz}\left(k,0,\omega\right)&=\left(c_{13}ik-c_{33}\alpha_1\eta_1\right)\overline{G}_1+\left(c_{13}ik-c_{33}\alpha_3\eta_2\right)\overline{G}_3\\&=0\end{aligned} \tag{4.108}$$

At $z = 0$, zero shear stress gives,

$$\begin{aligned} \overline{S}_{xz}(k,0,\omega) &= (ik\alpha_1 - \eta_1)\overline{G}_1 + (ik\alpha_3 - \eta_2)\overline{G}_3 \\ &= 0 \end{aligned} \tag{4.109}$$

Therefore written in matrix form, G_1, G_3 which govern the motion due to the Rayleigh waves, satisfy

$$\begin{bmatrix} c_{13}ik - c_{33}\alpha_1\eta_1 & c_{13}ik - c_{33}\alpha_3\eta_2 \\ ik\alpha_1 - \eta_1 & ik\alpha_3 - \eta_2 \end{bmatrix} \begin{Bmatrix} G_1 \\ G_3 \end{Bmatrix} = \begin{Bmatrix} 0 \\ 0 \end{Bmatrix} \tag{4.110}$$

For nontrivial solution of G_1, G_3, the determinant of the coefficient matrix in Equation (4.110) needs to be zero, which gives the frequency equation for the Rayleigh waves in the half-space:

$$(c_{13}ik - c_{33}\alpha_1\eta_1)(ik\alpha_3 - \eta_2) - (c_{13}ik - c_{33}\alpha_3\eta_2)(ik\alpha_1 - \eta_1) = 0$$

$$\frac{(c_{13}ik - c_{33}\alpha_1\eta_1)(ik\alpha_3 - \eta_2)}{(c_{13}ik - c_{33}\alpha_3\eta_2)(ik\alpha_1 - \eta_1)} = 1 \tag{4.111}$$

Substituting the expressions for α_1, α_3 from Equations (4.36,4.38), the above governing equation for the Rayleigh waves can be written as

$$\frac{\eta_1}{\eta_2}\frac{[-c_{13}^2k^2 - c_{13}c_{44}k^2 + c_{33}c_{11}k^2 - c_{33}c_{44}\eta_1^2 - c_{33}\rho\omega^2]\,[c_{11}k^2 - \rho\omega^2 + c_{13}\eta_2^2]}{[-c_{13}^2k^2 - c_{13}c_{44}k^2 + c_{33}c_{11}k^2 - c_{33}c_{44}\eta_2^2 - c_{33}\rho\omega^2]\,[c_{11}k^2 - \rho\omega^2 + c_{13}\eta_1^2]} = 1$$

$$\frac{\eta_1}{\eta_2}\frac{\left[c_{13}\left\{\eta_2^2 - \frac{c_{11}k^2}{c_{13}}\left(\frac{\rho c^2}{c_{11}} - 1\right)\right\}\right]}{\left[c_{13}\left\{\eta_1^2 - \frac{c_{11}k^2}{c_{13}}\left(\frac{\rho c^2}{c_{11}} - 1\right)\right\}\right]}\frac{\left[-c_{33}c_{44}\left\{\eta_1^2 + \frac{c_{13}}{c_{33}}k^2\left(\frac{c_{13}}{c_{44}} + 1\right) + \frac{c_{11}}{c_{44}}k^2\left(\frac{\rho c^2}{c_{11}} - 1\right)\right\}\right]}{\left[-c_{33}c_{44}\left\{\eta_2^2 + \frac{c_{13}}{c_{33}}k^2\left(\frac{c_{13}}{c_{44}} + 1\right) + \frac{c_{11}}{c_{44}}k^2\left(\frac{\rho c^2}{c_{11}} - 1\right)\right\}\right]} = 1$$

$$\frac{\eta_1}{\eta_2}\frac{\left[\eta_2^2 - \frac{c_{11}k^2}{c_{13}}\left(\frac{\rho c^2}{c_{11}} - 1\right)\right]}{\left[\eta_1^2 - \frac{c_{11}k^2}{c_{13}}\left(\frac{\rho c^2}{c_{11}} - 1\right)\right]}\frac{\left[\eta_1^2 + \frac{c_{13}}{c_{33}}k^2\left(\frac{c_{13}}{c_{44}} + 1\right) + \frac{c_{11}}{c_{44}}k^2\left(\frac{\rho c^2}{c_{11}} - 1\right)\right]}{\left[\eta_2^2 + \frac{c_{13}}{c_{33}}k^2\left(\frac{c_{13}}{c_{44}} + 1\right) + \frac{c_{11}}{c_{44}}k^2\left(\frac{\rho c^2}{c_{11}} - 1\right)\right]} = 1 \tag{4.112}$$

Defining, as before

$$A_1 = \frac{\eta_1}{k} \qquad A_2 = \frac{\eta_2}{k} \tag{4.113}$$

the above governing equation (Equation (4.112)) for the Rayleigh waves can be written as

$$A_1\left[A_2^2-\frac{c_{11}}{c_{13}}\left(\frac{c^2}{c_{1L}^2}-1\right)\right]\left[A_1^2+\frac{c_{13}}{c_{33}}\left(\frac{c_{13}}{c_{44}}+1\right)+\frac{c_{11}}{c_{44}}\left(\frac{c^2}{c_{1L}^2}-1\right)\right]= \tag{4.114}$$
$$A_2\left[A_1^2-\frac{c_{11}}{c_{13}}\left(\frac{c^2}{c_{1L}^2}-1\right)\right]\left[A_2^2+\frac{c_{13}}{c_{33}}\left(\frac{c_{13}}{c_{44}}+1\right)+\frac{c_{11}}{c_{44}}\left(\frac{c^2}{c_{1L}^2}-1\right)\right]$$

Using isotropic material properties, and the results from Equations (4.87,4.88,4.91,4.92) the above equation for Rayleigh waves reduces to

$$\frac{\left(2k^2-k_2^2\right)^2}{4k^2\eta_{1\text{iso}}\eta_{2\text{iso}}}=1 \tag{4.115}$$

which is the governing equation for Rayleigh waves in an isotropic half-space [40].

CHAPTER 5

Rayleigh to Lamb wave conversion at a delamination-like crack

The problem considered in this work is a half-space in which waves are excited by a point force F , resulting in mostly Rayleigh waves propagating along the surface. When these Rayleigh waves encounter a crack parallel to the surface of the half-space (e.g. a delamination), the top layer will act as a waveguide for Lamb waves, while the lower part will remain a half-space. Hence, at the leading edge of the crack, energy from the incident Rayleigh wave will transmit as new Lamb waves above the crack, and a Rayleigh wave below the crack. Additionally, part of the incident wave is also reflected. The amplitude of the reflected Rayleigh wave is, however, found to be negligible in both numerical simulations and laboratory experiments. Similarly, reflection and transmission at the trailing edge of the crack occurs. As soon as the Lamb waves interact with the trailing edge of the crack, they are partially transmitted to the subsequent half-space in the form of a new Rayleigh wave, and are partially reflected back into layer above the crack. Moreover, the Rayleigh wave propagating below the crack is expected to be mostly transmitted as a Rayleigh wave at the trailing edge.

This problem is motivated by delaminations of layers in composite sandwich panels as illustrated in Figure (5.1). If, for example, the face sheet with thickness $2H$ separates from the core of a three-layer sandwich panel, where the core layer is a thick plate-like layer (e.g. honeycomb core), the previously described wave conversion will occur at the edges of the delaminated region.

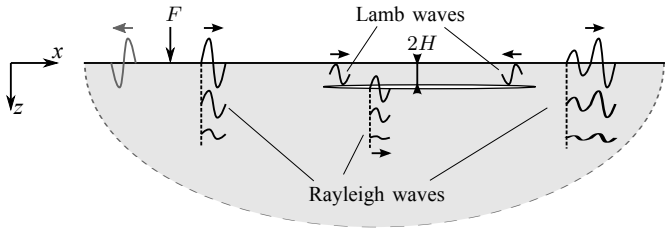

Figure 5.1: Wave conversion at delamination-like cracks near surface of a half-space for an incident Rayleigh surface wave

In this work, a square aluminum plate with lateral dimensions of 304.8 mm (12 in.) and thickness of 10 mm in the y-direction is considered as a prototype of the delamination problem. Note, when comparing the dimensions of this plate with the wavelengths in the considered frequency range, the plate can be considered as a half-space. As explained in more details later, an artificial crack is sawed into the plate at 1.78 mm from one side of the plate using electrical discharge machining. The aluminum plate (Al 6061 T-6) has a Young's modulus of $E = 69\,\mathrm{GPa}$, a Poisson's ratio $\nu = 0.3269$, a shear modulus μ given by $E/(2+2\nu)$, and density $\rho = 2700\,\mathrm{kg/m^3}$.

The excitation force on the surface of the plate generates both body waves (P- and S-waves) and Rayleigh waves. The speeds of the body waves, c_1 for P- and c_2 for S-waves, where

$$c_1^2 = \frac{E(1-\nu)}{\rho(1+\nu)(1-2\nu)} \tag{5.1}$$

and

$$c_2^2 = \frac{E}{2\rho(1+\nu)} \tag{5.2}$$

in aluminum are $c_1 = 6120\,\mathrm{m/s}$ and $c_2 = 3103\,\mathrm{m/s}$, respectively. It is well known from the solution of Lamb's problem [1] that the wave field near the surface of the plate is dominated by the Rayleigh waves within a distance of a few wavelengths from the source. Moreover, the reflected waves from the edges of the plate have no influence on the wave field in the time duration of interest due to the large dimensions of the plate. Nonetheless, the wave speeds are necessary for the calculations

of Rayleigh and Lamb wave speeds, as described in the following subsection.

5.1 Rayleigh Surface Waves

Rayleigh wave speed c_R can be determined by solving the characteristic equation

$$\left(2-\frac{c_R^2}{c_2^2}\right)^2-4\sqrt{1-\frac{c_R^2}{c_1^2}}\sqrt{1-\frac{c_R^2}{c_2^2}}=0 \tag{5.3}$$

A good approximation [42] is given by

$$c_R \approx \frac{0.862+1.14\nu}{1+\nu} \tag{5.4}$$

for most metals. This approximate solution can also be used as an initial guess for solving Equation (5.3). For the studied aluminum plate, the Rayleigh wave speed is 2891 m/s (Equation (5.4) yields 2888 m/s).

Furthermore, the energy of Rayleigh waves is concentrated near the surface, making this kind of wave appealing for NDE of damages near the surface of a structure. For the sake of clarity, the displacement and stress fields $\mathbf{u}\left(\mathbf{x},t\right)=\overline{\mathbf{U}}\left(z\right)e^{i(kx-\omega t)}$ and $\boldsymbol{\sigma}\left(\mathbf{x},t\right)=\overline{\boldsymbol{S}}\left(z\right)e^{i(kx-\omega t)}$ due to Rayleigh waves are given below.

$$\overline{U}=iA\left(ke^{-\eta_1 z}-\frac{k^2+\eta_2^2}{2k}e^{-\eta_2 z}\right) \tag{5.5}$$

$$\overline{V}=0 \tag{5.6}$$

$$\overline{W}=A\left(-\eta_1 e^{-\eta_1 z}+\frac{k^2+\eta_2^2}{2\eta_2}e^{-\eta_2 z}\right) \tag{5.7}$$

$$\overline{S}_{xx}=-A\mu\left(\left(2\eta_1^2+k_2^2\right)e^{-\eta_1 z}-\left(k_2^2+\eta_2^2\right)e^{-\eta_2 z}\right) \tag{5.8}$$

$$\overline{S}_{zz}=A\mu\left(k_2^2+\eta_2^2\right)\left(e^{-\eta_1 z}-e^{-\eta_2 z}\right) \tag{5.9}$$

$$\overline{S}_{xz}=-2iA\mu k\eta_1\left(e^{-\eta_1 z}-e^{-\eta_2 z}\right) \tag{5.10}$$

where $\eta_1^2=k^2-k_1^2$, $\eta_2^2=k^2-k_2^2$, $k_1=\frac{\omega}{c_1}$ and $k_2=\frac{\omega}{c_2}$. ω is the angular frequency, k is the wavenumber and c_1 and c_2 are the P and S wave speeds.

5.2 Guided Lamb Waves

For a homogeneous isotropic elastic plate with a thickness of $2H$, the dispersion relations for guided symmetric Lamb wave motion can be expressed in the form [40]

$$\left(2k^2 - k_2^2\right)^2 \cosh\left(\eta_1 H\right) \sinh\left(\eta_2 H\right) - 4k^2 \eta_1 \eta_2 \sinh\left(\eta_1 H\right) \cosh\left(\eta_2 H\right) = 0 \quad (5.11)$$

and for antisymmetric Lamb wave motion by

$$\left(2k^2 - k_2^2\right)^2 \sinh\left(\eta_1 H\right) \cosh\left(\eta_2 H\right) - 4k^2 \eta_1 \eta_2 \cosh\left(\eta_1 H\right) \sinh\left(\eta_2 H\right) = 0 \quad (5.12)$$

where $\omega = 2\pi f$ is the angular frequency, and k is the wavenumber. In subsequent discussions, symmetric waves are labeled as S_m and antisymmetric waves are labeled A_n with $m, n = 0, 1, 2, \ldots$, respectively.

The graphical solutions of Eqs.(5.11) and (5.12) for the phase velocity c, which is generally a function of frequency, are called dispersion curves. The group velocity c_g of the waves can be obtained from the dispersion curves using the relation

$$c_g = \frac{c}{1 - \frac{\omega}{c}\frac{dc}{d\omega}} \quad (5.13)$$

The displacement and stress fields for antisymmetric Lamb waves propagating the

the x direction in the xz plane are given by

$$\overline{U} = -iA_{\mathrm{a}}\left(k\sinh\left(\eta_1 z'\right) - \frac{\left(2k^2-k_2^2\right)\sinh\left(\eta_1 H\right)}{2k\sinh\left(\eta_2 H\right)}\sinh\left(\eta_2 z'\right)\right) \tag{5.14}$$

$$\overline{W} = -A_{\mathrm{a}}\left(\eta_1\cosh\left(\eta_1 z'\right) - \frac{\left(2k^2-k_2^2\right)\sinh\left(\eta_1 H\right)}{2\eta_2\sinh\left(\eta_2 H\right)}\cosh\left(\eta_2 z'\right)\right) \tag{5.15}$$

$$\overline{S}_{xx} = A_{\mathrm{a}}\mu\left(\left(2\eta_1^2+k_2^2\right)\sinh\left(\eta_1 z'\right) - \frac{\left(2k^2-k_2^2\right)\sinh\left(\eta_1 H\right)}{\sinh\left(\eta_2 H\right)}\sinh\left(\eta_2 z'\right)\right) \tag{5.16}$$

$$\overline{S}_{zz} = -A_{\mathrm{a}}\mu\left(2k^2-k_2^2\right)\left(\sinh\left(\eta_1 z'\right) - \frac{\sinh\left(\eta_1 H\right)}{\sinh\left(\eta_2 H\right)}\sinh\left(\eta_2 z'\right)\right) \tag{5.17}$$

$$= -A_{\mathrm{a}}\mu\left(2k^2-k_2^2\right)\sinh\left(\eta_1 H\right)\left(\frac{\sinh\left(\eta_1 z'\right)}{\sinh\left(\eta_1 H\right)} - \frac{\sinh\left(\eta_2 z'\right)}{\sinh\left(\eta_2 H\right)}\right) \tag{5.18}$$

$$\overline{S}_{xz} = -2iA_{\mathrm{a}}\mu k\eta_1\left(\cosh\left(\eta_1 z'\right) - \frac{\left(2k^2-k_2^2\right)^2\sinh\left(\eta_1 H\right)}{4k^2\eta_1\eta_2\sinh\left(\eta_2 H\right)}\cosh\left(\eta_2 z'\right)\right) \tag{5.19}$$

$$= -2iA_{\mathrm{a}}\mu k\eta_1\cosh\left(\eta_1 H\right)\left(\frac{\cosh\left(\eta_1 z'\right)}{\cosh\left(\eta_1 H\right)} - \frac{\cosh\left(\eta_2 z'\right)}{\cosh\left(\eta_2 H\right)}\right) \tag{5.20}$$

with $\mathbf{u}\left(\mathbf{x},t\right) = \overline{\mathbf{U}}\left(z\right)e^{i(kx-\omega t)}$ and $\boldsymbol{\sigma}\left(\mathbf{x},t\right) = \overline{\boldsymbol{S}}\left(z\right)e^{i(kx-\omega t)}$.

The expressions above are given for a coordinate system with the origin in the middle of the plate. The coordinates can be transformed into the global coordinate system that is also used for expressing Rayleigh waves through $z' = z - H$.

Similarly, the expressions for the symmetric Lamb wave motion are given by

$$\overline{U} = iA_{\mathrm{s}}\left(k\cosh\left(\eta_1 z'\right) - \frac{\left(2k^2-k_2^2\right)\cosh\left(\eta_1 H\right)}{2k\cosh\left(\eta_2 H\right)}\cosh\left(\eta_2 z'\right)\right) \tag{5.21}$$

$$\overline{W} = A_{\mathrm{s}}\left(\eta_1\sinh\left(\eta_1 z'\right) - \frac{\left(2k^2-k_2^2\right)\cosh\left(\eta_1 H\right)}{2\eta_2\cosh\left(\eta_2 H\right)}\sinh\left(\eta_2 z'\right)\right) \tag{5.22}$$

$$\overline{S}_{xx} = -A_{\mathrm{s}}\mu\left(\left(2\eta_1^2+k_2^2\right)\cosh\left(\eta_1 z'\right) - \frac{\left(2k^2-k_2^2\right)\cosh\left(\eta_1 H\right)}{\cosh\left(\eta_2 H\right)}\cosh\left(\eta_2 z'\right)\right) \tag{5.23}$$

$$\overline{S}_{zz} = A_{\mathrm{s}}\mu\left(2k^2-k_2^2\right)\left(\cosh\left(\eta_1 z'\right) - \frac{\cosh\left(\eta_1 H\right)}{\cosh\left(\eta_2 H\right)}\cosh\left(\eta_2 z'\right)\right) \tag{5.24}$$

$$= A_{\mathrm{s}}\mu\left(2k^2-k_2^2\right)\cosh\left(\eta_1 H\right)\left(\frac{\cosh\left(\eta_1 z'\right)}{\cosh\left(\eta_1 H\right)} - \frac{\cosh\left(\eta_2 z'\right)}{\cosh\left(\eta_2 H\right)}\right) \tag{5.25}$$

$$\overline{S}_{xz} = iA_{\mathrm{s}}\mu k\eta_1\left(\sinh\left(\eta_1 z'\right) - \frac{\left(2k^2-k_2^2\right)^2\cosh\left(\eta_1 H\right)}{4k^2\eta_1\eta_2\cosh\left(\eta_2 H\right)}\sinh\left(\eta_2 z'\right)\right) \tag{5.26}$$

$$= 2iA_{\mathrm{s}}\mu k\eta_1\sinh\left(\eta_1 H\right)\left(\frac{\sinh\left(\eta_1 z'\right)}{\sinh\left(\eta_1 H\right)} - \frac{\sinh\left(\eta_2 z'\right)}{\sinh\left(\eta_2 H\right)}\right) \tag{5.27}$$

For the studied aluminum plate, the region above the delamination-like crack has a thickness of $2H = 1.78\,\text{mm}$, and the dispersion curves are computed for the P and S wave speeds given above. The results are shown in Figure (5.2), where solid curves denote symmetric waves and dashed curves denote antisymmetric waves. Additionally, the Rayleigh wave speed is plotted as a dotted line. In the frequency range of interest, i.e. 100 to 500 kHz, the symmetric wave S_0 propagates much faster than Rayleigh waves. The antisymmetric wave A_0, however, propagates with a similar wave speed as that for Rayleigh waves. Below approximately 280 kHz, Rayleigh waves are faster, while above this frequency, A_0 waves are slightly faster. Hence, wave signals have to be analyzed carefully in order to distinguish between the different waves. Therefore, numerical simulations are carried out first, which allow for a more detailed analysis than experiments.

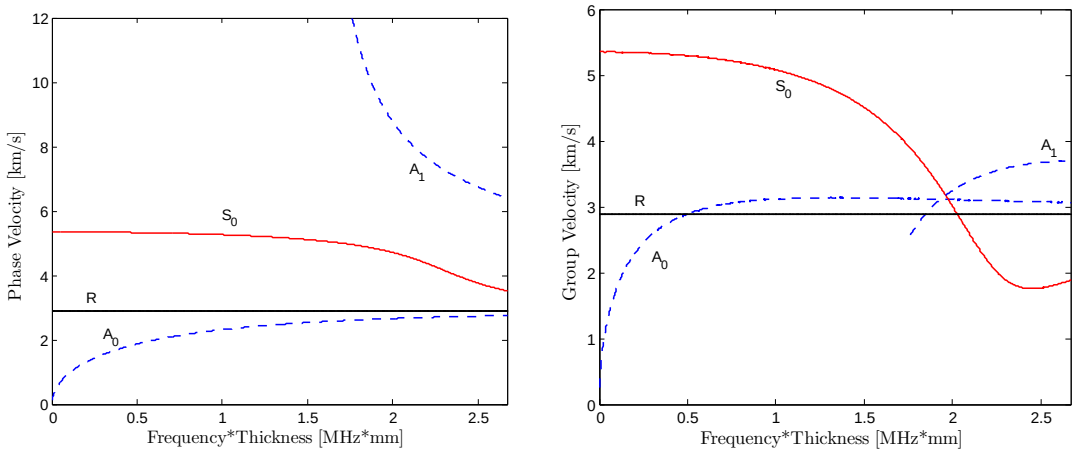

(a) Phase velocity

(b) Group velocity

Figure 5.2: Dispersion curves for an aluminum plate with a thickness of $2H = 1.78\,\text{mm}$. Symmetric modes are shown as solid lines, antisymmetric as dashed lines. The velocity of the Rayleigh surface wave for this material is shown as black lines.

5.3 Wave Scattering

Energy-based scattering coefficients e_i and amplitude-based scattering coefficients s_i are defined as

$$e_i = \frac{E_i}{E_{\text{inc}}} \qquad \text{and} \qquad s_i = \frac{\sqrt{E_i}}{\sqrt{E_{\text{inc}}}} = \frac{a_i}{a_{\text{inc}}}, \tag{5.28}$$

where E denotes the energy of a wave and a the corresponding amplitude. Hence, the scattering coefficient for the transmitted Rayleigh wave e_{RR} is the ratio of the energy E_{RR} of the transmitted wave and the incident Rayleigh wave $E_{\text{inc}} = E_{\text{R}}$.

In order to determine the scattering coefficients, the power flow P through an arbitrary cross-section A of the waveguide in the x-direction with the normal vector $\mathbf{n} = \mathbf{e}_x$, which is given by

$$P = -\int_A \sigma_{ij} n_j \dot{u}_i \, \mathrm{d}A = -\int_A \sigma_{ix} \dot{u}_i \, \mathrm{d}A \tag{5.29}$$

is considered. The time-average over one period $T = \frac{2\pi}{\omega}$ of the power flow is then given by

$$\langle P \rangle = \frac{1}{T}\int_0^T P \, \mathrm{d}t = \frac{-\omega}{2}\int_A \operatorname{imag}\left(\overline{S}^*_{xx}\overline{U} + \overline{S}^*_{yx}\overline{V} + \overline{S}^*_{zx}\overline{W}\right) \mathrm{d}A \tag{5.30}$$

where $(\cdot)^*$ indicates complex conjugate. The total energy E of a harmonic wave with n_{p} periods is then

$$E = n_{\text{p}} T \langle P \rangle \tag{5.31}$$

Inserting displacements and stresses from Equations (5.5)-(5.10) into Equation (5.30) and carrying out the integration in the z-direction, yields the time-average power flow per unit length of a Rayleigh wave as

$$\begin{aligned}\langle P_{\text{R}} \rangle = \frac{A^2\omega\mu}{2}\Bigg[k\left(\frac{2\eta_1^2 + k_2^2}{2\eta_1} - \frac{(2k^2 - k_2^2)}{\eta_1 + \eta_2} - \frac{(2k^2 - k_2^2)(2\eta_1^2 + k_2^2)}{2k^2(\eta_1 + \eta_2)} + \frac{(2k^2 - k_2^2)^2}{4k^2\eta_2}\right) \\ + \eta_1\left(k - \frac{(2k^2 - k_2^2)}{2k\eta_2(\eta_1 + \eta_2)} - \frac{k(2k^2 - k_2^2)}{\eta_2(\eta_1 + \eta_2)} + \frac{(2k^2 - k_2^2)^3}{8k\eta_1\eta_2^3}\right)\Bigg]\end{aligned} \tag{5.32}$$

The amplitude A in the above equation depends on the boundary conditions of the problem, i.e. on the load F for the incident Rayleigh wave and on the interface conditions at the leading and trailing edges of the crack for transmitted and reflected waves. While the amplitude of the incident wave can be determined analytically (see Equations (5.5)-(5.10), the amplitude of transmitted and reflected Rayleigh waves are determined from finite element simulations, which are described in the following section.

In a similar way, the time-average power flow per unit length of an antisymmetric Lamb wave can be determined by inserting displacements and stresses from Equations(5.14)-(5.20)) into Equation (5.30), resulting in

$$\begin{aligned}\langle P_{\mathrm{a}}\rangle = \frac{A_{\mathrm{a}}^2\omega\mu}{4}\Bigg[&\frac{k}{\eta_1}\sinh\left(2\eta_1 H\right)\left(k_2^2+4\eta_1^2\right)-2Hkk_2^2\\ &\frac{\left(2k^2-k_2^2\right)}{k\eta_2}\frac{\sinh\left(\eta_1 H\right)}{\sinh\left(\eta_2 H\right)}\frac{\sinh\left(\left(\eta_1+\eta_2\right)H\right)}{\eta_1+\eta_2}\left(2k^2\left(\eta_2+2\eta_1\right)+k_2^2\left(\eta_2-\eta_1\right)+2\eta_1^2\eta_2\right)\\ &\frac{\left(2k^2-k_2^2\right)}{k\eta_2}\frac{\sinh\left(\eta_1 H\right)}{\sinh\left(\eta_2 H\right)}\frac{\sinh\left(\left(\eta_1-\eta_2\right)H\right)}{\eta_1-\eta_2}\left(2k^2\left(\eta_2-2\eta_1\right)+k_2^2\left(\eta_2+\eta_1\right)+2\eta_1^2\eta_2\right)\\ &\frac{\left(2k^2-k_2^2\right)^2}{4k\eta_2^3}\frac{\sinh^2\left(\eta_1 H\right)}{\sinh^2\left(\eta_2 H\right)}\sinh\left(2\eta_2 H\right)\left(4k^2-3k_2^2\right)\\ &\frac{\left(2k^2-k_2^2\right)^2}{2k\eta_2^2}\frac{\sinh^2\left(\eta_1 H\right)}{\sinh^2\left(\eta_2 H\right)}Hk_2^2\Bigg]\end{aligned} \tag{5.33}$$

where the amplitude A_{a} again depends on the boundary conditions of the problem and is identified from finite element simulations. For this problem, mostly antisymmetric waves are expected to be generated at the edges of the crack.

The time-average power flow per unit length of a symmetric Lamb wave can be determined by inserting displacements and stresses from Equations (5.21-5.27)

into Equation (5.30), resulting in

$$\begin{aligned}\langle P_{\mathrm{s}}\rangle = \frac{A_{\mathrm{s}}^2\omega\mu}{4}\Bigg[&\frac{k}{\eta_1}\sinh\left(2\eta_1 H\right)\left(k_2^2+4\eta_1^2\right)-2Hkk_2^2\\ &\frac{\left(2k^2-k_2^2\right)}{k\eta_2}\frac{\cosh\left(\eta_1 H\right)}{\cosh\left(\eta_2 H\right)}\frac{\sinh\left(\left(\eta_1+\eta_2\right)H\right)}{\eta_1+\eta_2}\left(2k^2\left(\eta_2+2\eta_1\right)+k_2^2\left(\eta_2-\eta_1\right)+2\eta_1^2\eta_2\right)\\ &\frac{\left(2k^2-k_2^2\right)}{k\eta_2}\frac{\cosh\left(\eta_1 H\right)}{\cosh\left(\eta_2 H\right)}\frac{\sinh\left(\left(\eta_1-\eta_2\right)H\right)}{\eta_1-\eta_2}\left(2k^2\left(\eta_2-2\eta_1\right)+k_2^2\left(\eta_2+\eta_1\right)+2\eta_1^2\eta_2\right)\\ &\frac{\left(2k^2-k_2^2\right)^2}{4k\eta_2^3}\frac{\cosh^2\left(\eta_1 H\right)}{\cosh^2\left(\eta_2 H\right)}\sinh\left(2\eta_2 H\right)\left(4k^2-3k_2^2\right)\\ &\frac{\left(2k^2-k_2^2\right)^2}{2k\eta_2^2}\frac{\cosh^2\left(\eta_1 H\right)}{\cosh^2\left(\eta_2 H\right)}Hk_2^2\Bigg]\end{aligned} \tag{5.34}$$

5.4 Numerical Modeling and Simulations

In order to investigate the class of problems described above, transient finite element (FE) simulations are conducted. For the considered homogeneous isotropic linearly elastic aluminum plate, different two-dimensional plane-strain models are created in the commercial software package Abaqus.

First, a thin layer with a thickness of 1.78 mm and a thick layer with a thickness of 298.22 mm are modeled. The plate is then assembled through tie constraints between the two layers, enforcing continuity, i.e. equal displacements, at the interface. Using this method, the delamination-like crack can easily be introduced in the form of a zero volume delamination by untying the neighboring nodes in the damaged region. In the simulations, the leading edge of the crack is 50 mm away from the concentrated force input F (which is at $x = 0$), and the delamination is 50 mm long. At the bottom edge of the plate, a fixed boundary is introduced, i.e. $\mathbf{u} = 0$, while all other edges are considered traction free, except for the concentrated force at the top edge. This model will be referred to as the "tie model".

Since the zero volume delamination implemented in the tie model does not in-

troduce a singularity in the stress at the leading and trailing edges of the crack, a second model is considered. Instead of implementing an elliptical crack with non-zero volume, which has also been shown to give excellent results [43], crack tip elements are implemented in Abaqus with the delamination-like crack being the seam. By applying crack tips in Abaqus, strain is proportional to $\frac{1}{\sqrt{r}}$ with r being the distance from the crack tip. The size and location of the delamination are identical to the ones of the tie model. In the following, this model will be referred to as the "crack tip model".

For both models, mostly 4-node bilinear elements (CPE4) are used with a spatial resolution of about 0.5 mm, which is about ten times smaller than the smallest wave length of the Lamb and Rayleigh waves in the considered frequency range. In order to implement the crack tips, 6-node and 8-node quadratic elements are used in the surrounding area. Since this results in a slight irregularity in the mesh, the crack tip model has 237,815 elements, while the tie model has 240,000 elements. To calculate the transient dynamic response to a given concentrated force input F, Abaqus' implicit time integration with a fixed time step of 0.1 µs is used and simulations are conducted up to 80 µs simulation time.

In order to study mode conversion at the leading edge of the aforementioned delamination-like crack more thoroughly, another smaller model is considered as well. In this "leading edge model", as shown in Figure (5.3), three nodes are of particular interest: at M1, the induced Rayleigh wave is measured, at M2, the Lamb wave that is generated at the crack tip, and at M3, the transmitted Rayleigh wave below the delamination-like crack, respectively. With the reduced dimensions, the model requires less computation time and simulations for varying excitation frequencies can be carried out more easily.

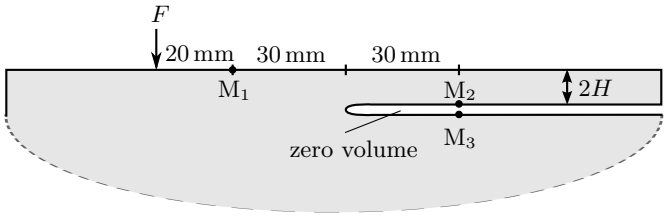

Figure 5.3: Model to investigate mode conversion at leading edge of a delamination-like crack in a half-space

5.5 Results

In a first step, the modeling techniques "tie model" and "crack tip model", as described in the previous section, are compared for a three-cycle sinusoidal tone burst enclosed in a Hann window (also called Hanning window) with the central frequency at 200 kHz. The relatively short tone burst is used to avoid superposition of the wave of interest with other (reflected) waves. Results of the conducted simulations are shown in Figure (5.4). In Figure (5.4a) the normalized displacements in the z direction at the same node in the delamination zone are compared, and in Figure (5.4b), wave signals from after the damaged area are shown. Solid lines denote results from the crack tip model and dashed lines denote results from the tie model. It can be seen that the results from the tie model coincide with those from the crack tip model. Moreover, only the left propagating Lamb wave that is generated at the trailing edge of the crack, as shown in Figure (5.4a), reveals a practically negligible difference between the two models. Hence, this also confirms the accuracy of the results from past research [34, 30] in which a zero volume delamination with sufficiently fine meshes were used for modeling such defects. It should be noted that the distinction between the two models would be more prominent closer to the crack tip, where the singular field dominates. The distinction appears to be negligible in the guided wave dominated far field.

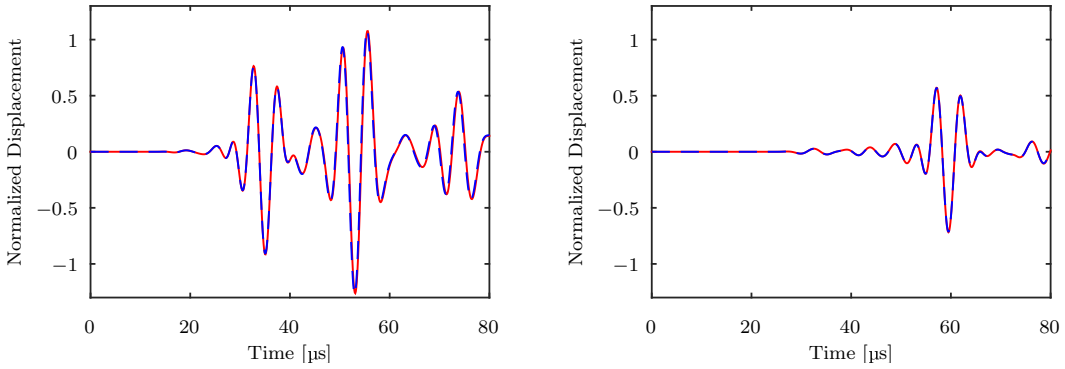

(a) In delamination zone at $x = 75\,\text{mm}$ (b) After delamination zone at $x = 150\,\text{mm}$

Figure 5.4: Comparison of normalized displacements in the z direction at the surface of a thick damaged plate from simulations with the crack tip model (solid) and the tie model (dashed) at $f = 200\,\text{kHz}$.

In the next step, wave propagation is studied in detail using the determined wave speeds from Sections (5.1) and (5.2). To this end, the displacements are analyzed at two locations on the surface of the plate. In Figure (5.5), the normalized displacements in the z direction that are calculated at $x = 25\,\text{mm}$ and $x = 150\,\text{mm}$ are shown for $f = 200\,\text{kHz}$. In Figure (5.5a), the incident Rayleigh wave R$\rightarrow$ can clearly be identified using the corresponding wave speed and position. When this incident R$\rightarrow$ wave interacts with the leading edge of the delamination-like crack, almost no reflection occurs. Instead, the wave is partially transmitted to an A_0 wave, propagating in the ligament above the crack that now acts as a waveguide for Lamb waves, and partially to a Rayleigh wave that propagates along the surface of the half-space below the crack. When the $RA_0\rightarrow$ wave encounters the trailing edge of the crack, it is partially reflected as a left propagating wave $A_0\leftarrow$. Continuing on the path of this wave, it is again partially transmitted as a Rayleigh wave when the wave interacts with the leading edge of the crack. Hence, the second wave in the signal is denoted as $RA_0R\leftarrow$.

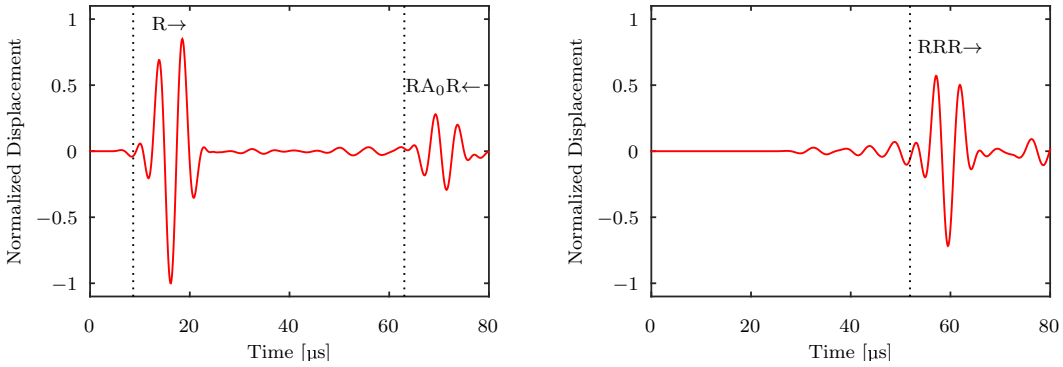

(a) In delamination zone at $x = 75\,\text{mm}$ (b) After delamination zone at $x = 150\,\text{mm}$

Figure 5.5: Normalized displacements in the z direction at various locations on the surface of a thick damaged plate for $f = 200\,\text{kHz}$.

It should also be noted, that the Rayleigh wave RR→ is almost completely transmitted at the trailing edge of the crack such that there is no RRR← in the signal. Note, the waves are denoted by their current wave type, i.e. A_m for antisymmetric waves and R for Rayleigh waves, and including their propagation history with the most recent wave type being at the end of the sequence. Additionally, the current propagation direction is denoted by $\rightarrow$ for right and by $\leftarrow$ for left propagating waves, respectively.

In Figure (5.5b) the normalized displacements in the z direction from beyond the crack at $x = 150\,\text{mm}$ are shown. Considering the wave speeds, the main wave packet can be identified as an RRR→ wave. This wave might be superimposed with the $RA_0R\rightarrow$ wave but since the wave speeds of Rayleigh and A_0 waves at 200 kHz are very similar (see Figure (5.2b)), a clear distinction cannot be made. However, a low but significant amplitude before the arrival time of previously mentioned waves can also be noticed. Dividing the distance $x = 150\,\text{mm}$ by the time at which the first non-zero signal can be observed leads to an average group velocity of about 5500 m/s and can therefore not be associated with any expected propagating wave. The fastest expected propagating wave that could be detected

is the $RS_0R\rightarrow$ wave, which possibly arrives around 44 µs and therefore would be significantly later in time but still might explain part of the non-zero signal. Nonetheless, the investigation of this phenomenon has to be addressed again in future work.

The frequency dependence of mode conversion at a delamination-like crack is analyzed next. The leading edge model is evaluated first for varying excitation frequencies. Scattering coefficients e_i are determined from Equation (5.28) using the semi-analytical approach from Equations (5.31-5.33). Thereby, the amplitudes A for Rayleigh waves and A_a for Lamb waves are determined by comparing displacements from FE simulations with normalized theoretical values at, for example, $z = 0$. In Figure (5.6), the determined transmission coefficient for Rayleigh to Rayleigh wave conversion is shown for frequencies between 100 and 500 kHz and marked by $\times$. Additionally, the Rayleigh to Lamb wave transmission coefficient is denoted by $+$.

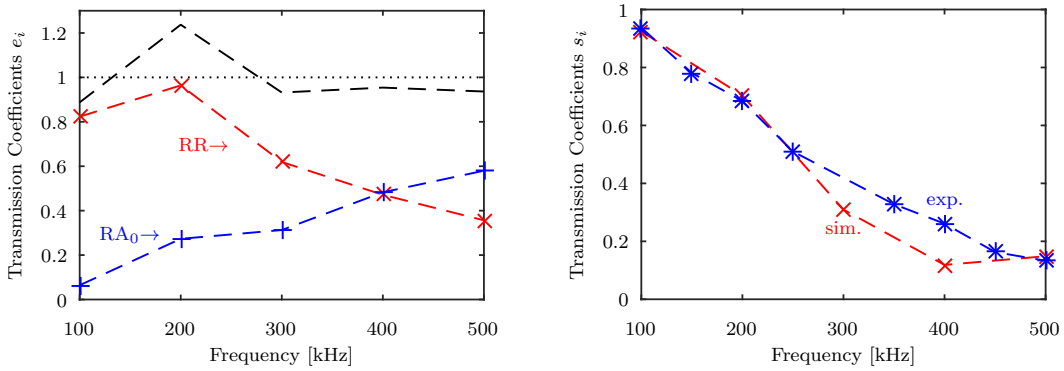

(a) Rayleigh to Lamb wave $RA_0 \rightarrow$ (+) and Rayleigh to Rayleigh wave RR→ (×) transmission at leading edge of the crack

(b) Rayleigh to Rayleigh wave RRR→ transmission through the delamination zone; experimental results (*) for a 25.4 mm and FE results (×) for a 50 mm delamination zone

Figure 5.6: Transmission coefficients for mode conversion at the delamination-like crack for varying frequencies

In order to examine the transmission of the induced Rayleigh wave to the transmitted Rayleigh wave RRR$\rightarrow$ through the whole delamination zone, in Figure (5.6b), the transmission coefficient is shown for frequencies from 100 to 500 kHz. The results reveal a decreasing transmission of the incident Rayleigh wave with increasing frequency.

In order to visualize the effect of a delamination-like crack, the displacement fields of waves propagating in the delamination zone are shown in Figure (5.7) at frequencies 200 kHz and 500 kHz. For $f = 200$ kHz, Lamb waves propagate slower through the damaged area than Rayleigh waves below the crack, which is due to the difference in the group velocities (cf. Figure (5.2)). For $f = 500$ kHz, the opposite behavior can be seen, as Lamb waves propagate faster than Rayleigh waves. These effects need to be incorporated into damage detection systems through careful signal processing.

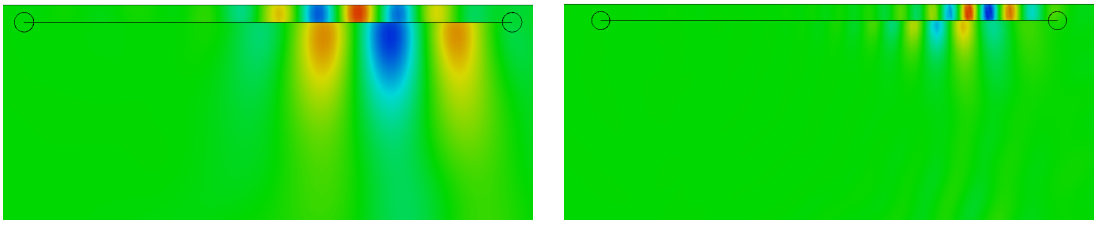

(a) A_0 waves are slower than Rayleigh waves at 200 kHz

(b) A_0 waves are faster than Rayleigh waves at 500 kHz

Figure 5.7: Displacement fields in the delamination zone, showing propagating Lamb and Rayleigh waves at different frequencies

In the final step, the displacements at the surface of the plate at various locations are compared for the undamaged and damaged cases. The normalized displacements in the z direction at $x = 75$ mm and $x = 150$ mm are shown in Figure (5.8). The displacements for an undamaged plate are shown as dashed lines,

while displacements for the damaged plate are shown as solid lines. In Figure (5.8a), there is a clear difference between the undamaged and damaged cases even without a detailed analysis of the signals. When considering a measurement after the delamination zone, as shown in Figure (5.8b), it becomes clear why a detailed understanding of the underlying phenomena is necessary. In this case, not only is the amplitude of the Rayleigh wave RRR→ reduced but also part of the incident wave's energy is now propagating as an additional Rayleigh wave, whose arrival time depends on the speed of the Lamb wave propagating above the delamination-like crack.

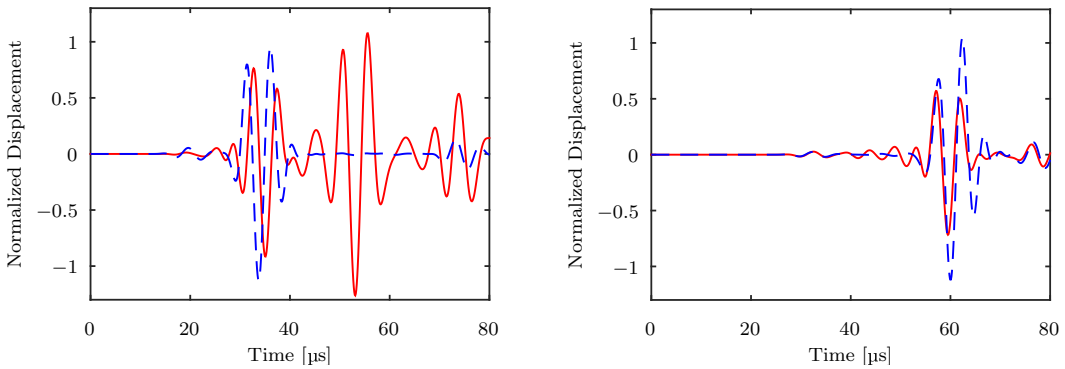

(a) In the delamination zone at $x = 75\,\text{mm}$ (b) After delamination zone at $x = 150\,\text{mm}$

Figure 5.8: Normalized displacements in the z direction at various locations on the surface of the undamaged (dashed lines) and damaged (solid lines) plate for $f = 200\,\text{kHz}$

5.6 Experimental Validation

In this section, the response of a thick aluminum plate to a dynamic load is obtained from experiments. After an introduction to the general experimental setup in Section (5.6.1), wave propagation in the undamaged case is compared to simulation results in Section (5.6.2). This ensures correctness of the validation methodology. Then in Section (5.6.3), experiments with a damaged aluminum plate are conducted and results are compared to those obtained from numerical

simulations.

5.6.1 Experimental Setup

Laboratory experiments are carried out using an ultrasonic system in the pitch-catch mode augmented by a fixture that allows accurate placement of the actuating and sensing transducers in repeated tests, thereby simulating a large array with an arbitrary number of sources and receivers. The waves are induced and recorded by a pair of identical broadband PZT transducers (Digital Wave B-225). The transducers are placed on the top edge of the plate, as shown in Figure (5.9), using a Plexiglas face sheet that is attached to the plate. An array of holes with the diameter equal to that of the transducers is drilled into the sheet, ensuring identical transducer locations in repeated experiments. The transmission of ultrasound is supported by the application of an ultrasonic gel couplant (Sonotech). A five-cycle sinusoidal tone burst enclosed in a Hann window with the central frequency at 200 kHz, produced by an arbitrary waveform generator (Stanford Research Systems), is used as the driving signal V of the source transducer. Note that for the experiments, a tone burst that consists of more cycles than in previous numerical simulations is preferable, reducing distortion effects due to the frequency response of the transducer. A signal conditioner (Digital Wave FM-1) is used to amplify and filter the received signals. The input and received signals are digitized and recorded using an oscilloscope (Agilent 54624A) with up to 200 MHz sampling frequency.

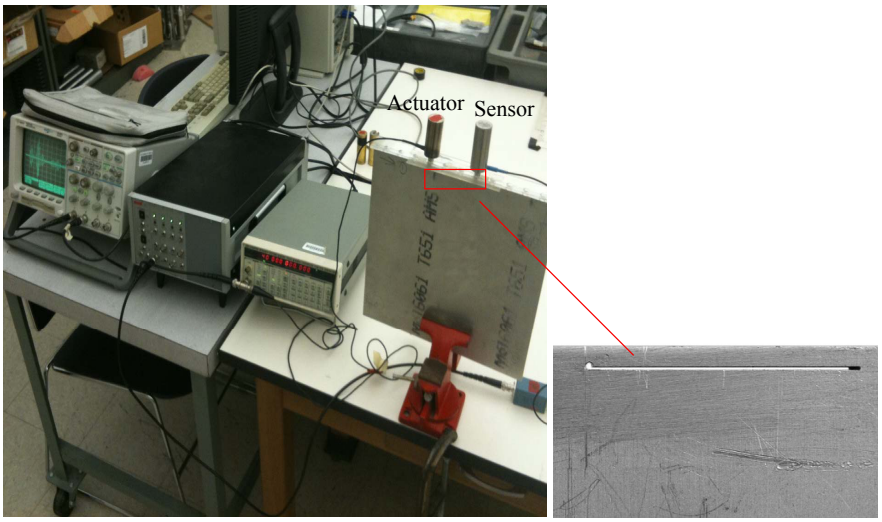

Figure 5.9: The laboratory experimental setup including oscilloscope, signal conditioner, function generator and transducers on the edge of a thick aluminum plate, and a close-up view of the delamination-like crack

The generated input signal $V(t)$ is thereby of the form

$$V(t) = \frac{1}{2}\left[1 - \cos\left(\frac{2\pi f t}{n_{\mathrm{p}}}\right)\right]\sin(2\pi f t) \tag{5.35}$$

where f is the central frequency and n_{p} is the number of cycles. However, the signal from Equation (5.35) is modified by various components of the test setup before it is transmitted as a force on the specimen. In a similar manner, the received signal differs from the displacement available from simulations. Hence,the force applied in numerical simulations has to be modified appropriately to allow for a comparison with experimental results. In frequency domain, the modified force $F^{*}(\omega)$ is calculated from the frequency-domain relation

$$F^{*}(\omega) = \frac{V_{\mathrm{exp}}(\omega)}{U_{\mathrm{sim}}(\omega)} F(\omega) \tag{5.36}$$

where $V_{\mathrm{exp}}(\omega)$ is the experimentally received signal at a given location, and $U_{\mathrm{sim}}(\omega)$ is the displacement at the same location in the simulation model for the force $F(\omega)$. Once $F^{*}(\omega)$ is obtained, the inverse Fourier transform is simply

applied to determine the modified input force for the FE simulations. An example of such a modified signal with a 200 kHz central frequency is shown in Figure (5.10), along with the original force signal.

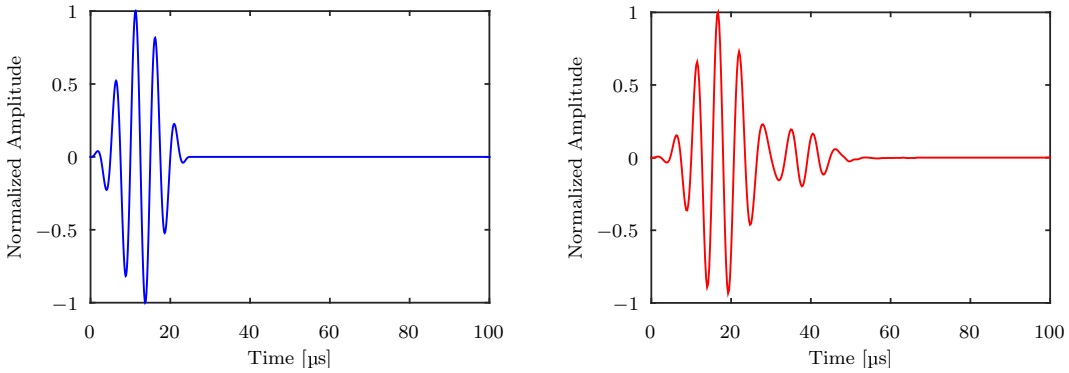

(a) Original force F; used as input signal in experiments

(b) Modified force F^*; used as input force in simulations

Figure 5.10: Original and modified narrow-band input signals with center frequency $f = 200\,\text{kHz}$

5.6.2 Undamaged Plate

First, an FE simulation is carried out using the tie model as described in Section (5.4). In this case, however, the tie-bond is applied to all neighboring nodes of the lower and upper part of the plate, resulting in a homogeneous undamaged 2D model of the plate. As mentioned before, the forcing function used in the FE model is now the modified force F. The recorded outputs are the displacement components normal to the surface at various positions. In the experiment, the same aluminum plate is used for measurements in both the undamaged and damaged case. In the undamaged case, the opposite side of the plate is used and, due to the sufficiently large dimensions, the damaged area does not influence the measurements in this case. With the actuating transducer at $x = 0\,\text{mm}$, which is 76.2 mm (3 in) away from the edge of the plate, measurements are conducted

with the receiving transducer placed at identical positions to those used in the simulations.

The experimentally and numerically determined responses to the induced force at $f = 200\,\text{kHz}$ are compared in Figure (5.11) for two receiver locations at $x = 76.2\,\text{mm}$ and $x = 127\,\text{mm}$. Results from experiments are shown as solid lines, while results from simulations are plotted as dashed lines. In the signal, two waves can be identified: the first wave packet with high amplitude is the induced Rayleigh wave R→, while the second smaller wave packet is a reflected wave from the (left) edge of the plate. It can be seen that there is good agreement between the experimental and numerical results at both receiver locations.

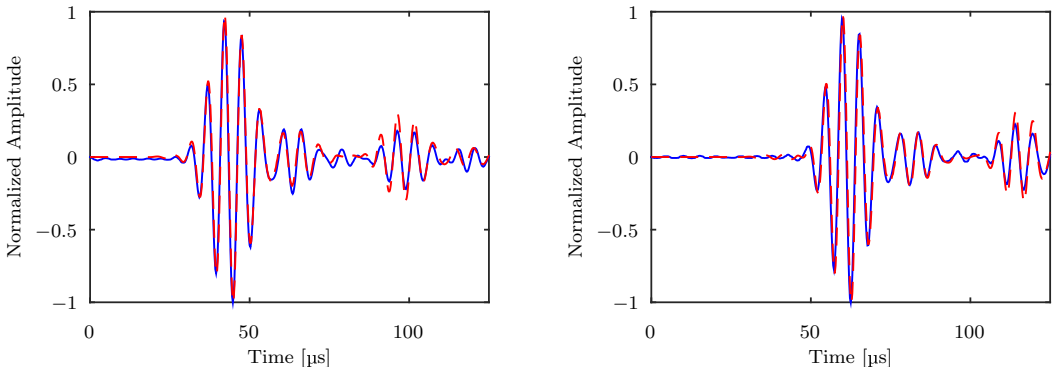

(a) $x = 76.2\,\text{mm}$ (b) $x = 127\,\text{mm}$

Figure 5.11: Comparison of experimentally received signal (solid blue lines) and simulation result (dashed red lines) for various locations along the top surface of an undamaged aluminum plate for $f = 200\,\text{kHz}$

5.6.3 Damaged Plate

More important than the experimental validation of wave propagation in the undamaged case, numerical findings for the damaged plate are also verified experimentally. In this case, a crack parallel to the surface of the plate with a length of 25.4 mm (1 in) is sawed into the specimen using electrical discharge machining,

such that the leading edge of the crack is located at 63.5 mm (2.5 in) from the source and 1.78 mm below the surface.

The experiments are performed similarly to the ones for the undamaged case, i.e. measurements are conducted at various positions along the surface of the plate near the crack. Numerical FE simulation are carried out using the tie model, as described in Section (5.4). For the input force, again the modified source F^* is applied. Displacements in the z direction are recorded at the same positions as in the experiments.

The results for both experimentally and numerically recorded signals at two receiver locations $x = 76.2$ mm (above the crack) and $x = 127$ mm (after the crack) are shown in Figure (5.12), where results from experiments are shown as solid lines and results from FE simulations as dashed lines, respectively. The simulated waveforms can again be seen to have the same major characteristics as those in the experiments. However, in Figure (5.12a), the agreement between simulation and experiment is acceptable but not perfect. This might be due to the fact that the measurement is taken exactly in the middle of the relatively short crack, which causes superposition of left and right going Lamb waves. Due to minor differences in the group velocities between the experiment and the simulation, superposition of the two waves is not identical. As can be seen from Figure (5.12b), the recorded signals of the right propagating Rayleigh wave, which is transmitted through the delamination zone, are very close in the simulation and the experiment.

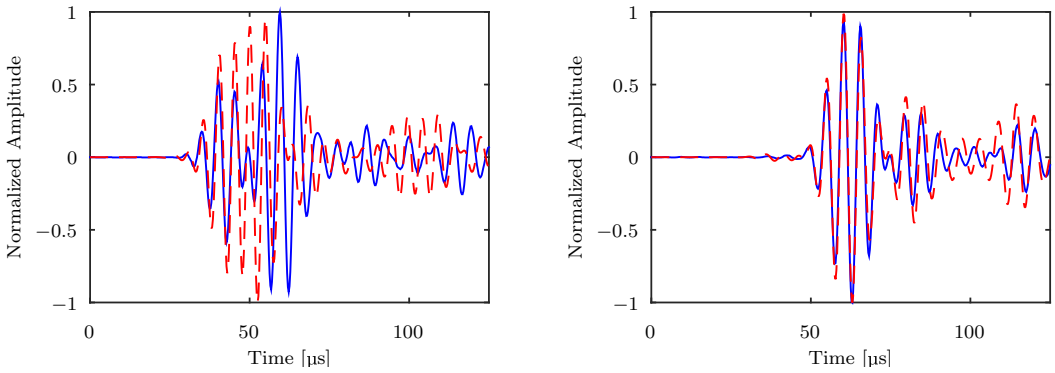

(a) In delamination zone at $x = 76.2\,\text{mm}$ (b) After delamination zone at $x = 127\,\text{mm}$

Figure 5.12: Comparison of experimentally received signals (solid blue lines) and simulation results (dashed red lines) for various locations along the top surface of a damaged aluminum plate for $f = 200\,\text{kHz}$

CHAPTER 6

Concluding Remarks

From the study of propagation of Lamb waves through plates carried out in this thesis, the following remarks can be made as a summary.

- The displacements and stresses associated with the propagation of waves in a plate are highly influenced by the nature of the load generating the wave motion in the frequency range of 100 kHz to 0.5 MHz.
- The energy carried by the waves differ significantly depending on the type of load generating the waves.
- The rocking load induces Lamb waves with the least energy within the frequency range considered. For low frequencies, Lamb waves generated due to the uniform vertical load, carries the highest amount of energy. For some mid frequencies, in the range considered, the Lamb waves generated due to the uniform shear load carries a little more energy than those generated by the uniform vertical load, but again decreases for higher frequencies.
- The non-propagating waves near the source do not contribute to any net average energy flow per cycle.
- When a Rayleigh wave hits a crack in a half space, with increasing frequency, more energy is transmitted as Lamb waves at the leading edge of the defect. This can be attributed to the fact that more of the Rayleigh wave energy is concentrated near to the surface of the half-space. Furthermore,

with increasing frequency, less energy is transmitted at the trailing edge of the delamination like crack. Hence, the measured Rayleigh wave after the delamination zone is of lower amplitude for higher frequencies.

- There is a pressing need for simulations and experiments for realistic problems involving composite structural composites containing hidden defects.

References

[1] H. Lamb. On waves in an elastic plate. *Proc. Roy. Soc. London*, Ser. A 93:114–128, 1917.

[2] M. Ewing, W. S. Jardetzky, and F. Press. *Elastic Waves in Layered Media*. McGraw-Hill, New York, 1957.

[3] K. Aki and P. G. Richards. *Quantitative Seismology, Theory and Methods*. Freeman, San Francisco, 1980.

[4] A. H. Nayfeh. *Wave Propagation in Layered Anisotropic Media: With Applications to Composites*. Elsevier Science, Amsterdam, 1995.

[5] J. L. Rose. *Ultrasonic Waves in Solid Media*. Cambridge University Press, New York, 1999.

[6] A. K. Mal and S.-S. Lih. Elastodynamic response of a unidirectional composite laminate to concentrated surface loads: Part i. *J. Appl. Mech.*, 59:878–886, 1992.

[7] S.-S. Lih and A. K. Mal. Elastodynamic response of a unidirectional composite laminate to concentrated surface loads: Part ii. *J. Appl. Mech.*, 59:887–892, 1992.

[8] S.-S. Lih and A. K. Mal. On the accuracy of approximate plate theories for wave field calculations in composite laminates. *Wave Motion*, 21:17–34, 1995.

[9] L. M. Brekhovskikh. *Waves in Layered Media*. Academic Press, New York, 1960.

[10] D. Guo, A. K. Mal, and K. Ono. Wave theory of acoustic emission in composite laminates. *Journal of Acoustic Emission*, 14:S19–S46, 1996.

[11] D. E. Chimenti. Guided waves in plates and their use in material characterization. *Applied Mechanics Review*, 50:247–284, 1997.

[12] M. R. Karim, A. K. Mal, and Y. Bar-Cohen. Inversion of leaky lamb wave data by simplex algorithm. *J. Acoust. Soc. Am.*, 88(1):482–491, 1990.

[13] Y. Bar-Cohen, A. Mal, and S.-S. Lih. Nde of composite materials using ultrasonic oblique insonification. *Materials Evaluation*, 51(11):1285–1295, 1993.

[14] L. Wang and F. G. Yuan. Group velocity and characteristic wave curves of lamb waves in composites: Modeling and experiments. *Composites Science and Technology*, 67:1370–1384, 2007.

[15] Z. Chang and A. K. Mal. Wave propagation in a plate with defects. *Review of Progress in QNDE*, 17:121–128, 1998.

[16] S. Banerjee, A.K. Mal, and W.H. Prosser. Analysis of transient lamb waves generated by dynamic surface sources in thin composite plates. *J. Acoust. Soc. Am.*, 115(5):19051911, 2004.

[17] L. J. Gibson and M. J. Ashby. *Cellular Solids: Structure and Properties*. Cambridge University Press, Cambridge, U.K., 2 edition, 1997.

[18] John Gary and Marvin A Hamstad. On the far-field structure of waves generated by a pencil lead break on a thin plate. *Journal of acoustic emission*, 12(3-4):157–170, 1994.

[19] WH Prosser, MA Hamstad, J Gary, and A O'Gallagher. Finite element and plate theory modeling of acoustic emission waveforms. *Journal of nondestructive evaluation*, 18(3):83–90, 1999.

[20] Brian R Mace, Denis Duhamel, Michael J Brennan, and Lars Hinke. Finite element prediction of wave motion in structural waveguides. *The Journal of the Acoustical Society of America*, 117(5):2835–2843, 2005.

[21] L Gavrić. Computation of propagative waves in free rail using a finite element technique. *Journal of Sound and Vibration*, 185(3):531–543, 1995.

[22] Svante Finnveden. Spectral finite element analysis of the vibration of straight fluid-filled pipes with flanges. *Journal of Sound and Vibration*, 199(1):125–154, 1997.

[23] Christoph Schaal, Stefan Bischoff, and Lothar Gaul. Analysis of wave propagation in periodic 3d waveguides. *Mechanical Systems and Signal Processing*, 40(2):691–700, 2013.

[24] Fabien Treyssede and Laurent Laguerre. Investigation of elastic modes propagating in multi-wire helical waveguides. *Journal of sound and vibration*, 329(10):1702–1716, 2010.

[25] Christoph Schaal. *Fuzzy Arithmetical Assessment of Health Monitoring for Multi-Wire Cables using Ultrasonic Waves*. Der Andere Verlag, 2014.

[26] Sauvik Banerjee, Fabrizio Ricci, and Ajit Mal. Autonomous health monitoring of composite structures using a statistical damage index approach. In *The 14th International Symposium on: Smart Structures and Materials & Nondestructive Evaluation and Health Monitoring*, pages 65321U–65321U. International Society for Optics and Photonics, 2007.

[27] Mathias Fink. Time reversal of ultrasonic fields. i. basic principles. *Ultrasonics, Ferroelectrics, and Frequency Control, IEEE Transactions on*, 39(5):555–566, 1992.

[28] Hyun Woo Park, Hoon Sohn, Kincho H Law, and Charles R Farrar. Time reversal active sensing for health monitoring of a composite plate. *Journal of Sound and Vibration*, 302(1):50–66, 2007.

[29] Buli Xu and Victor Giurgiutiu. Lamb waves time-reversal method using frequency tuning technique for structural health monitoring. In *The 14th International Symposium on: Smart Structures and Materials & Nondestructive Evaluation and Health Monitoring*, pages 65290R–65290R. International Society for Optics and Photonics, 2007.

[30] Ajit Mal, Fabrizio Ricci, Himadri Samajder, and Harsh Baid. Nde of composite structures using ultrasonic guided waves. In *SPIE Smart Structures and Materials+ Nondestructive Evaluation and Health Monitoring*, pages 86950E–86950E. International Society for Optics and Photonics, 2013.

[31] Younho Cho and Joseph L Rose. An elastodynamic hybrid boundary element study for elastic guided wave interactions with a surface breaking defect. *International Journal of Solids and Structures*, 37(30):4103–4124, 2000.

[32] Stefan Bischoff, Christoph Schaal, and Lothar Gaul. Efficient wave scattering analysis for damaged cylindrical waveguides. *Journal of Sound and Vibration*, 333(18):4203–4213, 2014.

[33] Gennady Shkerdin and Christ Glorieux. Lamb mode conversion in a plate with a delamination. *The Journal of the Acoustical Society of America*, 116(4):2089–2100, 2004.

[34] Sunil Kishore Chakrapani and Vinay Dayal. The interaction of rayleigh waves with delaminations in composite laminates. *The Journal of the Acoustical Society of America*, 135(5):2646–2653, 2014.

[35] John A Judge, Douglas M Photiadis, Joseph F Vignola, Brian H Houston, and Jacek Jarzynski. Attachment loss of micromechanical and nanomechanical resonators in the limits of thick and thin support structures. *Journal of Applied Physics*, 101(1):013521, 2007.

[36] GF Miller and H Pursey. The field and radiation impedance of mechanical radiators on the free surface of a semi-infinite isotropic solid. In *Proceedings of the Royal Society of London A: Mathematical, Physical and Engineering Sciences*, volume 223, pages 521–541. The Royal Society, 1954.

[37] Y Jimbo and K Itao. Energy loss of a cantilever vibrator. *Journal of the Horological Institute of Japan*, 47:1–15, 1968.

[38] Mikio Takemoto, Hideo Nishino, and Kanji Ono. Wavelet transform-applications to ae signal analysis. *Acoustic Emission-Beyond the Millennium*, pages 35–56, 2000.

[39] Milton Abramowitz and Irene A Stegun. *Handbook of mathematical functions: with formulas, graphs, and mathematical tables*. Number 55. Courier Corporation, 1964.

[40] Ajit K Mal and Sarva Jit Singh. *Deformation of elastic solids*. Prentice Hall, 1991.

[41] Harsh Kumar Baid. Detection of damage in a composite structure using guided waves. 2012.

[42] Jan Achenbach. Wave propagation in elastic solids (north-holland series in applied mathematics and mechanics). 1987.

[43] Jungki Lee and Ajit Mal. A volume integral equation technique for multiple inclusion and crack interaction problems. *Journal of applied mechanics*, 64(1):23–31, 1997.